Universidade de São Paulo

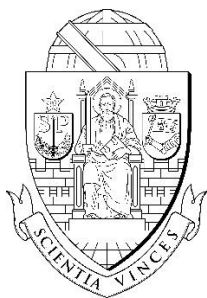Universitat Politècnica de València

Kayo Santana Barros

Treatment, by electrodialysis, of a synthetic wastewater from the cyanide-free brass electroplating and study on ion transport: recovery of water and chemicals

Supervisor (USP): Prof. Dr. Denise C. R. Espinosa

Supervisor (UPV): Prof. Dr. Valentín Pérez-Herranz

São Paulo / València

June - 2020

Universidade de São Paulo

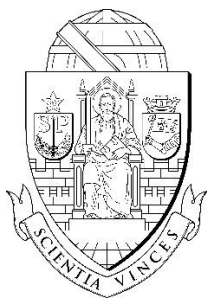Universitat Politècnica de València

Kayo Santana Barros

Tratamiento, por electrodiálisis, de aguas residuales sintéticas de la electrodeposición de latón libre de cianuro y estudio del transporte de iones: recuperación de agua y productos químicos

Supervisora (USP): Prof. Dr. Denise C. R. Espinosa

Supervisor (UPV): Prof. Dr. Valentín Pérez-Herranz

São Paulo / València

Junio - 2020

Universidade de São Paulo

Universitat Politècnica de València

Kayo Santana Barros

Tratamento, por eletrodiálise, de águas residuais sintéticas da eletrodeposição de latão livre de cianeto e estudo sobre transporte de íons: recuperação de água e produtos químicos

Orientadora (USP): Prof. Dr. Denise C. R. Espinosa

Orientador (UPV): Prof. Dr. Valentín Pérez-Herranz

São Paulo / València

Junho - 2020

Kayo Santana Barros

Treatment, by electrodialysis, of a synthetic wastewater from the cyanide-free brass electroplating and study on ion transport: recovery of water and chemicals

Corrected version – Versão corrigida

(Versão original encontra-se na unidade que aloja o Programa de Pós-graduação)

Ph.D. Thesis presented to the Graduate Program in Chemical Engineering at the Departamento de Engenharia Química, Escola Politécnica da Universidade de São Paulo, Brazil and the Graduate Program in Industrial Engineering and Production at the Universitat Politècnica de València, Spain, to obtain the dual degree of Doctor of Philosophy in Science.

Supervisor at USP: Prof. Dr. Denise C. R. Espinosa

Supervisor at UPV: Prof. Dr. Valentín Pérez-Herranz

São Paulo / València

2020

Este exemplar foi revisado e corrigido em relação à versão original, sob responsabilidade única do autor e com a anuência de seu orientador.

São Paulo, _____ de _____ de _____

Assinatura do autor: _____

Assinatura do orientador: _____

Catalogação-na-publicação

Universidade de São Paulo
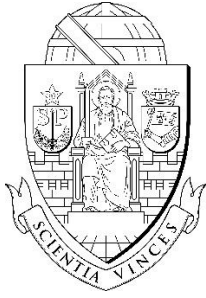
Universitat Politècnica de València

TESIS

Presentada en co-tutela en vía de obtener el

DOCTORADO

de la **Universitat Politècnica de València**

y

de la **Universidade de São Paulo**

Realizada por:

Kayo Santana Barros

Dirigida por:

Prof. Dr. Denise C. R. Espinosa

Prof. Dr. Valentín Pérez-Herranz

Dedico este trabalho a todas as pessoas que me proporcionam amor e inspiração.

ACKNOWLEDGEMENTS

I would like to express my sincere gratitude to those who helped, taught and encouraged me to work towards my goals.

To my supervisors, Prof. Denise Crocce Romano Espinosa and Prof. Valentín Pérez-Herranz, who guided me throughout this project. It has been a great pleasure and honor to have them as my supervisors.

To Prof. Jorge Alberto Soares Tenório, for accepting me in his research group.

To Prof. Montserrat García Gabaldón and Prof. Emma M. Ortega, for being so kind and helpful during my stay in València, Spain.

To my colleagues from Larex/USP, for the friendship and the enjoyable moments. I would like to express my special thanks to Tatiana Scarazzato, for providing me valuable helps for my investigation.

To all my colleagues from UPV, for the friendship and the incredible moments in València throughout the best year that I had in my life.

To the members of the thesis committee, for generously offering their time and knowledge to improve the research.

To Valdir, for being so patient and supportive of my life goals.

To my friends, especially those from Belo Horizonte, Caeté, São Paulo, Uberlândia and València, for providing me friendship and encouragement.

To my mother, Maria Alice; my father, Robson and my sister, Renata; for supporting me with love and showing how proud they are of me / À minha mãe, Maria Alice; ao meu pai, Robson e à minha irmã, Renata; por me apoiarem com amor e por demonstrarem o quão orgulhosos estão de mim.

ABSTRACT

Growing concerns about environment and human health have led to the development of cleaner industrial processes. In recent years, the replacement of cyanide by EDTA in the brass electroplating baths has been assessed. However, the treatment of the wastewater generated has not been studied yet. Traditionally, wastewaters from electroplating processes are treated by chemical precipitation, which requires the addition of chemicals and produces sludges that are disposed in hazardous waste landfills. Hence, other techniques must be investigated and electrodialysis is a promising alternative since it allows the recovery of metals and water. Although electrodialysis is generally operated at current densities lower than the limiting current density of the membrane system (underlimiting), researchers have verified that operations at current densities above the limiting one (overlimiting) improve the ions transfer. To ensure its feasibility, studies on transport properties of ionic species are crucial and, among the dynamic characterization methods, chronopotentiometry stands out, since the dynamic voltage response in time can be analyzed. Therefore, this thesis aims to propose an alternative to the treatment of a synthetic solution that simulates the major wastewater from the cyanide-free brass electroplating industry. Firstly, chronopotentiometric tests were performed to compare transport properties of Cu^{2+} ions, in acid medium, across two ion-exchange membranes, the PC-SK and the HDX100. The use of HDX membrane in electrodialysis showed to be more appropriate, due to its lower tendency of fouling/scaling occurrence. Then, transport properties of copper and zinc complexes, present in the synthetic wastewater from the brass electroplating, across the anion-exchange membrane HDX200 were assessed. The effects of the solution pH, Cu^{2+}/Zn^{2+} proportion and EDTA concentration on the transport properties were studied. For the solution with Cu^{2+}/Zn^{2+} proportion of 0.4, an insoluble species was formed. Therefore, the synthetic wastewater with this metals proportion was treated, by electrodialysis in underlimiting and overlimiting conditions, to assess the influence of the current regime and the presence of insoluble species on the extraction of ions. The overlimiting operation was more advantageous since water splitting and electroconvection accounted for the improvement of the extraction of ions. Besides, chronopotentiometric studies showed that fouling/scaling occurrence was reduced. Then, the used membranes were forwarded to a three-stage cleaning procedure and the cleaning solution with 0.1 mol NaOH/L was the most appropriate. Lastly, ions from the concentrated solution obtained by electrodialysis were recovered into the electroplating bath. Cyclic voltammetric studies and electrodeposition tests were conducted at a rotating disk electrode. Uniform brass electrodeposits, with brightness and without cracks were obtained using the original electroplating bath and after the recovery of ions from electrodialysis, especially under agitation and at lower voltages than those already tested in literature. Thus, electrodialysis showed to be a feasible alternative for recovering water and inputs from the evaluated wastewater.

Keywords: electrodialysis; chronopotentiometry; brass electrodeposition; water recovery; chemicals recovery.

RESUMO

Preocupações crescentes com o meio ambiente e com a saúde humana têm levado ao desenvolvimento de novos processos industriais. Nos últimos anos, a substituição do cianeto pelo EDTA nos banhos de eletrodeposição de latão tem sido avaliada. No entanto, o tratamento dos resíduos líquidos gerados ainda não foi estudado. Tradicionalmente, resíduos líquidos provenientes de indústrias galvânicas são tratados por precipitação química, que requer a adição de reagentes e produz lamas que são descartadas em aterros de resíduos perigosos. Portanto, outras técnicas devem ser investigadas e a eletrodiálise é uma alternativa promissora, pois permite recuperar os metais e a água. Embora a eletrodiálise seja geralmente operada sob densidades de corrente inferiores à densidade de corrente limite do sistema da membrana (*underlimiting*), alguns pesquisadores têm verificado que operações sob densidades de corrente superiores à limite (*overlimiting*) intensificam a transferência dos íons. Para garantir sua viabilidade, estudos sobre propriedades de transporte das espécies iônicas são cruciais, e dentre os métodos de caracterização dinâmica, a cronopotenciometria se destaca por permitir a análise da diferença de potencial entre as membranas em função do tempo. Portanto, esta tese tem como objetivo propor uma alternativa ao tratamento de uma solução sintética que simula o principal resíduo líquido proveniente da indústria de eletrodeposição de latão, isenta de cianeto, com EDTA. Primeiramente, testes cronopotenciométricos foram realizados a fim de comparar as propriedades de transporte dos íons Cu^{2+}, em meio ácido, através de duas membranas trocadoras de cátions, a PC-SK e a HDX100. O uso da HDX mostrou-se mais adequado, devido à menor tendência de ocorrência de incrustações na sua superfície. Em seguida, foram avaliadas as propriedades de transporte dos complexos de cobre e zinco, presentes no resíduo líquido da eletrodeposição de latão, através da membrana trocadora de ânions HDX200. Os efeitos do pH, proporção de Cu^{2+}/Zn^{2+} e concentração de EDTA foram investigados. Com a solução de proporção Cu^{2+}/Zn^{2+} de 0,4; uma espécie insolúvel foi formada. Portanto, o resíduo líquido com essa proporção de metais foi tratado, por eletrodiálise, em condições *underlimiting* e *overlimiting*, para avaliar o efeito da intensidade de corrente e a presença de espécies insolúveis na extração dos íons. A operação *overlimiting* foi mais vantajosa, já que a quebra das moléculas de água e eletroconvecção favoreceram a extração dos íons. Além disso, estudos cronopotenciométricos mostraram que as incrustações nas membranas foram reduzidas. Em seguida, as membranas foram submetidas a um procedimento de limpeza em três etapas e a solução de NaOH em 0,1 mol/L foi a mais adequada. Por fim, os íons da solução concentrada obtida por eletrodiálise foram recuperados no banho. Estudos de voltametrias cíclicas e eletrodeposições foram realizados em um eletrodo de disco rotativo. Depósitos uniformes de latão e com brilho foram obtidos utilizando o banho original e após a recuperação dos íons, principalmente sob agitação e em potenciais inferiores aos que já foram testados na literatura. Portanto, a eletrodiálise se mostrou uma alternativa viável para recuperar água e insumos do resíduo líquido avaliado.

Palavras-chave: eletrodiálise; cronopotenciometria; eletrodeposição de latão; recuperação de água; recuperação de produtos químicos.

RESUMEN

Las crecientes preocupaciones por el medio ambiente y la salud humana han llevado al desarrollo de nuevos procesos industriales. En los últimos años, se ha evaluado la sustitución del cianuro por EDTA en los baños de electrodeposición de latón. Sin embargo, el tratamiento de las aguas residuales generadas no se ha estudiado aún. Tradicionalmente, los efluentes de los procesos de electrodeposición se tratan por precipitación química, que requiere la adición de reactivos y produce lodos que se almacenan en los vertederos de residuos peligrosos. Por lo tanto, es necesario investigar otras técnicas y la electrodiálisis es una alternativa prometedora, ya que permite la recuperación de metales y del agua. Aunque la electrodiálisis generalmente se opera a corrientes inferiores a la corriente límite del sistema de membrana (*underlimiting*), algunos investigadores han verificado que las operaciones a corrientes superiores a la límite (*overlimiting*) intensifican la transferencia de iones. Para garantizar su viabilidad, los estudios sobre las propiedades de transporte de los iones son cruciales y, entre los métodos de caracterización, la cronopotenciometría destaca por permitir el análisis del voltaje en función del tiempo. Por lo tanto, esta tesis tiene por objetivo proponer una alternativa al tratamiento de una disolución sintética que simula las aguas residuales de la industria de electrodeposición de latón libre de cianuro. Primero, se realizaron pruebas cronopotenciométricas para comparar las propiedades de transporte de iones Cu^{2+}, en medio ácido, a través de dos membranas de intercambio iónico, la PC-SK y la HDX100. El uso de la HDX en electrodiálisis demostró ser más apropiado debido a su menor tendencia a formar incrustaciones. Luego, se evaluaron las propiedades de transporte de los complejos de cobre y zinc, presentes en las aguas residuales de la electrodeposición de latón, a través de la membrana de intercambio aniónico HDX200. Se estudiaron los efectos del pH, la proporción Cu^{2+}/Zn^{2+} y la concentración de EDTA sobre las propiedades de transporte. Para la disolución con una proporción Cu^{2+}/Zn^{2+} de 0.4, se formó una especie insoluble. Por lo tanto, se trataron las aguas residuales con esta proporción de metales, por electrodiálisis en condiciones *underlimiting* y *overlimiting*, para evaluar la influencia de la corriente eléctrica y la presencia de especies insolubles en la extracción de los iones. La operación *overlimiting* se mostró más ventajosa, ya que la hidrólisis del agua y la electroconvección mejoraran la extracción de los iones. Además, los estudios cronopotenciométricos mostraron que se reducen las incrustaciones. Luego, las membranas se sometieron a un procedimiento de limpieza de tres etapas y la disolución de limpieza con 0.1 mol de NaOH/L se mostró más apropiada. Finalmente, los iones de la disolución concentrada obtenida por electrodiálisis se recuperaron en el baño de electrodeposición. Se realizaron estudios de voltametría cíclica y pruebas de electrodeposición en un electrodo de disco rotatorio. Se obtuvieron depósitos de latón uniformes y con brillo, utilizando el baño original y después de la recuperación de iones, especialmente con agitación y a voltajes más bajos que los ya probados en la literatura. Por lo tanto, la electrodiálisis demostró ser una alternativa factible para recuperar agua y materias primas de las aguas residuales evaluadas.

Palabras clave: electrodiálisis; cronopotenciometría; electrodeposición de latón; recuperación del agua; recuperación de productos químicos.

RESUM

Les creixents preocupacions pel medi ambient i la salut humana han conduït al desenvolupament de nous processos industrials. En els últims anys, s'ha avaluat la substitució del cianur per EDTA als banys d'electrodeposició de llautó. No obstant això, el tractament de les aigües residuals generades no s'ha estudiat encara. Tradicionalment, els efluents dels processos d'electrodeposició es tracten per precipitació química, que requereix l'addició de reactius i produeix fangs que s'emmagatzemen en els abocadors de residus perillosos. Per tant, és necessari investigar altres tècniques i l'electrodiàlisi és una alternativa prometedora, ja que permet la recuperació de metalls i de l'aigua. Tot i que l'electrodiàlisi generalment s'opera a corrents inferiors al corrent límit del sistema de membrana (underlimiting), alguns investigadors han verificat que les operacions a corrents superiors al límit (overlimiting) intensifiquen la transferència de ions. Per garantir la seua viabilitat, els estudis sobre les propietats de transport dels ions són crucials i, entre els mètodes de caracterització, la cronopotenciometria destaca per permetre l'anàlisi del voltatge en funció del temps. Per tant, aquesta tesi té per objectiu proposar una alternativa al tractament d'una dissolució sintètica que simula les aigües residuals de la indústria d'electrodeposició de llautó lliure de cianur. Primer, es van realitzar proves cronopotenciomètriques per comparar les propietats de transport de ions Cu^{2+}, en medi àcid, a través de dues membranes d'intercanvi iònic, la PC-SK i l`HDX100. L'ús de l'HDX en electrodiàlisi va demostrar ser més apropiat a causa de la seua menor tendència a formar incrustacions. Després, es van avaluar les propietats de transport dels complexos de coure i zinc, presents a les aigües residuals de l'electrodeposició de llautó, a través de la membrana d'intercanvi aniònic HDX200. Es van estudiar els efectes del pH, la relació molar Cu^{2+}/Zn^{2+} i la concentració d'EDTA sobre les propietats de transport. Per a la dissolució amb una proporció Cu^{2+}/Zn^{2+} de 0,4, es va formar una espècie insoluble. Per tant, es van tractar les aigües residuals amb aquesta proporció de metalls per electrodiàlisi en condicions underlimiting i overlimiting, per avaluar la influència del corrent elèctric i la presència d'espècies insolubles en l'extracció dels ions. L'operació overlimiting es va mostrar més avantatjosa, ja que la hidròlisi de l'aigua i l'electroconvecció milloren l'extracció dels ions. A més, els estudis cronopotenciomètrics van mostrar que es redueixen les incrustacions. Després, les membranes es van sotmetre a un procediment de neteja de tres etapes i la dissolució de neteja amb 0,1 mol d'NaOH/L es va mostrar més apropiada. Finalment, els ions de la dissolució concentrada obtinguda per electrodiàlisi es van recuperar al bany d'electrodeposició. Es van realitzar estudis de voltametria cíclica i proves d'electrodeposició en un elèctrode de disc rotatori. Es van obtenir dipòsits de llautó uniformes i brillants, en utilitzar el bany original i després de la recuperació de ions, especialment amb agitació i a voltatges més baixos que els ja provats en la literatura. Per tant, l'electrodiàlisi va demostrar ser una alternativa factible per recuperar aigua i matèries primeres de les aigües residuals avaluades.

Paraules clau: electrodiàlisi; cronopotenciometria; electrodeposició de llautó; recuperació d'aigua; recuperació de productes químics.

CONTENTS

LIST OF FIGURES

LIST OF TABLES

LIST OF SYMBOLS

A	Disc area
a_j	Activity of the species j
C	Electrolyte concentration
C_t^j	Concentration of the species j at a given time
C_0^j	Concentration of the species j in the initial state
D_j	Diffusion coefficient of the species j
D_m	Electrolyte diffusion coefficient in the membrane phase
E	Electric potential difference
E^0	Standard electrode potential
F	Faraday constant
g	Gravitational acceleration
I	Electric current
I_d	Diffusion current
I_k	Kinetic current
i	Electric current density
i_{lim}	Limiting current density
$\vec{J_J}$	Flux density of the species j
J_j^m	Flow of counterions through the membrane
J_j^s	Flow of counterions in the solution
K	Equilibrium constant
k	Kinetic rate constant
L	Effective radius of the membrane when it is circular

Q	Ionic equivalent charge
U	Electric potential
R	Molar gas constant
R_{elec}	Electrical resistance
R_1/R_3	Electrical resistance at underlimiting condition / overlimiting condition
Sc	Schmidt number
T	Temperature
t	Time
$\overline{t_j}$	Transport number of an ion j in the membrane phase
t_j	Transport number of an ion j in the solution
U	Electric potential
U_m	Membrane potential drop
U_Ω	Initial membrane potential drop
$U_{m,f}$	Final membrane potential drop
U_c	Membrane potential drop related to the concentration overvoltage
$\vec{V}$	Velocity vector of the fluid
x	Directional coordinate
z_j	Charge of the ionic species j
α_1/α_3	Slope of the tangential line of the CVC at the ohmic and overlimiting regions
δ	Thickness of the diffusion boundary layer
δ_m	Thickness of the membrane
ΔC_g	Concentration gradient between the boundary layer of the membrane interface and the bulk solution
ε	Fraction of conductive area of the membrane

λ	Conductivity
v	Kinematic viscosity
v_j	Stoichiometric coefficient of the species j
τ	Transition time
ω	Rotation speed

LIST OF ABBREVIATIONS

ABNT	Brazilian Association for Technical Standards
AEM	Anion-exchange membrane
BSA	Bovine serum albumin
CEM	Cation-exchange membrane
ChP	Chronopotentiogram
CIMD	Current-induced membrane discharge
CVC	Current-voltage curve
CV	Cyclic voltammetry
DBL	Diffusion boundary layer
EC	Electroconvection
ED	Electrodialysis
EDS	Energy Dispersive X-ray Spectroscopy
EDL	Electric double layer
EDTA	Ethylenediaminetetraacetic acid
FTIR-ATR	Fourier-transform Infrared Spectroscopy - Attenuated Total Reflectance
NBR	Associação Brasileira de Normas Técnicas
PCA	Polymerchemie Altmeier GmbH
PC%	Percent concentration
PE%	Percent Extraction
ICP-OES	Inductively Coupled Plasma Optical Emission Spectrometry
RDE	Rotating disk electrode
SEM	Scanning electron microscopy

1.   INTRODUCTION

1.1.   Background

Electroplating is the deposition of a thin layer of the desired coating, by means of electrolysis, on an object to alter the characteristics of its surface. This process is frequently applied to provide decorative aspects to an object, to improve the surface, engineering or mechanical properties, or a combination of them [1]. Common electroplating processes use copper, zinc, nickel, chromium, gold, and silver, besides metal alloys. The plating of copper-zinc alloys, also known as brass, is widely used for decorative finishes, protection of steel and promotion of rubber adhesion to steel and other metals [2,3]. The most employed electrolyte for brass plating is based on cyanides, since this complexing agent brings the reduction potentials of both metals closer together, forming stable complexes [4]. However, the use of cyanide in the electroplating industry has been discouraged in recent years.

One of the major drawbacks of the cyanide in the brass plating bath is the disposal of the wastes generated, due to the increasing stringency of the environmental legislations, besides its toxicity [5]. Hence, concerns about environment and human safety have prompted the development of cyanide-free brass plating baths less hazardous and able to provide deposits with quality comparable to cyanide.

Brenner [6] published a review, in 1963, on some cyanide-free complexing agents for electrodepositing brass alloys and, from that study, several alternative complexing agents have been tested in literature [4,7,8]. In recent years, Almeida et al. [9,10] evaluated the electrodeposition of brass with EDTA and obtained deposits with brightness, uniform color, regular composition and without cracks. Hence, among the cyanide-free complexing agents tested in literature, EDTA has shown to be a promising alternative.

The metal electroplating process involves three main stages: the surface preparation, the electrodeposition, and the post-treatment of the objects. Each stage is followed by rinsing steps, which are responsible for the major proportion of wastewater in the electroplating process, since the drag out of chemicals from

the electroplating baths generates a toxic rinsing water (11,12). The most used technique for treating wastewaters from electroplating industries is the chemical precipitation in alkaline medium (13). Despite its simplicity, this method implies the addition of chemicals and produces sludges that are filtrated, dehydrated and disposed in hazardous waste landfills (14). Therefore, increasing attention has been given to alternative techniques to treat wastewaters, such as ion-exchange, adsorption, membrane and biological processes (15,16). Membrane processes, driven by pressure, concentration and potential difference, have been extensively assessed in recent years (13,17,18) and, among them, electrodialysis has shown special relevance in literature.

Electrodialysis (ED) is a membrane separation process that allows the extraction and recovery of ions by applying an electrical potential difference between two electrodes separated by anion- and cation-exchange membranes. This technique was proposed in 1890, by Maigrot and Sabates (19), to demineralize sugar syrup and, from the 1950s, it has been mostly used for producing drinking water from brackish water sources. Traditionally, electrodialysis is conducted at underlimiting current regimes, under 70 % - 80 % of the limiting current density of the membrane/solution system to avoid concentration polarization phenomena (20). Nevertheless, some authors have assessed the operation in overlimiting conditions, since an improved ionic transport across the membranes has been observed, besides the reduction of the membrane area (21,22).

Considering its advantages and possibilities of adaptations, electrodialysis has become a multifunctional process, being used for several applications, such as in industrial wastewaters treatment, in the pharmaceutical and food industry, production of organic acids and ultrapure water (23). Some of the advantages of electrodialysis over competing technologies are:

- Raw materials can be concentrated, whereas the treated solution can be reused, promoting water reclamation and the recovery of ionic species.
- The process can be adjusted in function of the feed solution quality (24) and adapted to other applications (25).
- Minimal impact on the environment compared to other techniques, since no sludge is formed (26,27).

- Units sized to fit any application (25,27).

- Operation without addition of further chemicals, at ambient temperature (23) and without pressurization (28).

- Membrane life expectancy between 8-10 years (28).

- Simple start-up and shut-down of the process for intermittent operation (24), being also possible to be operated continuously (29).

Besides the evolution of electrodialysis systems, the properties of membranes have often been improved to ensure a more efficient ionic transport, selective to the ions to be separated, with lower energy consumption and manufacturing cost. For determining the transport properties of ions across the membranes, several dynamic characterization methods can be used, such as steady-state current-voltage curves, impedance spectroscopy, cyclic voltammetry (potential sweeps) and chronopotentiometry.

Chronopotentiometry is an electrochemical method widely used to investigate transport properties and reactions that occur in electrolytic solutions at electrodes (30–32) and membranes (33–35). For the latter, a current density is applied to a system with an electrolytic solution separated by membranes, a working electrode and a counter electrode. The potential variation is measured on each side of the membrane as a function of time. Compared to other dynamic characterization methods, the use of chronopotentiometry stands out, since it allows a detailed evaluation of the contribution of the potential in different dynamic states of the membrane/solution system. Current-voltage curves at steady-state conditions can also be constructed, allowing the determination of important properties of the system (36). Finally, both curves provide information on the transport competition between ions and the formation of insoluble species at the membrane surface, also known as fouling and scaling.

In view of the need for cyanide-free brass plating baths technically and economically viable, the present thesis aimed at assessing the treatment, by electrodialysis at underlimiting and overlimiting current regimes, of a synthetic wastewater generated in the brass electrodeposition with EDTA as complexing agent. The ion-exchange membranes used in the electrodialysis tests were chosen based on chronopotentiometric studies conducted using solutions with cupric ions in acid medium and two different cation-exchange membranes, one

homogeneous and the other heterogeneous. After the electrodialysis tests, the membranes were evaluated and forwarded to a three-stage chemical cleaning in alkaline medium. In addition, the main transport properties of species across the anion-exchange membrane used in electrodialysis were investigated, by chronopotentiometry, in function of several conditions of the synthetic wastewater. Finally, a rotating disk electrode was used for evaluating, by means of cyclic voltammetry and electrodeposition tests, the influence of the rotation speed on the quality of the brass electrodeposits, besides the recovery of EDTA, copper and zinc ions from the concentrated solution, obtained by electrodialysis, into the electroplating bath.

1.2.   Scientific and technical contributions

The toxicity of cyanide compounds has prompted an effort to discover complexing agents less harmful to the environment and that offer deposits with similar quality (7,37,38). In recent years, Almeida et al. (9,10) have shown that the substitution of cyanide by EDTA is promising, since good deposits were obtained. The authors focused their studies, especially that performed in galvanostatic mode, on the bath with 70% of Cu^{2+} and 30% of Zn^{2+}. Besides, the experiments were carried out in the absence of agitation. Several works have been published to evaluate the effect of agitation on deposits using a rotating disk electrode (RDE), since this may avoid stagnation of the reactants, increase the deposition rates, dissipate from the surface, incorporate particles in the coating and modify the deposit properties, such as the grain size, stress and hardness control (39–41). Hence, in the thesis, a RDE was used to study the brass electrodeposition with EDTA and a bath with 30% of copper and 70% of zinc, which is generally used in industries.

Since the conventional method used to treat wastewaters from electroplating industries presents several limitations, researchers have put effort into making feasible other techniques and, among them, electrodialysis has shown to be a promising alternative. Recently, several studies on the use of electrodialysis for extracting and recovering ions from electroplating processes have been published (42–46). The tests are, in general, conducted in underlimiting conditions, since researchers still have concerns about the

influence of overlimiting phenomena on the fouling/scaling occurrence. Therefore, we proposed a novel electrodialysis operated in overlimiting condition to explore the water splitting phenomenon and electroconvection, aiming at recovering water and concentrated solutions for reuse.

After long-term concentration operations with ED, the membranes cleaning is crucial to restore the membrane performance and to extend its life, since fouling and scaling can cause an increase in the electrical resistance, a decrease in the permselectivity and membrane alterations (47). In general, authors use some well-known protocols for studying the influence of artificial ageing on some membrane features (48,49). Herein, a three-stage cleaning procedure in alkaline medium was evaluated, which favors the viability of the electrodialysis use.

Chronopotentiometry has been extensively used in studies on transport properties of ionic species across membranes (20,50–54). Compared to other characterization methods, such as impedance spectroscopy and cyclic voltammetry, it provides a direct access to the voltage contributions in different states of the membrane/solution system. It also provides more detailed information compared to steady-state voltage or current-sweeps, since the dynamic voltage response in time can be analyzed (55–57). Considering its advantages, chronopotentiometry was used in the thesis for evaluating transport properties of solutions that, from the best of our knowledge, have not been assessed in literature yet. This is crucial for the technical and economic viability of electrodialysis. Hence, the determination of the main transport properties of species in solutions, such as limiting current density, electrical resistances, plateau length, transport number, transition time and fraction of conductive area, enhances the possibility of electrodialysis to be a competitive technique to the conventional methods used for treating wastewaters.

1.3.   Structure of the thesis

The thesis was subdivided into four topics, as shown in the illustrative scheme of Figure 1. The studies performed in each stage of the work are described below.

- Topic I: Transport properties of Cu^{2+} ions in acid medium across a homogeneous and a heterogeneous cation-exchange membrane were evaluated, by chronopotentiometry, and the behavior of the chronopotentiometric and current-voltage curves were assessed in function of the solution concentration and the membranes morphology. Limiting current densities, ohmic resistances, plateau lengths, transport numbers and transition times were determined, and the tendency of fouling and scaling occurrence was investigated. The results were compared for choosing which type of membrane must be employed in topic II and topic III.

- Topic II: Transport properties of copper and zinc complexes, present in a synthetic wastewater from the brass electrodeposition with EDTA, across an anion-exchange membrane were investigated, by chronopotentiometry. Solutions at some pH conditions, molar ratios of Cu^{2+}/Zn^{2+} ions and concentrations of EDTA were evaluated. The transport competition between species and the fouling occurrence were assessed in function of the behavior of the chronopotentiometric and current-voltage curves.

- Topic III: A synthetic cyanide-free wastewater from the brass electroplating with EDTA was treated by two long-term electrodialysis tests, one performed in underlimiting condition and the other in overlimiting condition. The experiments aimed at obtaining a treated solution in appropriate conditions to be reused in the rinsing operations and a concentrated solution that was forwarded to electroplating tests (topic IV). After the electrodialysis tests, chronopotentiometric measurements were performed for evaluating the influence of the membranes use on their features. Finally, the used membranes were forwarded to a three-stage cleaning procedure in alkaline medium and their properties were evaluated by means of chronopotentiometry, FTIR-ATR and SEM-EDS analyses.

- Topic IV: Cyclic voltammetric curves were constructed and electrodeposition tests at a rotating disk electrode were conducted using the brass electroplating bath with EDTA. The effects of the rotation speed, galvanostatic/potentiostatic mode, charge density and bath concentration were studied. Lastly, the recovery of ions in the concentrated solution, obtained by electrodialysis in topic III, was evaluated. The quality of the deposits was assessed in function of visual analysis and SEM-EDS analysis.
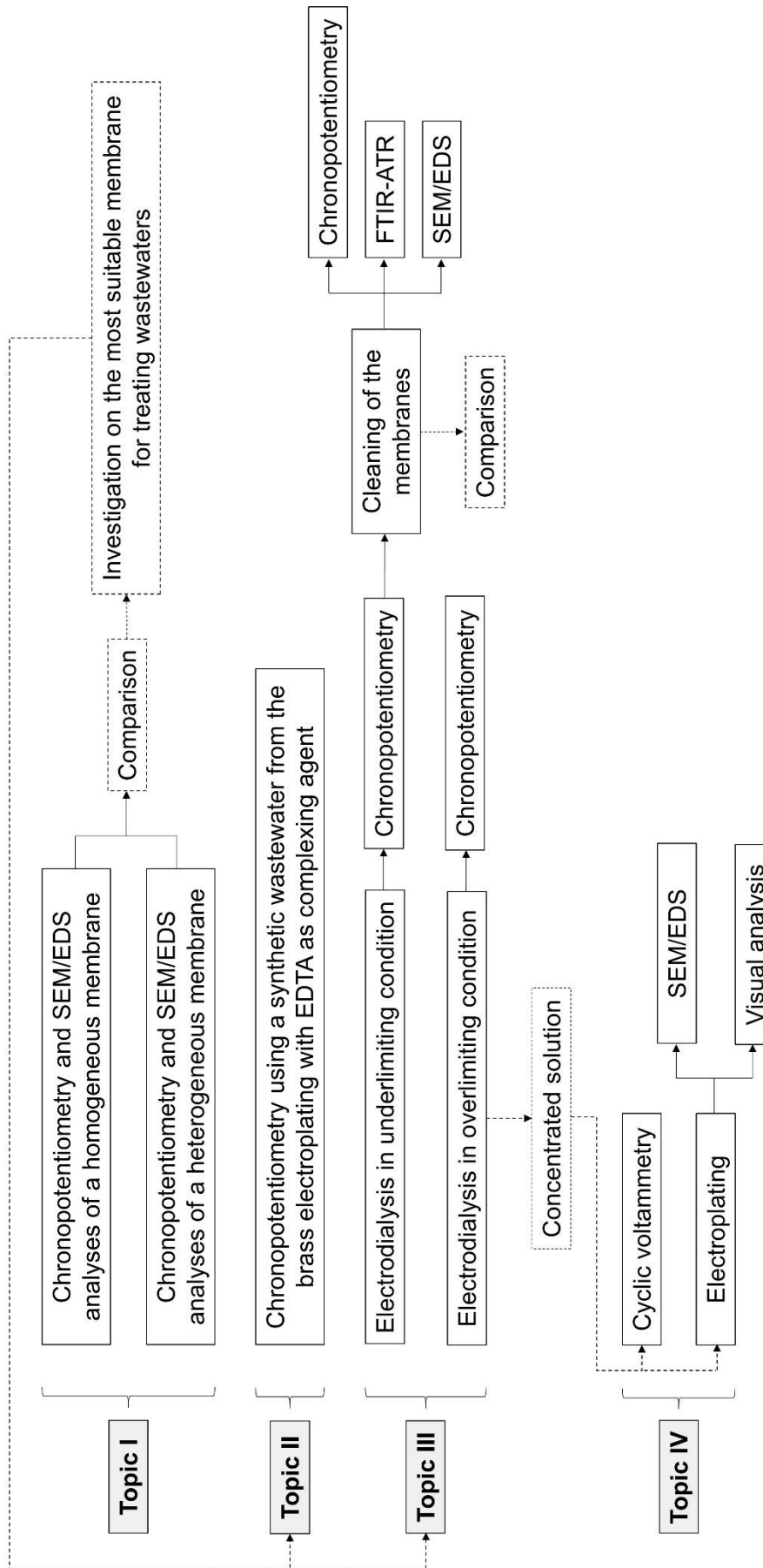
Figure 1 - Structure of the thesis.

2.   OBJECTIVES

The main objective of this work is to investigate, by means of chronopotentiometry, the transport properties of ionic species present in a synthetic wastewater from the cyanide-free brass electrodeposition with EDTA as a complexing agent across an ion-exchange membrane, besides evaluating the feasibility of the treatment, by electrodialysis, of the synthetic wastewater. In addition, the study aims to assess the quality of the brass electrodeposits after recovering the ions into the electrolytic bath. The thesis was subdivided into four topics and the specific objective of each step is presented below.

- Topic I: To evaluate, by chronopotentiometry, the transport properties of Cu^{2+} ions in acid medium across a heterogeneous and a homogeneous membrane for determining which one is more appropriate to treat wastewaters by electrodialysis.

- Topic II: To investigate, by chronopotentiometry, the transport properties of complexes of Cu-EDTA and Zn-EDTA across an anion-exchange membrane involved in the treatment, by electrodialysis, of the wastewater from the cyanide-free brass electrodeposition with EDTA.

- Topic III: To assess the treatment of the cyanide-free wastewater, by electrodialysis in underlimiting and overlimiting conditions, from the brass electrodeposition, and to evaluate a three-stage chemical cleaning of the membranes after treating the wastewater by means of chronopotentiometry, SEM-EDS and FTIR-ATR.

- Topic IV: To investigate, by means of cyclic voltammetry and electrodeposition tests at RDE, the influence of the rotation speed on the quality of brass electrodeposition with EDTA. The recovery of the concentrated solution obtained by electrodialysis into the electrodeposition bath was also assessed in function of the quality of the electrodeposits

3.   BIBLIOGRAPHIC REVIEW

3.1.   Electroplating process

Metal finishing operations use electrochemical principles and are employed in several types of industries to provide desirable characteristics to materials, such as corrosion resistance, hardness, electrical conductivity, chemical stability, homogeneity of the material or to provide decorative aspect (44,58). Several operations are involved in metal finishing and the main three stages are the surface preparation (cleaning and surface activation), the plating (electroplating and coatings) and the rinsing of the pieces (59).

In the surface preparation, organic pollutants, such as oil and grease, are removed prior to the electroplating process, since they can affect negatively the quality of the deposits. Hence, the first stage in most plating plants is the removal of oil and grease by the aqueous or solvent degreasing. The presence of metal-oxides has also a negative impact on the efficiency of the process. Therefore, pickling, etching and descaling steps are present in the preparation stage to remove oxide-layers and scales.

The plating process consists of depositing the metal on a part by passing electric current through a series of electrolytic baths, and the number of tanks used and their chemical constituents depend on each objective (1). The part to be covered by the metal is the cathode and is usually made of metal or plastic, whereas the anode is typically a plate of the metal to be deposited.

Each stage mentioned above is accompanied by rinsing stages with water, which generates wastewaters with metals and other substances present in the electrolytic bath, such as complexing agents and additives used to improve the quality and characteristics of the deposits (60). Rinsing presents mainly two objectives: to reduce the contamination of an electrolytic bath by the process solution of a preceding bath through drag out, and to stop chemical reactions on the parts surface.

The most common electroplating processes use copper, nickel, chromium, zinc, gold and silver (59). Copper is a metal with extensive industrial applications due to its properties of electric conductivity, ductility and thermal conductibility,

being mainly used, in industry, in plastic electroplating, printed wiring boards, zinc die casting, automotive bumpers, rotogravure rolls, electrorefining and electroforming (61). Hence, its deposition has become more attractive especially in the industry of semiconductors, due to its processing temperature, selectivity and cost (62). In industries, the electroplating of copper is generally conducted in the presence of cyanide in alkali pH or without cyanide in acid medium. In recent years, some baths have been developed to replace cyanide due to the risks of hydrogen cyanide formation, but in general, the stability or characteristics of the deposits are affected (61). When acid medium is employed, copper sulfate ($CuSO_4$) and sulfuric acid (H_2SO_4) are generally used, and the water from the rinsing step, which is the main effluent generated in this process, contains between 0.1 g/L – 1.0 g/L of Cu^{2+}, hindering its disposal in the environment (63).

The deposition of zinc in electroplating industries is generally performed to protect iron or steel parts from corrosion, by covering them with a layer of the metal in two ways: surface coating and sacrificial anode, since zinc is less noble than iron. Hence, the part is previously introduced into a pickling bath with a solution of $ZnCl_2$, NH_4Cl and HCl or H_2SO_4 to remove impurities and finally it is electrodeposited. At the end of the process, the effluent generated contains between 10 – 80 g/L of HCl, 5 – 150 g/L of $ZnCl_2$ and 80 – 150 g/L of $FeCl_2$ (64). This is the effluent from zinc electrodeposition generally treated in the literature (64–68).

3.2.   Brass plating process

In addition to the electrodeposition of a metal, it is also possible to combine two or more metals in the bath in concentrations that guarantee some desired properties of the parts. Baths composed of zinc and copper ions form brass alloys and are used for bright decorative finishes on wire goods, as a thin layer on bright nickel present in hardware, for antique or other dark finishes, in the manufacture of radial tires for passenger vehicles, trucks and of high pressure hoses, and to provide adherence of rubber to steel (2,3). However, for electrodepositing two or more metals simultaneously, their reduction potentials must be similar. According to the Nernst equation, the variation of the reduction potential is possible by changing the cations activity, as represented by Equation 1 (69). In this equation,

the term E represents the potential (in volts) of the system, E^0 is the standard electrode potential, R, T and F are the universal gas constant, temperature and Faraday constant, respectively, n is the number of electrons involved in the stoichiometry of the reaction, v_j is the stoichiometric coefficient of the species j, a_j is the activity of the species j and indices "ox" and "red" refer to the species that oxidize and reduce, respectively.

$$E = E^0 - \frac{RT}{nF} \cdot \left(\sum_{ox} v_j ln a_j - \sum_{red} v_j ln a_j \right) \qquad \text{Equation 1}$$

In the case of brass, copper and zinc have values of standard reduction potential quite different: $E^0_{Cu} = +0.342V$ and $E^0_{Zn} = -0.7618V$. Therefore, complexing agents that have greater affinity for one of the cations and that are able to reduce the activity of the noblest metal (copper, in this case) are generally added to the bath to allow the electrodeposition of both metals (7,70).

3.3.   Replacement of cyanide in the brass plating bath

Conventionally, the electrolytic bath for brass electrodeposition presents cyanide as complexing agent due to the stability of the complexes, which guarantees the simultaneous deposition of copper and zinc, besides ensuring a uniform color and regular composition even on parts with irregular structures. The plating bath of brass is usually composed of copper cyanide, zinc cyanide, sodium cyanide, sodium bicarbonate, sodium carbonate, ammonia and presents pH close to 10 (71). However, it is widely known that cyanide is toxic and requires pH control to avoid accidents that may cause the death of people in contact with the hydrogen cyanide, in addition to the possibility of extinction of the fauna and flora of the region (72). Hence, its toxicity and the need of the maintenance and control of the solutions have prompted an effort to discover eco-friendly complexing agents able to produce brass deposits with similar quality.

Brenner (6) published a review, in 1963, on some complexing agents alternative to cyanide for electrodepositing brass alloys and, from that study, several authors evaluated the quality of the deposits of these metals using cyanide-free baths. Some complexing agents already evaluated are

glycerol (6,73),   glycine (5,72),   sorbitol (8,74),   ethylenediaminetetraacetic acid (EDTA) (9,10),   citrate (75),   pyrophosphate (76), pyrophosphate-oxalate (77),   triethanolamine (7),   glucoheptonate (78), nitrilotriacetic   acid (79),   tartrate (3),   choline   acetate (4), bis(trifluoromethylsulfonyl)imide (38) and d-mannitol (37). Among them, EDTA is interesting since it is widely used as a complexing agent in the electrodeposition of metals (80,81).

3.4.   The use of EDTA as a complexing agent

EDTA, or ethylenediaminetetraacetic acid, is an organic compound with four carboxylate and two amine groups, as shown in Figure 2. Among the cyanide-free complexing agents alternative to cyanide already tested, the use of EDTA is interesting since it is a compound with well-known properties, due to the lower risks that it offers to the population and to the environment, besides the facility of purchasing it.
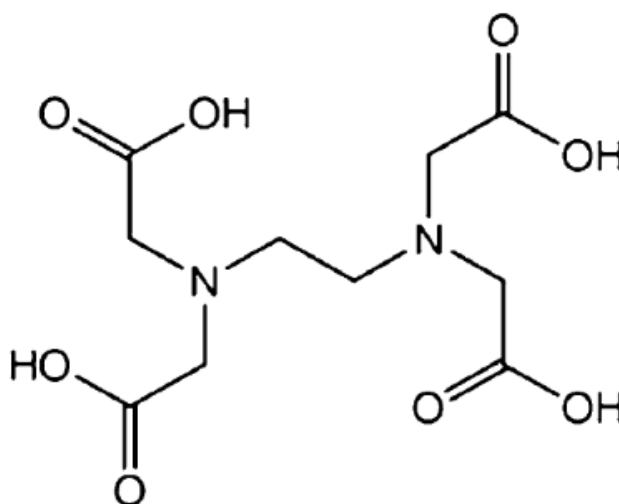
Figure 2 - Molecular structure of EDTA (Adapted from ref. (82))

EDTA has been tested in the literature as a complexing agent for a variety of purposes, such as in electrodeposition of metals (9,10,80,81,83,84), adsorption (85,86), reverse osmosis (87,88), ultrafiltration (89), dialysis (90), electrolysis (91) and in the separation of different cations in solution by electrodialysis (92–97).

In recent years, EDTA was assessed as a complexing agent in the brass electrodeposition in potentiotastic mode by Almeida et al. (98). The authors assessed the influence of the deposition potential and the Cu^{2+}/Zn^{2+} molar ratio (0.4, 1.0 and 2.3) on the composition, morphology and phase composition of the brass deposits. The best conditions to obtain smooth brass deposits were found to be the voltage of -1.45 V for the baths with Cu^{2+}/Zn^{2+} of 2.3 and 1.0, whereas for the bath with Cu^{2+}/Zn^{2+} of 0.4, the best condition was -1.60 V. The deposits obtained were gold in color. Shortly thereafter, Almeida et al. (9) assessed the brass deposition with EDTA in galvanostatic mode. The applied current density and the duration of the experiments influenced the quality of deposits. In general, the deposits were free of cracks and continuous, covering the substrate completely. The authors obtained current efficiencies greater than 90 % at the lowest deposition current densities.

The use of EDTA as a complexing agent in electrodialysis processes has also been frequently assessed. Chaudhary et al. (92) evaluated the use of electrodialysis to separate nickel and cobalt by exploring the differences between the formation constants of Ni-EDTA and Co-EDTA complexes in a system with 2 and 3 compartments. For the two-compartment system, the authors obtained smaller separation of ions compared to the three-compartment one, since although Ni-EDTA complexes did not pass through the cation-exchange membrane, EDTA was destroyed at the anode and released Ni^{2+} ions into the solution, which passed through the membrane along with Co^{2+} towards the cathode. Thus, the importance of the presence of EDTA in the ionic separation was confirmed. When the authors assessed the EDTA concentration, they found that when it exceeded the stoichiometry required to complex nickel, the transport percentage of both metals through the membrane was hindered. The Co:Ni molar ratio was also evaluated, keeping the Ni:EDTA ratio constant. In this case, it was found that the separation decreased with the nickel content increasing. For the three-compartment system, the results of separation were better than those of the two-compartment one, since the anion-exchange membrane present in the three-compartment system cell prevented the reaching of free Ni^{2+} to the cathode compartment. Even using the three-compartment system, the authors verified that, although the increase in EDTA led to an increase in the cobalt purification

at the cathode, a reduction in the separation efficiency occurred due to the increase of the transport of cobalt towards the anode.

The separation of calcium and cadmium was evaluated by Kubal et al. (94) using EDTA as a complexing agent under various conditions and the experimental results were compared with those predicted by speciation curves. The authors found that, at the lowest pH tested (1.5), 40 % of the Cd^{2+} present in the central compartment was transported to the anode, although speciation curves predicted the complexation of 60 % of the metal. It was also observed that at pH 1.5, the applied current carried mainly H^+, Na^+ and NO_3^- ions through the membranes. For pH 2, the theoretical results were similar to the experimental ones, and it was found that more than 90 % of the Cd^{2+} removed from the central compartment was transported to the anode. Finally, for pH values above 2, the experimental results of transport of Ca^{2+}, Cd^{2+} and EDTA were not in agreement with the speciation curves since an unexpected amount of Cd^{2+} was found at the cathode compartment. Although the authors expected a higher transport rate of free Ca^{2+} than Cd-EDTA complexes due to the differences between the species size, it was observed that, for pH values above 2, both species presented a similar transport rate. This was justified by the formation of a species involving Ca-Cd-EDTA that hindered the transport of free Ca^{2+} through the cation-exchange membrane.

Cherif et al. (95) studied the selective separation of Ag^+ from Cu^{2+} and Zn^{2+} ions by electrodialysis using EDTA in acidic and alkali medium. Cu^{2+} and Zn^{2+} ions would be separated at the anode, whereas Ag^+ ions would be separated at the cathode. When EDTA was added, the authors verified that although the complexation of Cu^{2+} and Zn^{2+} in alkali medium improved the separation between the two metals and silver, the current efficiency for the ions extraction decreased due to the greater transfer of ammonia, sodium and nitrate through the membranes.

The separation of Li^+ and Co^{2+} was evaluated by Iizuka et al. (97) using electrodialysis with a bipolar membrane and EDTA. The authors verified a relationship between pH and the concentration of EDTA in the separation of ions due to the competition between the species present in solution. The extraction rates of Li^+ were higher using the lowest initial EDTA concentrations and pH 4,

whereas the highest Co^{2+} extraction rates were obtained under equimolar conditions of EDTA and pH 4.

3.5.   Electroplating industry waste

Metal surface treatment is one of the major industrial processes that generates solid (sludge) and liquid wastes containing mainly inorganic anions and metals, which are toxic even in diluted solutions (16). Approximately 1 % of the hazardous waste in Europe is generated by the electroplating industry (99).

The electroplating process is followed by rinsing stages with water to remove the residual process solutions from the surfaces of the pieces and to stop chemical reactions that occur on it. The water used in the rinsing baths becomes contaminated during the cleaning process due to the drag-out from preceding baths. Hence, used rinsing water is usually the major waste stream from electroplating facilities (11).

3.6. Conventional treatment of wastewaters from electroplating industries

The conventional techniques used to treat wastewaters from electroplating industries may generate a sludge that is classified as hazardous waste according to the Brazilian standards (NBR) from Associação Brasileira de Normas Técnicas (ABNT), NBR 10004:2004 (100), besides being classified as hazardous or dangerous waste according to the European Directive 2008/98/EC (101).

The presence of metal ions in the effluent generated in the electroplating process causes concerns due to the risks to health and to the environment. Excess of zinc in the body causes stomach cramps, lung disorders, nausea, vomiting and anemia (13), whereas the excess of copper can cause disturbances such as vomiting, cramps, convulsions or death (102). Thus, environmental laws have become increasingly stringent to prevent the contamination of waters and soils by metals.

Chemical precipitation with hydroxide is the conventional method used in electroplating industries for treating the effluents due to its simplicity, cost and easy control of pH (103), besides the possibility of removing the metal hydroxides by flocculation and sedimentation (13). Generally, $Ca(OH)_2$ or NaOH   is

used (104), and for increasing the contaminant removal, coagulants such as alum and ferric salts are added. These compounds increase the removal of metals from the effluent by neutralizing the surface charge of the contaminants and causing their destabilization, which allows the formation of floc particles (105).

Although the precipitation of metals with hydroxide is widely used in industries, this process presents some limitations. The need of coagulants and the sludge formation hinder its final disposal (106). In addition, some hydroxides formed are amphoteric, and when several metals are present in the solution, the ideal pH to precipitate a metal may be responsible for the solubilization of other metals in solution. Besides, the presence of complexing agents in the solution may inhibit the metallic precipitation (13).

Another method commonly used to treat the effluent from electroplating industries is sulfide precipitation, which presents some advantages over hydroxide precipitation, such as the reactivity of sulfides with metal ions, solubility of the metal sulfide over a wide pH range, relative independence of the presence of most complexing agents, possibility of removing chromates and dichromates without the preliminary reduction of chromium, possibility of obtaining good selectivity when several metals are present, besides the higher density and stability of the metal sulfide sludge generated compared to the metal hydroxide sludge, which facilitates the next treatment steps (103). However, besides generating toxic (H_2S) and corrosive substances, colloidal precipitates tend to be formed, which may cause some inconveniences in the filtration and sedimentation steps (13).

Considering the limitations involved in the chemical precipitation with hydroxide and sulfide, alternative methods can be employed for treating effluents from the electroplating industry and, among them, electrodialysis has been frequently evaluated in the literature in recent years.

3.7. Electrodialysis

Electrodialysis is a process that involves two physical mechanisms: dialysis and electrolysis. In electrodialysis, the former describes the transport of species driven by a concentration gradient between both sides of an ion-exchange membrane, whereas the latter is controlled by the rate of migration

of ions under the application of an electric field (107). Electrodialysis systems comprise a series of cation- (CEM) and anion-exchange membranes (AEM) arranged alternately. Cation-exchange membranes consist of dense polymeric films which bear negative fixed charges and are permeable to cations, while anion-exchange membranes have positive charges in their structure and are ideally permeable only for anions. Consequently, cations are repelled by anion-exchange membranes and anions by cation-exchange membranes. Two electrodes placed at the side compartments accomplish the function of working and counter-electrodes. When an electric field is applied between them, cations migrate towards the cathode and anions migrate in the opposite direction, towards the anode. As a result of the imposed electric field and the alternating disposition of anion- and cation-exchange membranes, the feed solution is converted into two product streams: a concentrate and a diluate solution. In modern industrial plants, more than 200 pairs of cells are generally used to ensure an efficient separation. In most cases, the geometry of the cells of the diluted and concentrated solutions are identical, as well as the flow direction, to avoid differences in hydrostatic pressure and the occurrence of convection between the solutions (23). Figure 3 presents a schematic drawing of an electrodialysis system.
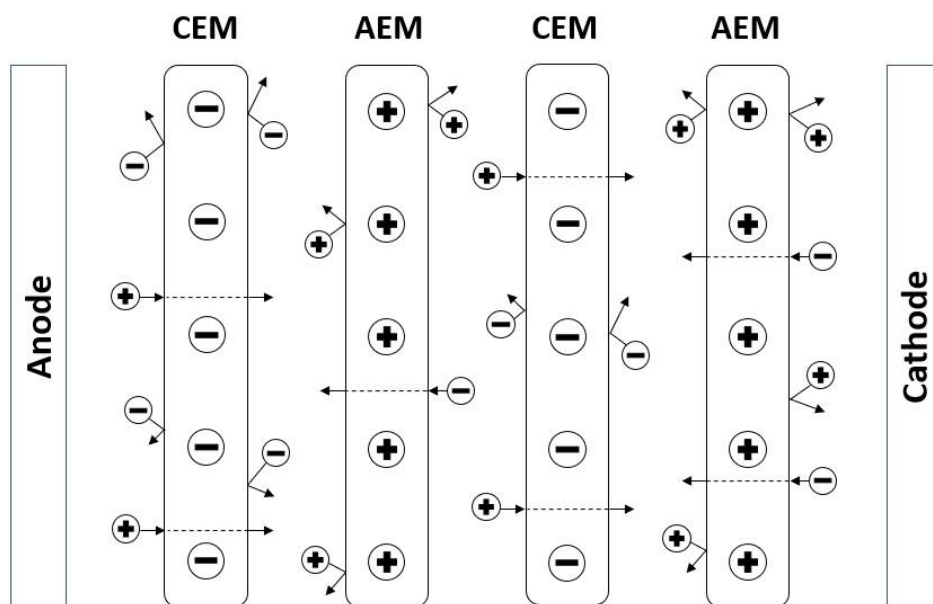
Figure 3 - A schematic diagram of an electrodialysis system.

The choice of membranes is the key factor in electrodialysis, since they allow or block the ions passage, depending on the purpose of the separation. Membranes can be classified as homopolar and bipolar. The homopolar ones have a cation- or anion-exchange layer that allows the passage of counterions and the exclusion of co-ions. Bipolar membranes contain a cation- and an anion-exchange layer and are widely used to produce acids and alkalis by exploring the water splitting phenomenon (56). There are two types of homopolar membranes in relation to their functional groups in the polymer matrix: the cation-exchange ones, which have fixed groups with negative charges, and the anion-exchange ones, which have fixed groups with positive charges. In cation-exchange membranes, the fixed anionic groups are in equilibrium with cations of the solution, which are called counterions. In turn, anions of the solution are repelled by the similarity of the charge type of the cation-exchange membrane and are called co-ions. In contrast, in anion-exchange membranes, cations are the co-ions and anions are the counterions (108). This phenomenon is known as Donnan exclusion and occurs for the electroneutrality achievement between the charges of the polymeric matrix and the ions in solution.

Figure 4 presents a schematic representation of a polymer matrix of a cation-exchange membrane with cations and anions from a solution to be treated by electrodialysis.
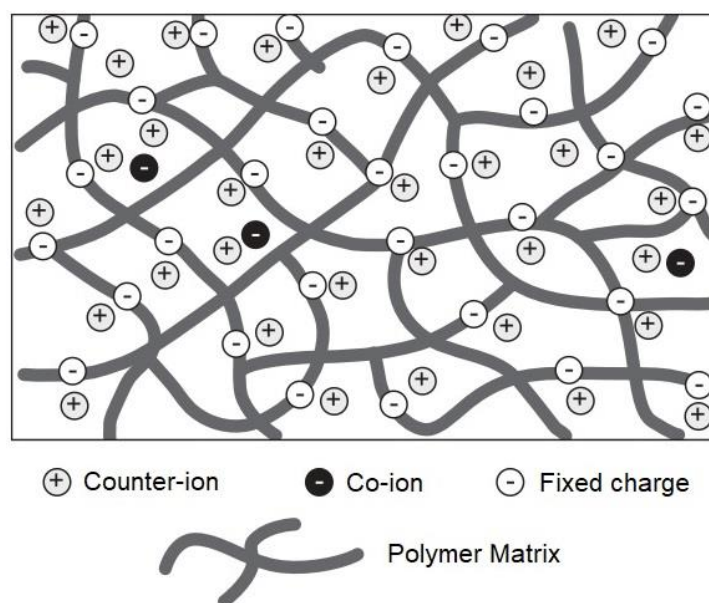
Figure 4 - Schematic representation of a polymer matrix of a cation-exchange membrane equilibrated in an electrolyte (adapted from ref. (23)).

Different types of membranes can be found, and their differences are, for example, due to the density of the polymer chain, concentration and type of fixed charges, as well as its hydrophobic or hydrophilic character (23). In general, the most desirable properties of the membranes are higher selectivity to counterions than to co-ions (i.e., greater permselectivity), lower electrical resistance to guarantee a lower potential drop during the process, higher mechanical stability, moderate degree of swelling, reasonable degree of crosslinking, chemical stability to maintain stable in a pH range and in the presence of oxidizing agents, thermal stability to support temperature differences and lower production cost (46,108).

Concerning heterogeneity, two main types of membranes can be found: the heterogeneous and the homogeneous ones. In homogeneous membranes, the fixed functional groups are uniformly distributed throughout the matrix, whereas in the heterogeneous ones, the fixed groups are non-uniformly distributed and separated by uncharged binding polymer, which enhances its mechanical resistance (109). Two other types of membrane are the mosaic and amphoteric ones. The former is composed of both cation- and anion-exchange domains randomly distributed in a neutral polymer matrix (110,111), whereas amphoteric membranes present randomly distributed weak acid and weak basic groups (112). Figure 5 shows a scheme of the classification of ion-exchange membranes.
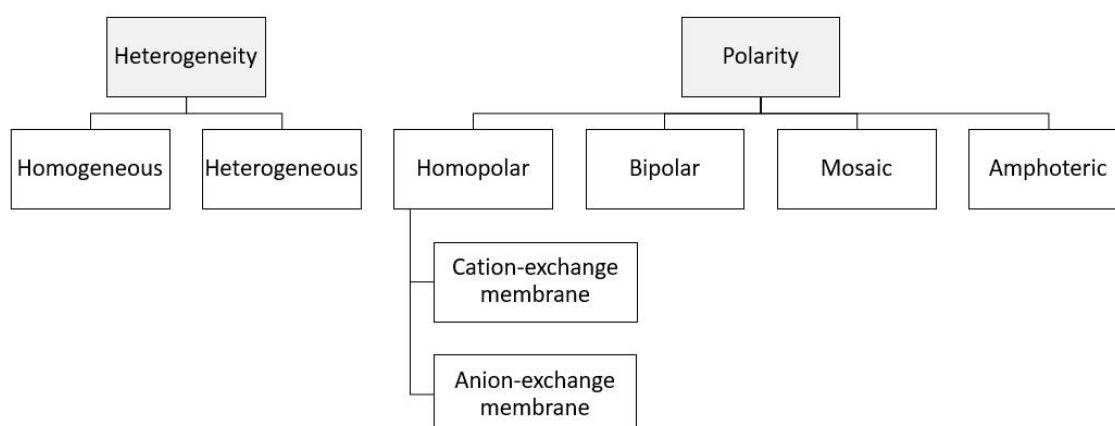
Figure 5 - Classification of membranes according to their heterogeneity and polarity.

The transport rate of a species in the membrane and in solution is determined by its concentration, mobility, and by the applied driving force (23). Generally, the transport of an ion j in the solution or in the membrane is described by the extended Nernst-Plank equation adapted with the convective term (113), which is represented by Equation 2.

$$\vec{J_j} = -D_j \left(\nabla C_j + z_j C_j \frac{F}{RT} \nabla U \right) + C_j \vec{V} \qquad \text{Equation 2}$$

In Equation 2, $\vec{J_j}$, D_j, z_j, and C_j represent the flux density, diffusion coefficient, charge and concentration of the ionic species j, respectively; U is the electric potential, $\vec{V}$ is the velocity vector of the fluid; F, R, T are the Faraday constant, the molar gas constant and the temperature, respectively. The first term on the right side of Equation 2 represents the diffusion, the second one the migration and the third one the convection. Equation 2 can be used under consideration of several assumptions. The first one involves assuming the effect of concentration gradients on activity coefficients neglected, that is, the same deviation of non-ideality for the solutions at each side of a membrane is considered. It can be also considered that there is no short-range interaction between ions (those acting at the lowest distances of intermolecular separation). Furthermore, the diffusive and electric mobility of the ions are considered identical. In general, all the hypotheses presented above are reasonable for electrodialysis systems (114).

The transport of ions in the solutions between the two electrodes results in a transport of electric charges: cations move towards the cathode, while anions migrate towards the anode. Hence, the electrolytic solution/electrode system obeys the same mathematical relation of a current transport by a metallic conductor material: Ohm's Law, represented by Equation 3 (115), where U, R_{elec} and I are the potential between the two electrodes, the electrical resistance and the electric current, respectively, and n is the number of electrolytic cells. In an electrodialysis cell, four resistances to the mass transfer can be considered: the resistance of the cation- and anion-exchange membranes, and the resistance of the dilute and concentrate compartments.

$$U = n R_{elec} I \qquad \text{Equation 3}$$

For decades, electrodialysis has been mostly used for desalination of brackish water and seawater (108). In recent years, it has been considered for several purposes, such as the recovery of sulfuric acid from acid mine drainage (116), concentration, purification and demineralization of food products (117,118) deacidification of juices (29), purification of green tea (119), protein concentration (120), separation of organic acids (121,122), removal of potassium hydrogen tartrate from wine (123), treatment of solutions with molybdate (124), extraction of dissolved solids in the effluent from the shale gas production (125), remediation of contaminated soil with metals (126) and for extracting and recovering metals from the electroplating industry (27,46,64,127-132).

Regardless of the solution to be treated, the choice of membranes is the key factor in electrodialysis. For the separation efficiency, some characteristics of the membrane to be used must be considered, such as its ionic conductivity, mechanical resistance, chemical stability and manufacturing cost (133,134).

Besides the characteristics provided by the manufacturer, it is also important to perform studies on membrane characterization to determine some properties that depend on the solution to be treated, such as the limiting current density, electrical resistance and transport number of ions in the membrane. The latter represents the fraction of current carried by each type of ion in the absence of concentration gradients. The energy consumed to change the type of transport mechanism must also be evaluated. In addition, it is essential to know the fraction of conductive area of the membrane and its distance from ideality, besides the tendency of fouling and scaling occurrence. In these undesirable phenomena, the deposit of organic and inorganic material, respectively, occurs on the surface of the membrane and may block the ions passage due to the poisoning phenomenon, which leads to an increase in resistance (124).

Besides the factors that influence any separation process by electrodialysis, the presence of weak electrolytes and complexes in the solution to be treated can modify the ionic transport and affect the membrane properties (135). The lower mobility of complexes hinders their transport and causes a decrease in the current efficiency of the ion transport (95), which leads to an increase of the membrane resistance (135,136).

Some recent developments (18,137,138) showed the effectiveness of electrodialysis and bipolar electrodialysis batch systems for purifying fermentation broths and producing chemical precursors from biomass, which are basically weak organic electrolytes. Unlike strong electrolytes, which completely dissociate into their respective ions, weak electrolytes are characterized by forming ionic species with different valences, mobilities and ionic charges depending on the pH, the ionic strength of the solution or the molar concentration. Therefore, depending on the degree of dissociation of the weak electrolyte that predominates in the solution, its transport across ion-exchange membranes will occur at different speeds. The ionic charges of the species directly or indirectly affect which ion is preferentially transported, the electrical resistance of the electrodialysis cell, the mass transfer efficiency and the energy efficiency of the overall process. Melnikov et al. (139) reported that the existing models used for predicting the transport-structural parameters of ion-exchange membranes are not applicable to weak electrolytes and further studies are required for a comprehensive description of the transport of weak electrolytes through ion-exchange membranes.

Aouad et al. (136) suggested that some complexes are able to neutralize part of the fixed charges of the membranes, since the transport of chloride through an AEM decreased in the presence of zinc complexes, whereas the transport of sodium increased. Therefore, evaluating the membranes to be used in electrodialysis is crucial, besides the influence of the molar ratio between the complexes and free ions on the transport properties of the membrane, as well as the influence of the species concentration and the solution pH. For performing these evaluations, methods of dynamic characterization of membranes may be used, such as chronopotentiometry, cyclic voltammetry, impedance spectroscopy and steady-state voltage, or current sweeps (140).

3.8.   Chronopotentiometry

Among the methods of electrochemical characterization generally used in studies involving membranes, the use of chronopotentiometry is interesting since it allows a direct access of the contribution of the potential in different states of the membrane/solution system (57). Therefore, this technique has been

frequently used to evaluate membranes properties by assessing the chronopotentiograms (ChP) and current-voltage curves (CVC) constructed by this method (36,55,57,141–143).

Chronopotentiometric studies are often conducted using a three-compartment cell and two membranes; in general, one is an anion- and the other is a cation-exchange membrane. Two electrodes are introduced in the side compartments to apply a specific current density, and two reference electrodes immersed in Luggin capillaries on each side of the membrane under study for measuring the potential drop (U_m) over a given time. Cells with more compartments may also be employed to minimize the influence of reactions on the potential measurements (55,144,145).

Chronopotentiometric curves (or chronopotentiograms - ChPs) allow evaluating the behavior of membranes and the determination of some properties, such as the fraction of conductive area, transport number of ions in the membrane, which indicates the fraction of current carried by an ion across the membrane, and transition time. The latter corresponds to the moment at which the depletion of ions occurs at the membrane surface due to the intense occurrence of concentration polarization. This will be discussed in section 3.9.1. Figure 6 presents a representation of typical chronopotentiometric curves obtained with monopolar membranes.
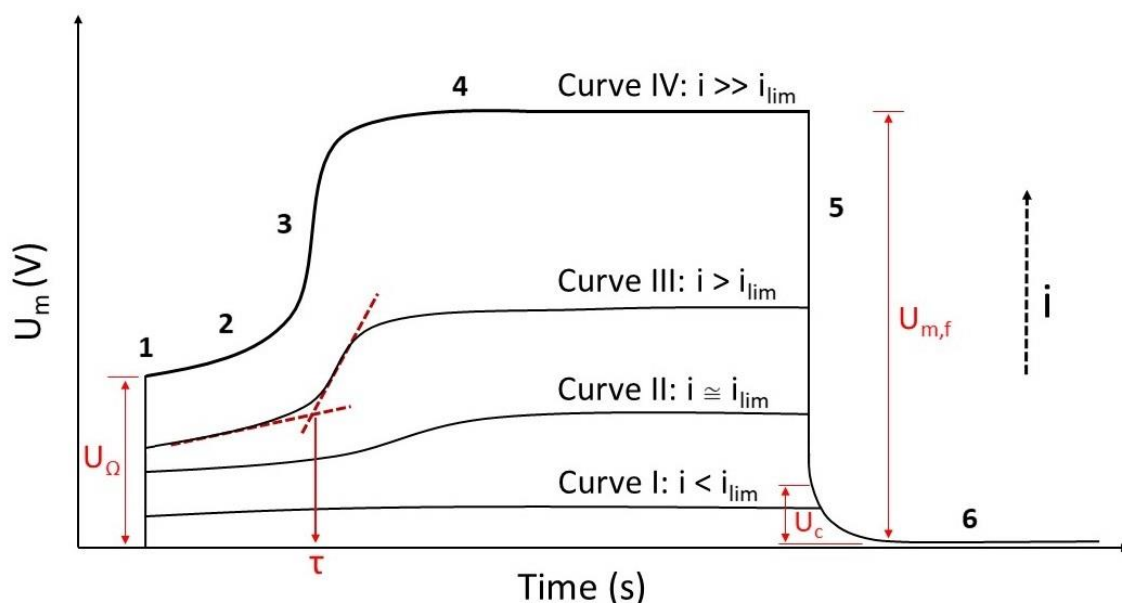
Figure 6 - Representation of typical chronopotentiometric curves of monopolar membranes.

According to Figure 6, chronopotentiometric curves present well-defined regions and distinct behaviors depending on the applied current density. By curve I, we can see that its voltage presents a constant value. This occurs when the applied current density is lower than the limiting current density (i_{lim}) of the membrane system, which is the current density responsible for the depletion of ions near its surface as a consequence of intense concentration polarization. Hence, in the case of curve I, the applied current density is not high enough to cause the depletion of ions in the diffusion boundary layer (DBL) due to the intense concentration polarization. The potential difference recorded is constant over time and this is only due to the ohmic drop caused by the electrolyte/membrane system. The concentration polarization phenomenon and the limiting current density will be discussed in detail in section 3.9.1.

When the applied current density is slightly increased (curve II), the curve presents a subtle inflection related to the increase of the membrane voltage at a certain time, due to the beginning of depletion of ions in the diffusion boundary layer and the formation of concentration gradients in the vicinity of the membrane. As the applied current density increases, this inflection point becomes more evident (compare curve II with curve III).

For current densities greater than the limiting current density of the membrane (curve IV), six different regions may be distinguished:

- Region 1: Before imposing a current density to the system, the potential drop across the membrane under evaluation is zero. When the current is switched-on, an immediate increase in the potential drop appears in the chronopotentiometric curve. This initial potential drop (U_{Ω}) is related to the ohmic contribution of the membrane system (146).

- Region 2: A slow increase in the potential drop is shown, which is due to the development of small concentration gradients in the solution near the membrane surface. This is governed mainly by electro-diffusion mechanisms (55). When an underlimiting current is applied (as shown by curve I), this region 2 extends even during long times and, in this case, region 3 is not reached.

- Region 3: Here, the curve shows an inflection point at which the voltage increase becomes more pronounced in a short time, due to the occurrence of intense concentration polarization. At this moment, the concentration of counterions in the solution near the membrane layer reaches values close to zero, which leads to the resistance to tend to infinity, since the voltage shows a sudden increase. This occurs only when the applied current density is greater than the limiting current density of the membrane (compare curve I with curve IV). In region 3, it is possible to determine the elapsed time for the ion depletion in the diffusion boundary layer, which is called transition time - τ, as shown in Figure 6. Other methods may be used for determining transition times, such as by the maximum of the time derivative of the potential drop (147). This will be shown in the section 3.8.1.

- Region 4: In this region, the system reaches a steady-state condition, where the potential drop ($U_{m,f}$) remains virtually constant until the current ceases. This occurs since the system develops another way to support itself with the emergence of overlimiting mechanisms of current transfer, such as electroconvection, gravitational convection and dissociation of water molecules. In studies that involve construction of current-voltage curves, this $U_{m,f}$ value is the one plotted against the applied current density.

- Region 5: It shows when the current density is switched-off and the voltage suddenly drops to a residual value that slowly disappears with time. The remained voltage difference across the membrane after interrupting the current represents the concentration overvoltage (U_c) (148). This results from the differences in the concentration profiles created at both sides of the membranes while the current is imposed. For bipolar membranes, additional plateaus may be verified in region 5 (56).

- Region 6: This last region describes the diffusion relaxation of the system, in which the voltage remains at zero value over a long time.

3.8.1. Transition time

As already mentioned, when the concentration polarization phenomenon takes place intensively due to the operation at current densities greater than the limiting current density of the membrane system, it is possible to determine the elapsed time for the electrolytic concentration to reach zero and for the voltage to tend to infinity. This property can be experimentally determined by chronopotentiometric curves, by determining the point of intersection of the tangential lines of the regions before and after the voltage increase (inflection point), as shown in Figure 6.

The transition time can also be mathematically determined. In 1899, Sand (149) developed an equation that was adapted by Lerche and Wolf (150) and applied by Audinos and Pichelin (151) to homogeneous membranes. The latter authors evaluated the non-steady-state transport of counterions considering a homogeneous surface, in contact with univalent electrolytes and without electroconvection. The Sand Equation was developed from Fick's second law (147), which presents the change in the electrolytic concentration as a function of time and distance (Equation 4), where C is the electrolyte concentration, x is the directional coordinate and t is time.

$$\frac{\partial C(x,t)}{\partial t} = D \frac{\partial^2 C(x,t)}{\partial x^2}$$
Equation 4

Equation 4 has an analytical solution and requires two boundary conditions for its resolution. In the initial state ($t = 0$), concentration C is expressed by Equation 5.

$$C(x,0) = C_0$$
Equation 5

In positions sufficiently distant from the membrane, Equation 6 is also valid since we are evaluating the semi-infinite diffusion problem.

$$C(x \rightarrow \infty) = C_0$$
Equation 6

Equation 7 expresses the flow of counterions through the membrane (J_j^m), which principally occurs by migration, while Equation 8 expresses the flow in the solution (J_j^s), which occurs due to migration and diffusion (151). In these equations, $\bar{t}_j$ and t_j represent the transport number in the membrane and solution phase, respectively. In this case, D, $\bar{t}_j$ and t_j are assumed not to depend on the electrolytic concentration.

$$J_j^m = \frac{i\bar{t}_j}{zF} \qquad\qquad \text{Equation 7}$$

$$J_j^s = \frac{it_j}{zF} + D\left(\frac{\partial C}{\partial x}\right)_{x=0} \qquad\qquad \text{Equation 8}$$

The flow of ions through the membrane and within the solution are equal. Hence, combining Equation 7 and Equation 8, a boundary condition is obtained, which relates the concentration of the counterion on the membrane surface ($x = 0$) at a nonzero time (Equation 9).

$$\left(\frac{\partial C}{\partial x}\right)_{x=0} = -\frac{i}{zFD}\left(\bar{t}_j - t_j\right) \qquad\qquad \text{Equation 9}$$

Finally, the Equation of Fick's second law can be solved by applying Laplace transform (Equation 10) (144).

$$C(x,t) = C_0 - \frac{i(\bar{t}_j - t_j)}{zFD}\left[2\sqrt{\frac{Dt}{\pi}}\,exp\left(-\frac{x^2}{4Dt}\right) - x.erfc\left(\frac{x}{2\sqrt{Dt}}\right)\right] \quad \text{Equation 10}$$

For $x = 0$, Equation 11 is obtained, which relates the concentration of ions on the surface of the membrane as a function of time.

$$C(0,t) = C_0 - \frac{i}{zFD}\left(\bar{t}_j - t_j\right)2\sqrt{\frac{Dt}{\pi}} \qquad\qquad \text{Equation 11}$$

Thus, by verifying that the ions concentration at the membrane decreases with time, Sand (149) developed the well-known Sand Equation (Equation 12) from the Nernst-Planck equation assuming a stagnant diffusion layer of infinite thickness near the membrane (152). This equation allows calculating of the time elapsed for the depletion of ions on the membrane surface, widely known as transition time (τ).

$$\tau = \frac{\pi D}{4} \left(\frac{z_j F}{\overline{t_j} - t_j} \right)^2 \left(\frac{C_0}{i} \right)^2$$

Equation 12

3.8.2. Fraction of conductive area

Choi and Moon (153) modified the Sand equation and included a term relative to the fraction of the conductive area, allowing the equation use in studies with heterogeneous membranes. The modified Sand Equation can be seen in Equation 13 and is widely used in chronopotentiometric studies to determine the fraction of conductive area (ε) or the transport number of counterions in the membrane phase ($\overline{t_j}$). The term of the transport number in the solution (t_j) can be calculated by using the diffusion coefficients, according to Equation 14, where D_c and D_a are the diffusion coefficients of the cationic and anionic species, respectively (154).

$$\tau = \frac{\varepsilon^2 \pi D}{4} \left(\frac{z_j F}{\overline{t_j} - t_j} \right)^2 \left(\frac{C_0}{i} \right)^2$$

Equation 13

$$t_j = \frac{D_j}{(D_c + D_a)}$$

Equation 14

As shown in the development of the equation that relates concentration to time, the term of electrolyte diffusion coefficient (D) was considered to be independent of the concentration. In 2016, Mareev et al. (155) evaluated the inclusion of the concentration dependence in this term by developing the term $D_{(c)}$, which considers the concentration variation in agitated solutions. The

authors used NaCl solutions (0.002, 0.02 and 0.2 mol/L) in the chronopotentiometric tests and verified that $D_{(c)}$ can be used in chronopotentiometric studies with any membrane or electrolyte.

For determining the fraction of conductive area using chronopotentiometry, a figure of transition time (τ) vs. $(C_0/i)^2$ is constructed, as shown in Figure 7. In general, curves with a correlation coefficient close to a line are obtained. Therefore, the coefficient of the curve can be related to Equation 13 and ε can be determined, since the other terms are generally known. The solutions used for determining ε are generally composed of single salts such as NaCl or KCl. The value of $\bar{t_j}$ is generally given by manufacturers or it may be determined by the Hittorf or emf method.
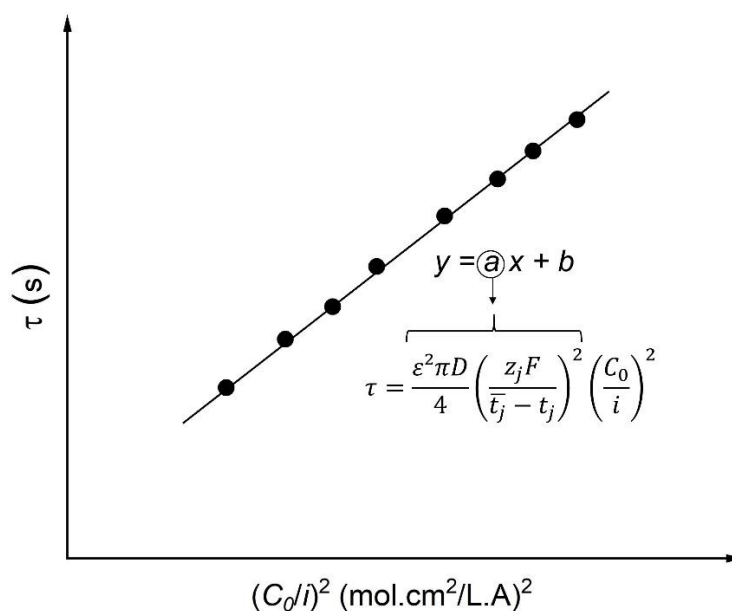
Figure 7 - Representation of the (τ) vs. $(C_0/i)^2$ curve for determining the fraction of membrane conductive area.

Recently, results of transition time obtained by chronopotentiometry for anion- and cation-exchange membranes were compared to those obtained by X-ray computed microtomography (156), since the latter provides a detailed analysis of the membrane structure both on its surface and in its volume. The authors verified that for homogeneous membranes, experimental transition times agreed with theoretical predictions based on Sand equation. In turn, transition times were not well predicted by the Sand equation in case of the heterogeneous ion-exchange membranes.

3.8.3. Transport number

The transport number is a very important property considered in studies of electrodialysis, since it measures the fraction of current density carried by each type of ions through the membrane and is a measure of the current efficiency (thus, the membrane selectivity) (131). In addition, the difference between the transport number in the solution and in the membrane is responsible for the occurrence of concentration polarization. In the case of cation-exchange membranes, the transport number indicates the fraction of current that is associated with the transport of cations, whereas in anion-exchange membranes, the transport number indicates the fraction of current that is associated with the transport of anions. In ideal conditions, this property presents a value close to 1 for counterions and close to zero for co-ions.

In the early 1990s, the transport number of counterions in the membranes was often determined by radiotracer measurements (157–161). However, it has been replaced with the development of simpler and more modern techniques. The transport number began to be conventionally determined by two methods: the Hittorf (157,162–164) and, mainly, the emf method (165–169). In recent years, the authors have frequently used chronopotentiometry, together with the modified Sand equation (Equation 13), to determine the transport number of ions in membranes. Obviously, all the other terms of the equation must be known, including the fraction of conductive area of the membrane. Then, the modified Sand Equation may be employed to determine the transport number of an ion in the membrane phase by using the same procedure described for determining the fraction of conductive area. In this case, the coefficient of the curve of (τ) vs. (C_0/i)^2 (Figure 7) is equal to the Sand equation and only $\overline{t_j}$ is an unknown term, which can be finally determined.

3.8.4. Fouling and scaling

Depending on the metals present in the solution and the pH, insoluble species may be formed on the membrane surface or inside it during electrodialysis. This phenomenon is called fouling when the attached species is organic, and scaling when it is inorganic. Fouling and scaling are undesirable in

electrodialysis, since they increase the electrical resistance, decrease the permselectivity and alter the membrane properties (170)

The formation of insoluble species on cation- and anion-exchange membranes occurs when current densities above the limiting one are applied, which leads to water splitting and the consequent formation of H^+ and OH^- at its surface. When water splitting occurs at a cation-exchange membrane, protons tend to intensively pass through the membrane, while OH^- ions are retained on its surface, leading to an increase of the local pH. These OH^- ions may react with metal ions and form mainly hydroxides and oxides that adhere to the monopolar structure of the membrane (142). At anion-exchange membranes, the opposite phenomenon occurs: OH^- ions intensively pass through the membrane, whereas protons are retained on its surface, which causes a pH reduction. In general, the formation of insoluble species on the surface of anion-exchange membranes due to water splitting is more difficult to occur than on the cation-exchange ones. The evaluation of this phenomenon is very important for the electrodialysis efficiency, since the formation of precipitates causes an increase of the potential drop and increases the resistance of the membrane (140).

The formation of insoluble species on the monopolar membranes surface can be verified in the chronopotentiometric curves by some non-expected behaviors (36,57,140,142,143), which are represented in Figure 8. In the curve, a rapid increase in the potential drop occurs and it does not reach a constant value (52,140,142,171,172). The presence of additional plateaus during the system relaxation is also a typical behavior when a precipitate is formed at the membrane, as shown in Figure 8 (140,142,143,171,172). In this case, the voltage remains at non-zero values for long periods of time, and the change in the equilibrium at the solution adjacent to the DBL when the current is switched-off leads to the hindered recombination of the precipitates with protons or hydroxides in the bipolar junction (173).
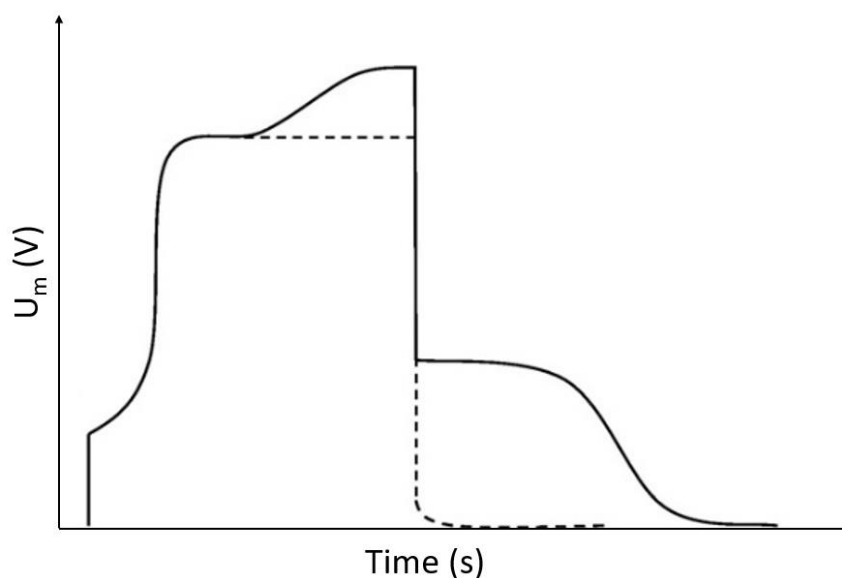
Figure 8 – Schematic representation of a chronopotentiogram with precipitate formation (full line). Dashed line corresponds to a classical shape of a chronopotentiogram for a monopolar membrane (adapted from ref. (142)).

Using chronopotentiometry, Marder et al. (140) evaluated the transport properties of solutions with different metals: nickel, manganese, copper, cobalt and zinc. The authors verified the formation of additional plateaus only with solutions of cobalt and nickel, due to the formation of the insoluble species $Co(OH)_2$ and $Ni(OH)_2$, respectively. Some years later, the effect of boric acid on the transport properties of nickel was evaluated (142) and the deposition of $Ni(OH)_2$ was also verified on the surface of the cation-exchange membrane. Also using chronopotentiometry, Taky et al. (174) studied the transport properties of solutions containing Cr^{3+} and observed the formation of $Cr(OH)_3$ at the CEM.

In some cases, the visual observation of precipitate formation is possible. Martí-Calatayud et al. (36) evaluated the transport of mixture solutions of $Fe_2(SO_4)_3$ and Na_2SO_4 emulating the composition of acid mine drainage through two different membranes, one homogeneous and the other heterogeneous. At the end of the experiments, the authors visually verified the presence of precipitates that were suggested by chronopotentiograms.

Chronopotentiometry has been used not only to investigate the formation of precipitates and scaling in metallic solutions, but also to evaluate the influence of some substances on the fouling occurrence and on the fraction of conductive area of membranes. Freijanes et al. (175) evaluated the influence of glucose on

membrane properties using NaCl and KCl solutions. The authors noted that in diluted solutions, the transition times were lower in the presence of glucose due to the reduction of the effective area of the membrane by this substance. Similar results were observed by Shahi et al. (176). Also using chronopotentiometry, they verified that the presence of glycine in NaCl solutions reduced the ions migration due to the blockage of functional groups of the membrane matrix. Similarly, Park et al. (177) evaluated the influence of bovine serum albumin (BSA) on the transport properties of KCl solutions and noted that this substance increased the membrane heterogeneity. The authors verified the occurrence of a chemical adsorption of BSA on the cation-exchange membrane and a chemical+electrostatic adsorption on the anion-exchange one, causing the reduction of its fraction of conductive area. Kang et al. (178) studied the influence of lysine on the properties of two membranes and noted that they were affected by molecules with molar mass greater than 70 g/mol. Chronopotentiometry allowed the authors to verify that the fraction of conductive area was reduced with the increase of the molar mass of the counterion.

Choi and Moon (153) assessed the influence of pore size of three ion-exchange membranes, being two homogeneous and the other heterogeneous, on the behavior of chronopotentiograms using some amine chloride solutions. Only ions smaller than the pore of the membrane could cross it, since when the size of the pore was smaller than the transporting ion, it behaved as a non-conductive area. From the curves obtained, it was clear that ions with greater size were responsible for lower values of fraction of membrane conductive area.

3.9.   Current-voltage curves

In addition to the chronopotentiograms, chronopotentiometry allows constructing curves of current versus voltage in the steady state. Current-voltage curves (CVC), also known as polarization curves, are widely used in studies involving electrodialysis, since they provide a general overview of the membrane resistance over a wide range of current densities. Moreover, relevant information about the system can be obtained from these curves, such as the limiting current density, the electric resistance of the membrane (the one corresponding to the

quasi-ohmic regime and also at the overlimiting one), the energy required to change the mechanism of ion transport (associated with the plateau length), and also qualitative information regarding the overlimiting mechanisms of current transfer and transport competition between different species. Figure 9 shows a typical CVC of a monopolar membrane.
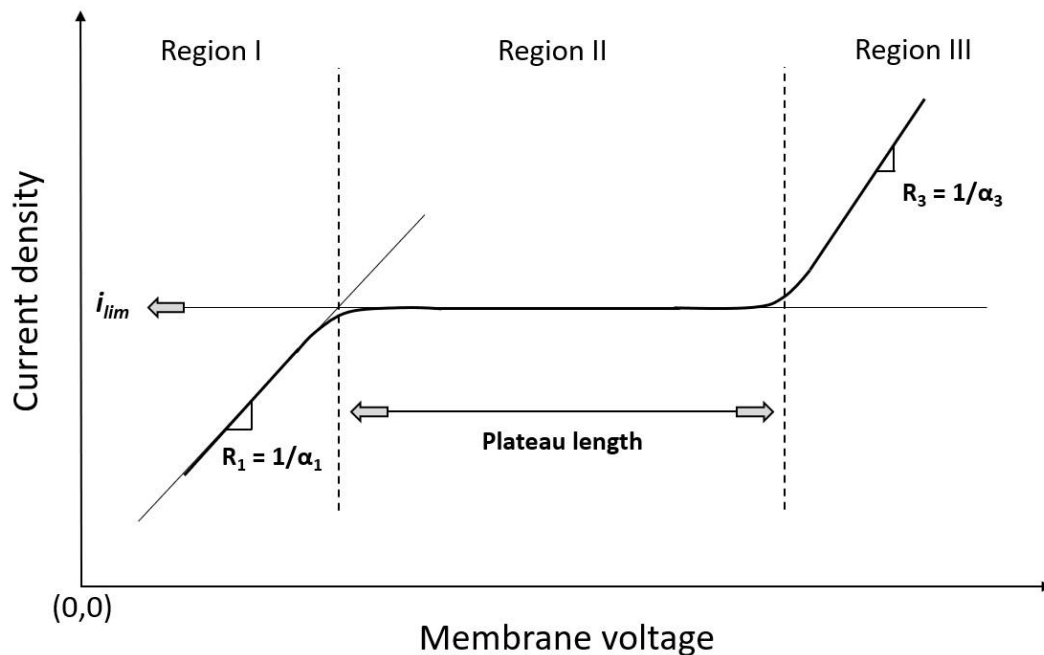
Figure 9 - Typical CVC of a membrane.

As shown in Figure 9, the CVC can be divided into three regions based on the slopes of the curve: region I, II and III. In region I, also called quasi-ohmic region, the current and the voltage show a linear relationship. In this case, the flow of ions that cross the membrane increases proportionally with the electric field, and the system obeys Ohm's law. By region I, it is possible to determine an important property of electrodialysis: the ohmic resistance of the membrane/electrolyte system (R_1), which can be obtained by the inverse of the slope (α_1) of the tangential line of this region. The ohmic resistance of the membrane/electrolyte system is an important property that indicates the contribution of the membrane and the diffusion layer adjacent to the cell voltage (143).

After the linear relationship of region I, the curve reaches region II, in which the current density remains virtually constant with the voltage increase. This

region is also known as the plateau region. At the inflection of the curve, that is, at the intersection of the tangents of region I and II, the limiting current density is reached. As previously explained, in this condition, there is no increase in the current flow across the membrane due to the scarcity of ions on the membrane surface (at the diluate side), even with an increase in the applied transmembrane voltage. By region II of the CVC, it is possible to determine the plateau length, which represents the energy required to change the mass transfer mechanism in the solution layer adjacent to the membrane from diffusion and migration to overlimiting transfer mechanisms (143).

Finally, in region III, a new region of current increasing with voltage appears due to the activation of overlimiting transport mechanisms, such as the gravitational convection, electroconvection and water splitting, which allow the increase in ionic transfer through the membrane (57,140). The electric resistance of region III (R_3) can also be determined by the same methodology of the quasi-ohmic region, that is, by the inverse of the slope (α_3) of its tangential line.

3.9.1. Concentration polarization and limiting current density

Polarization is a well-known phenomenon involved in studies of electrodes and in all membrane processes (179). In the case of ion-exchange membranes, it is associated with the preferential transport of counterions through the membrane phase and the consequent concentration gradient between the bulk solution and the vicinity of the membrane. Hence, in ion-exchange membrane studies, this is often called "concentration polarization". This reduction in the concentration of ions at the ion-exchange membrane surface causes a sudden increase in the voltage and in the resistance during the polarization. Therefore, the measurement of potential over time gives us valuable information about the system under study. The potential measurement is described in detail in the classical investigation of polarization by Cooke (180,181) and by Forgacs (182).

The concentration polarization is a phenomenon that occurs in electrodialysis due to the difference between the transport number of counterions in the solution and in the membrane phase (147). The proposed model for a concentration profile from a membrane-electrolyte interface states that a mass balance of counterions inside the membrane and in the interface must exist. The

mass balance considers ion transport by diffusion and electromigration according to Equation 15. A scheme of the concentration profile at the membrane-solution interface during electrodialysis is shown in Figure 10.

$$\frac{it}{F} + \frac{D\ (C_1 - C_2)}{\delta_1} = \frac{i\bar{t}}{F} - \frac{D_m(C_3 - C_2)}{\delta_m}$$

Equation 15
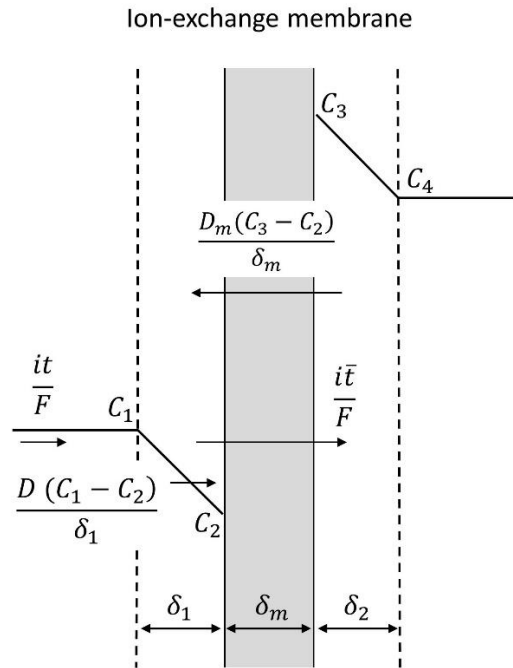
Figure 10 - Concentration profile at the membrane-solution interface during electrodialysis (adapted from ref. (183)).

In Equation 15 and Figure 10, C_1 is the ion concentration in the bulk solution on the diluted solution, C_2 is the ion concentration at the membrane surface on the diluted side, δ_1 is the thickness of the diffusion layer on the diluted side, D_m is the diffusion coefficient in the membrane phase, C_3 is the ion concentration at the membrane surface on the concentrated side and δ_m is the membrane thickness. The first term on the left side of Equation 15 is related to the ion transport due to electromigration, while the second term is related to diffusion, both occurring in the solution layer next to the membrane interface. Since they have the same direction, the left side of the equation is a sum of both first and second terms. In turn, in the membrane phase (right side of Equation 15) the first term is related to the electromigration from the diluted side towards the concentrated one. The second term shows an opposite sign and corresponds to

the diffusion transport. Since ionic concentration C_3 is higher than C_2, the diffusion transport tends to occur in the opposite direction.

In the diluate compartment, where the diluted solution is in contact with the cation-exchange membrane, the transport number of cations in the solution is smaller than on the membrane surface. The same behavior is valid for anions in the bulk solution and on the surface of the anion-exchange membrane. At a certain moment, a concentration gradient between the surface adjacent to the membrane and the bulk solution is established. This gradient results in a diffusive transport of electrolytes, which reaches a steady-state condition when ions in the bulk solution migrate, by diffusion, to the membrane interface to minimize the concentration gradient previously established by the difference in the ionic transport rate. While the diffusion is able to supply ions in the boundary layer, the system remains in steady-state condition. When the applied driving force (electrical field) is such that the diffusion is no longer able to supply enough ions to compensate the migration flux through the membranes, ion depletion occurs on the surface of the membrane at the interface of the diluted solution. At this moment, the system leaves the previous condition of steady-state, and an increase in the applied voltage does not lead to an increase of the current density, which is defined as limiting current density (117). Hence, an increase in the energy consumption occurs without increasing the ion transport through the membranes.

Figure 11 presents a schematic drawing illustrating the evolution of concentration profiles of counterions in the diffusion boundary layer at different current densities. The electric double layer (EDL) at each side of the membrane is also represented in the figure. This is an interfacial region with thickness typically in order of several nanometers and it is situated between the ion-exchange membrane and the adjacent solution (184,185). The EDL is formed due to the generation of an electric field by the fixed charges on the surface of the membranes. The electric field generated is responsible for Coulomb forces that attract ions with opposite charge, which creates the EDL (111,186). In Figure 11, the different behaviors of ions supply are due to the change from diffusion and migration to overlimiting phenomena as the mechanism of ion transport, as discussed further on.
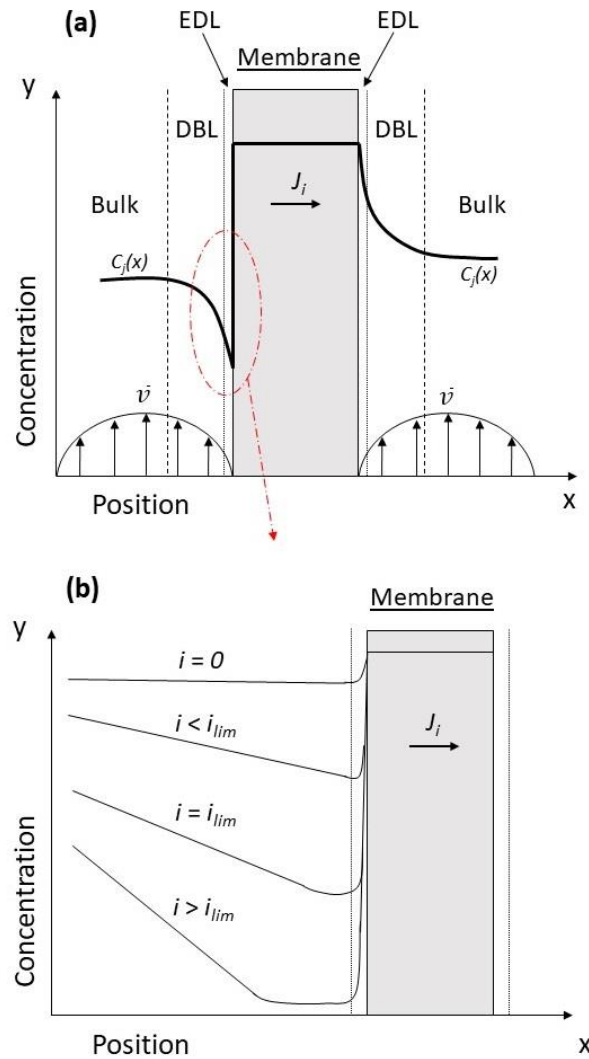
Figure 11 - Schematic drawing illustrating the evolution of concentration profiles of counterions in the diffusion boundary layer at different current densities.

The concepts used so far in the studies of concentration polarization derived from the Nernst film model (187,188). This model considers the existence of a "Nernst diffusion layer" region between the membrane/solution interface and the bulk solution, also known as diffusion boundary layer. During the development of this model, Nernst considered that, at this thin region, there is no variation in the electrolytic composition and no convection phenomenon, being the mass transport controlled by diffusion-migration (112). The concept reported by Nernst was later improved by Levich (187), since he considered the occurrence of convective transport within the DBL (112) and developed an equation that is going to be presented.

When the limiting current density is exceeded and the concentration polarization phenomenon becomes intense, a mass transfer limitation occurs and any increase in the voltage or current density that passes through the membrane does not increase the ionic transport. Generally, the extra energy is spent in secondary reactions, such as the dissociation of water ($H_2O \rightarrow H^+ + OH^-$) (109). The limiting current density, considering a solution of a single salt completely dissociated, can be calculated by the equation developed by Peers in 1956, represented by Equation 16 (189). In this equation, under the local electroneutrality assumption, the limiting current density is reached when the concentration of counterions reaches zero on the surface of the membrane.

$$i_{lim} = \frac{DC_0F}{\delta(\overline{t_j} - t_j)}$$ Equation 16

Equation 16 is a rearrangement of Equation 15, considering that the diffusion of ions in the membrane phase is negligible and that a limiting current density exists, above which the concentration polarization phenomenon may occur. In the equation, δ is the thickness of the diffusion boundary layer, defined as the distance from the membrane to the cross point of the tangents drawn to the concentration profile at the interface and bulk solution. This can be estimated by the Levich Equation represented by Equation 17 (190) and it is affected by the hydrodynamic conditions of the electrolyte solution, such as the stirring strength or flow rate of the solution.

$$\delta = \frac{L^{1/4}}{0.7(Sc^{1/4})\left(g\Delta C_g/4v^2\right)^{1/4}}$$ Equation 17

In Equation 17, L is the effective radius of the membrane when it is circular, g is the gravitational acceleration, Sc is the Schmidt number, v is the kinematic viscosity of the solution, ΔC_g is the concentration gradient between the boundary layer of the membrane interface and the bulk solution. In the condition of limiting current density, $\Delta C_g = C_0$, since the concentration of ions on the interface is zero.

Equation 16 provides the theoretical limiting current density and involves the calculation of several unknown terms, including the transport number of ions

in the membrane. Its use is especially complex when considering a solution that is not composed of a monovalent single salt. In this case, it may be impossible to obtain the necessary parameters. The real limiting current density can be determined directly from the current-voltage curves obtained by chronopotentiometry (124,172,191,192), by determining the intersection point of the tangential lines of regions I and II of the CVC, as shown in Figure 9.

The membrane heterogeneity influences the current-voltage curves and, according to Volodina et al. (193), the limiting current density is the property that presents greater differences between the homogeneous and heterogeneous membranes. In their study performed by chronopotentiometry, the values of i_{lim} obtained for the heterogeneous membranes were smaller than for the homogeneous ones. According to the authors, the non-uniform distribution of the local current density in the conductive areas (where the current lines are condensed) leads to the ion depletion in these regions firstly, which is responsible for the inflection point in the current-voltage curves. Then, the theoretical limiting current density was calculated by the Lévêque equation for the two types of membranes. For the homogeneous ones, the values calculated and those experimentally obtained by chronopotentiometry were very similar. However, for the heterogeneous membranes, the calculated values were higher than the experimental ones. Therefore, Volodina et al. (193) verified that the tangential electrolytic diffusion towards the conducting regions is responsible for the higher current density in the conducting regions of the heterogeneous membranes than in the homogeneous uniform areas.

Current-voltage curves of heterogeneous and homogeneous membranes were also evaluated, by chronopotentiometry, by Pismenskaya et al. (55). The authors also verified a higher current density in the conductive areas of the heterogeneous membranes and a lower electrolytic concentration in these regions, when compared to the homogeneous ones under the application of the same total current density. The heterogeneous membranes showed a slower increase of the current density with the voltage due to the presence of non-conductive regions and the tangential electrolytic diffusions. Shortly thereafter, Volodina et al. (193) constructed current-voltage curves of homogeneous and heterogeneous membranes by chronopotentiometry, and verified that the local limiting current density through conducting regions of a

heterogeneous membrane is several times higher than the average limiting current through a homogeneous membrane.

Marder et al. (140) reduced the fraction of conductive area of a homogeneous membrane in 80 %, 60 % and 45 % and evaluated their CVCs by chronopotentiometry. The authors verified that the limiting current decreased in a linear relationship with the reduction of the fraction of conductive area. The relation of the limiting current density with fouling occurrence was also studied. Lee et al. (194) verified that the occurrence of foulant deposition and chemical binding to the functional groups led to the decrease of the limiting current density, since the fraction of conductive area decreased.

Marder et al. (140) evaluated CVCs constructed for the same homogeneous membrane and different chloride solutions to compare the limiting current density values obtained experimentally with those calculated by the classical Nernst diffusion layer theory. The values obtained by the two methods were very close and, in both cases, i_{lim} presented the same order: cobalt > zinc > nickel = copper > manganese. The difference between the values of i_{lim} for each evaluated metal was justified by the gravitational convection.

The relation between the limiting current density and the liquid flow rate has also been investigated (195). This effect is virtually unnoticeable in solutions concentrated in salts, due to the lower contribution of the thickness of boundary layer in this condition. However, in diluted solutions, changes in the hydrodynamic conditions influence the values of limiting current density. The thickness of the diffusion boundary layer at the membrane surface is reduced by the increase of the solution flow, which increases the limiting current density and enhances the performance of the separation. This is also in agreement with Peers equation (Equation 16).

3.9.2. The presence of additional inflection points in chronopotentiograms and current-voltage curves

Some authors have verified the presence of two inflection points in current-voltage curves and chronopotentiograms, which are related to distinct limiting current densities. Pismenskaya et al. (196) constructed CVCs in galvanodynamic mode with solutions containing HPO_4^{2-} and PO_4^{3-} and a modified

AEM selectively permeable to monovalent anions. The authors verified the presence of two waves in the CVCs and related them to the alteration of the diffusion layer resistance after the depletion of the first species and the intense changes of pH inside the membrane. This displacement of the equilibrium condition and the alteration of the species being transported through the membranes occurred because weak electrolytes undergo shifts in equilibrium due to concentration polarization. These shifts imply a change in the species present near the membrane. The same behavior in current-voltage curves was observed by Melnikova et al. (197) using NaH_2PO_4 and $KC_4H_5O_6$ solutions.

Other authors verified the presence of two plateaus in CVCs using chronopotentiometry. Martí-Calatayud et al. (172) verified two plateaus using solutions of $Cr_2(SO_4)_3$. In this case, the CVCs obtained agreed with the chronopotentiograms, since multiple transition times were also verified. At the lowest current densities, the transport of Cr^{3+} and Fe^{3+} preferentially occurred through the membranes, while the depletion of complexed ions occurred more intensively at higher current densities. A decrease in the resistance between the two limiting current densities was also observed, which may have occurred due to the dissociation of the Cr(III) complex within the membrane, and the subsequent enrichment of the membrane phase in multi-charged ions. Melnikova et al. (197) constructed CVCs with solutions of NaH_2PO_4 and also verified the presence of two limiting current densities. The first one appeared when the NaH_2PO_4 salt diffusion to the membrane surface was saturated and the second was related to the saturation of the H^+ flux when the membrane was almost completely converted into the HPO_4^{2-} form. Scarazzato et al. (198) also verified the presence of two transition times in the ChP testing solutions with etidronic acid and copper ions. The authors justified it by the transport of different species after the equilibrium change in the membrane. The first and the second transition times were attributed to the passage of $HHEDP^{3-}$ and $[CuHEDP]^{2-}$, respectively. However, the current-voltage curves obtained were typical, without the presence of two limiting current densities. Zook et al. (199) related the two transition times to the results of spectroelectrochemical microscopy and confirmed that the inflections in the ChP appeared exactly when the free ionophore and ion-ionophore complex concentrations approached zero at the membrane-solution interface.

Butylskii et al. (33) showed that besides the ions competition, there may be another cause of the appearance of more than one transition time in chronopotentiograms, and this is related to the membrane heterogeneity. Two transition times were obtained by the authors by testing a commercial heterogeneous anion-exchange membrane and two prepared cation-exchange membranes in a 0.02 mol/L NaCl solution. They verified that the first transition time appears in heterogeneous membranes when the concentration of ions at the conductive regions reaches a value very close to zero. In turn, the second transition time appears when the electrolyte concentration reaches a very small value at the whole surface of the membrane, including the conductive and non-conductive regions. Similar results were obtained by Mareev et al. (34). The authors identified the nature of the two transition times present in chronopotentiograms of a heterogeneous membrane by using mathematical modeling. They verified that the first transition time appeared when the diffusive transport of ion from the solution to the conductive areas reached its limiting condition. From this moment, electroconvective vortices appeared in the limit of the conductive/non-conductive regions. The second transition time appeared when the electroconvection-diffusion ion delivery to the overall membrane surface achieved its limiting value.

3.9.3. Electric resistance

The resistance that ions face when transported through the solution and the membranes in an electrodialysis system is one of the most important properties for the separation viability, since the lower the resistance, the lower the energy consumption. The total resistance involved in electrodialysis is the sum of different resistances that ions face during their transport. Its value depends on some factors intrinsically related to the membrane, the type of solution and the cell configuration, such as the spacing between the membranes and electrodes (36,200). In industries, the intermembrane distance tends to be the smallest for reducing the resistance (23).

Membranes with larger thickness and those with reinforcing fibers present higher electrical resistances. Heterogeneous membranes, in general, also present higher electrical resistances due to the more tortuous counterion

pathway. Membranes with higher concentrations of ionic charges in the matrix present lower resistances, since this increases the attraction between membrane/ions (108). The greater content of water also abruptly reduces the resistance, since it leads to larger conducting interstices and a greater ion mobility through the membrane (164). The type of solution also influences the resistance: the presence of organic species, such as glucose, affects the water structure in the regions near the ions, and therefore, their hydration sphere and the corresponding Stokes radius. A decrease in the Stokes radius leads to a decrease in the resistance of the ion movement through the liquid, since it increases the conductivity and the ions mobility (175).

For determining the electrical resistance of the quasi-ohmic region, several direct current methods can be used, and one of the simplest methods is by calculating the inverse of the slope of the tangential line of the current-voltage curve (Figure 9). The resistance behavior obtained by direct current methods is quite different depending on the solution concentrations (112). Several authors have found that, in diluted solutions, the decrease of the resistance with an increasing concentration is very pronounced, whereas in concentrated solutions, the resistance is independent of the concentration increase (186,201,202). However, these methods do not allow distinguishing which type of resistance (the pure membrane resistance, the resistance of the DBL and the resistance of the interfacial ionic charge transfer through the double layer) is dominant in function of the electrolyte concentration.

Since direct current methods do not allow differentiating each resistance, authors have studied the resistance as a function of the electrical conductivity of the system (186,195,203). In these works, it was verified that at lower concentrations, the main resistance that controls the system is that caused by the diffusion boundary layer at the interface between the membrane/solution, whereas at higher concentrations, this resistance is no longer important. For identifying and differentiating each type of resistance, electrochemical impedance spectroscopy is generally used (201,204–206).

Długołecki et al. (201) used the electrochemical impedance spectroscopy to differentiate the resistances under different conditions of the solution. In addition to verifying the dominance of the DBL resistance at lower concentrations, they observed that the pure resistance of the membrane is the most important at

higher electrolytic concentrations. The authors also verified a decrease in the DBL resistance with the flow rate increase from 100 ml/min to 800 ml/min. Finally, it was found that the pure membrane resistance decreases with the temperature increase.

Chronopotentiometry has often been used to evaluate electrical resistances of systems operating in underlimiting and overlimiting conditions. Stodollick et al. (207) used chronopotentiometry to determine the resistance in overlimiting currents of a bipolar membrane by constructing current-voltage curves. The authors observed that the resistance in overlimiting conditions follows an exponential law and depends on the pH and ionic strength only with regard to the absolute level of the current. The relationship between the ohmic resistance (R_1) and the resistance of the overlimiting region (R_3) obtained by chronopotentiometry has also been evaluated (36,57,194,208–210). Assuming that the overlimiting regime is preferably governed by electroconvection, Choi et al. (209) verified that the resistance of the third region (R_3) decreases with the Péclet number, or with the increase of the Stokes radius of the ion, since greater ions enhance the mixing intensity. In this case, larger ions reduce the R_3/R_1 ratio.

In addition to the polarization curves, the chronopotentiograms also provide valuable information on the resistance. The ohmic potential drop in non-polarized state of a membrane quantifies the resistance associated with the membrane and the solution (55,172). Therefore, the greater the final value of the voltage registered for an applied current density, the greater its electrical resistance. Some authors have observed that after the steady-state stage in chronopotentiograms, the voltage may vary and, consequently, the resistance. As already mentioned, the voltage increase suggests the formation of some precipitate at the membrane when the limiting current density is exceeded, which can block the ions passage and increase the resistance (140–142). Scarazzato et al. (198) observed an increase in the potential drop of chronopotentiograms, which may have occurred due to the formation of uncharged species after the reduction of the pH on the membrane surface. The reduction of the voltage during the application of a current density above the limiting one has also been observed and is related to water splitting and the change in the equilibrium of the species transported through the membrane. In

this case, the generation of H^+ and OH^- intensifies the transport of some species through the membrane due to their ionic mobility (56), leading to a change in the pH of the diffusion boundary layer, and the occurrence of the dissociation of species (36). According to Kniaginicheva et al. (211), the total resistance begins to decrease due to the dominance of water splitting when $i/i_{lim} > 2$.

3.9.4. Plateau length

After the inflection point related to the limiting current density in the current-voltage curves, a plateau zone is reached, where the current density remains virtually constant with voltage increase (See Figure 9). This behavior occurs due to the depletion of ions in the diffusion boundary layer and the consequent increase of the resistance tending to infinity. From a voltage value, the water splitting phenomenon takes place and new current carriers are provided (H^+ and OH^-). Besides, overlimiting mechanisms of ion transport take place, such as gravitational convection and/or electroconvection. From this condition, the system reaches the overlimiting regime and the delivery of ions to the membrane surface is improved. In the polarization curves, the plateau length is a transition zone between the underlimiting region and the overlimiting one. Therefore, the plateau length indicates the membrane potential drop that must be surpassed to change the main ionic transport mechanism from diffusion and migration to overlimiting mechanisms.

The plateau length depends on both the solution tested in electrodialysis and on the membrane. In general, this property tends to decrease with the increase of electrolyte concentration (141,143,172,212). However, in some cases, the inverse behavior may occur due to the size of the ions that preferentially pass through the membrane (198). As already mentioned, Choi et al. (209) verified that bigger ions tend to enhance the solution mixing, which reduces the resistance of the third region (R_3). Therefore, ions with greater Stokes radius and, consequently, with higher Péclet number, facilitate the transition to the overlimiting regime at lower transmembrane voltages and reduce the plateau length. This behavior has already been verified by chronopotentiometry with cation-exchange membranes (53).

The counterion hydration number also influences the plateau length, as verified by Gil et al. (213). The authors constructed CVCs, by chronopotentiometry, for $MgCl_2$, $CaCl_2$ and NaCl solutions using a heterogeneous cation-exchange membrane and the plateau length decreased with cations in the following order: $Na^+ > Ca^{2+} > Mg^{2+}$. This was related to the degree of hydration of cations, since more hydrated ions, such as Mg^{2+}, engage larger volumes of water in their movement, which favors electroconvection and reduces the plateau length. It means that when ions with higher degree of hydration are present in the solution, the onset of electroconvection occurs at a lower voltage value (214). Recently, Gil et al. (146) also constructed CVCs using solutions of $MgCl_2$, $CaCl_2$, NaCl and observed the same tendency of plateau length decrease in the presence of ions in the following order: $Na^+ > Ca^{2+} > Mg^{2+}$. In addition to the higher degree of hydration of Mg^{2+} ions than the others, the lowest plateau length obtained with $MgCl_2$ solution was justified by the greatest Stokes radius of Mg^{2+}. As it was verified by Choi et al. (209), ions that present greater Stokes radius favor the activation of electroconvection at lower voltage values, which reduces the plateau length.

The structure of the membrane also influences the plateau length. Choi and Moon (215) constructed CVCs of anion-exchange membranes after their use in electrodialysis under overlimiting conditions, for evaluating the behavior of the curves in function of the changes in the membrane structure caused by water splitting. The CVCs were constructed for both sides of the membranes: for the front side, where ion depletion and water splitting occurred during electrodialysis, and for the back side, where ions were concentrated. The authors verified that one of most remarkable changes observed after the alterations on the membrane structure due to water splitting were in the plateau length. The OH^- ions generated due to water splitting converted quaternary amines into tertiary amines. Also, part of these amines may have been converted into their neutral forms, resulting in a reduction of charged groups and leading to an increase of the plateau length. Therefore, the plateau length was observed to increase at increasing inhomogeneity degrees of the membrane. A few years later, Ibanez et al. (216) performed a chronopotentiometric study on the relationship between membrane structures and plateau length. The authors constructed CVCs with membranes cast on a glass plate and dried in air; the

results revealed remarkable differences in plateau length, especially when the orientation of the membrane towards the feed was changed. Then, Marder et al. (140) modified the fraction of conductive area of a CEM and also verified, by chronopotentiometry, that the plateau length increased with the reduction of this property. According to Verodina et al. (193), this is due not only to the non-uniformity of the distribution of the layer near the membrane, but also due to the non-uniformity of the distribution of the current lines passing through the membrane, as shown in Figure 12. Other authors found the same tendency of increase in plateau length when the heterogeneity is increased (216).

Fouling and scaling occurrence also affects the plateau length, since the deposition of insoluble species on the membrane surface reduces this property (42,170,194). In some cases, the reduction is so strong that the second and third regions of the CVC come together, making the determination of the third region of the CVC unfeasible (172). This is in accordance with the works of refs. (217,218), since they showed that fouled membranes lead to the onset of electroconvection at a lower voltage, which means the plateau length is reduced. Finally, several authors developed new membranes to reduce the plateau length and to promote the regime above the limiting current density operating at lower voltage values (52,166,215,219–221).
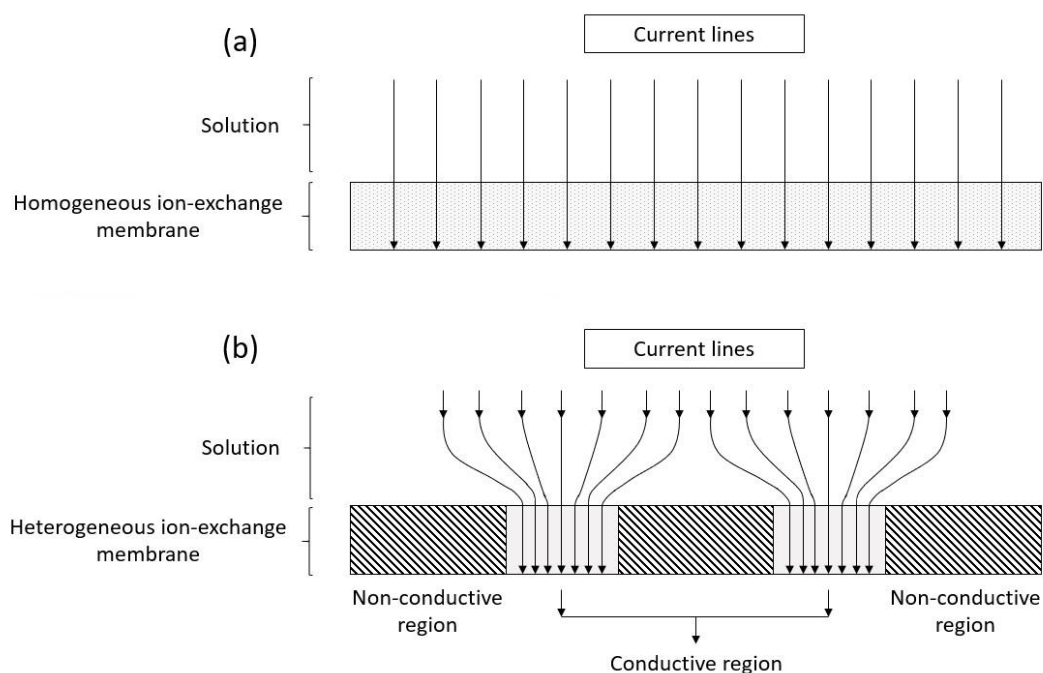
Figure 12 - Representation of the current line distribution close to the surface of (a) homogeneous and (b) heterogeneous ion-exchange membranes.

3.10. Electrodialysis operation under overlimiting conditions

Electrodialysis is conventionally operated under underlimiting conditions, by applying 70 % - 80 % of the limiting current density of the membrane system (45,222,223). In this condition, the system is principally governed by Ohm's law and showcases predictable behaviors. Some years ago, the application of a current density above the limiting one was only related to operational inconveniences, such as the formation and deposition of precipitated salts on the surface of the membranes, which can lead to its destruction, increase its resistance and unnecessary energy consumption related to water splitting. In recent years, several authors have considered the operation of electrodialysis under overlimiting conditions, since they have verified some advantages, such as the reduction of membrane area (215), reduction of apparatus dimensions (224), reduction of operating time and increase in ion transport (20).

The operation of electrodialysis at overlimiting condition is established from the occurrence of intense concentration polarization phenomenon. When concentration polarization is intensified, the saturation of current density occurs due to the ion depletion at the membrane vicinity. When the limiting current density is reached, the voltage (and, consequently, the electrical resistance) over a membrane surrounded by two DBL tends to infinity, theoretically. However, in practice, this does not occur since the system adjusts itself to continue transporting electric current. The first explanation given for this transport of current in overlimiting condition was the generation of H^+ and OH^- ions during the water splitting phenomenon, which was justified by the change in the solution pH on the membrane surface (113,225). However, in 1956, Frilette (226) experimentally found that besides there being no saturation of electric current, the saturation of Na^+ ions crossing a cation-exchange membrane did not occur, either, due to the convection phenomenon. Therefore, from Frilette (226) and Peers (189), the convection was also considered a justification for the current and ion transport under overlimiting condition.

With the aid of improved techniques and greater knowledge about the overlimiting condition, researchers began to discover other phenomena and mechanisms that occur simultaneously or as a result of water splitting and convection, such as the Kharkats effect (or exaltation effect) and the

current-induced membrane discharge (CIMD). In recent years, extensive efforts have been made to distinguish the effects of electroconvection and gravitational convection on the transfer of ions, besides understanding the different types and mechanisms of electroconvection, such as stable/unstable, bulk electroconvection, electroosmosis of the first and second kind (219,227–229).

3.10.1. Electroconvection

Electroconvection (EC) is one of the major responsible for ion transport when the system operates in overlimiting conditions. However, its mechanisms are not completely understood yet, although some information in literature are universally accepted. In theoretical studies on the types of convection, Rubinstein et al. (219,227,229–232) verified that, especially in homogeneous membranes, electroconvection results from the interaction between the electric field of the system and its respective space charge under conditions of deviation of the local electroneutrality condition. As a consequence, a nonpotential volume force grows strong enough to set in motion the fluid in the boundary layer adjacent to the membrane (57,215). For heterogeneous membranes with curved or electrically heterogeneous surface, Dukhin and Mishchuk (233,234) showed that the tangential components of electric current are necessary for the onset of electroconvection, since the curvature of the current lines toward the conducting regions causes the formation of vortices. In heterogeneous membranes, the accumulation of electric current lines leads to their distortion in the ion conductive pathways on the membrane surface, which is known as "funnel effect" (235). This tangential component of ion fluxes in the diffusion boundary layer enables the emergence of electroconvection in heterogeneous membranes. When electroconvection emerges, hydrodynamic instabilities are produced, since a non-uniform electric field is formed as a result of the intense variation of fluid velocity and concentration of ions at the DBL (214). Hence, vortexes are formed, and the system begins to be controlled by complex phenomena that will be mentioned below.

Electroconvection can be classified as stable or unstable, also known as Dukhin-Mishchuk EC mode and Rubinstein-Zaltzman EC mode, respectively (113,236). In the polarization curves, the registration of plateau

regions with a moderate increase in current density is related to the stable EC, while the great increase in the final region of the curve is related to unstable EC or water splitting (219,236). The unstable EC presents intense oscillations of current/voltage and this is responsible for the increased delivery of ions, contributing to better mass transfer. Moreover, unstable vortices cause the suppression of the undesirable water splitting phenomenon in comparison with stable vortices (54). Druzgalski et al. (237) showed how electrohydrodynamics become chaotic by using some concepts from turbulence theory such as Reynolds-averaging. These intense oscillations related to the unstable EC may be associated by breaking large vortices into smaller ones, which may merge again and generate new large vortices.

It is known that electroconvection occurs more intensively in more diluted solutions due to the higher thickness of the space charge region near the membrane surface (113,193,236). Diluted solutions exhibit stable electroconvection more intensively than concentrated solutions (218). The properties of membranes are also important to the stability of electroconvection. Experimental studies have shown that when the membrane is immobilized by casting a thin layer of an agarose-gel on its surface, the plateau is reached and the excess current noise cannot be observed, hindering the occurrence of electroconvection (238). According to Andreeva et al. (52), the surface modification of the membrane by casting a conducting film on its surface allows an earlier onset of unstable electroconvection, which leads to a decrease of the plateau length and, consequently, the energy consumption.

Some physical and mathematical models have been developed to explain the mechanisms involved in electroconvection. After Rubinstein and Shtilman (239), several works have been published to mathematically describe the overlimiting regime using the Nernst-Planck and Poisson equations (240,241). These models are developed for 1D systems and consider the appearance of space charge region and the consequent reduction of DBL. However, 1D models do not consider convection and are therefore unable to associate this variation of the DBL with the experimental results obtained that show an increase of ion transfer in the overlimiting regime. Simulations show that, when the current density is equal or greater than the limiting current density, differences in the behavior of polarization curves

constructed with models that do not consider electroconvection are visible (236). Therefore, 2D models, which consider convection besides diffusion as transfer mechanism of ions, were developed by Dukhin and Mishchuk (242) and Rubinstein et al. (243) from the Nernst-Planck-Poisson equation coupled with the Navier-Stokes equation. Other 2D models have been developed in the last years and they are often assessed in studies of mass transfer modeling on membranes, since they allow evaluating the concentration in function of the electric field in the overlimiting regime (147,214,233,244–248).

The use of chronopotentiometry, together with mathematical assessments based mainly on the 2D model, has generated very promising results in recent years in the field of overlimiting regime. Mareev et al. (34) identified, mathematically, the nature of two transition times present in chronopotentiograms of a heterogeneous membrane. The first transition time appeared when the diffusive transport of ion from the solution to the conductive areas reached its limiting condition, whereas the second transition time appeared when the electroconvection-diffusion ion delivery to the overall membrane surface achieved its limiting value. This mathematical evaluation was possible since the authors developed a 2D model, which also consider electroconvection besides diffusion as transfer mechanism. Mareev et al. (147) used a model based on 2D to simulate chronopotentiograms in underlimiting and overlimiting regions. The authors presented the diffusion layer thickness, δ, as a function of the Donnan potential drop at the interface between the membrane and the depleted solution. Simulated curves very close to the experimental ones were obtained. The authors also verified that the use of the Sand Equation for determining the transition time is valid only for current densities 1.5 times greater than the limiting current density of the membrane system.

Mareev et al. (249) proposed a 2D non-stationary model of ion transport through a membrane using a new formulation of the boundary conditions at the conductive areas. By applying an electric current stream function, they showed the non-uniformity of the distribution of current lines over the conductive regions and its influence on chronopotentiograms and electrochemical impedance spectra. Mareev et al. (250) reported an approach for a three-dimensional (3D) modeling of transient ion transfer across a heterogeneous surface. Theorical transition times were compared to those experimentally obtained by

chronopotentiometry and they agreed. The authors also evaluated the assumption of the uniform current density distribution proposed by Rubinstein et al. (235) and verified that shorter transition times than the experimental ones were obtained.

Experimental studies of electroconvection by evaluating ChPs and polarization curves without using a mathematical model are also often performed. Nebavskaya et al. (152) studied the influence of the ion exchange membrane surface charge and hydrophobicity in underlimiting and overlimiting regimes by chronopotentiometry. The authors noted that in underlimiting condition, the mass transfer rate is mainly affected by the membrane surface charge, while in overlimiting conditions, the main factor is the degree of hydrophobicity. This may be explained by the difference in the convection types in the underlimiting (electroosmosis of the first kind) and overlimiting regimes (electroosmosis of the second kind). Electroosmosis of the first kind occurs by the action of the tangential electric field upon the diffuse part of the electric double layer, whereas in the electroosmosis of the second kind, the tangential electric field acts upon the extended space charge of the nonequilibrium double layer (229,251).

The influence of the hydrophobicity of the membrane on the overlimiting regime was also verified by Pismenskaya et al. (252). They compared chronopotentiograms and current-voltage curves of virgin and used membranes after overlimiting experiments and suggested that intensive currents produced erosion of the ion-exchange polymer, which formed a continuous phase in the membrane. This erosion led to the exposure at the surface of particles with about 100 nm of relatively hydrophobic polyvinylchloride. The higher hydrophobicity or the surface was responsible for the increase in the electroconvective vortices. Korzhova et al. (253) also evaluated chronopotentiograms and polarization curves as a function of the deposits of hydrophobic non-conducting spots of a fluoropolymer after modifying of the membrane surface. The modified membranes showed higher amplitude of oscillations due to the greater hydrophobicity, lower voltage growth and lower water splitting rate. According to the authors, the hydrophobic spots favored higher tangential electric force applied more intensively to the equilibrium space charge region.

3.10.2. Gravitational convection

Another type of convection involved in the overlimiting regime is the gravitational one. Gravitational convection occurs by the non-uniform distribution of the solution density, which causes the Archimedes force, and together with the gravitational force, the fluid in the region near the membrane is set in motion (247,254). The Archimedes force is emerged as a result of the tendency of a body to be pushed out of the liquid's bulk onto its surface due to the lower density of the body if compared to the liquid's density (255). In an electrodialysis system, the rise of volume force is conditioned by gradients of concentration and/or temperature. Therefore, this phenomenon tends to occur more intensively in concentrated solutions, due to the higher Joule heating and higher concentration gradients. Theoretical (248,255–257) and experimental studies (21,55,144,145,193,240,258,259) on gravitational convection are frequently published. Among the techniques employed in the experimental studies, the use of chronopotentiometry has shown special relevance.

Pismenskaya et al. (55) verified that in a system with a 0.1 mol/L NaCl solution, the main overlimiting mechanism is gravitational convection, whereas in 0.01 mol/L NaCl systems, the main mechanism is electroconvection. The authors also verified a reduction of the potential drop in the ChPs after reaching a maximum point, which occurred due to the gravitational convection. This reduction was greater with the heterogeneous membrane than with the homogeneous one, since the heat produced in the heterogeneous membrane is greater and its dissipation is lower, due to its greater thickness and resistance. Therefore, the heat produced accumulated on the surface of the membrane and heated the depleted diffusion boundary layer.

Martí-Calatayud et al. (172) used chronopotentiometry to confirm that gravitational convection occurs even at current densities below the limiting current density. The authors noted that at currents below or slightly greater than the limiting one, gravitational convection is the main overlimiting mechanism, which causes a decrease in the thickness of the diffusion boundary layer and in the membrane potential drop. Krol et al. (144) evaluated chronopotentiometric and polarization curves obtained with the system in vertical and horizontal positions to evaluate the effects of gravitational convection. The authors verified

that, in the horizontal position, without any forced convection, the steady-state condition was not achieved in the chronopotentiograms, since the potential drop increased continuously with time. This occurred because concentration gradients in the depleted solution were established by gravitation force. Oscillations in potential drop caused by the gravitational convection were also verified. Hence, the work showed the importance of gravitational convection to a system under overlimiting regime. Pismenskaya et al. (258) also evaluated polarization curves by chronopotentiometry using systems in different positions. The authors verified that the differences between the curves obtained with the system in horizontal and vertical positions did not exceed 6 %. Therefore, gravitational convection could be neglected in their experiments.

The effects of gravitational convection are generally quite subtle. In addition to occurring only in concentrated solutions, gravitational convection is more intense in systems with greater intermembrane distances and in solutions with lower flow rates (259).

3.10.3. Water splitting

The water splitting phenomenon in membrane systems began to be intensively studied in the 1980s (260) and, in recent years, several works have been published to understand its mechanisms and consequences. Studies focused on water splitting performed by voltammetry, chronopotentiometry and electrochemical impedance spectroscopy are often performed, with the possibility of analyzing the evolution of the solution pH during the experiments (21,52). Water splitting takes place in a thin layer at the membrane interface (~1 nm thick) and it occurs as proton-transfer reactions between molecules of water and the charged groups of the membrane (260,261). When the applied current density approaches the limiting current density of the membrane system, the reaction rapidly increases (193). Therefore, water splitting becomes intense when the ions concentration on the surface of the membrane is comparable to the concentration of the H^+ and OH^- ions of the water (218).

The membrane type influences water splitting, and the range of the catalytic activity of ionogenic groups towards the water splitting reaction is presented as follows: $-N(CH_3)_3 < -SO_3H < =NH, -NH_2 < \equiv N$ (52,262). For this

reason, water splitting tends to occur more intensively at anion- than at cation-exchange membranes. This can be justified by the different mechanisms of the phenomenon in both types of membranes, which can be proven by the different pH variations in the membranes and by the polarization curves (263). Belova et al. (254) studied water splitting on two anion-exchange membranes by chronopotentiometry. The authors noted that with one of the membranes (MA-40M), the intensity of water splitting was lower than electroconvection, whereas with the MA-40 membrane, the electroconvection seemed to be suppressed by water splitting. Kang et al. (264) assessed the influence of the surface charge density on the water splitting behavior. They observed that the increase in the fixed charge density caused an increase in the water splitting intensity, which is in accordance with the classical electric field-enhanced water splitting theory. Kang et al. (165) used a Nafion membrane with an iron hydroxide/oxide deposited layer for evaluating the influence of inorganic substances on water splitting. The authors observed that the intensity of the phenomenon of the metal-embedded cation-exchange membranes was 10^4-10^5 times higher than those of the virgin membranes at the same conditions. They believed that the immobilized bipolar structure consisting of the H^+ and OH^- affinity groups increased the electric fields and the catalytic activity of the membrane.

Martí-Calatayud et al. (53) evaluated the relationship between current efficiency and plateau length by chronopotentiometry. They verified that water splitting was more relevant in curves with long plateaus, since greater values of transmembrane voltage are needed to reach the region of overlimiting currents. In contrast, in systems with lower plateau lengths, the tendency of water splitting occurrence is lower, since electroconvection takes place more intensively. The authors observed that the transfer of nickel ions through the membrane was favored by electroconvection in conditions of the lowest plateau lengths, while water splitting reduced the transfer efficiency.

The system configuration can also affect the rate of water splitting, which is negligible in systems with large distances between membranes, with or without agitation (265). The reduction of water splitting in pulsed-ED processes has also been evaluated in recent years, in addition to determining optimal conditions for pulse regimes, which consequently decreases fouling and scaling (266–268).

Another phenomenon, less evident, may occur associated with water splitting: the exaltation effect, which was firstly studied by Kharkats (269). This occurs by the generation of H^+ and OH^- ions and their presence in the region near the membrane since these ions may disturb the electric field and increase the exaltation of the transport of counterions. That is, OH^- ions generated in the depletion region attract cations from the salt and move them from the bulk solution to the interface, promoting their transport through the membrane, while H^+ ions promote the same mechanism with salt anions (257). In general, the exaltation effect is neglected due to the greater relevance of electroconvection and the fact that the mobility of H^+ and OH^- is 5 to 10 times greater than the mobility of salt ions. However, recently, Melnikova et al. (197) mathematically verified that this phenomenon is able to increase the transport of $H_2PO_4^-$ by 11 %.

Water splitting can also cause the current-induced membrane discharge (CIMD) (270). In this case, the intense passage of OH^- ions through anion-exchange membranes, which have weak basic functional groups, can deprotonate their charges. Consequently, the membranes lose permselectivity, that is, the passage of co-ions through the anion-exchange membrane increases. Studies performed by IR-spectroscopy (215) show that after the intense passage of OH^- ions through commercial anion-exchange membranes with quaternary amines, these functional groups are rapidly converted into tertiary and secondary amines, by Hofmann reaction (118,253). The process is intensified by the local Joule heating up to detachment of ionic groups.

Chronopotentiometric studies performed by Mikhaylin et al. (54) and Korzhova et al. (253) show that the presence of electroconvective unstable vortices lead to suppression of water splitting, since the competition between the two phenomena takes place. In this case, the vortices contribute to decreasing the OH^- concentration in the depleted boundary solution. Belova et al. (21) and Slouka et al. (271) noted the opposite effect: a partial suppression of electroconvection by water splitting at anion-exchange membranes. This may be related to the reduction of the space charge at the depleted interface by H^+ ions, since they have opposite charges compared to the space charge at the membranes, being able to reduce it. The same phenomenon is valid for OH^- at cation-exchange membranes (113).

4. MATERIALS AND METHODS

The thesis was subdivided into 4 topics. Firstly, the general materials and methods used in all the steps of the work will be presented. Then, the specific materials and methods of each topic will be shown.

4.1. Ion-exchange membranes

The membranes used in the studies on chronopotentiometry and electrodialysis were the anion-exchange membrane HDX200 and the cation-exchange membrane HDX100. Both were supplied by Hidrodex, are heterogeneous and have a structure with reinforcing fabrics at both surfaces to enhance its mechanical resistance. The HDX200 presents quaternary amine as fixed groups, whereas the HDX100 presents sulfonic acid. In topic I of the thesis, the cation-exchange membrane PC-SK was also evaluated, which was provided by Polymerchemie Altmeier GmbH (PCA).

The main characteristics of the membranes used in the study are shown in Table 1.

Table 1 - Main characteristics of HDX100, HDX200 and PC-SK membranes.

Parameter	HDX100	HDX200	PC-SK	Unit
Ion group attached	- SO_3^-	- NR_3^+	- SO_3^-	-
Water content	35-50	30-45	9	%
Ion exchange capacity	≥ 2.0	≥ 1.8	≥ 1	mol.kg^{-1} (dry)
Surface resistance (0.1 mol de NaCl)	≤ 20	≤ 20		Ohm.c m^{-2}
Permeselectivity	≥ 90 (0.1 mol KCl/0.2 mol KCl)	≥ 89 (0.1 mol KCl/0.2 mol KCl)	≥ 93 (0.1 mol KCl/0.5 mol KCl)	%
Burst strengh	≥ 06	≥ 0.6		MPa
Water permeability	≤ 0.1 (< 0.2 MPa)	≤ 0.2 (< 0.035 MPa)		mL.h.c m^{-2}
Thickness	450	450	130	µm

4.2.   Electrochemical cell for chronopotentiometric measurements

The chronopotentiometric experiments (Topic I, II and III) were conducted using a three-compartment cell with a cation- and anion-exchange membrane separating the central compartment from the cathode and anode, respectively. Two graphite electrodes were placed at the extremities of the cell, and during the experiments, some current values were imposed by a potentiostat/galvanostat (Autolab, PGSTAT 20). Ag/AgCl reference electrodes immersed in Luggin capillaries were installed on each side of the membrane for measuring the potential drop across the membranes. The experiments were conducted in duplicate, at room temperature and without stirring. For constructing the chronopotentiograms in topics I and II of the thesis, current pulses were applied for 180 seconds. Then, the relaxation process was allowed for 100 seconds before the next pulse was applied. In topic III, the current pulses were applied for 300 seconds and the relaxation step was allowed for 100 seconds. A schematic representation of the chronopotentiometric system is shown in Figure 13 (198).
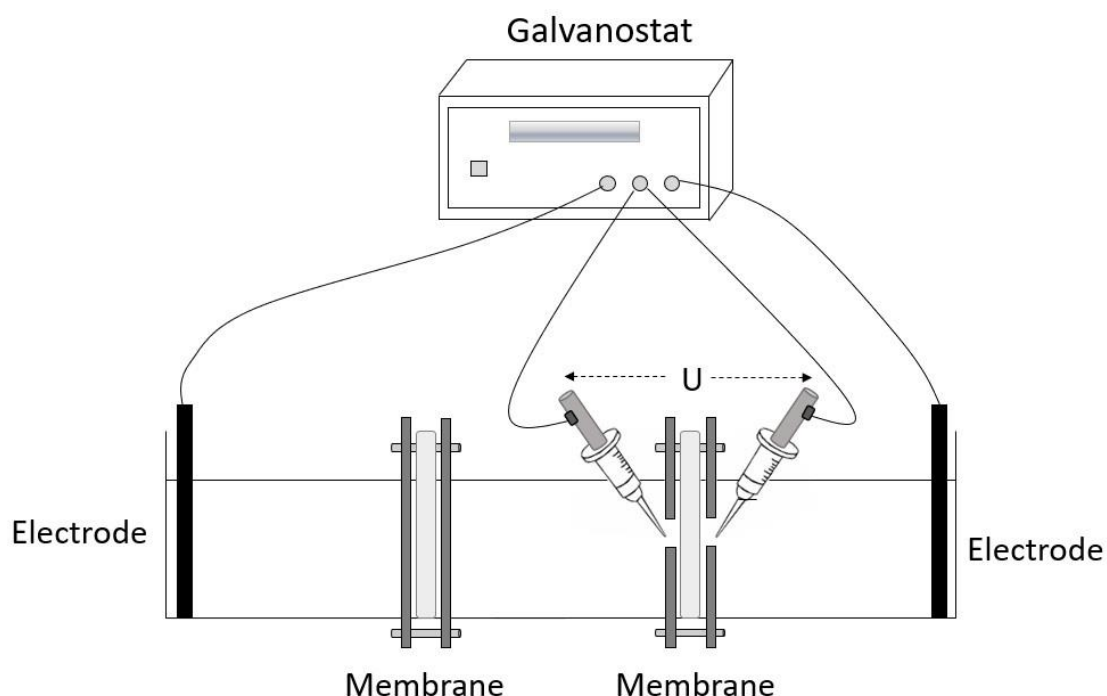
Figure 13 - Schematic representation of the chronopotentiometric setup.

4.2.1. Obtaining of current-voltage curves by chronopotentiometry

Current-voltage curves, which are represented in Figure 9, were obtained from the steady-state polarization voltage corresponding to each current pulse in the chronopotentiometric stage.

Limiting current densities (i_{lim}) were determined by the intersection of the tangential lines of the first (quasi-ohmic) and second (plateau) regions of the CVC, whereas the ohmic resistances (R_1) were calculated by the inverse of the slope of the tangential line ($1/\alpha_1$) of the first region. The plateau lengths were determined by the subtraction of the voltage related to the intersection of the tangential lines of the second + third regions of CVC and the intersection of the tangential lines of the first and second regions. Finally, the electric resistance of the overlimiting region (R_3) was calculated similarly to the ohmic one, i.e., by the inverse of the slope assigned to the overlimiting region.

4.3. Topic I: Chronopotentiometric study for evaluating the effect of the membrane morphology on the transport properties of Cu(II) through a homogeneous and a heterogeneous ion-exchange membrane

The chronopotentiometric experiments were carried out using a three-compartment cell as described in section 4.2. Two cation-exchange membranes were evaluated: HDX100 and PC-SK. The heterogeneous HDX200 membrane was used as auxiliary anion-exchange membrane.

4.3.1. Working solutions

For the evaluation of copper transport in different conditions, the study was carried out with solutions of $CuSO_4.5H_2O$ and H_2SO_4 varying the salt concentration, as shown in Table 2. The concentration values of sulfuric acid added in all systems were those responsible for the molar ratio of sulfate/acid equal to 1:1, and then the pH was adjusted with potassium hydroxide. All reagents employed were analytical grade.

Table 2 - Composition of the working solutions with Cu^{2+} ions in acid medium.

	Cu^{2+} (g/L)	pH	Molar ratio (sulfate:acid)
	0.1	3.0	1:1
	0.5	3.0	1:1
Working solutions	1.0	3.0	1:1
	1.5	3.0	1:1
	2.0	3.0	1:1

The conditions of Table 2 were chosen based on the study of Peng et al. (63), who analyzed 36 samples of wastewaters from 12 electroplating enterprises and verified that the Cu^{2+} concentration ranged from less than 0.1 g/L to almost 1.0 g/L while pH varied from 2.5 to 5.0. Besides, Öğütveren et al. (272) studied the removal of copper ions from electroplating wastewater and tested Cu^{2+} concentrations of 0.1 g/L, 0.2 g/L and 0.3 g/L, whereas Caprarescu et al. (273) tested the removal of copper from a solution with 1.0 g Cu^{2+}/L. Furthermore, according to Alebrahim et al. (274) the electroplating industries are contaminated with copper to the level of 0.5 g/L or more.

4.3.2. Visualization of the membranes structure

The structure of the cation-exchange membranes PC-SK and HDX100 was visualized using an electron scanning microscope (Phenom ProX) at 15 kV of accelerating voltage. Before the analysis, the membranes samples were immersed in distilled water for 24 h and dried at 50 °C for more 24 h.

4.3.3. Determination of the transport and membrane properties

The transport and membrane properties were determined by the construction of current-voltage and chronopotentiometric curves. The limiting current density, the electrical resistance and the plateau length were determined as described in section 4.2.1.

For the determination of the fraction of conductive area of the membranes, chronopotentiograms were constructed using a KCl solution with 0.1 mol/L and 0.3 mol/L for the HDX100 and PC-SK membrane, respectively. These solutions were chosen based on intermediate concentration values of the solutions used in

the determination of the permselectivity of each membrane by the suppliers (Table 1). Transition times (τ) were experimentally obtained by the intersection of the tangential lines of the first and second stages of the chronopotentiometric curves, as shown in Figure 6 (165). A figure of (τ) vs. (C_0/i)² was constructed for each membrane and the coefficient of the curve was equal to the modified Sand's equation (Equation 13). A representation of the curve of (τ) vs. (C_0/i)² is present in Figure 7. The transport number of counterion in the membrane phase ($\overline{t_j}$) was calculated by Equation 18 (108). For the calculation of t_j and the diffusion coefficient, the equivalent conductivity data (λ) was employed (154). As only ε was an unknown term in the Equation 13, it was finally determined.

$$\overline{t_j} = permselectivity * \left(1 - t_j\right) + t_j \qquad \text{Equation 18}$$

According to Herraiz-Cardona et al. (141), once the value of ε is known, the modified Sand's equation can be applied to determine the membrane transport number for any system. Thus, the fractions of conductive area obtained for both membranes with KCl solutions were used for the $\overline{t_j}$ determination of copper with the solutions of $CuSO_4.5H_2O$ + H_2SO_4 by Equation 13 and the linear slope between the transition times (τ) and (C_0/i)².

4.4.   Topic II: Chronopotentiometric study for evaluating the transport properties of the anion-exchange membrane used in the treatment of the synthetic cyanide-free wastewater from brass electrodeposition

The experiments were carried out using a three-compartment cell as described in section 4.2. The anion-exchange membrane evaluated was the heterogeneous HDX200, whereas the heterogeneous HDX100 was used as the auxiliary cation-exchange membrane.

4.4.1. Working solutions

Copper sulfate pentahydrate, zinc sulfate heptahydrate and EDTA sodium salt were used for preparing solutions based on the study carried out by

Almeida et al. (9,10). The authors tested the influence of the copper and zinc proportion present in the bath on the brass electrodeposition. In all solutions tested, the total concentration of metals (Cu^{2+} + Zn^{2+}) was kept constant at 0.2 mol/L and the molar proportions of Cu^{2+} and Zn^{2+} were variable. Three metals proportions were evaluated: 30%Cu+70%Zn, 50%Cu+50%Zn and 70%Cu+30%Zn, which presented Cu^{2+}/Zn^{2+} molar ratios of 0.4, 1.0 and 2.3, respectively. In the solutions, the molar ratio of EDTA/Cu^{2+} was 2.5 and the pH 14, since both metals are complexed by EDTA at this condition.

Here, the electroplating baths tested by Almeida et al. (9,10) were diluted in 1 % (v/v) for preparing the synthetic solutions of the wastewater. Besides the assessment of Cu^{2+}/Zn^{2+} molar ratios (0.4, 1.0 and 2.3), pH values between 9 – 12 and EDTA/Cu^{2+} molar ratios of 2.0, 2.5, 3.0 and 3.5 were evaluated. The lowest pH evaluated was 9 to guarantee the complexation of Zn^{2+} and Cu^{2+} ions and the greatest pH was 12 to prevent the membrane deterioration, which occurs under extreme pH conditions (215). The experimental conditions tested are found in Table 3.

Table 3 - Composition of the working solutions that simulate the wastewater from the cyanide-free brass electroplating industry.

Evaluation	ID	pH	Conductivity (µS/cm)	Cu^{2+}/Zn^{2+}	EDTA/Cu^{2+}	Concentration (mol/L)		
						Cu^{2+}	Zn^{2+}	EDTA
pH	I	9	780	1.0	2.5	0.0010	0.0010	0.0025
	II	10	810	1.0	2.5	0.0010	0.0010	0.0025
	III	11	948	1.0	2.5	0.0010	0.0010	0.0025
	IV	12	2360	1.0	2.5	0.0010	0.0010	0.0025
Cu^{2+}/Zn^{2+}	V	10	944	0.4	2.5	0.0006	0.0014	0.0015
	II	10	810	1.0	2.5	0.0010	0.0010	0.0025
	VI	10	632	2.3	2.5	0.0014	0.0006	0.0035
EDTA	VII	10	672	1.0	2.0	0.0010	0.0010	0.0020
	II	10	810	1.0	2.5	0.0010	0.0010	0.0025
	VIII	10	917	1.0	3.0	0.0010	0.0010	0.0030
	IX	10	1020	1.0	3.5	0.0010	0.0010	0.0035

For evaluating the influence of Cu^{2+} and EDTA on the transport properties, pH was fixed as 10 since speciation diagrams constructed with the aid of the *Hydra-Medusa* software (275) showed that both metals are complexed under this condition. This also avoids the presence of more OH^- ions in solution that could compete with the other anionic species.

4.5. Topic III: Treatment of the synthetic cyanide-free wastewater, by electrodialysis in underlimiting and overlimiting condition, from the brass electrodeposition with EDTA

4.5.1. Electrodialysis bench system

The electrodialysis tests were carried out in a five-compartment ED cell made of acrylic, separated by cation- and anion-exchange membranes with an active area of 16 cm^2, arranged alternately in a "Cathode (electrode)-AEM-CEM-AEM-CEM-Anode (electrode)" configuration. The flow channel width between two membranes was 1 cm. The five compartments were 8 cm×8 cm×1 cm in dimension and were connected to three 1 L independent reservoirs. The reservoirs with the solution to be treated and with the solution to be concentrated were labeled diluted and concentrated solutions, respectively, and both were fed with the synthesized wastewater (working solution). The reservoir connected to the electrode compartments was fed with a Na_2SO_4 solution to maintain the electrical conductivity. All the reservoirs were independently connected to centrifugal electro-pumps to produce the circulation of the solutions (80 L/h). A schematic representation of the electrodialysis system employed is presented in Figure 14, while the real ED system used is shown in Figure 15. The electrodes were made of titanium coated with titanium and ruthenium oxides ($70RuO_2/30TiO_2$) and present an active area of 16 cm^2 (4 cm×4 cm). Both electrodes were placed at the extremities and connected to an external power source. The determination of the limiting current density of the membranes was performed as described in section 4.5.3.
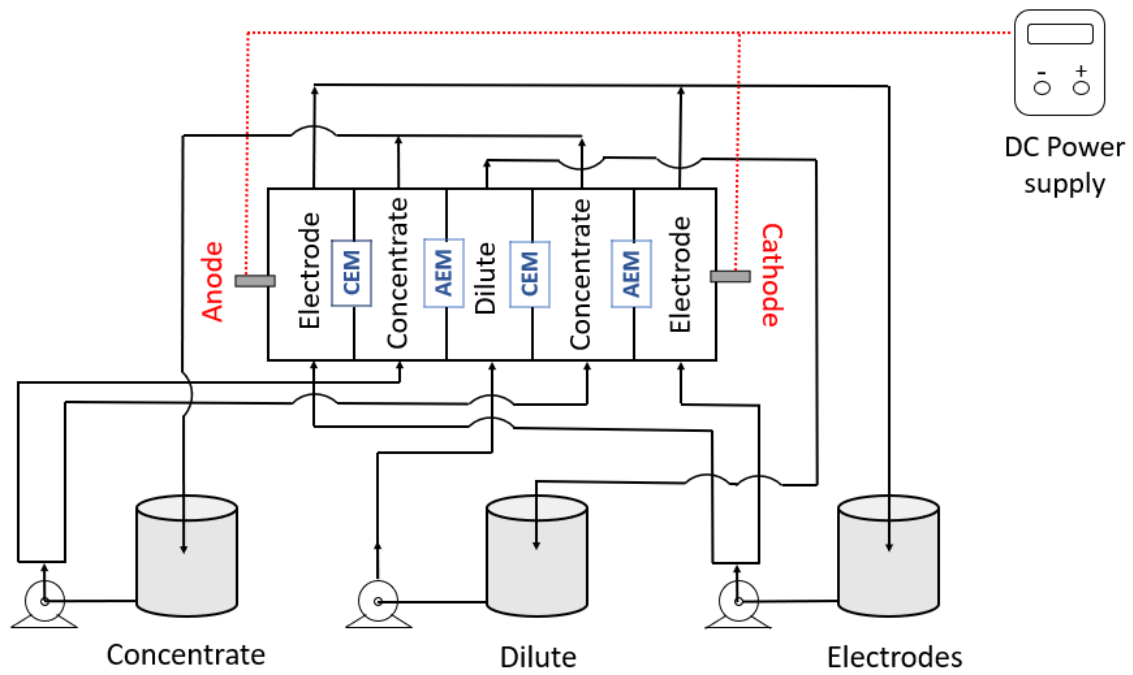
Figure 14 - Schematic representation of the electrodialysis system used.
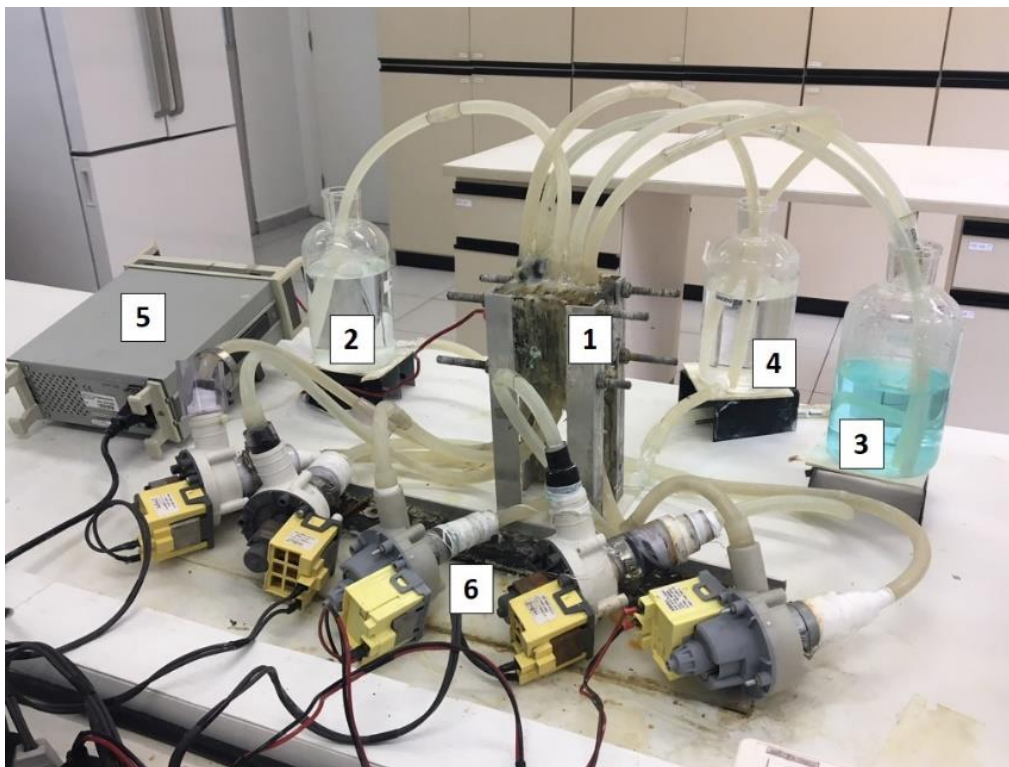
Figure 15 - Electrodialysis system with five compartments. 1 is the ED cell; 2 is the synthesized rinsing water; 3 and 4 are the concentrated and electrode solutions, respectively; 5 is the DC power supply and 6 refers to the pumps.

4.5.2. Experimental procedure

Two electrodialysis experiments were performed in long-term concentration tests: the underlimiting, and the overlimiting test. Initially, both dilute and concentrate compartments were fed with the working solution of the synthesized rinsing water, and the electrodes compartment, with the conductive solution of NaSO₄. A current density value established based on the current-voltage curves of both membranes was applied for transporting ions from the dilute compartment to the concentrate one. In the underlimiting test, the applied current density was 80 % of the limiting current density of the cation-exchange membrane (CEM), which was determined for the initial working solution. In the overlimiting test, the current density was 120 % of the i_{lim} of the anion-exchange membrane (AEM). This procedure was carried out until the conductivity of the diluted solution reached values close to tap water (~0.2 mS/cm). When this condition was reached, the diluted solution was replaced with the working solution and the experiment was conducted again, until its conductivity also reached ~0.2 mS/cm. Each renewal of the diluted solution was named "cycle". Four cycles were performed due to the occurrence of ionic transfer limitation by the diffusion mechanism between the dilute and concentrate compartments. The conductivity and pH of the three solutions were monitored throughout the cycles. At the end of each cycle, the diluted solution and 10 mL samples of the concentrate compartment were collected and forwarded to chemical analyses. The ED performance was evaluated in function of percent extraction (PE%) and percent concentration (PC%), according to Equation 19-Equation 20, where C_0^j and C_t^j are concentrations of an ion j in the initial state and at a given time, respectively. As PE% were calculated with data on the diluted solutions, the values obtained were lower than 100 %. For PC%, the values obtained after the first cycle were higher than 100 % since they were calculated with data on the concentrate compartment after each cycle, which means they were accumulative.

$$PE\% = \left(1 - \frac{C_t^j}{C_0^j}\right).100 \qquad \text{Equation 19}$$

$$PC\% = \left(\frac{C_t^j}{C_0^j} - 1 \right) . 100 \qquad\qquad \text{Equation 20}$$

After the last cycle, the membranes were forwarded to chronopotentiometric tests, as described in section 4.5.5.

4.5.3. Determination of the limiting current density of the membranes in the ED stack

For defining the current to be applied to the electrodialysis tests, current-voltage curves of both membranes were constructed using the same apparatus of the electrodialysis experiments. Platinum wires without an inert braid were placed at the interfaces of the anion- and cation-exchange membranes between the dilute and concentrate compartments. Voltmeters were connected directly to the platinum wires of both membranes. This configuration has already been used by other authors for determining limiting current densities of membranes (20,222).

Two CVCs were constructed: one for the anion-exchange membrane and another for the cation-exchange membrane. The curves were obtained by increasing the applied current densities gradually every 2 min, in 2 mA, with an interval of 3 minutes without current application. The potential differences between the AEM and CEM were measured immediately before the interruption of the current densities. Before the experiments, the membranes were equilibrated for 24 hours with the solutions to be used subsequently. The experiments were performed in duplicate.

The limiting current densities of both membranes were determined by the intersection of the tangential lines of the first and second regions of the CVC.

4.5.4. Working solutions

The synthetic rinsing water evaluated herein was prepared by the dilution of the electroplating bath assessed by Almeida et al. (9,10) in their study of brass electrodeposition using EDTA as a complexing agent and Cu^{2+}/Zn^{2+} molar ratio of 0.4.

The bath solution was prepared with $CuSO_4.5H_2O$ (0.06 mol/L), $ZnSO_4.7H_2O$ (0.14 mol/L), EDTA disodium salt (0.15 mol/L) and NaOH (3 mol/L). The working solution that simulated the rinsing water was prepared by diluting the electroplating bath in a 1 % v/v proportion in distilled water, and this solution was used to feed the dilute and concentrate reservoirs. Table 4 presents the initial conditions of the working solution used.

Table 4 - Initial conditions of the working solutions of the electrodialysis tests.

Molar concentration (mol/L)					
$CuSO_4.5H_2O$	$ZnSO_4.7H_2O$	EDTA	NaOH	pH	Conductivity (mS/cm)
0.0006	0.0014	0.0015	0.03	12.25	5.3

A Na_2SO_4 solution was used to feed the electrodes compartment. The conductivity of this solution was 11 mS/cm, about twice as great as the conductivity of the working solution, for reducing the resistance of the system. During the experiments, drops of a NaOH solution (40 % wt) were added to the electrodes reservoir for minimizing the influence of oxidation-reduction reactions on the solution conductivity and to maintain this parameter in approximately 11 mS/cm.

..

4.5.5. Chronopotentiometric measurements

After the electrodialysis tests, the membranes were forwarded to chronopotentiometric steps. Firstly, they were immersed separately in the working solution and equilibrated for 24 hours. Then, chronopotentiometric experiments were performed for evaluating the influence of each ED performed on the transport properties of the cation- and anion-exchange membranes. The chronopotentiometric system used here is described in section 4.2, whereas the methods for determining the transport properties are described in section 4.2.1.

4.5.6. Analytical methods

The concentration of copper and zinc ions was determined by energy dispersive X-ray fluorescence spectrometry (PANalytical Epsilon 3XL). The

concentration of sodium (Na^+) and sulfate (SO_4^{2-}) was ascertained by ion chromatography (IC Metrohm 858). Finally, the concentration of EDTA was determined by Total Organic Carbon analysis (Shimadzu TOC-L). Before the analyses, the solutions were filtered. The estimated relative error between the concentration values was below 5 %.

During the experiments, the conductivity and the pH of the solutions in the three reservoirs were monitored with a Sensoglass electrical conductivity meter and a Hanna PH21 pHmeter, respectively.

4.5.7. Cleaning procedure of the membranes

After the long-term electrodialysis and the chronopotentiometric measurements, the membranes used in the underlimiting test were removed from the electrodialysis stack and forwarded to a three-stage cleaning procedure. Alkaline solutions were used since Garcia-Vasquez et al. (118) assessed the ageing effects on the properties of a heterogeneous anion-exchange membrane under acidic and alkaline conditions; the membrane showed to be more resistant in alkaline medium. In addition to this, Scarazzato et al. (42) evaluated two cleaning procedures under acidic and alkaline conditions for the same AEM used in this thesis and verified that both procedures presented similar performance.

Both cation and anion-exchange membranes were rinsed with distilled water and immersed in the cleaning solution of NaOH (0.1 mol/L) for 72 hours. Then, the membranes were rinsed (24 h), immersed in the working solution (synthetic wastewater from the brass electrodeposition – Table 4) for equilibrium (24 h) and submitted to chronopotentiometry, for evaluating the transport properties after the first cleaning step. Chronopotentiometric and current-voltage curves were constructed for each membrane as described in section 4.2 and section 4.2.1. Then, the cleaning procedure was repeated twice, for 72 h, using more concentrated cleaning solutions of NaOH: 0.5 and 1.0 mol/L. Finally, the cleaned membranes were analyzed by means of FTIR-ATR spectroscopy and SEM-EDS for evaluating modifications in their structure.

For a better understanding of the cleaning and chronopotentiometric steps, the procedure is detailed in Figure 16.
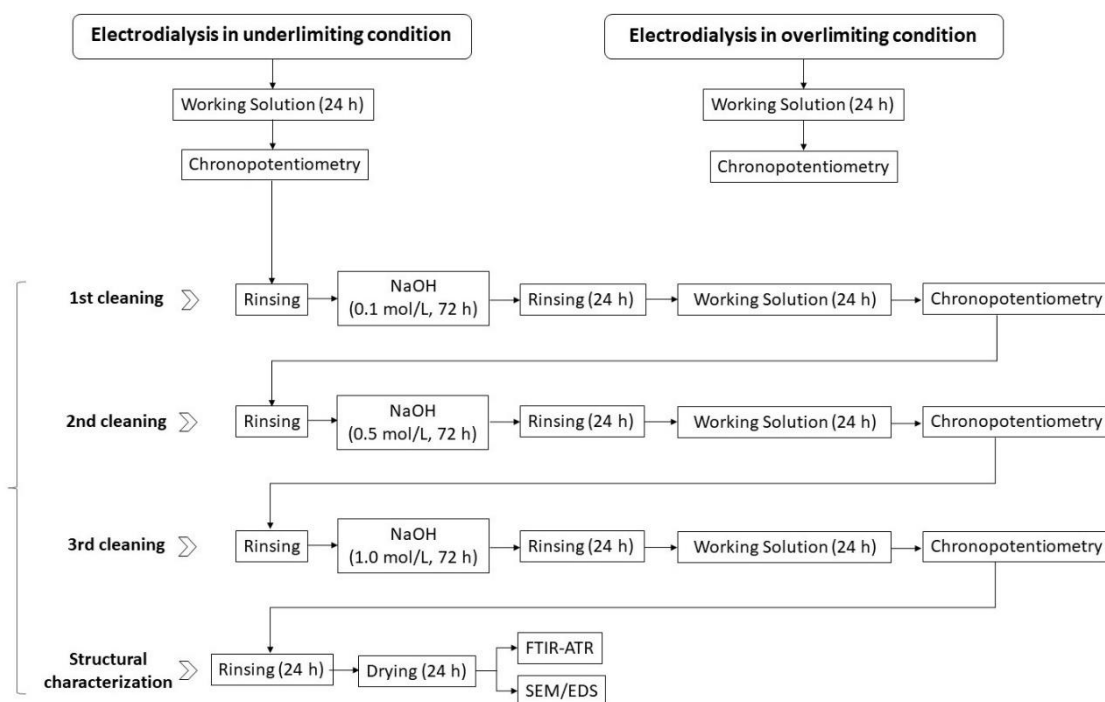
Figure 16 - Cleaning and chronopotentiometric procedures performed after electrodialysis.

4.6. Topic IV: Evaluation of brass electrodeposition at RDE from cyanide-free bath and the recovery of the metals and EDTA extracted, by electrodialysis, into the bath

The experiments of cyclic voltammetry and electrodepositions were conducted in a cell with three electrodes. In both experiments, the rotating disk electrode (RDE) of AISI 1010 steel enclosed in Teflon with 0.8 cm of diameter was used as working electrode. The reference and counter electrodes were made of Ag/AgCl and platinum, respectively. A representation of the cell used is shown in Figure 17.
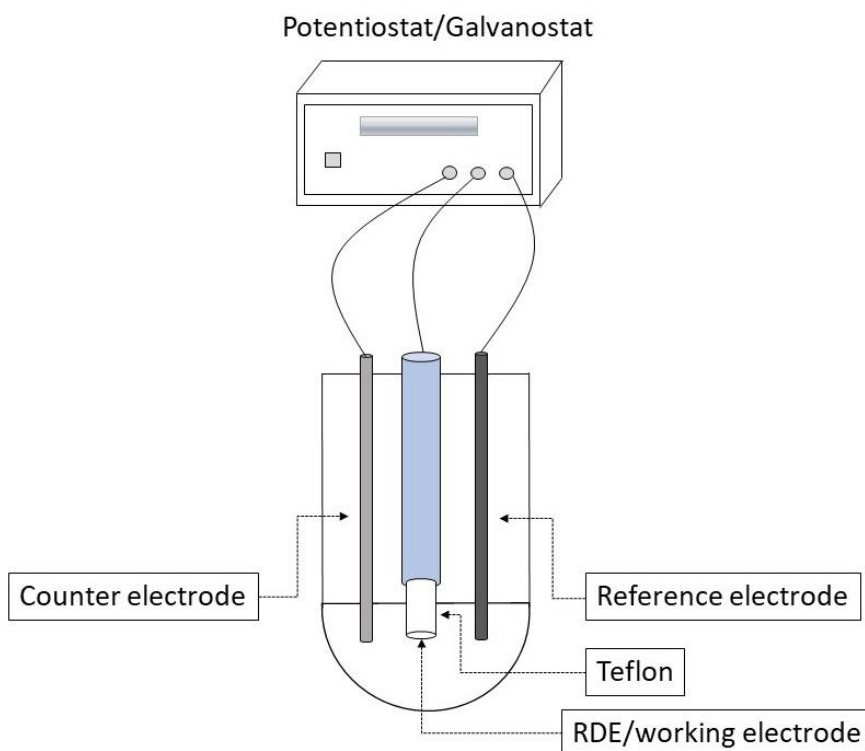
Figure 17 - Cell with three electrodes used in the experiments of cyclic voltammetry and electrodepositions.

Before each experiment, the working electrodes were polished with continuously finer grades of emery paper (240, 500 and 4000), rinsed with distilled water and dried. All the experiments were controlled using a potentiostat/galvanostat (Autolab PGSTAT 20) and conducted at room temperature.

The electroplating bath evaluated here was based on the works of Almeida et al. (9,10). The solutions were freshly prepared with copper sulfate pentahydrate, zinc sulfate heptahydrate and EDTA sodium salt. The pH of all solutions tested was 14. All reagents employed were analytical grade.

4.6.1. Cyclic voltammetry

Cyclic voltammetric studies were performed within the potential range of -2.0 V to 0.7 V, at a scan rate of 10 mV/s, with rotation speeds of 0, 500, 1000, 1500, 2000 and 2500 rpm. The curves were constructed using solutions with the metals together and separated in different concentrations. Table 5 presents all the conditions of the tested solutions.

Table 5 - Working solutions for the experiments of cyclic voltammetry.

	Cu^{2+} (M)	Zn^{2+} (M)	EDTA (M)	NaOH (M)	Rotation speed (rpm)
Only copper	0.03	-	0.15	3.0	
	0.06	-	0.15	3.0	
	0.10	-	0.15	3.0	0, 500, 1000, 1500, 2000, 2500
Only zinc	-	0.06	0.15	3.0	
	-	0.10	0.15	3.0	
	-	0.14	0.15	3.0	
Original bath	0.06	0.14	0.15	3.0	

4.6.2. Electrodeposition tests

For the brass electrodepositions, the bath with Cu^{2+} (0.06 mol/L), Zn^{2+} (0.14 mol/L), EDTA (0.15 mol/L) and NaOH (3.0 mol/L) was used. This bath presents molar ratio Cu^{2+}/Zn^{2+} equal to 0.4 and molar ratio EDTA/Cu^{2+} equal to 2.5. The influence of the rotation speed (0 – 1500 rpm) on the quality of the electrodeposits was evaluated, as well as the electrodeposition modes. The current densities applied to the galvanostatic tests were determined by the average of final values of the potentiostatic curves. The duration of the electrodepositions was 2.5 min, except in the charge density evaluation. Table 6 shows the conditions of the solutions tested in this section.

Table 6 - Conditions of the electrodeposition tests performed with the original bath.

Potentiostatic mode					
Cu^{2+} (M)	Zn^{2+} (M)	EDTA (M)	NaOH (M)	Potential (V)	Rotation speed (rpm)
0.06	0.14	0.15	3.0	-1.30, -1.35, -1.40, -1.45, -1.50	0, 500, 1000, 1500
Galvanostatic mode					
Cu^{2+} (M)	Zn^{2+} (M)	EDTA (M)	NaOH (M)	Current Density (mA/cm^2)	Rotation speed (rpm)
0.06	0.14	0.15	3.0	-3.2, -3.6, -4.0, -6.0, -15.1	0

Electrodeposition tests with 75 % (v/v) of the original bath and 25 % (v/v) of the concentrated solution obtained by the electrodialysis conducted in overlimiting condition were performed. This proportion was chosen based on the intermediate value tested by Scarazzato et al. (42) since they evaluated the addition of the concentrated solution from electrodialysis into the copper electroplating bath using proportions between 0-50%. Electrodepositions in potentiostatic (-1.3, -1.35, -1.4, -1.45, -1.5 V) and galvanostatic mode (-3.8, -4.2, -5.1 mA/cm²) were conducted. The current densities of the galvanostatic tests were also determined by the curves of the potentiostatic experiments.

Lastly, the concentration of EDTA, Cu^{2+} and Zn^{2+} ions in the solution obtained by the electrodialysis conducted in overlimiting condition was adjusted until reaching the concentration of the original bath. Electrodepositions with this adjusted bath were performed in potentiostatic (-1.4 V and -1.45 V) and galvanostatic mode (-4.0 and -6.0 mA/cm²).

After all the electrodeposition tests, the surface morphology of the deposits was investigated using scanning electron microscopy (SEM) and the composition of the deposits was analyzed using an energy dispersive X-ray analyzer (EDX) attached to the SEM.

5.   RESULTS AND DISCUSSION

5.1.   Topic I: Chronopotentiometric study for evaluating the effect of the membrane morphology on the transport properties of Cu(II) through a homogeneous and a heterogeneous ion-exchange membrane

5.1.1.   Visualization of the membranes structure

The structure of the HDX100 and PC-SK membranes was evaluated using an scanning electron microscope and as can be observed in Figure 18, the differences between the membranes are evident. The surface of HDX shows the presence of dispersed agglomerates of ion-exchange particles typical of heterogeneous membranes, whereas the SEM image of PC-SK shows a homogeneous and uniform braided structure.
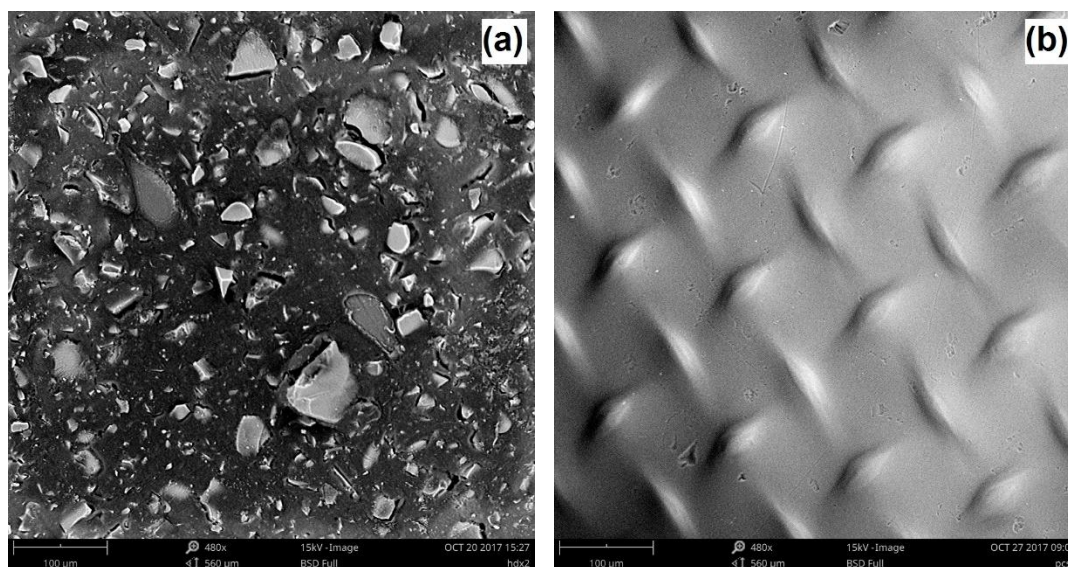
Figure 18 - SEM images of a) HDX100 and b) PC-SK membrane.

5.1.2.   Determination of fraction of conductive area of the membranes

The fraction of conductive area of the cation-exchange membranes was determined by constructing chronopotentiograms with a KCl solution together with the modified Sand's equation (Equation 13). For the determination of the transport number of K^+ ions in the solution (t_j), the equivalent conductivity

data (λ) was employed (154) and the value obtained was 0.491. For HDX and PC-SK, the permselectivity values used in Equation 18 were 0.9 and 0.93, respectively, which were provided by the suppliers (Table 1), and the $\overline{t_j}$ calculated for the membranes were 0.949 and 0.964.

With the $\overline{t_j}$ values, the KCl diffusion coefficient calculated using the Nernst-Einstein equation with the equivalent conductivity data ($D = 1.99\text{x}10^{-5}$ cm²/s) (154), and the linear slope between transition times (τ) and (C_0/i)² presented in Figure 19, the fraction of conductive area (ε) was finally calculated by Equation 13. The ε values obtained were 0.808 and 0.734 for the HDX and PC-SK membranes, respectively. The value of the former is in agreement with the literature, since Martí-Calatayud et al. (36) obtained the value of 0.804 for the same membrane.
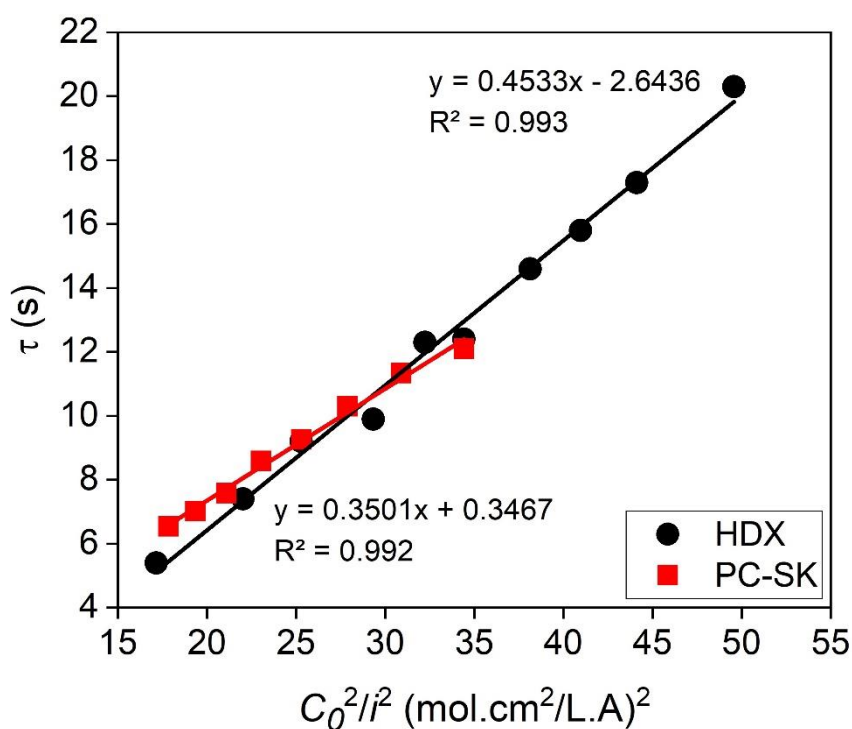
Figure 19 - Transition time (τ) as a function of (C_0/i)² for HDX and PC-SK membranes in contact with a KCl solution.

Although the fraction of conductive area is used for heterogeneous membranes, it can be also applied for homogeneous ones if it is considered as an effective parameter regulating some differences occurring between an ideal system and a real one. In general, the ε values of homogeneous membranes are

greater than of heterogeneous ones (36). In our study, the lower value of ε for PC-SK suggests that despite its homogeneity, its distance between the ideal and real conditions is greater and this may be explained by the preparation method of each membrane and their differences in the density of polymer network, the concentration of the fixed charges in the polymer, the water content, the thickness and ion exchange capacity (276). Moreover, according to Mikhaylin et al. (54), the membrane swelling characterized by the water uptake is the key factor of the ion transport, since when the water content increases, the membrane conductivity also increases and leads to larger conducting interstices and greater ion mobility across the membrane. According to the suppliers, PC-SK presents lower water content (9 %) than HDX100 (35-50 %), which can also affect the fraction of conductive area of PC-SK and the ions mobility.

5.1.3. Evaluation of chronopotentiometric curves of solutions with copper

Chronopotentiometric curves were constructed for the HDX100 and PC-SK membranes under application of some current densities. Figure 20 and Figure 21 show some curves obtained for the solution with 0.5 g Cu^{2+}/L and 2.0 g Cu^{2+}/L, respectively, sulfate/acid molar ratio of 1:1 and pH 3.
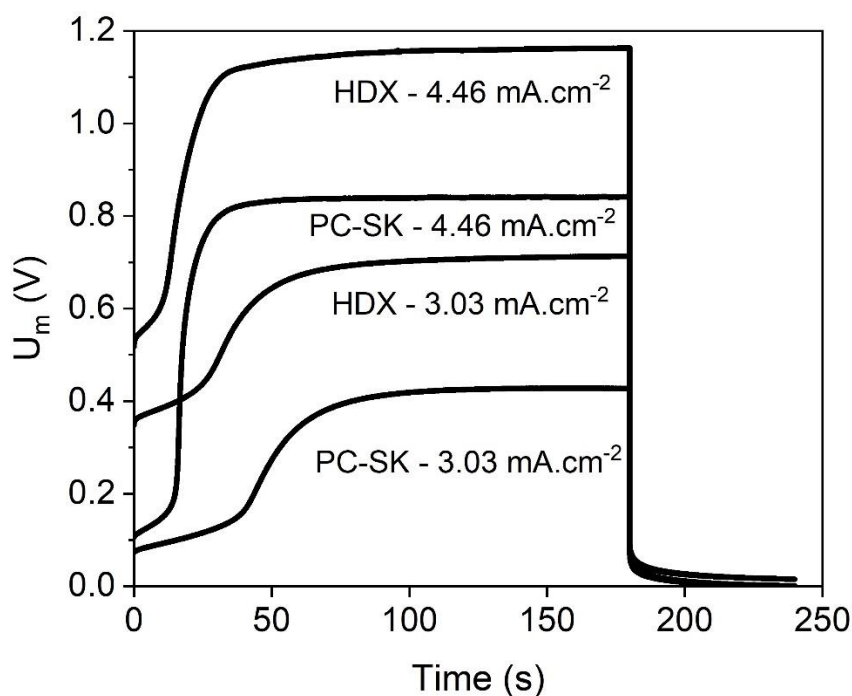
Figure 20 - Chronopotentiometric curves of a solution with 0.5 g/L of Cu^{2+} and pH 3.0 for HDX100 and PC-SK membranes.
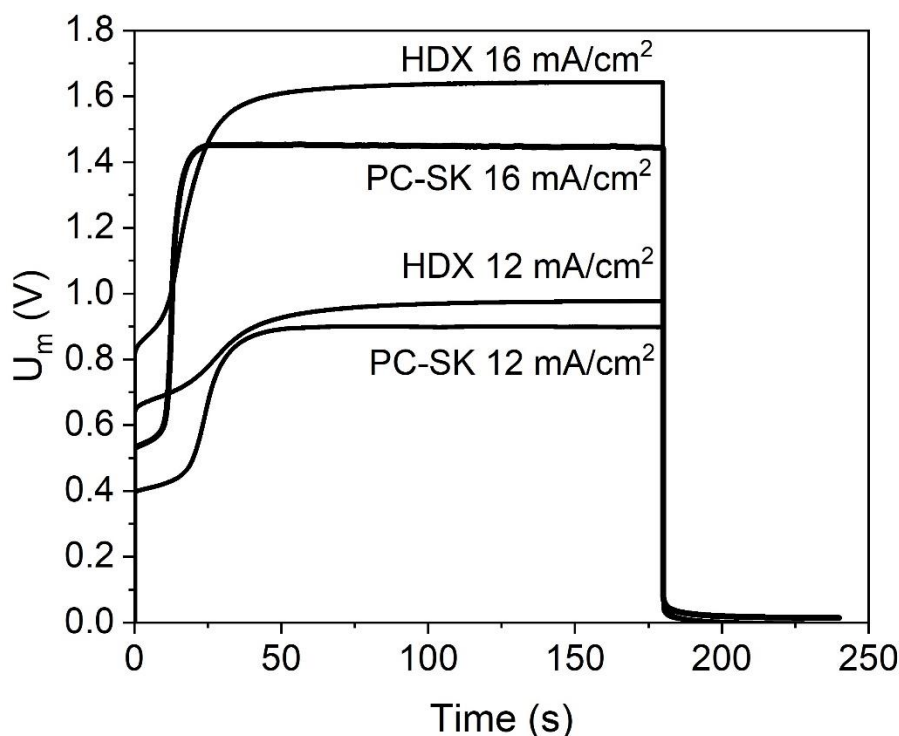
Figure 21 - Chronopotentiometric curves of a solution with 2.0 g/L of Cu^{2+} and pH 3.0 for HDX100 and PC-SK membranes.

Some differences between the curves can be noted. For both concentrations, the initial voltages of the membranes, or ohmic potential drops, are greater for HDX than for PC-SK at the same applied current density. This behavior is in accordance with the results of ohmic resistances that will be shown in the next section and, as will be discussed, this can be explained by the more tortuous counterion pathway caused by the heterogeneous structure of HDX. In general, differences in transition times in both solutions were subtle, which means the zero concentration of electrolyte at the surface of both membranes was reached virtually at the same time, under the same applied current density.

When the system reached a steady-state, where the voltage no longer varied with time, the curves of both membranes did not show oscillations typical of water splitting occurrence or electroconvection (55,211,257), since a linear behavior was obtained for all applied current densities. Hence, both membranes did not show differences in their behavior regarding the occurrence of overlimiting phenomena.

Differences in the behavior of the potential drop evolution with time can also be observed in the chronopotentiometric curves, especially when the lowest current densities were applied, since the increase in potential drop during

concentration polarization was very fast for the homogeneous membrane. This led to a sharp inflexion point of the PC-SK when the voltage began to be constant, whereas for the heterogeneous membrane it was smother. This behavior may be explained by the more irregular distribution of ion-exchange sites in the HDX membrane (36). The final voltage value for the same applied current density was higher with HDX than with PC-SK, which indicates that HDX has a higher electrical resistance (36).

The curves obtained were typical of a monopolar membrane, since they showed no additional inflexion point before the steady-state and when the current was switched-off. Hence, the curves did not suggest formation of precipitates even when the limiting current density was surpassed for both membranes. Speciation diagrams of solutions with Cu^{2+} concentrations of 0.1 g/L, 0.5 g/L, 1.0 g/L, 1.5 g/L, 2.0 g/L and sulfate/sulfuric acid molar ratio of 1:1 were constructed with the aid of *Hydra-Medusa* software (275) (not shown) and the molar concentration of the main ionic species in solution were obtained from the graphs. Table 7 presents the molar concentrations (in mmol/L) obtained for the most diluted (0.1 g Cu^{2+}/L) and concentrated solution (2.0 g Cu^{2+}/L) of Table 2.

Table 7 - Molar concentration of the main species in the solutions with 0.1 g Cu^{2+}/L and 2.0 g Cu^{2+}/L.

	Concentration of the species in mmol/L							
	Solution prepared with 0.1 g/L of Cu^{2+}							
Ionic species	pH 1	pH 2	pH 3	pH 4	pH 5	pH 6	pH 7	pH 8
H^+	95.28	9.46	1.00	0.10	0.01	0.00	0.00	0.00
HSO_4^-	2.69	1.36	0.23	0.02	0.00	0.00	0.00	0.00
Cu^{2+}	1.47	1.22	1.05	0.99	0.88	0.03	0.00	0.00
SO_4^{2-}	0.28	1.43	2.38	2.47	2.54	2.78	3.05	3.05
$CuSO_4$	0.08	0.34	0.51	0.52	0.46	0.02	0.00	0.00
	Solution prepared with 2.0 g/L of Cu^{2+}							
H^+	99.54	9.82	1.00	0.10	0.01	0.00	0.00	0.00
HSO_4^-	43.35	18.37	3.03	0.32	0.05	0.01	0.00	0.00
Cu^{2+}	16.22	6.10	4.06	3.71	0.32	0.01	0.00	0.00
SO_4^{2-}		4.43	19.23	31.77	33.42	47.64	52.97	52.97	61.09
$CuSO_4$	14.96	24.66	26.98	26.06	3.33	0.16	0.00	0.00

Besides the ionic species shown in Table 7, the presence of insoluble species was also verified in the speciation diagrams. For the diluted solution, the formation of the insoluble species $Cu_3(SO_4)(OH)_4$ and $Cu_4(SO_4)(OH)_6$ occurs at pH 5 and 6, respectively, while CuO is formed at pH 7 and 8. For the concentrated solution, $Cu_3(SO_4)(OH)_4$ and $Cu_4(SO_4)(OH)_6$ are formed at pH 5 and 6, while at pH 7 and 8 $Cu_4(SO_4)(OH)_6$ and CuO are formed, respectively. As observed in Figure 20 and Figure 21, even considering the precipitate formation, chronopotentiometric curves did not show additional inflexion points when overlimiting current densities were applied under all conditions tested.

The absence of additional inflexion points in the curves with cupric ions was also verified by Marder et al. (140), since the chronopotentiograms obtained by the authors were typical of monopolar membranes. Besides, Martí-Calatayud et al. (36) evaluated some transport properties of a $Fe_2(SO_4)_3$ solution with the same heterogeneous membrane tested here (HDX100) and also verified that, in some conditions, it did not show the second inflexion point typical of bipolar membranes, which appears when precipitates are formed on the membrane surface.

5.1.4. Evaluation of the CVC behavior for both membranes

Comparisons between the HDX and PC-SK membranes were also made by constructing current-voltage curves of both membranes (Figure 22) using a solution with 0.5 g Cu^{2+}/L and pH 3, for evaluating the differences regarding the limiting current density, plateau length, electric ohmic resistance and the behavior of the curves.
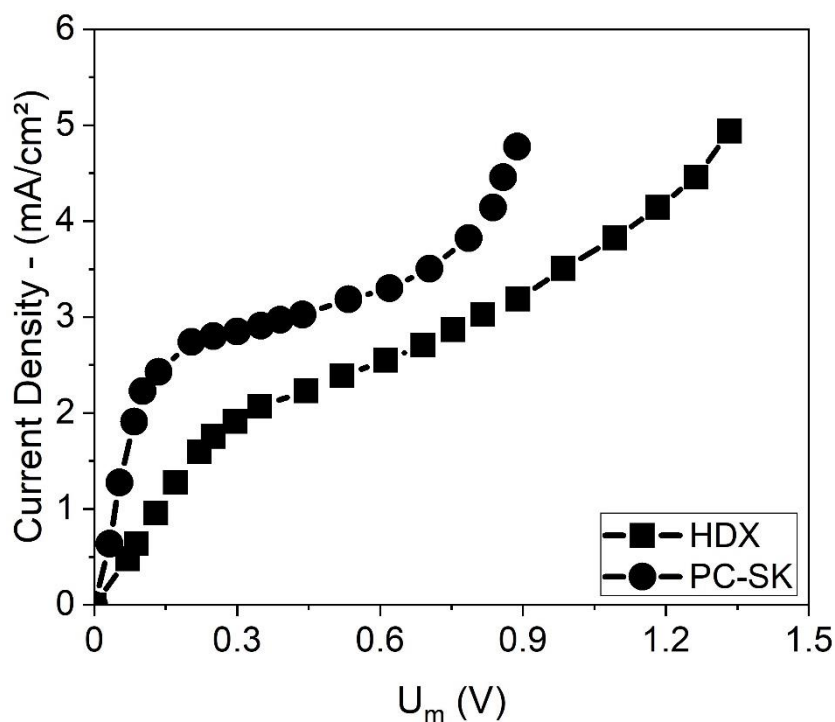
Figure 22 - CVC for a solution with 0.5 g Cu^{2+}/L and pH 3 for HDX and PC-SK membranes.

As observed in Figure 22, HDX100 showed lower limiting current density values than PC-SK, which is in accordance with the i_{lim} values of heterogeneous and homogeneous membranes determined by Volodina et al. (193). The heterogeneity of HDX membrane was responsible for a higher local current density through its conducting regions and, consequently, the interfacial electrolyte concentration at these regions was lower compared to the homogeneous PC-SK for the same applied current density. Besides, for compensating the difference between the interfacial concentration at the conducting and non-conducting regions of HDX, tangential diffusions occurred and were responsible for the slower growth of current density with the voltage compared to PC-SK (55), as shown in Figure 22. We can also observe that, for an applied current density, the voltage of HDX was higher than of PC-SK, which occurred due to the higher thickness and resistance of the former (55).

The plateau length of the HDX membrane showed lower values than the PC-SK in all conditions tested. Some authors (193,216) obtained higher values of plateau length for heterogeneous membranes than for homogeneous ones and attributed it to the nonuniform DBL thickness distribution and the consequent nonuniform current lines distribution. However, in our work, the plateau length

decreased with the increase of the fraction of conductive area, which was also observed by Marder et al. (140). Hence, the plateau length does not depend only on the membrane heterogeneity, but also on the distance between the ideal and the real system (ε).

As verified in Figure 22 and as will be shown further on, HDX showed higher ohmic resistance than PC-SK under all conditions assessed. This general trend may be explained by the heterogeneous surface of HDX and the more tortuous counterion pathway, since the presence of rich areas in inert binder hinders the connection between the conducting channels available for the copper transport (36,117,277). In heterogeneous membranes, the electrolyte diffusion from the bulk solution occurs in normal and tangential directions along the non-conductive regions, which enhances the resistance that the current faces to cross the membrane.

5.1.5. Effect of Cu^{2+} concentration on the transport properties across the membranes

The influence of copper concentration on the transport properties of the HDX100 and PC-SK cation-exchange membranes was evaluated by means of the construction of chronopotentiometric and current-voltage curves for solutions at pH 3 and Cu^{2+} concentrations of 0.1 g/L, 0.5 g/L, 1.0 g/L, 1.5 g/L and 2.0 g/L. Figure 23 shows the curves of limiting current density and ohmic resistance in function of Cu^{2+} concentration for both membranes.
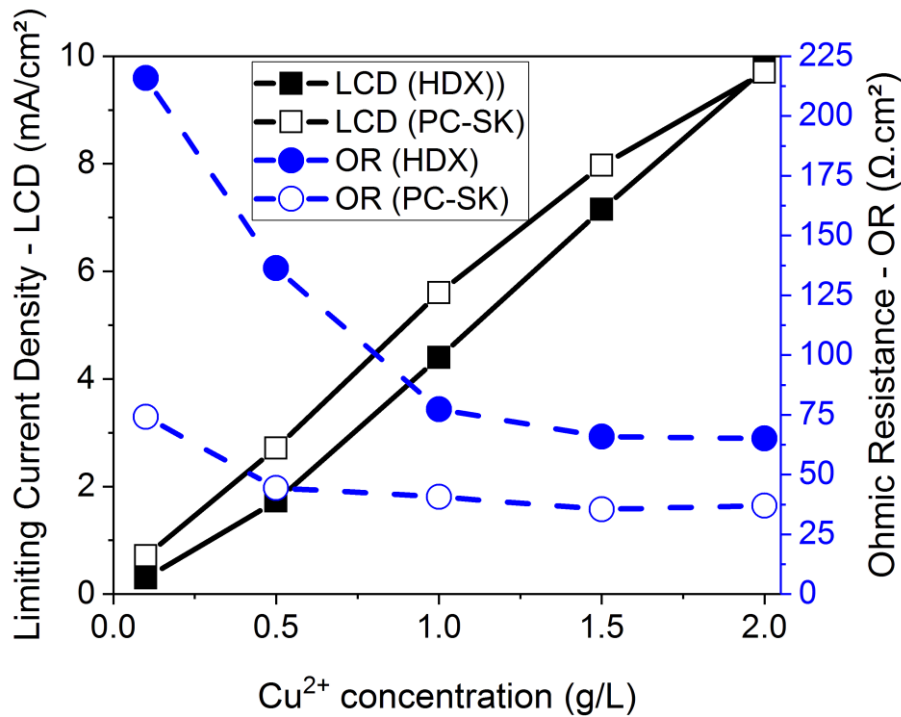
Figure 23 - Effect of Cu²⁺ concentration on the limiting current density and ohmic resistance at pH 3.0 for both membranes.

According to Figure 23, for the heterogeneous and the homogeneous membranes, the increase in Cu²⁺ concentration from 0.1 g/L to 2.0 g/L caused an increase in the limiting current density, which was also observed by other authors for other metals tested (57,143). This can be related to the proportional relationship between these variables in the classical concentration polarization theory (278), expressed by Equation 21:

$$i_{lim} = \frac{zAFC_0D}{\delta(\bar{t_i} - t_i)}$$
Equation 21

In Equation 21, δ is the thickness of the diffusion boundary layer, C_0 is the counterion concentration in the bulk solution, A is the membrane area, D is the electrolyte diffusion coefficient, z is the counterion charge, F is the Faraday's constant, $\bar{t_i}$ and t_i are the counterion transport number in the membrane and in the solution, respectively.

As shown in Figure 23, for the HDX and PC-SK membranes, the ohmic resistance decreased with the Cu²⁺ concentration increase. This decreasing behavior may be explained by the greater facility that ions face to escape from

the fixed charges of the membrane when they are in higher concentrations and the consequent contribution to a greater conductivity in the diffusion boundary layer, which leads to lower values of electric resistance (57,143). However, for concentrations above 0.5 g/L, the curve of PC-SK tended to be constant, while for HDX it continued decreasing.

Długołecki et al. (201) used electrochemical impedance spectroscopy to distinguish the three types of resistance involved in membrane processes: the pure membrane resistance, the resistance of the diffusion boundary layer and the resistance of the interfacial ionic charge transfer through the electric double layer. The authors verified that, in diluted solutions, the resistance of the DBL is dominant, whereas in concentrated solutions, the pure membrane resistance is the dominant one. Hence, when the increase in copper concentration did not lead to a decrease in the resistance, the membranes achieved a sufficiently high concentration of cupric ions at the conductive regions that made the DBL resistance insignificant, and with PC-SK this occurred before and more intensively than HDX due to their morphology differences. As showed, the homogeneous PC-SK presents 73.4 % of conductive area, whereas the heterogeneous HDX100 presents 80.8 %, which means the distribution of cations on their surfaces is different and as the copper concentration increases, the conductive regions of PC-SK presents a higher local concentration of cupric ions compared to HDX at a certain moment. This suggestion is in accordance with the work of Volodina et al. (193). They verified that the local limiting current density through conducting regions of heterogeneous membranes is several times higher than the average limiting current through the homogeneous membranes; consequently, the boundary concentration near the conducting regions of the heterogeneous membrane is smaller when compared to the homogeneous one. Besides, PC-SK presents lower water content (9 %) than HDX100 (35 % - 50 %), lower conductivity as a consequence of the lower water content (134) and lower ion-exchange capacity (1 meq/g) compared to HDX (2 meq/g), which disfavored the passage of cupric ions through the PC-SK and led to its higher boundary concentration, as mentioned above.

Figure 24 shows the curves of plateau length and transport number in the membrane in function of Cu^{2+} concentration for the PC-SK and HDX100.
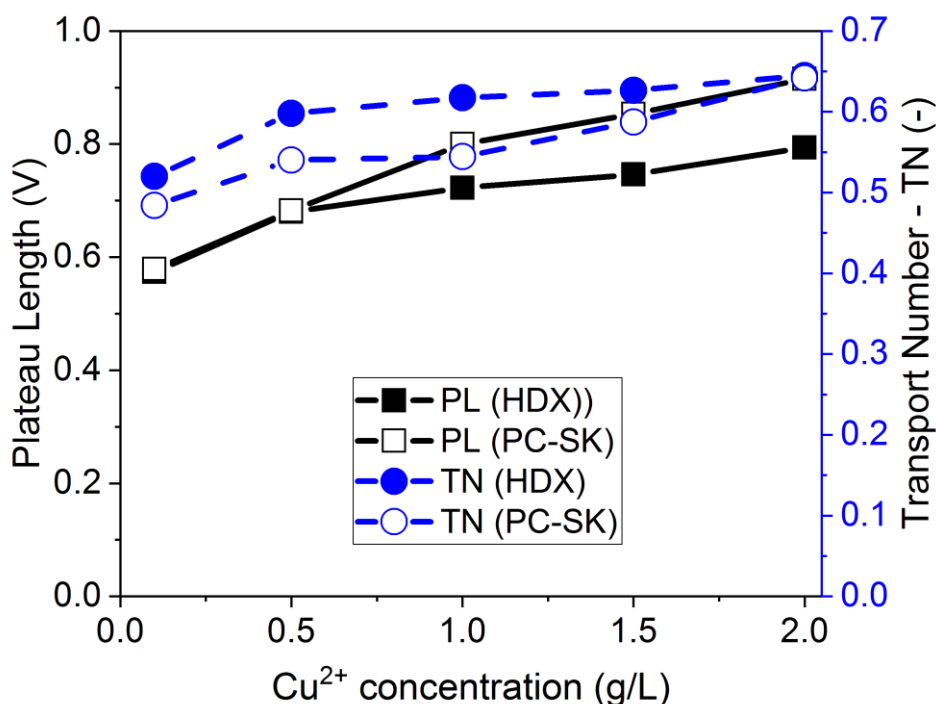
Figure 24 - Effect of Cu^{2+} concentration on the plateau lengh and transport number at pH 3.0 for both membranes.

According to Figure 24, the plateau length of HDX tended to be virtually constant with the Cu^{2+} increase whereas for PC-SK it increased, although some authors verified the contrary for other membranes and solutions (141,143). However, as showed by Ibanez et al. (216), the plateau length is not only related to the solution concentration, but also to the surface and heterogeneity of the membrane. Besides, Scarazzato et al. (198) determined the plateau length for some etidronic solutions using the anion-exchange membrane HDX200 and verified that the addition of KCl caused an increase in the plateau length because of the competition between Cl$^-$ and the anionic chelates, which present a greater molecular volume than Cl$^-$ ions. Here, the solution pH was adjusted by adding KOH and as the copper concentration increased, the volume of hydroxide added also increased until reaching pH 3. This may explain the increase in plateau length, since K$^+$ ions have smaller Stokes radius than Cu^{2+} (1.25 Å and 3.25 Å, respectively (279)) and smaller Péclet number, since the Péclet number is proportional to the ionic radius. According to Choi et al. (209), ions having smaller Stokes radius disfavor the intensity of electroconvection, which increases the plateau length.

Lastly, the relationship between copper concentration and its transport number in the membranes was evaluated. Although this property is generally reduced with increasing concentration, according to Figure 24, the transport number increased with the increase in the Cu^{2+} concentration. This result is in accordance with Martí-Calatayud et al. (143), who explained this behavior by the occurrence of electroconvection and the higher valence of metal ions than protons. In this case, the affinity of the ion-exchanging sites of the membrane for Cu^{2+} ions was enhanced with the increasing concentration of copper, which enhanced its transport number. We can also observe that the transport number values were lower than 0.7 for all copper concentrations tested, which is related to the competition between Cu^{2+}, H^+ and K^+ ions, since H^+ and K^+ are smaller than Cu^{2+} and tend to cross the membrane more easily due to their greater mobility (280) (D_{H^+} = 9.311x10^{-5} cm²/s; D_{K^+} = 1.957x10^{-5} cm²/s; $D_{Cu^{2+}}$ = 0.714x10^{-5} cm²/s (154)). Besides, as in diluted solutions the membrane behaves as an ideal cation-exchange (281), we can suggest that the increase in the electrolyte concentration caused a failure in Donnan exclusion and allowed the invasion of co-ions (SO_4^{2-}) through the membrane. According to Figure 24, the transport number of PC-SK was lower than HDX in all conditions tested, which may be explained by the higher value of water content and fraction of conductive regions of HDX compared to PC-SK, besides its higher thickness (282).

5.1.6. Evaluation of chronopotentiograms of both membranes with a more concentrated solution

Chronopotentiometric curves were constructed for a more concentrated solution with 5.0 g Cu^{2+}/L, pH 3 and molar ratio of sulfate/acid of 1:1 for verifying if the solutions tested herein do not form precipitate regardless of concentration, since Marder et al. (140) did not verify precipitate formation with copper solutions. The CVC of this membrane system was also constructed (not shown) and the limiting current density was determined. Figure 25 presents chronopotentiometric curves obtained for both membranes when applied 33.4 mA/cm², which is an overlimiting current for both membranes.
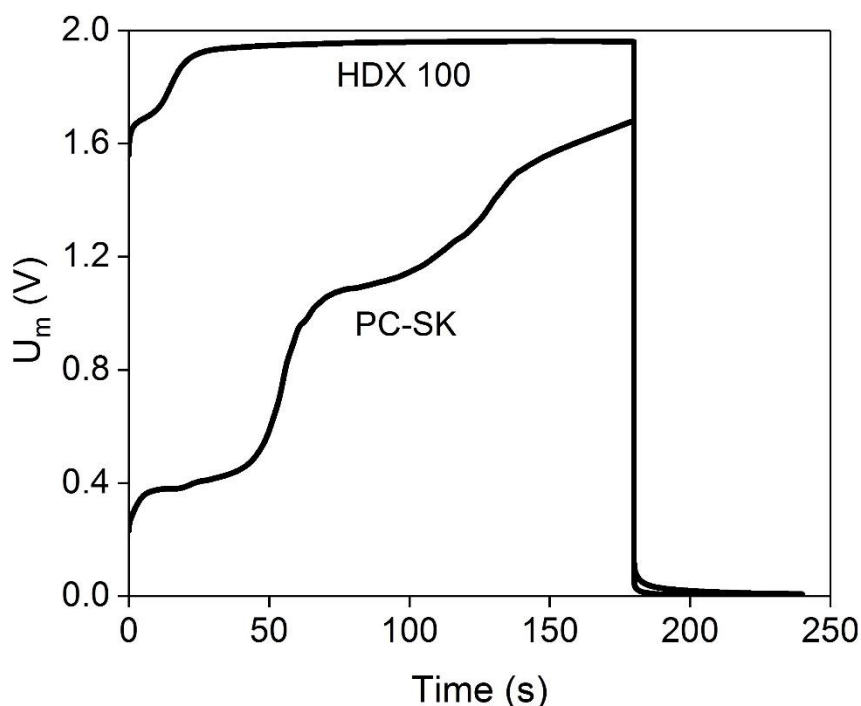
Figure 25 - Chonopotentiometric curve of HDX and PC-SK membranes for a solution with 5.0 g Cu^{2+}/L, pH 3.0, under application of 33.4 mA/cm².

According to Figure 25, when a current density of 33.4 mA/cm² was applied, the HDX membrane did not show additional inflexion points in the chronopotentiometric curve even with the solution more concentrated in copper, whereas the PC-SK clearly showed it. Besides, the PC-SK membrane did not achieve a steady-state condition before the relaxation of the membrane system since the voltage continued increasing after the second inflexion point. This behavior occurred due to the recombination of the products from water splitting and the blockage of the interstices of PC-SK by the precipitate formed, turning it into non-conductive areas (36). This difference in the membranes behavior may be explained by the achievement of a greater local concentration of cupric ions at the conductive regions of PC-SK compared to HDX. Besides the homogeneity of PC-SK, its lower fraction of conductive area, water content and ion-exchange capacity than HDX led to its greater tendency to form precipitate. In this case, the local concentration of Cu^{2+} at the conductive regions of PC-SK was high enough to form the insoluble species on its surface.

At the end of the experiments, a blue solid material could be seen at the anodic surface of PC-SK effectively in contact with the solution, which

corresponded to the precipitate that caused the additional inflexion point in the chronopotentiometric curve. In turn, although the precipitate may have been formed inside the HDX, there was no solid material on its surface at the end of the experiment, which is in accordance with its chronopotentiogram in Figure 25. Figure 26 shows the membranes before and after the chronopotentiometric experiments conducted with the solution with 5 g Cu^{2+}/L and pH 3.
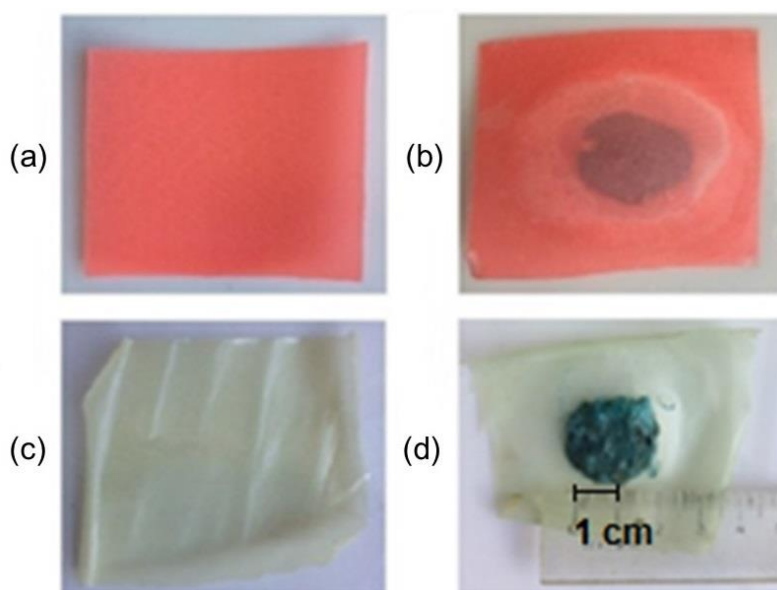
Figure 26 - HDX100 (a,b) and PC-SK (c,d) membranes before and after, respectively, the chronopotentiometric experiments for a concentrated solution.

At the end of the experiments, the pH of the bulk solution in the anodic side compartment of the cation-exchange membranes was measured. For the HDX, the final pH was 3.3, whereas for PC-SK it was 4.2. This difference in pH confirms the behavior of the chronopotentiogram regarding the precipitate shown in Figure 26, since intense water splitting occurred at the PC-SK. As H^+ ions tended to pass intensively through the PC-SK and co-ions tended to be excluded from the membrane, OH^- ions accumulated at the anodic surface and caused an increase in pH at the diffusion boundary layer (172,283). Although the precipitate is formed at pH above 5, as verified in section 5.1.3, when PC-SK was used, the pH at its diffusion boundary layer must have achieved a higher value than the pH of the bulk solution, since the precipitate was formed at its surface.

For the determination of the precipitate formed, a speciation diagram for the solution with 5.0 g Cu^{2+}/L was constructed (not shown) with the aid of

Hydra-Medusa software. According to the curves, the precipitate visually observed on the PC-SK membrane at the end of the chronopotentiometric experiments was $Cu_3SO_4(OH)_4$, $Cu_4(SO_4)(OH)_6$ or CuO, This may be explained by the intense pH variation at the depleted diffusion layer adjacent to the CEM as a result of water splitting and the rapid H^+ transport through the membrane, which increased the concentration of hydroxyl ions at the interface.

5.1.7. Conclusions

Transport properties of cupric ions across the heterogeneous HDX100 and homogeneous PC-SK membrane were determined, by chronopotentiometry, and the behavior of their chronopotentiometric and current-voltage curves were evaluated in function of the solution concentration and the membranes morphology.

Differences between the membranes virtually did not cause changes in the behavior of the limiting current density and transport number with the Cu^{2+} increasing. However, a non-expected increase in plateau length was verified as the concentration increased and this may be related to the membranes surface and to the presence of K^+ ions from the KOH added for the pH adjustment.

The ohmic resistance decreased as the concentration increased and, at a certain moment, it tended to be constant. However, for PC-SK the resistance tended to be constant from 0.5 g Cu^{2+}/L, whereas for HDX this occurred from 1.0 g Cu^{2+}/L. This difference regarding the ohmic resistance was related to the homogeneity of PC-SK and the higher boundary concentration at its conductive regions compared to the heterogeneous HDX100, besides its lower fraction of conductive region, lower water uptake, lower conductivity and lower ion-exchange capacity. Experiments with a concentrated solution (5.0 g Cu^{2+}/L) were also conducted and the chronopotentiometric curves showed an additional inflection point typical of bipolar membranes only with PC-SK. This occurred due to the formation of a precipitate, which was confirmed by the visualization of a solid blue material at the surface of PC-SK at the end of the chronopotentiometric experiments.

Since the characteristics of the cation-exchange membrane HDX100 and the anion-exchange HDX200 are very similar (Table 1), besides the lower

tendency of HDX100 to form precipitates at its surface than PC-SK, in the next topics of the thesis, only the heterogeneous HDX200 was used as anion-exchange membrane.

5.2. Topic II: Chronopotentiometric study for evaluating the transport properties of the anion-exchange membrane used in the treatment of the synthetic cyanide-free wastewater from brass electrodeposition

For understanding the influence of the ionic species present in all the solutions assessed in this topic (Table 3) on the membrane properties, the reactions of the species and their stability constants were obtained from the database of the *Hydra-Medusa* software (275). They are present in Equations (A1) – (A52) in Appendix.

As shown in Appendix, the use of EDTA as complexing agent involves many soluble and insoluble species formed with Cu^{2+}, Zn^{2+}, SO_4^{2-} from the sulfates and Na^+ from the NaOH used for the pH adjustment. As the pH of the solution in the chronopotentiometric system varies mainly at the interface of membrane/solution due to the transport of H^+ through the CEM and OH^- through the AEM, speciation diagrams were constructed with the aid of the *Hydra-Medusa* software for the initial composition of solutions I-IX (Table 3); the molar concentration of the main ionic species were obtained from the curves. The results are present in Table 8, where the anionic equivalent charge of the solutions is also expressed, which was calculated by the product of the concentration (C_j) of the anionic species and their charge (z_i), as expressed by Equation 22.

$$Q_{eq}^- = \sum |z_j| C_j$$

Equation 22

Table 8 - Molar concentration of the main ionic species in the initial composition of solutions I - IX.

	Concentration in mmol/L								
	I	II	III	IV	V	VI	VII	VIII	IX
Working Solution									
Cu^{2+}	1.00	1.00	1.00	1.00	0.60	1.40	1.00	1.00	1.00
Zn^{2+}	1.00	1.00	1.00	1.00	1.40	0.60	1.00	1.00	1.00
EDTA	2.50	2.50	2.50	2.50	1.50	3.50	2.00	3.00	3.50
Na^+	3.89	4.12	4.43	11.81	3.50	4.66	4.27	3.42	5.05
pH	9	10	11	12	10	10	10	10	10
Main ionic species in equilibrium									
OH^-	0.01	0.10	1.00	9.82	0.10	0.10	0.10	0.10	0.10
Na^+	3.45	3.80	4.05	10.99	3.39	4.31	4.13	3.28	4.71
SO_4^{2-}	1.85	1.89	1.94	1.83	1.91	1.91	1.90	1.95	1.94
$NaSO_4^-$	0.04	0.04	0.04	0.11	0.03	0.04	0.04	0.03	0.05
$Na(EDTA)^{3-}$	0.01	0.06	0.24	0.43	0.00	0.19	0.00	0.10	0.21
$EDTA^{4-}$	0.00	0.02	0.09	0.06	0.00	0.07	0.00	0.05	0.07
$HEDTA^{3-}$	0.46	0.41	0.16	0.01	0.00	1.21	0.00	0.83	1.19
$Zn(EDTA)^{2-}$	1.00	1.00	0.97	0.75	1.30	0.59	0.99	1.00	0.99
$Cu(EDTA)^{2-}$	1.00	0.99	0.92	0.53	0.15	1.36	0.99	0.99	0.99
$Zn(EDTA)OH^{3-}$	0.00	0.00	0.03	0.22	0.00	0.00	0.00	0.00	0.00
$Cu(EDTA)OH^{3-}$	0.00	0.01	0.08	0.46	0.00	0.01	0.01	0.01	0.01
Anionic equivalent charge (meq/L)									
Q^-_{eq}	9.16	9.42	10.60	19.77	6.85	12.38	7.91	11.01	12.51

As the objective of the electrodialysis is to extract and to recover Cu^{2+}, Zn^{2+} and EDTA present in the wastewater from the brass electrodeposition, the mole fraction of the soluble complexes with Cu^{2+} (x_{Cu}) was calculated by Equation 23, with Zn^{2+} (x_{Zn}) by Equation 24, and the mole fraction of the free species and complexes that involve these three components ($x_{Cu,Zn,EDTA}$) by Equation 25 using data of Table 8.

$$x_{Cu} = \frac{n_{CuEDTA^{2-}} + n_{CuEDTAOH^{3-}}}{n_t} * 100 \qquad \text{Equation 23}$$

$$x_{Zn} = \frac{n_{ZnEDTA^{2-}} + n_{ZnEDTAOH^{3-}}}{n_t} * 100 \qquad \text{Equation 24}$$

$$x_{Cu,Zn,EDTA} = \frac{\begin{array}{c} n_{NaEDTA^{3-}} + n_{EDTA^{4-}} + n_{HEDTA^{3-}} + n_{ZnEDTA^{2-}} + \\ n_{CuEDTA^{2-}} + n_{Zn(EDTA)OH^{3-}} + n_{CuEDTA^{2-}} \end{array}}{n_t} * 100 \qquad \text{Equation 25}$$

In Equation 23-Equation 25, n_j represents the number of moles of species j and n_T represents the total number of moles present in each solution. Table 9 presents the results of the mole fractions (x_{Cu}, x_{Zn} and $x_{Cu,Zn,EDTA}$) for solutions I-IX.

Table 9 - Mole fraction of the anionic soluble species and complexes with Cu^{2+}, Zn^{2+} and EDTA in solutions I - IX.

	Mole fraction (%) in solutions I – IX								
	I	II	III	IV	V	VI	VII	VIII	IX
x_{Cu} (%)	12.8	12.0	10.5	3.9	2.0	14.0	12.2	12.0	9.7
x_{Zn} (%)	12.8	12.0	10.5	3.9	17.6	6.0	12.2	12.0	9.7
$x_{Cu,Zn,EDTA}$ (%)	31.6	29.9	26.2	9.8	19.7	35.0	24.5	35.7	33.8

5.2.1. Effect of pH

Figure 27 was constructed with data on the initial concentrations of the main ionic species in solution I (pH 9), II (pH 10), III (pH 11) and IV (pH 12) present in Table 8.

As verified, the pH increase caused an increase in the concentration of the complexes $Zn(EDTA)OH^{3-}$ and $Cu(EDTA)OH^{3-}$ and a decrease of the complexes $Zn(EDTA)^{2-}$ and $Cu(EDTA)^{2-}$, which is very advantageous for the ionic separation since the attraction of ions towards the exchange sites of opposite polarity increases with the increase of the charge of the ion (280,284). The

concentration of Na(EDTA)$^{3-}$ species also increased with the solution pH, whereas an opposite behavior occurred for HEDTA^{3-} species.
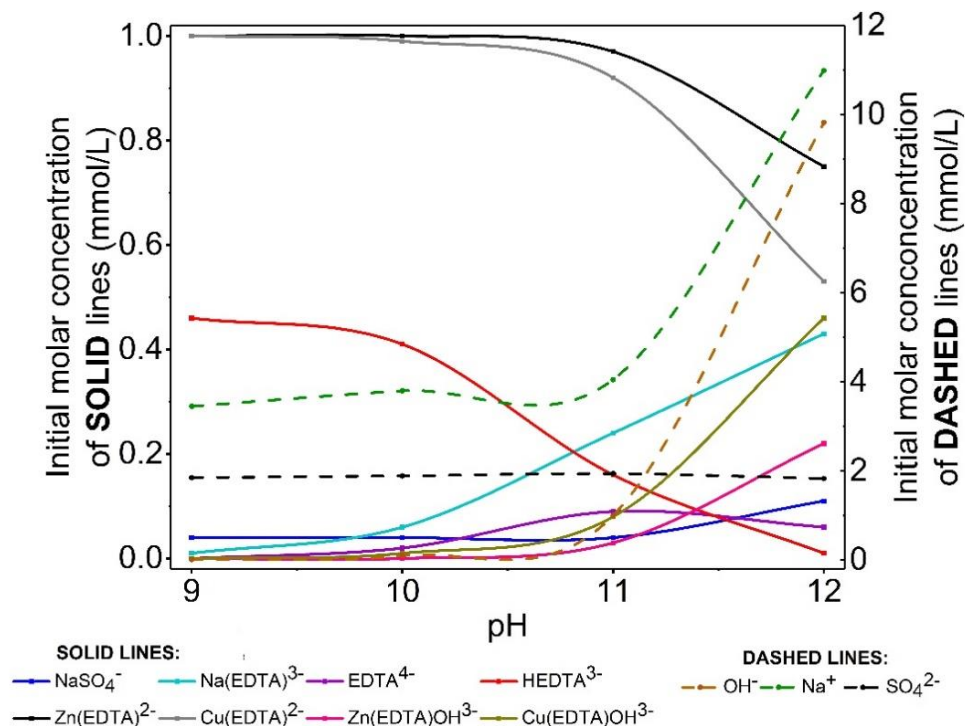
Figure 27 - Initial molar concentration of the main ionic species in solution I (pH 9), II (pH 10), III (pH 11) and IV (pH 12).

Current-voltage and chronopotentiometric curves under 0.64 mA/cm² for solutions I - IV were constructed for verifying the influence of pH on the properties of the membrane. Figure 28 and Figure 29 present the curves obtained and Table 10 presents the values of limiting current density, electric ohmic resistance and plateau length for each solution.
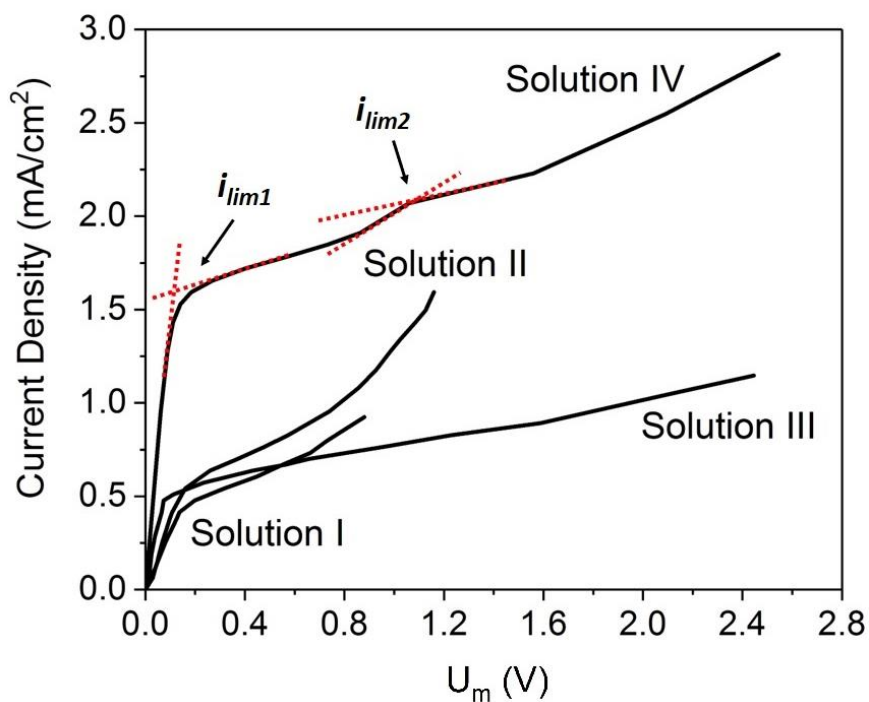
Figure 28 - Current-voltage curves for solutions I (pH 9), II (pH 10), III (pH 11) and IV (pH 12).
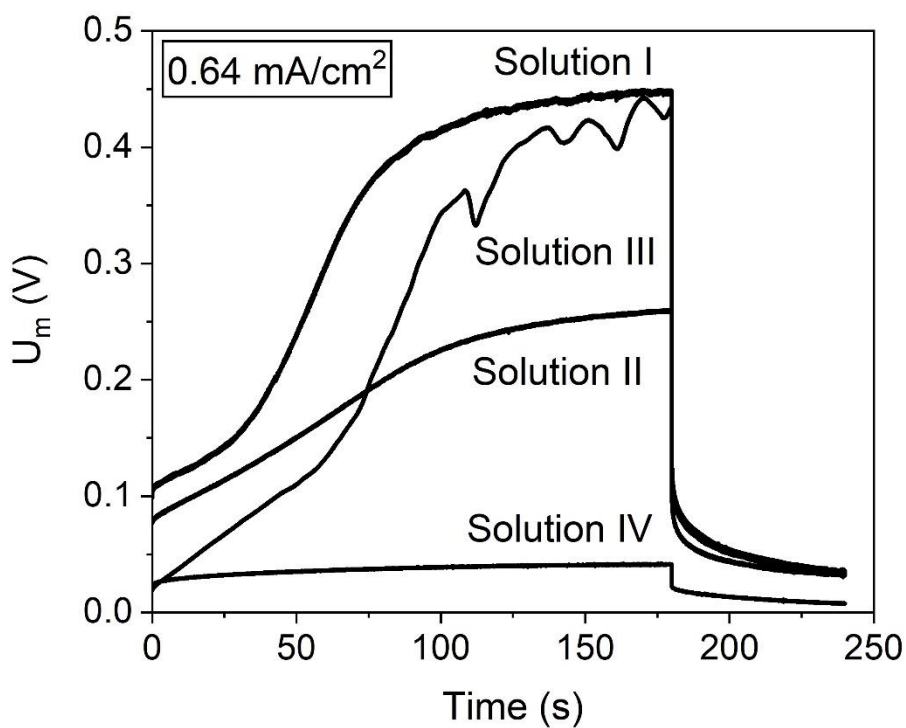
Figure 29 - Chronopotentiometric curves for solutions I (pH 9), II (pH 10), III (pH 11) and IV (pH 12) under 0.64 mA/cm².

Table 10 - Limiting current density, ohmic resistance and plateau length for solutions I (pH 9) – IV (pH 12).

Evaluation	Sol.	pH	Cu^{2+}/Zn^{2+}	$EDTA/Cu^{2+}$	Limiting current density (mA/cm²)	Ohmic resistance ($\Omega.cm^2$)	Plateau length (V)
pH	I	9	1.0	2.5	0.45	320.1	0.5
	II	10	1.0	2.5	0.54	225.6	0.6
	III	11	1.0	2.5	0.56	155.7	-
	IV	12	1.0	2.5	1.59 (i_{lim1}) 2.07 (i_{lim2})	68.0	1.4

According to Figure 28, the increase in pH from 9 to 12 caused some alterations in the shape of the current-voltage curves. Typical CVCs with the three regions clearly defined were obtained with solutions I-II. In the curve of solution III, the third region was not well defined, whereas the curve IV presented two limiting current densities. These differences between the curves are related to the differences regarding the change of diffusion and migration as the main mechanisms of mass transfer to overlimiting mechanisms. This is because plateau length is related to the energy required to overcome the diffusion layer and favor, for example, electroconvection and water splitting (285). As observed in Figure 27/Table 8 the concentrations of the main anionic species present in solutions I and II are very similar (SO_4^{2-}, $Zn(EDTA)^{2-}$, $Cu(EDTA)^{2-}$ and $HEDTA^{3-}$), which explains the similar typical CVC obtained only for these two solutions.

According to Figure 29, the chronopotentiometric curves for solutions I and II were also typical of monopolar membranes and did not show unexpected behaviors (140). Concerning the transport properties calculated, Table 10 shows that when the pH was increased from 9 (Sol. I) to 10 (Sol. II), the limiting current density enhanced by 20 % mainly due to the increase in the concentration of hydroxyl ions (900 %), since the other compounds did not vary so expressively (Figure 27/Table 8). This behavior is consistent, since the anionic equivalent charge also increased and when more anionic ions are in solution, the ionic depletion in the diffusion boundary layer is more difficult to occur. The plateau length was also increased by 20 %, which means OH^- ions enhanced the energy required to change the diffusion mechanism to electroconvection in this

pH range. Choi et al. (209) verified that the plateau length increases with the decrease of the Péclet number, which is proportional to the Stokes radius of a given ion. Hence, the higher concentration of OH^- and its smaller Stokes radius enhanced the energy required to destroy the diffusion boundary layer. Similar results were obtained by other authors that evaluated the influence of the increase in H^+ concentration on the plateau length of CEMs (53).

When pH was increased from 10 (Sol. II) to 11 (Sol. III), the limiting current density was not affected, since despite the increase of OH^- ions (900 %), $Na(EDTA)^{3-}$ (300 %) and $EDTA^{4-}$ (350 %) (Figure 27/Table 8), the concentration of $HEDTA^{3-}$, $Cu(EDTA)^{2-}$ and $Zn(EDTA)^{2-}$ decreased. As will be shown further on, complexes with copper and zinc seem to have greater influence on the membrane properties than the free species or complexes without the metals. For solution III, the CVC (Figure 28) obtained did not show the third region, since after the achievement of the limiting current density, the curve presented a continuous plateau that did not suggest a change in the type of transport mechanism, which hindered the determination of the plateau length. This anomalous shape of the CVC may be explained by the increase in the concentration of OH^- ions and their transport by the Grotthus mechanism. In this case, hydroxyl ions carry the charge by "tunnelling" from one water molecule to another without bringing liquid volume into motion. Hence, this mechanism hinders the occurrence of electroconvection and alters the behavior of the plateau length (143,257). The chronopotentiometric curve of the solution at pH 11 (Figure 29) also presented a non-expected behavior, since oscillations with an increase in the potential drop was verified during the concentration polarization. This may have occurred due to the formation of a precipitate at the membrane, since ion transfer is a dynamic process, in which the concentration and pH vary especially at the membrane surface. Hence, the faster transport of OH^- ions compared to the complexes may have been responsible for an accumulation of H^+ ions on the boundary layer, which caused a decrease in the pH on the cathodic side of the membrane and led to the formation of a precipitate.

For the pH increase from 11 (Sol. III) to 12 (Sol. IV), an increase of 184 % was verified in the limiting current density. Despite the reduction of $HEDTA^{3-}$ of 94 %, and the reduction of $Cu(EDTA)^{2-}$ of 42 %, this increase in the limiting current density occurred mainly due to the increase of $Cu(EDTA)OH^{3-}$ (475 %),

Zn(EDTA)OH^{3-} (633 %) and OH$^-$ (882 %) (Figure 27/Table 8). Under pH 12 (Sol IV), another unexpected behavior in the CVC was observed, since after the first inflexion point related to the limiting current density (i_{lim1}), the curve achieved a plateau zone and then showed another inflexion point (i_{lim2}) before reaching the third region. The presence of two inflexion points in the CVC was also observed by Pismenskaya et al. (196) with weak-electrolyte anions through anion-exchange membranes and by Martí-Calatayud et al. (172) for a diluted solution of Cr$_2$(SO$_4$)$_3$, which was attributed to the change of the prevailing species that crossed the membrane as the current density was increased. According to Figure 27/Table 8, the prevailing negatively charged species in solution IV are OH$^-$ (9.82 mmol/L), SO$_4^{2-}$ (1.83 mmol/L) and Zn(EDTA)$^{2-}$ (0.75 mmol/L). Hence, considering the initial composition of solution IV, we can infer that OH$^-$ ions were intensively transferred across the membrane under the lowest applied current densities, due to their greater concentration and smaller Stokes radius than the other species. When the first limiting current density was reached, the depletion of hydroxyl ions occurred at the DBL. Then, the applied current density was increased and the other species in solution, such as SO$_4^{2-}$ and Zn(EDTA)$^{2-}$, were depleted at the DBL, leading to the second limiting current density. Note that the difference between the values of i_{lim1} and i_{lim2} is 0.48 mA/cm², which is within the same order of magnitude of the i_{lim} of the other solutions shown in Table 10. According to Table 8, the concentrations of the species in solution did not show changes in the same order of OH$^-$ when the pH was increased to 12. Hence, this supports that i_{lim1} appeared due to the depletion of OH$^-$ ions, whereas i_{lim2} appeared due to the depletion of the other ionic species.

The plateau length was enhanced in solution IV due to the presence of Zn(EDTA)OH^{3-} and Cu(EDTA)OH^{3-}. Hence, more energy was required to change the diffusion as the main transport mechanism to electroconvection with these species in solution. The increase in plateau length with the anionic equivalent charge was also verified (Table 8) and this is in agreement with the results obtained by Scarazzato et al. (198). The authors also observed that the plateau length was reduced when the Péclet number increased and they related it to the tendency of ions with larger Stokes radius (and higher Péclet number) to activate overlimiting mechanisms earlier. Here, according to Figure 27/Table 8 and Table 10, the plateau length increased with the increase of the complexes with

higher Stokes radius [Zn(EDTA)OH^{3-}, Cu(EDTA)OH^{3-} and Na(EDTA)$^{3-}$] compared to the complexes that decreased with the pH increase [Zn(EDTA)$^{2-}$, Cu(EDTA)$^{2-}$ and HEDTA^{2-}]. However, according to Table 8, the concentration of OH$^-$ ions was more than 10 times greater than the complexes in solution IV. Considering its molar concentration, its Stokes radius lower than the other species and its transport by the Grotthus mechanism, these ions may have been responsible for the increase in plateau length. This suggestion is supported by the analysis of solutions I and II, since the molar concentration of OH$^-$ is equal or lower than the other anionic species; the plateau length did not show an expressive variation in these two solutions if compared to solution IV.

As the current density of Figure 29 was lower than the i_{lim} of the membrane system with solution IV, its ChP did not show an increase in the potential drop, since intense concentration polarization did not occur. In this case, the registered voltage was only due to the ohmic drop and the resistance of the membrane. Figure 30 presents chronopotentiograms for the solution IV under two overlimiting current densities. As verified, the behavior of the curves is in accordance with its CVC with two limiting current densities, since the ChP under 2.2 mA/cm² and 2.5 mA/cm² presented an additional inflexion point related to a second transition time.
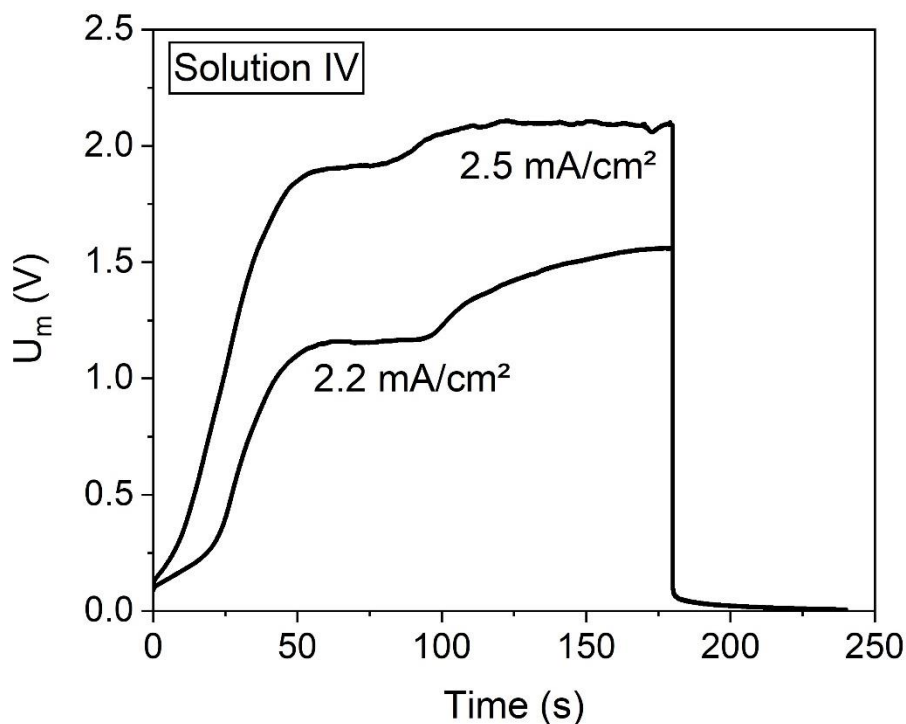
Figure 30 - Chronopotentiometric curves for solution IV under 2.2 mA/cm² and 2.5 mA/cm².

The same behavior on ChPs was observed by Scarazzato et al. (198) for a solution with Cu^{2+} ions and etidronic acid (HEDP). They attributed the first inflexion point to the transport of $HHEDP^{3-}$ and the second one to the $[CuHEDP]^{2-}$ because of the preferential transport of hydroxyl ions through the AEM and a consequent pH change on the membrane surface. In our work, the same discussion of the CVC for the solution IV is valid for its ChP, which means the first transition time occurred because of the depletion of OH^- ions in the boundary layer and the second transition time was due to the transport of the other species, such as SO_4^{2-} and $Zn(EDTA)^{2-}$.

Finally, the ohmic resistance was also determined for each pH condition. According to the results shown in Table 10, it decreased with the pH increase from 9 to 12 (320.1 $\Omega.cm^2$ to 68 $\Omega.cm^2$, respectively) due to the increase of the solution conductivity (Table 3) and the facility that ions faced to cross the membrane (46,57). The ohmic resistance also decreased with the increase of the anionic equivalent charge; this can be explained by the tendency of ions to escape from the fixed charges more easily when they are in greater concentrations and by the higher conductivity in the diffusion boundary layer (57,143). However, in electrodialysis, increasing the solution pH may disfavor the zinc, copper and EDTA transport through the AEM due to the competition between complexes and OH^-, since hydroxyl ions are smaller than the anionic complexes and present greater mobility. This competition between the species can also be seen in Table 9. The fraction of soluble compounds decreased from 12.8 % to 3.9 % (those with copper and zinc) and from 31.6 % to 9.8 % (those with EDTA) when pH was increased from 9 to 12, which occurred mainly because of the OH^- from the hydroxide used for the pH adjustment. Hence, at pH 12, the energy required for the ionic separation is mainly used for transporting hydroxyl ions and not for extracting metals and EDTA.

5.2.2.   Effect of the Cu^{2+}/Zn^{2+} molar ratio

The influence of the fraction of copper and zinc ions present in the solution on the membrane properties was also evaluated. Solutions with Cu^{2+}/Zn^{2+} molar ratios of 0.4, 1.0 and 2.3 were assessed. For all solutions tested, the $EDTA/Cu^{2+}$ molar ratio was 2.5 and the pH 10. Figure 31 was constructed with data from

Table 8 and presents the initial molar composition of the solutions with Cu^{2+}/Zn^{2+} molar ratio of 0.4 (Sol V), 1.0 (Sol II) and 2.3 (Sol VI). Table 11 presents the results of limiting current density, ohmic resistance and plateau length.
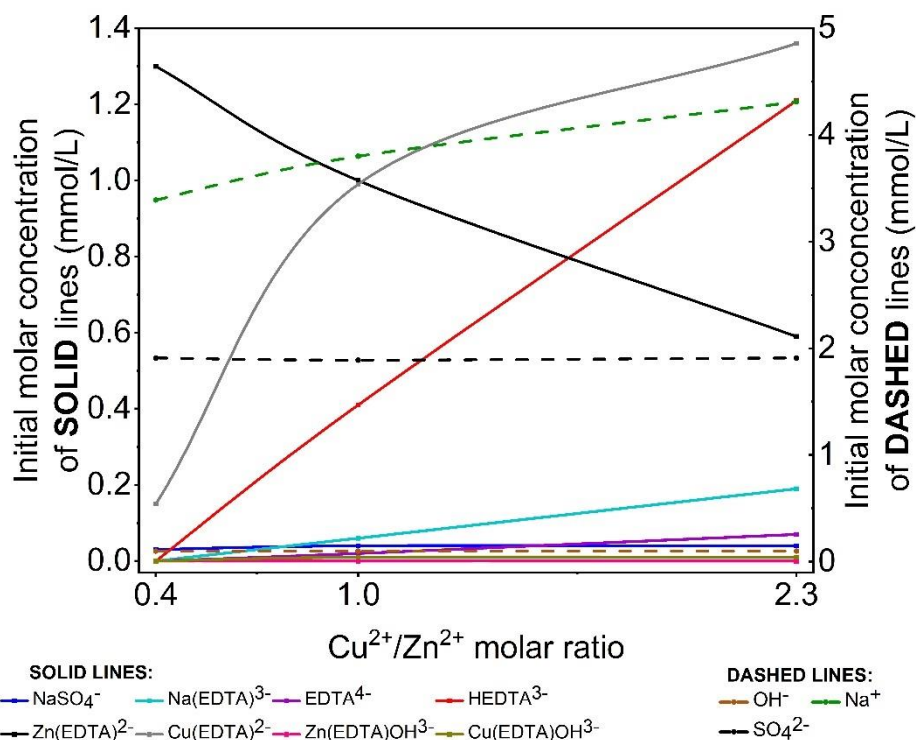
Figure 31 - Initial molar concentration of the main ionic species in solution V (Cu^{2+}/Zn^{2+} of 0.4), II (Cu^{2+}/Zn^{2+} of 1.0) and VI (Cu^{2+}/Zn^{2+} of 2.3).

Table 11 - Limiting current density, ohmic resistance and plateau length in Cu^{2+}/Zn^{2+} molar ratios of 0.4, 1.0 and 2.3.

Evaluation	Sol.	pH	Cu^{2+}/Zn^{2+}	$EDTA/Cu^{2+}$	Limiting current density (mA/cm²)	Ohmic resistance (Ω.cm²)	Plateau length (V)
	V	10	0.4	2.5	0.27	235.3	
Cu^{2+}/Zn^{2+}	II	10	1.0	2.5	0.54	225.6	0.6
	VI	10	2.3	2.5	0.76	231.3	0.7

According to Table 11, the limiting current density was enhanced as the Cu^{2+}/Zn^{2+} molar ratio increased. When Cu^{2+}/Zn^{2+} increased from 0.4 to 1.0, the increase in limiting current density was of 100 % due to the increase of $Cu(EDTA)^{2-}$ of 560 % and the formation of $HEDTA^{3-}$ in higher concentration than

the other species (Figure 31/Table 8). When Cu^{2+}/Zn^{2+} was increased from 1.0 to 2.3, the limiting current density was increased by 40.7 % with the increase in the concentration of $EDTA^{4-}$ (250 %), $Na(EDTA)^{3-}$ (216.7 %) and $HEDTA^{3-}$ (195.1 %). In this case, although the complex with copper $[Cu(EDTA)^{2-}]$ increased only by 37.4 %, it must have been responsible for the increase in the limiting current density, since complexes with copper and zinc seem to influence the transport properties more than the complexes without the metals. This was briefly shown in section 5.2.1 and will be discussed in more detail in section 5.2.3.

In turn, the resistance did not vary when the Cu^{2+}/Zn^{2+} molar ratio was increased from 0.4 to 2.3. Although the anionic equivalent charge increased from 6.85 mmol/L to 12.38 mmol/L when Cu^{2+}/Zn^{2+} increased (Table 8), the solution conductivity decreased from 944 μS/cm to 632 μS/cm (Table 3). This may account for the constant values of resistances shown in Table 11.

Current-voltage curves and chronopotentiograms under 0.45 mA/cm² of solutions with Cu^{2+}/Zn^{2+} molar ratios of 0.4 (Sol V), 1.0 (Sol II) and 2.3 (Sol VI) were also evaluated (Figure 32 and Figure 33, respectively).
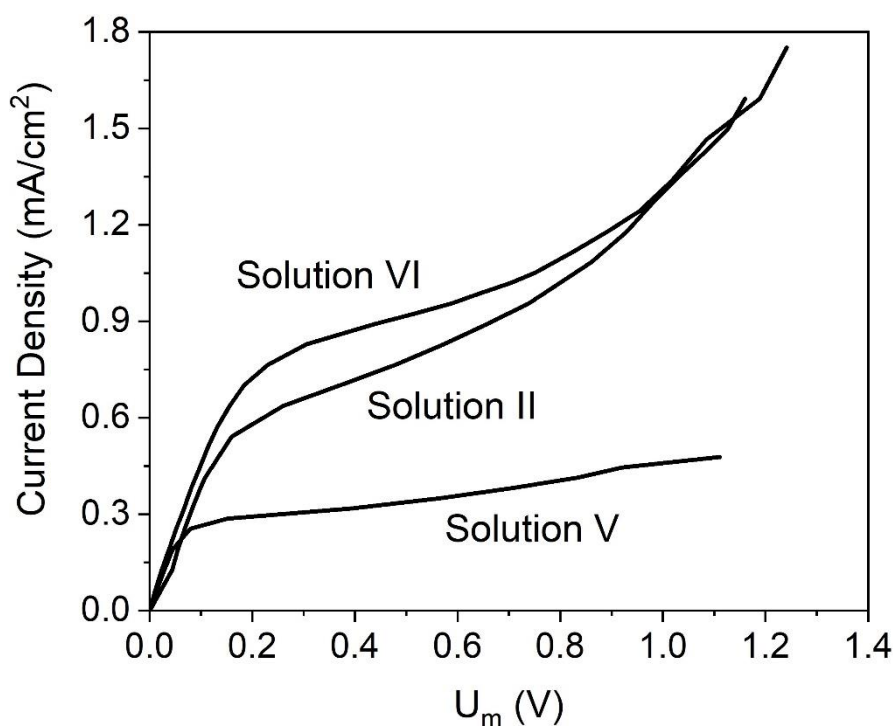
Figure 32 - Current-voltage curves for solutions with Cu^{2+}/Zn^{2+} of 0.4 (Sol V), 1.0 (Sol II) and 2.3 (Sol VI).
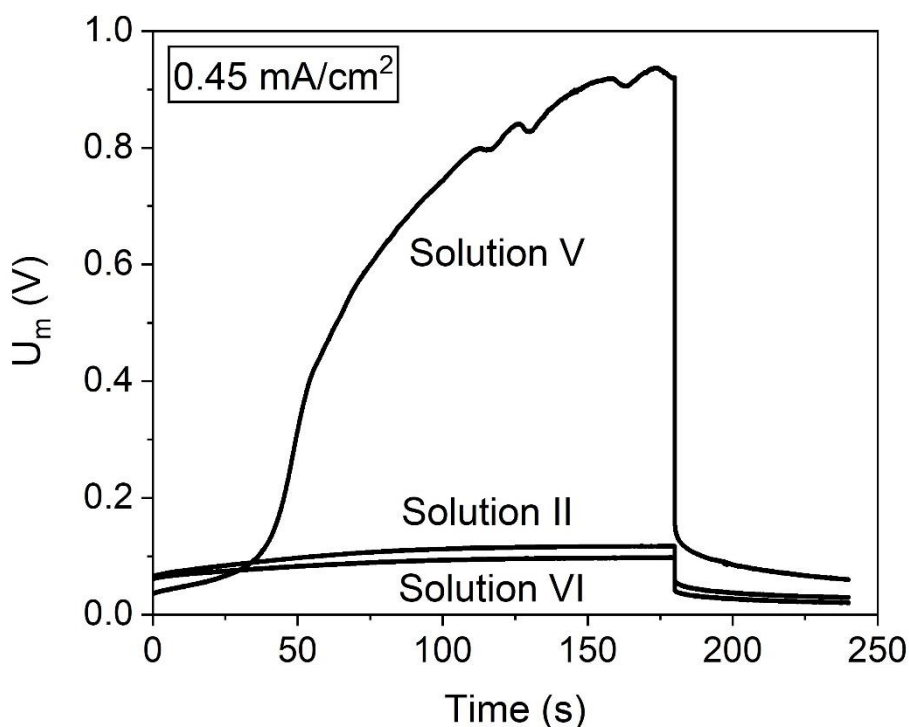
Figure 33 - Chronopotentiometric curves for solutions with Cu^{2+}/Zn^{2+} molar ratios of 0.4 (Sol V), 1.0 (Sol II) and 2.3 (Sol VI) under 0.45 mA/cm².

According to Figure 32, the CVC of solution V (Cu^{2+}/Zn^{2+} of 0.4) was not the typical curve with three regions, since after the achievement of the limiting current density, the plateau extended and the third region was not visualized, which hindered the determination of the plateau length. This occurred because of the formation of a precipitate at the membrane surface. Besides the ionic species shown in Table 8, the formation of the solid species ZnO and mainly CuO was verified for solution V, with Cu^{2+}/Zn^{2+} molar ratio of 0.4. In the speciation diagram constructed with the composition of this solution (not shown), the pH range in which CuO is present was verified to be approximately 7-13. Hence, when the concentration of Cu^{2+} is lower than Zn^{2+}, the tendency of precipitate formation increases, which may deposit on the membrane surface, leading to its destruction and increasing the energy consumption of electrodialysis (141). The formation of CuO on the membrane surface with solution V was also verified on the ChP (Figure 33) because of the oscillations after the inflexion point related to the concentration polarization achievement, besides the absence of the constant behavior before the relaxation of the system.

For solutions with concentration of Cu^{2+} equal or higher than Zn^{2+} (solution II and VI, respectively), the CVCs did not show unexpected behaviors,

since no precipitate was formed. As observed in Figure 33, under 0.45 mA/cm²
the occurrence of concentration polarization was not verified for solutions II
and VI, since their i_{lim} were greater than 0.45 mA/cm². Hence, Figure 34 presents
ChPs for both solutions under the current density of 1.08 mA/cm².
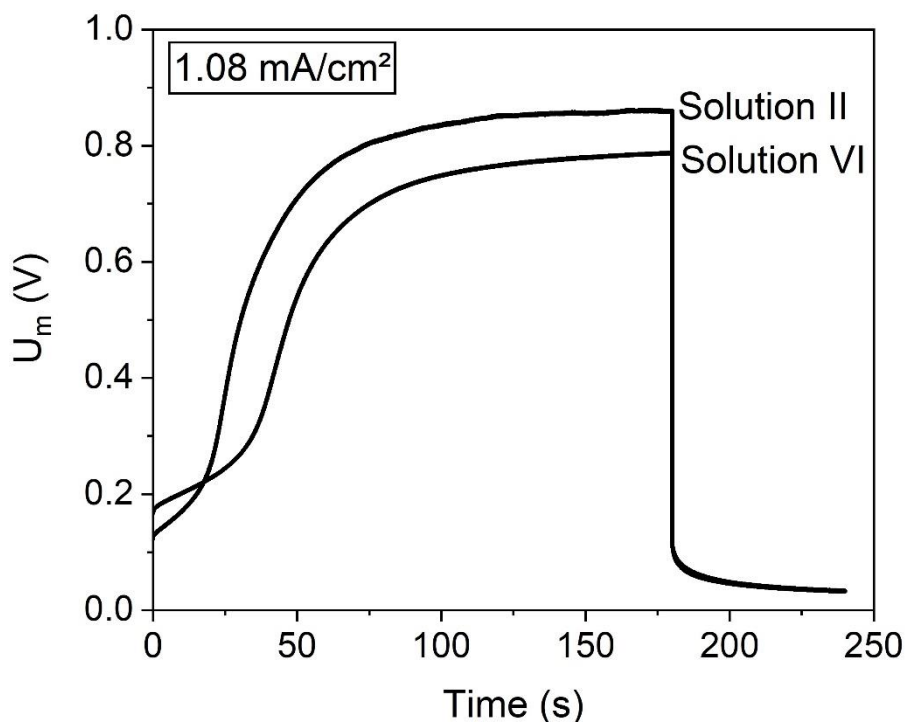
Figure 34 - Chronopotentiometric curves for solutions with Cu^{2+}/Zn^{2+} molar ratio of
1.0 (Sol II) and 2.3 (Sol VI) under 1.08 mA/cm².

According to Figure 34, the ChPs of solutions II and VI (and all the ChPs
under other current densities) confirm the absence of precipitate for these
solutions, which is in accordance with their CVCs. The plateau length of these
solutions was also calculated; according to Table 11, they enhanced by
increasing the Cu^{2+}/Zn^{2+} molar ratio from 1.0 to 2.3, since the anionic equivalent
charge increased from 9.42 to 12.38 meq/L (Table 3).

Concerning the fraction of the species in solution that involve copper, zinc
and EDTA (Table 9), when the molar ratio of Cu^{2+}/Zn^{2+} was increased from 0.4
to 2.3, the fraction of the soluble complexes with copper enhanced from 2 %
to 14 %, whereas the fraction of the soluble complexes with zinc decreased from
17.6 % to 6 % and the species with EDTA increased from 19.7 % to 35 %.
Considering the precipitate formed with Cu^{2+}/Zn^{2+} of 0.4 and the higher limiting
current density for the solution with molar ratio of 2.3, in electrodialysis, the most

interesting metals molar ratio may be 1.0, since it guarantees an equal distribution of the complexes with zinc and copper, preventing the precipitate formation and higher energy consumption.

5.2.3. Effect of EDTA

The influence of EDTA on the transport properties was also assessed. Figure 35 was constructed with data from Table 8 and presents the initial molar composition of solutions with EDTA/Cu^{2+} molar ratio of 2.0 (Sol VII), 2.5 (Sol II), 3.0 (Sol VIII) and 3.5 (Sol IX), whereas Table 12 presents the results of limiting current density, ohmic resistance and plateau length obtained in EDTA/Cu^{2+} molar ratios between 2.0 – 3.5, pH 10 and Cu^{2+}/Zn^{2+} molar ratio of 1.0.
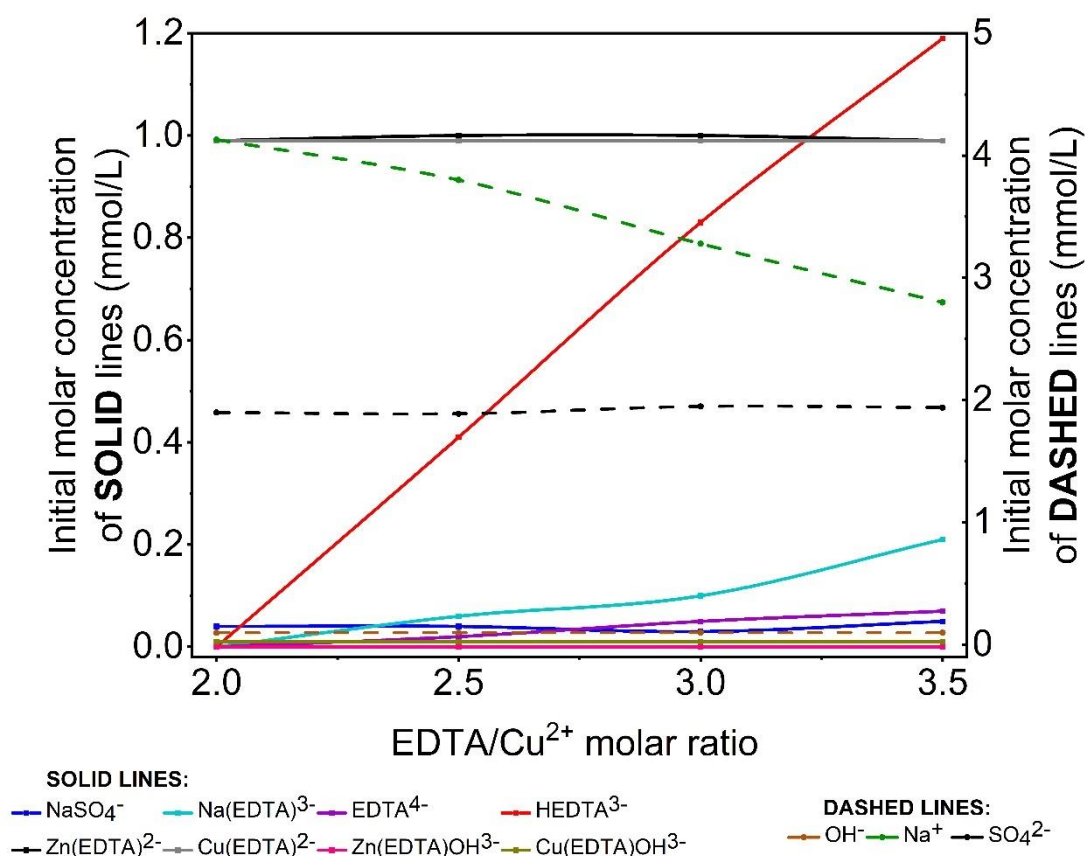
Figure 35 - Initial molar concentration of the main ionic species in the solution with EDTA/Cu^{2+} of 2.0 (Sol VII), 2.5 (Sol II), 3.0 (Sol VIII) and 3.5 (Sol IX).

Table 12 - Limiting current density, ohmic resistance and plateau length in EDTA/Cu^{2+} molar ratio between 2.0 - 3.5.

Evaluation	Sol.	pH	Cu^{2+}/Zn^{2+}	EDTA/Cu^{2+}	Limiting current density (mA/cm²)	Ohmic resistance (Ω.cm²)	Plateau length (V)
EDTA	VII	10	1.0	2.0	0.53	202.3	0.6
	II	10	1.0	2.5	0.54	225.6	0.6
	VIII	10	1.0	3.0	0.61	219.9	0.6
	IX	10	1.0	3.5	0.62	219,2	0.6

According to Table 12, the increase in EDTA caused an increase in the limiting current density only from EDTA/Cu^{2+} molar ratio 2.5 to 3.0. Despite the increase in Na(EDTA)$^{3-}$, EDTA^{4-}, HEDTA^{3-} (Figure 35/Table 8) and the increase in the anionic equivalent charge when the molar ratio was increased from 2.0 to 2.5 (Table 8), there was no variation in the limiting current density. This indicates the lower influence of the presence of these complexes (without copper and zinc) on the limiting current density when they are in lower concentration. When the ratio of EDTA/Cu^{2+} increased from 2.5 to 3.0, the limiting current density increased by 13.0 %, since in this case, the concentration of EDTA^{4-}, HEDTA^{3-} and Na(EDTA)$^{3-}$ was higher (increase of 150.0 %, 102.4 % and 66.7 %, respectively). For the increase in the EDTA/Cu^{2+} molar ratio from 3.0 to 3.5, the limiting current density maintained constant.

Figure 35/Table 8 show that the increase in EDTA did not lead to any change on the molar concentration of the complexes with copper and zinc ions [Zn(EDTA)$^{2-}$, Cu(EDTA)$^{2-}$, Zn(EDTA)OH^{3-} and Cu(EDTA)OH^{3-}], since the metals were already complexed in EDTA/Cu^{2+} molar ratio 2.0 and the addition of EDTA influenced only the formation of Na(EDTA)$^{3-}$, EDTA^{4-} and HEDTA^{3-}. Therefore, the results suggest that the addition of EDTA to the synthetic wastewater is not necessary, since the molar ratio of EDTA/Cu^{2+} tested by Almeida et al. (9,10) was 2.5 and it is sufficient for the copper and zinc separation by electrodialysis.

The plateau length was not altered with the increase of EDTA concentration. As the complexes with copper and zinc [Zn(EDTA)$^{2-}$, Cu(EDTA)$^{2-}$, Zn(EDTA)OH^{3-} and Cu(EDTA)OH^{3-})] did not show any change on their molar

concentration when EDTA was increased from 2 to 3.5, we can suggest that they are the major responsible for the change in plateau length, while the species and complexes without copper and zinc [$EDTA^{4-}$, $HEDTA^{3-}$ and $Na(EDTA)^{3-}$] virtually do not affect this property.

Figure 36 and Figure 37 present the CVC and the ChP under 1.15 mA/cm², respectively, for solutions VII, II, VIII and IX to evaluate the influence of EDTA addition on the curves behavior.
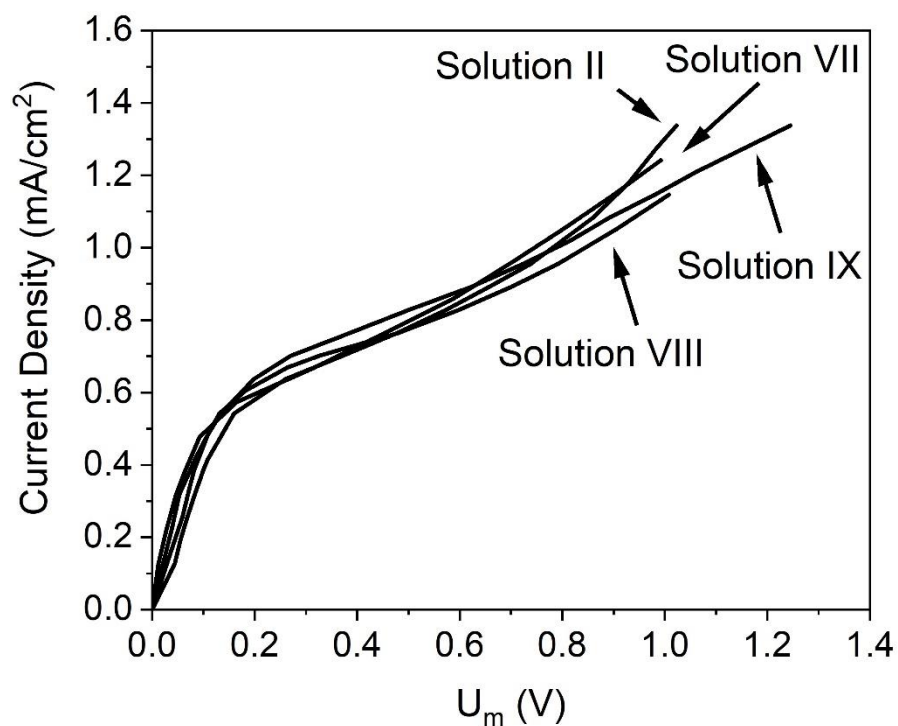
Figure 36 - Current-voltage curves for solutions with EDTA/Cu^{2+} of 2.0 (Sol VII), 2.5 (Sol II), 3.0 (Sol VIII) and 3.5 (Sol IX).
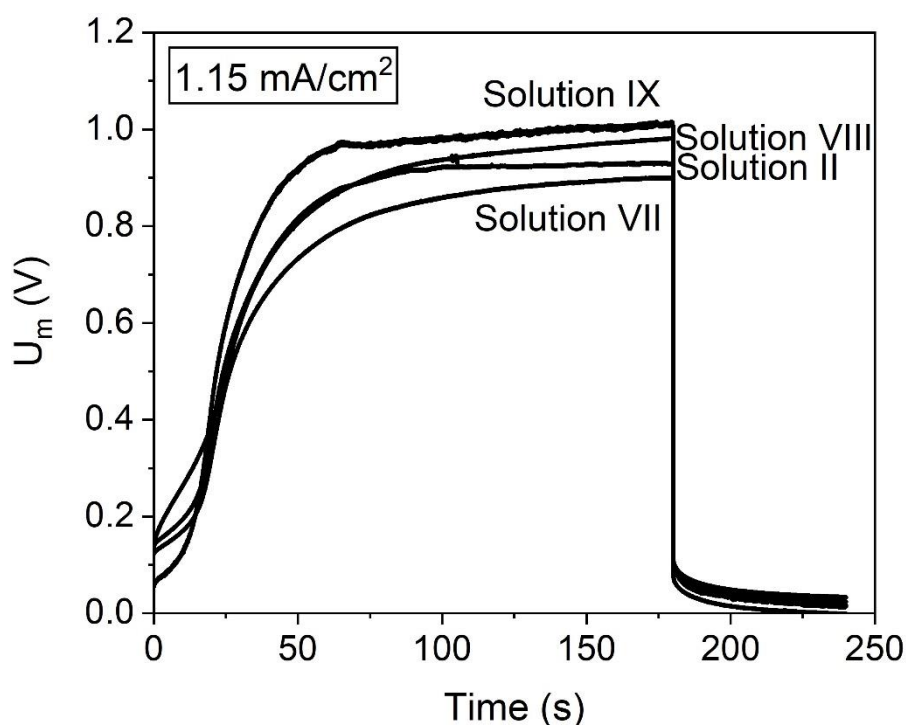
Figure 37 - Chronopotentiometric curves for solutions with EDTA/Cu^{2+} of 2.0 (Sol VII), 2.5 (Sol II), 3.0 (Sol VIII) and 3.5 (Sol IX) under 1.15 mA/cm².

According to Figure 36, the current-voltage curves for all tested solutions were very similar, since they presented three regions clearly defined and did not suggest precipitate formation. The ChPs (Figure 37) for the solutions were also very similar and presented similar transition times, which means although the species Na(EDTA)$^{3-}$, EDTA^{4-} and HEDTA^{3} increased with the increase in EDTA/Cu^{2+} molar ratio, the time elapsed for the depletion of counterions in the DBL was the same for the solutions. Hence, the behavior of the curves confirms the absence of precipitate formation for these solutions and the non-influence of the EDTA concentration on the formation of insoluble species.

Finally, according to Table 9, the fraction of the complexes with copper and zinc did not show remarkable changes when the EDTA/Cu^{2+} molar ratio was increased from 2 – 3.5 (12.2 % to 9.7 %), while the fraction of species with EDTA increased from 24.5 % to 33.8 %. This confirms that, in electrodialysis, the ratio 2.5 should be adopted, since the addition of EDTA influences only the formation of Na(EDTA)$^{3-}$, EDTA^{4-} and HEDTA^{3-}, whereas the formation of complexes with the metals that should be extracted from the wastewater was not altered.

5.2.4. Conclusions

Transport properties of the anion-exchange membrane HDX200 were investigated in function of the species in solutions with copper-zinc complexes at some pH values, molar ratios of Cu^{2+}/Zn^{2+} and concentrations of EDTA. The pH solution influenced the transport properties. Typical CVCs and ChPs were obtained for pH 9 and 10, whereas for pH 11 the CVC did not show the third region, which may have occurred due to the transport of OH^- ions by the Grotthus mechanism. For pH 12, the CVC showed two limiting current densities; the first one was related to the depletion of OH^- ions and the second one to the other ionic species in solution, such as SO_4^{2-} and $Zn(EDTA)^{2-}$. The chronopotentiograms showed an unexpected additional inflexion point, which agreed with the presence of two limiting current densities in the CVC. The ohmic resistance decreased with the pH increase since the conductivity and the anionic equivalent charge enhanced, whereas the plateau length showed an increase with pH due to the increase of $Zn(EDTA)OH^{3-}$ and $Cu(EDTA)OH^{3-}$. In general, complexes with copper and zinc mainly accounted for the alterations in transport properties.

The Cu^{2+}/Zn^{2+} molar ratio influenced the limiting current density, although it virtually did not affect the plateau length or, mainly, the resistance. When the concentration of copper was lower than zinc, the formation of CuO was verified in the speciation diagram, in the CVC and in the chronopotentiogram. Hence, in the next topic, the synthetic wastewater from the brass electrodeposition with Cu^{2+}/Zn^{2+} molar ratio of 0.4 was used for evaluating the influence of insoluble species on the electrodialysis operation in underlimiting and overlimiting conditions.

The addition of EDTA virtually did not affect the transport properties. The behavior of the CVCs and ChPs was not influenced by the complexing agent, since typical and very similar curves were obtained. The fraction of complexes with copper and zinc did not change when the EDTA/Cu^{2+} molar ratio was increased from 2 – 3.5. Hence, it is recommended to maintain the EDTA/Cu^{2+} molar ratio of 2.5 in electrodialysis, since this is the molar ratio present in the bath of brass electrodeposition.

5.3.   Topic III: Treatment of the synthetic cyanide-free wastewater, by electrodialysis in underlimiting and overlimiting condition, from the brass electrodeposition with EDTA

For understanding the influence of the species present in solution on the properties of the membranes, a speciation diagram for the initial composition of the working solution was constructed with the aid of the *Hydra-Medusa* software (275) (Figure 38). Then, the concentrations of the main ionic species in the initial solution, under pH 12.25, were determined, and the results are presented in Table 13. As observed, the species in the highest concentration is the cation Na^+, which is the only species in solution that theoretically crosses the cation-exchange membrane. Regarding the anionic species, those in the highest concentrations in the solution are OH^-, SO_4^{2-}, $Zn(EDTA)^{2-}$ and $Zn(EDTA)OH^{3-}$. The presence of two insoluble species can also be observed: CuO and ZnO, which influenced the results of percent extraction and percent concentration.
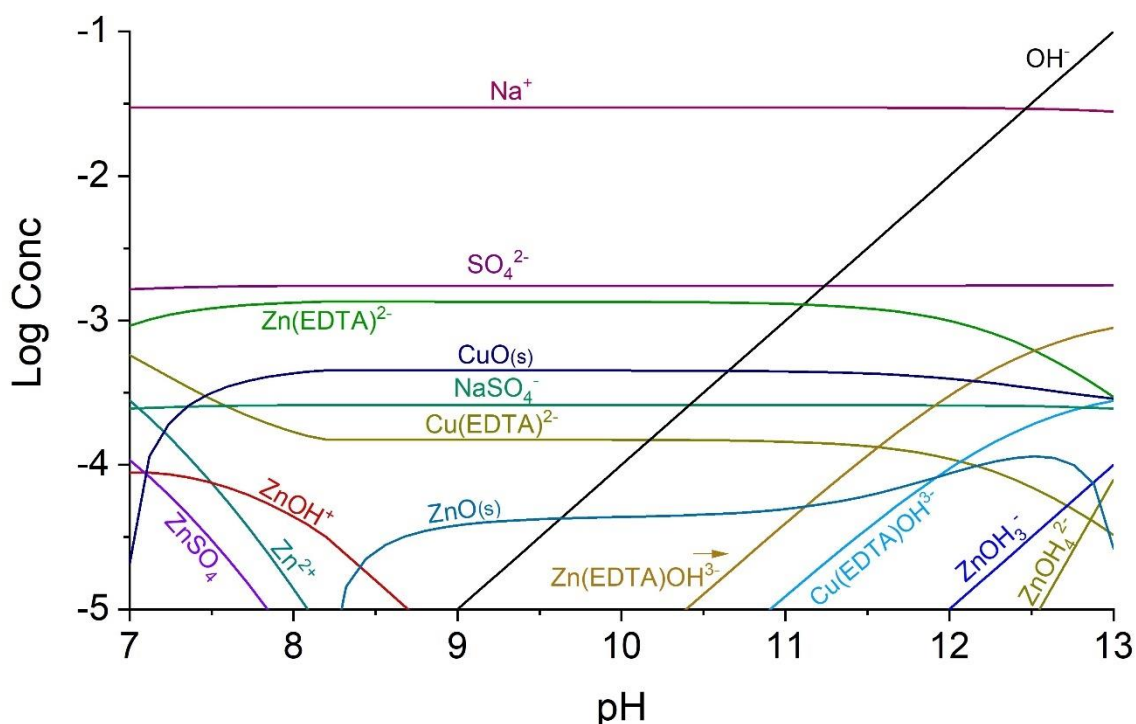
Figure 38 - Speciation diagram constructed with the composition of the working solution of the electrodialysis test.

Table 13 - Molar concentration of the main ionic species in the initial composition of the working solution.

	Concentration (mmol/L)
Na^+	29.44
OH^-	17.42
SO_4^{2-}	1.75
$Zn(EDTA)^{2-}$	0.83
$Zn(EDTA)OH^{3-}$	0.43
$NaSO_4^-$	0.26
$Cu(EDTA)OH^{3-}$	0.14

5.3.1. Obtaining of current-voltage curves in the electrodialysis stack

The current-voltage curves of the anion- and cation-exchange membranes were constructed for determining their limiting current density. The curves obtained are depicted in Figure 39 and the error in the i_{lim} determination between the duplicate curves was 3.5 % and 0.7 % for the AEM and CEM, respectively.
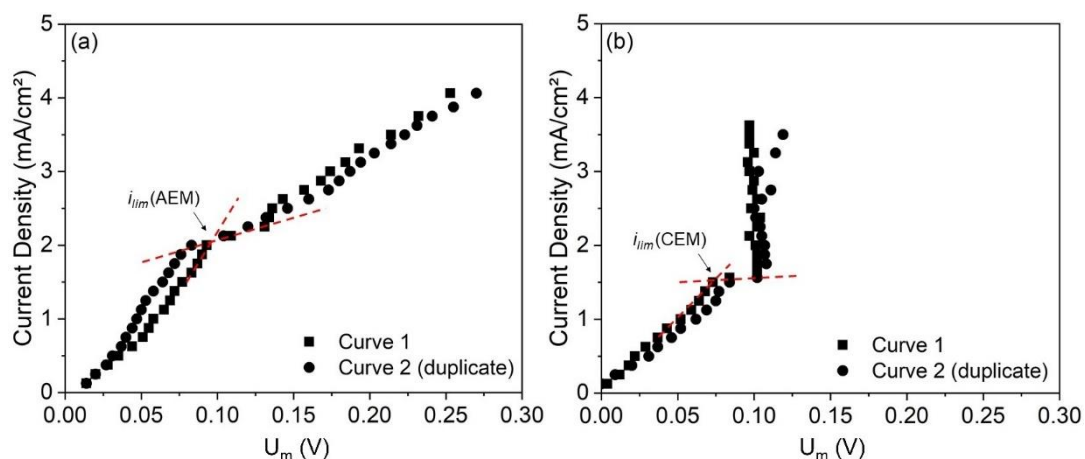
Figure 39 – Current-voltage curves in duplicate of the a) anion- (AEM) and b) cation-exchange membrane (CEM).

As observed, the AEM curve (Figure 39a) presented two limiting current densities: one at 0.5 mA/cm² and another at 2.0 mA/cm². This behavior was already seen for ampholyte-containing solutions due to the different forms of species depending on the local pH (197) and for other systems where the

prevailing species that passes through the membranes changes as the current density is increased (172,196). The species that passes at each current density depends on its size, molar concentration and mobility/diffusion coefficient. Here, the first limiting current density for the AEM ($i_{lim1,AEM}$ = 0.5 mA/cm²) must be related to the depletion of OH⁻ ions, due to its greater concentration in relation to the anionic species and mobility (Table 13), whereas the second one ($i_{lim2,AEM}$ = 2.0 mA/cm²) must be related to the depletion of anionic species in lower concentrations, such as SO_4^{2-} and complexes with EDTA. This is in accordance with the results presented in Topic II (section 5.2.1), since two limiting current densities were verified in the chronopotentiograms constructed for the solution with Cu-Zn-EDTA at pH 12 and, in both studies, the same ionic species were responsible for each i_{lim}. Then a plateau was reached, and the third region showed the usual linear behavior. For defining the current applied to the electrodialysis test in overlimiting condition, we considered the i_{lim} of the AEM as 2.0 mA/cm², since only at current densities above this one we can see the third region of the current-voltage curve, where overlimiting phenomena occur.

For the cation-exchange membrane (Figure 39b), the curve showed a linear relation in the first region, but in the third one, the potential drop kept virtually constant with the current density increase. This occurred due to the very fast and intense ionic transport through the CEM under overlimiting conditions, as will be discussed further on. Despite the absence of the linear behavior in the third region, the limiting current density of the CEM could be determined ($i_{lim,CEM}$ = 1.5 mA/cm²), since the change in the slope after the first region was evident.

Finally, the higher value of limiting current density for the AEM was due to the greater concentration of the anionic species than of the cationic species in the solution (Table 13), besides the higher mobility of OH⁻ compared to the other species in solution.

5.3.2. Electrodialysis

Two electrodialysis experiments were conducted in long-term concentration tests. Table 14 presents the current density applied to each test performed with the relations between these current densities and the limiting

current densities of both membranes. As observed, in the underlimiting experiment, the applied current density was lower than the i_{lim} of both membranes (80 % and 60 % of the i_{lim} of the CEM and AEM, respectively). In the overlimiting experiment, both membranes were in overlimiting conditions, since the i applied was 60 % and 20 % above the i_{lim} of the CEM and AEM, respectively. The limiting current densities were determined with the working solution in its initial state. As the concentration of the dilute compartment decreased throughout the tests, the limiting current density also decreased. Hence, in the underlimiting test, the system may have operated in overlimiting condition from a certain moment.

Table 14 - Relation between the current densities applied to each experiment and the limiting current densities of the membranes.

Experiment	Applied current density (mA/cm²)	Relation between the i applied and the i_{lim} of both membranes	
		CEM	AEM
Underlimiting	1.2	80 % of i_{lim}	60 % of i_{lim}
Overlimiting	2.4	160 % of i_{lim}	120 % of i_{lim}

Figure 40 and Figure 41 present the visual aspect of the four solutions involved in the underlimiting and overlimiting tests, respectively: the original bath before its dilution, the synthetic rinsing water (or working solution), the treated and the concentrated solutions obtained after the 4th cycle.
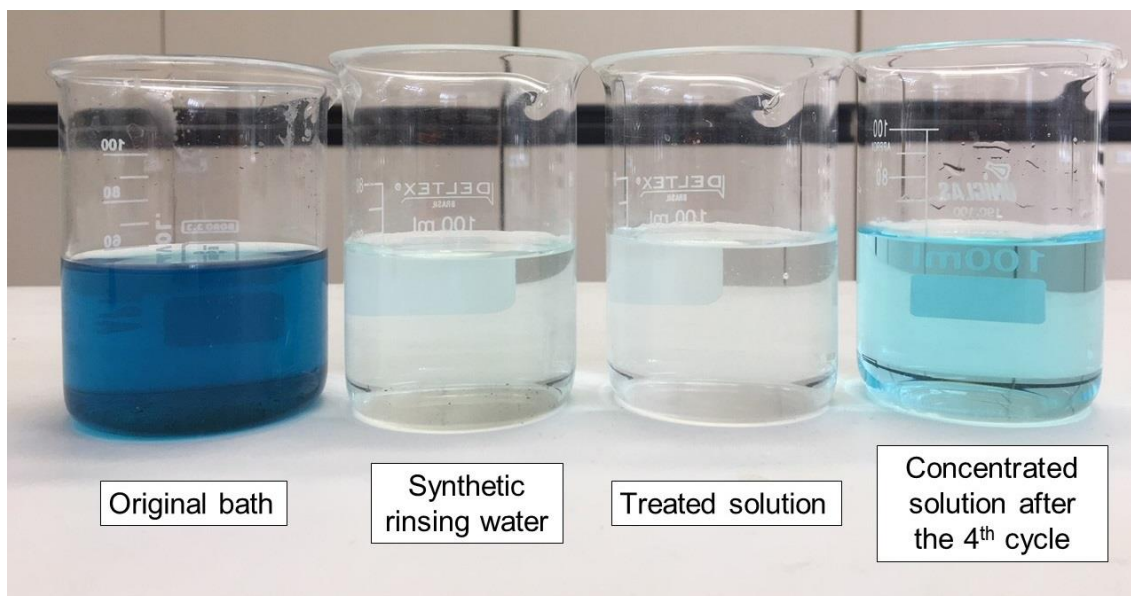
Figure 40 - Visual aspect of the original bath, the synthetic rinsing water, the treated solution (diluted) and the concentrated solution after the 4th cycle of the underlimiting test.
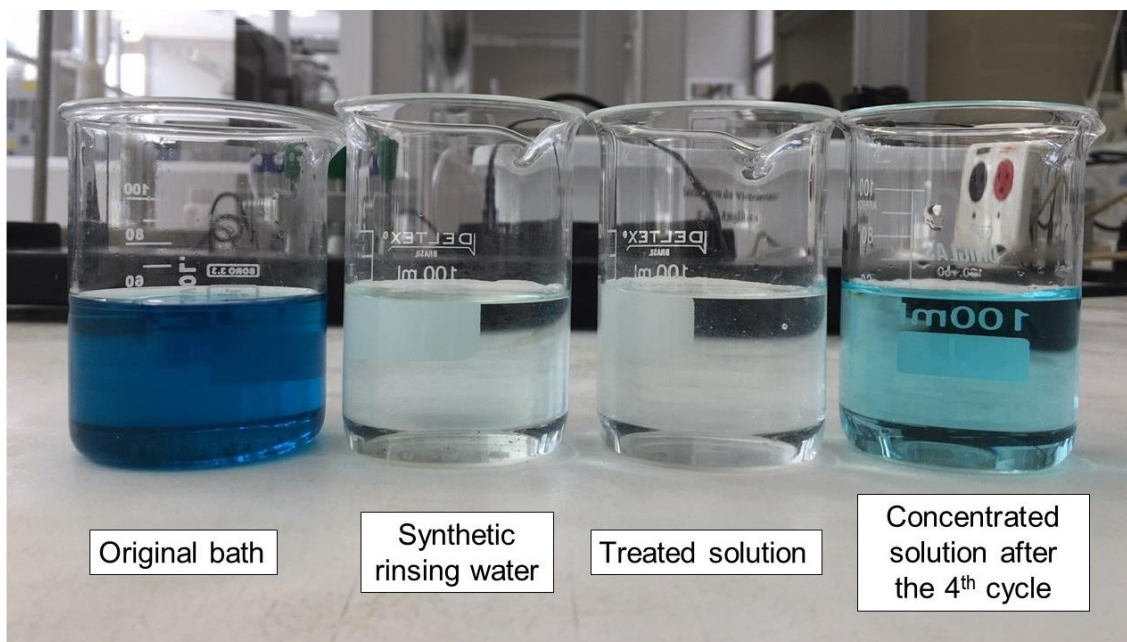
Figure 41 - Visual aspect of the original bath, the synthetic rinsing water, the treated solution (diluted) and the concentrated solution after the 4th cycle of the overlimiting test.

5.3.2.1.   Evaluation of the solution conductivity

Figure 42 presents the conductivity of the concentrate and dilute compartments throughout the four cycles performed in the electrodialysis tests.
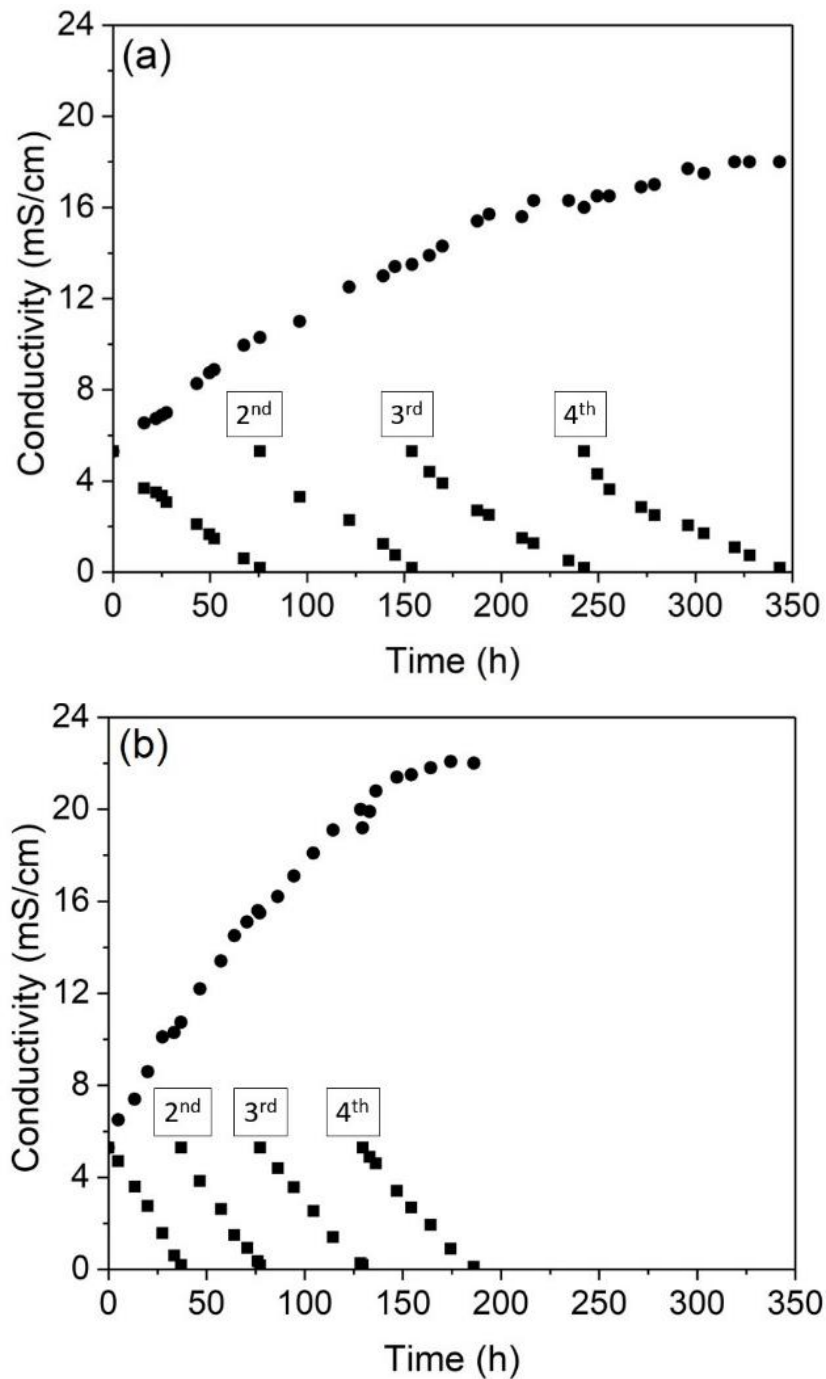
Figure 42 - Conductivity of the concentrated (●) and diluted (■) solutions during the 4 cycles of the a) underlimiting and b) overlimiting tests.

As expected, the increase in the current density decreased the operation time, from 344 hours to 186 hours. Concerning the conductivity of the concentrate compartment after each cycle, Figure 42 shows that the overlimiting test accounted for the highest conductivity achieved in all cycles. As the conductivity of the dilute compartment was the same after all the cycles in the

experiments (~0.2 mS/cm), the difference in the conductivity of the concentrated solutions suggests that the increase of the current density caused a change in the type of species that preferentially passed through the membranes. This is also going to be shown in the chemical analyses. The behavior of the conductivity of the diluted solutions was different for each experiment. Note that in the overlimiting test, the decrease in conductivity was virtually linear, whereas in the underlimiting test, a change in the slope of the curves occurred throughout each cycle. This may be explained by the diffusion of ions from the concentrate compartment to the dilute one since the concentration gradient increased throughout the tests. Hence, the effect of diffusion on ion transport was greater in the underlimiting test than in the overlimiting one.

The final pH values of the diluted and concentrated solutions after each cycle of the electrodialysis tests are presented in Table 15. Note that the pH values of the diluted solutions from the overlimiting experiment were higher than those from the underlimiting test. This may be related to the occurrence of water splitting during the overlimiting tests and the reaction of protons with complexes and insoluble species, as will be discussed.

Table 15 - Final pH of the diluted and concentrated solutions after the four cycles of the electrodialysis tests.

	Final pH			
	Underlimiting test		Overlimiting test	
Cycle	Diluted	Concentrated	Diluted	Concentrated
1st	10.8	12.4	10.7	12.4
2nd	10.2	12.3	10.8	12.5
3rd	10.1	12.3	10.9	12.6
4th	9.9	12.2	10.4	12.6

5.3.2.2.   Percent concentration and percent extraction

Table 16 presents the concentration, in ppm, of the species copper, zinc, EDTA, sodium and sulfate in the concentrate and dilute compartments. Here, the concentration of sodium present in EDTA was discounted. Although the initial solution of the synthetic wastewater was prepared with 0.0014 mol/L of Zn^{2+}

(Table 4), or ~90 ppm of Zn^{2+}, Table 16 shows that its initial concentration in the experiments, determined by analytical method, was about 60 ppm. This difference occurred due to the formation of a precipitate with zinc, which was visually observed before the electrodialysis tests. The precipitate formation was expected, as shown in the speciation diagram in Figure 38.

Table 16 - Concentration (in ppm) of copper, zinc, EDTA, sodium and sulfate in the concentrate and dilute compartments.

		Underlimiting test		Overlimiting test	
Initial solution	Copper	36		36	
	Zinc	62		59	
	EDTA	544		546	
	Sodium	784		768	
	Sulfate	273		265	
		Electrodialysis			
		Underlimiting test		Overlimiting test	
		Diluted	Concentrated	Diluted	Concentrated
Cycle 1	Copper	4	63	4	66
	Zinc	11	114	8	107
	EDTA	100	1013	88	986
	Sodium	25	2322	24	2607
	Sulfate	14	1569	5	2244
Cycle 2	Copper	6	89	5	97
	Zinc	13	156	9	156
	EDTA	117	1478	88	1496
	Sodium	27	3837	18	4284
	Sulfate	9	3457	14	4351
Cycle 3	Copper	7	116	6	124
	Zinc	16	196	12	202
	EDTA	144	1849	103	1962
	Sodium	24	5575	20	5733
	Sulfate	9	5279	13	6375
Cycle 4	Copper	7	143	5	161
	Zinc	18	233	9	257
	EDTA	162	2242	82	2430
	Sodium	20	7477	13	8405
	Sulfate	20	7142	22	9580

The results of the desalination of the feed solution in each of the four cycles were expected to be similar in the experiments, since the system was carried out in quasi steady-state conditions. The differences showed in Table 16, for both electrodialysis tests, are explained by the formation of insoluble species and by their reactions with protons during overlimiting phenomena, as will be discussed further on. With data from Table 16, the percent concentrations of Cu, Zn and EDTA were calculated, as shown in Figure 43.
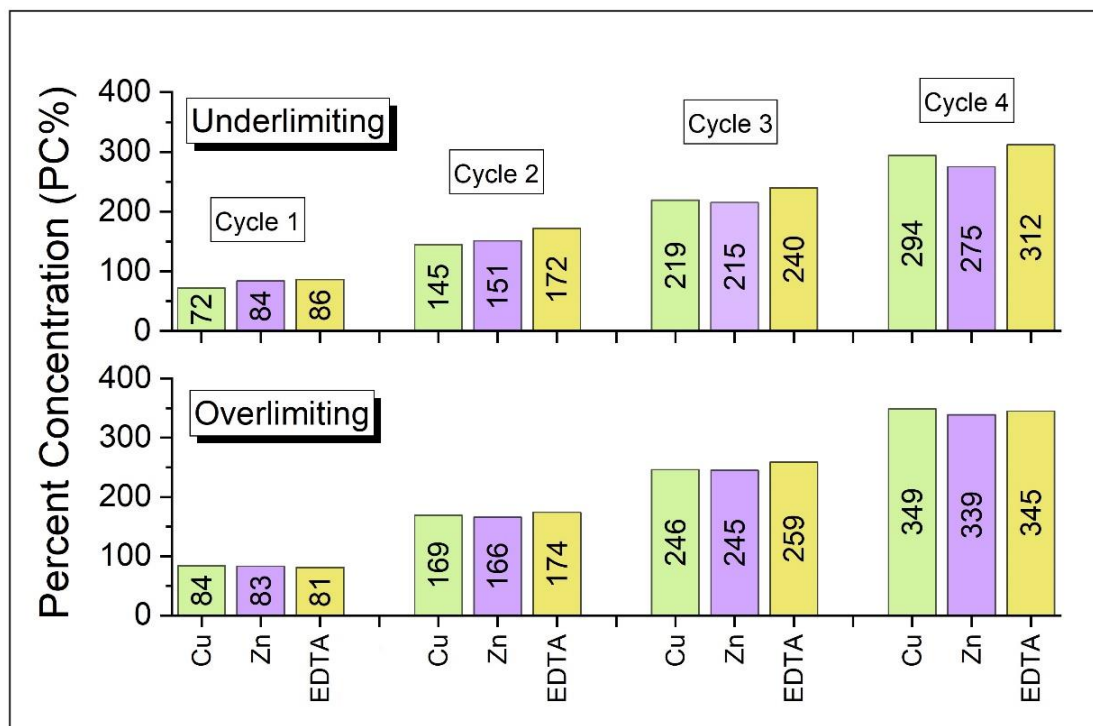
Figure 43 - Percent Concentration of Cu, Zn and EDTA obtained in the experiments.

According to Figure 43, the species that preferentially crossed the membranes and their concentrations depended on the applied current density, as suggested by Figure 42, regarding the values of final conductivities of the concentrate compartment. Note that, in general, the highest percent concentrations of copper and zinc were those obtained in the overlimiting test. For EDTA, the percent concentration maintained virtually constant in the first two cycles, whereas it also increased in the 3rd and 4th cycles in the overlimiting test.

The highest percent concentrations of copper, zinc and EDTA in the overlimiting test can be explained by the water splitting phenomenon. Zabolotsky et al. (240) tested different configurations of electrodialysis and

observed that in overlimiting conditions, part of the H^+ ions at the CEM may have migrated from the AEM as a result of water splitting at this membrane. Hence, the results presented in Figure 43, and those shown further on, suggest that intense water splitting occurred on the surface of the AEM in overlimiting condition. It is well-known that water splitting occurs mainly at anion-exchange membranes, due to their higher catalytic activity with respect to this phenomenon (263,286). During the intense migration of hydroxyl ions through the anion-exchange membrane, protons accumulated on its cathodic side, which led to a pH decrease. This caused the reaction of insoluble species, such as CuO and ZnO, with protons, which led to the formation of Cu^{2+} and Zn^{2+} (Equation 26 and Equation 27). As shown in Figure 38, in pH lower than approximately 8.3 and 7, there is no ZnO and CuO, respectively, in the working solution.

$$CuO(s) + 2H^+ \leftrightarrow Cu^{2+} + H_2O \qquad\qquad \log K = 7.66 \qquad \text{Equation 26}$$

$$ZnO(s) + 2H^+ \leftrightarrow Zn^{2+} + H_2O \qquad\qquad \log K = 11.16 \qquad \text{Equation 27}$$

Considering the very dynamic behavior of electrodialysis in relation to the concentration and pH of the diluted solution, especially on the membrane surface, reactions present in Equation 28-Equation 31 may also have taken place, which also form Cu^{2+} and Zn^{2+} ions. The values of equilibrium constant at 25ºC for the equations are from refs. (287,288), except for Equation 28 and Equation 30. For Equation 28, *log K* was calculated by combining the values from Equation 29 and Equation 32, whereas for Equation 30, *log K* was calculated by combining Equation 31 and Equation 33. The reactions of hydroxides of copper and zinc with protons are also shown in Equation 34 and Equation 35 (288).

$$Cu(OH)_2 + H^+ \leftrightarrow (CuOH)^+ + H_2O \qquad\qquad \log K = 9.3 \qquad \text{Equation 28}$$

$$(CuOH)^+ + H^+ \leftrightarrow Cu^{2+} + H_2O \qquad\qquad \log K = 8.0 \qquad \text{Equation 29}$$

$$Zn(OH)_2 + H^+ \leftrightarrow (ZnOH)^+ + H_2O \qquad\qquad \log K = 7.94 \qquad \text{Equation 30}$$

$$(ZnOH)^+ + H^+ \leftrightarrow Zn^{2+} + H_2O \qquad \log K = 8.96 \qquad \text{Equation 31}$$

$$Cu(OH)_2 + 2H^+ \leftrightarrow Cu^{2+} + 2H_2O \qquad \log K = 17.3 \qquad \text{Equation 32}$$

$$Zn(OH)_2 + 2H^+ \leftrightarrow Zn^{2+} + 2H_2O \qquad \log K = 16.9 \qquad \text{Equation 33}$$

$$Cu(OH)_2(s) + 2H^+ \leftrightarrow Cu^{2+} + 2H_2O \qquad \log K = 8.68 \qquad \text{Equation 34}$$

$$Zn(OH)_2(amorp) + 2H^+ \leftrightarrow Zn^{2+} + 2H_2O \qquad \log K = 12.48 \qquad \text{Equation 35}$$
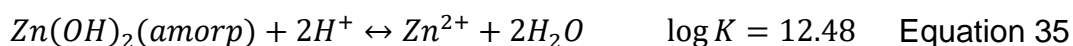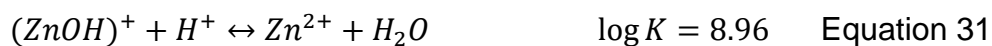
Then, the free metals Cu^{2+} and Zn^{2+} migrated from the AEM to the CEM as a result of the intense electric field and electroconvection, which allowed their transport to the concentrate compartment through the cation-exchange membrane. As presented in Table 14, the i applied to the overlimiting test was 160 % of the i_{lim} of the CEM, which means that the attraction of cations towards this membrane was very intense. This also explains the current-voltage curve presented in Figure 39 for the CEM, since the resistance of its third region was very low due to the intense transport of cations. The reaction of complexes of Cu-EDTA and Zn-EDTA with protons also occurred during water splitting, which led to the increase of the EDTA transfer through the anion-exchange membrane mainly during the 3rd and 4th cycles (Figure 43).

Finally, it is known that in the case of CEM, water splitting is enhanced due to protonation-deprotonation reactions of metallic precipitates, such as copper and zinc hydroxides and oxides. The general water dissociation reaction involving metal ions was formulated by Ganych et al. (289) and it can be seen in Equation 36 and Equation 37. For AEMs, the formation of metal complexes can also catalyze the water dissociation, since they participate as active sites in the protonation-deprotonation reactions (290). Hence, the presence of insoluble species and metal complexes may also have favored water splitting at both membranes facing the diluted solution.

$$R - [Metal(H_2O)_2]^{z+} + H - OH \rightleftarrows \qquad \text{Equation 36}$$
$$R - [Metal(H_2O)OH]^{(z-1)+} + H_3O^+$$

$$R - [Metal(H_2O)OH]^{(z-1)+} + H - OH \rightleftarrows \qquad \text{Equation 37}$$
$$R - [Metal(H_2O)_2]^{z+} + OH^-$$
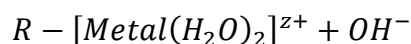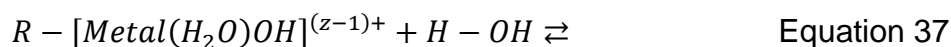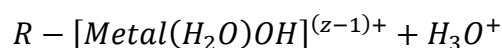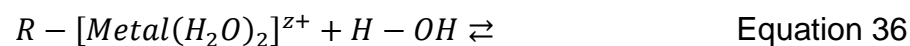
The suggestion of the occurrence of intense water splitting is also in agreement with the results obtained in section 5.2 (Topic II of the thesis), since it was verified, by chronopotentiometry, that an insoluble species was formed at the AEM surface. Oscillations typical of fouling/scaling by insoluble species were observed in the chronopotentiograms, besides the absence of the third region in the current-voltage curve for the solution with the same composition evaluated herein, but at pH 10.

With data of the diluted solutions from Table 16, the percent extractions (PE%) of copper, zinc, EDTA, sodium and sulfate were calculated and the results are present in Figure 44.
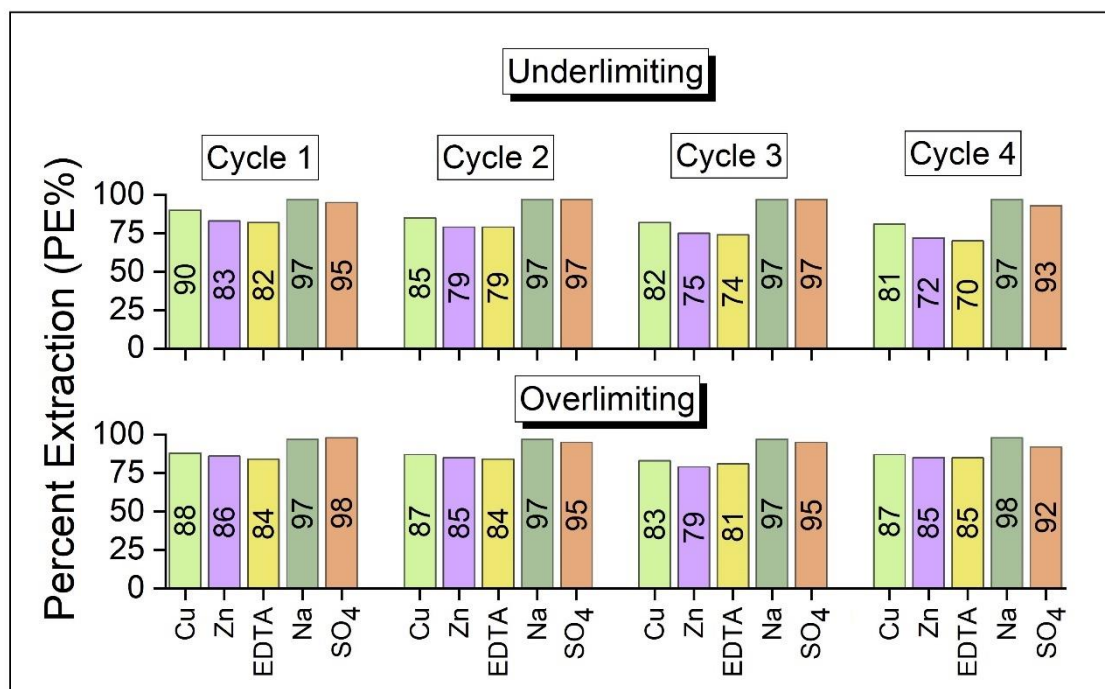
Figure 44 - Percent Extraction of Cu, Zn, EDTA, Na and SO_4 obtained in the electrodialysis experiments.

As verified in Figure 44, in general, the values of percent extraction of the species are relatively close in both experiments, except for Zn in cycle 2, EDTA in cycle 3, Cu, Zn and EDTA in cycle 4. The percent extraction was calculated in function of the concentration of species in the dilute compartment after each cycle in relation to its initial concentration. Therefore, similar PE% values for Cu and Zn were obtained in both experiments because, in the underlimiting test, some species were present in the solid state and were not quantified in the chemical analyses, whereas in the overlimiting experiment these species were transported to the concentrate compartment due to water splitting. For EDTA, the complexes dissociation occurred more intensively during the 3rd and 4th cycles, which explains the highest values of PE%. These results are in accordance with the results of percent concentration already showed and will be confirmed by the mass balance (section 5.3.2.3). For Na^+ and SO_4^{2-} species, differences in the PE% were virtually not verified among the experiments, since they were already present in the free form (Table 13). Hence, they were not influenced by the water splitting phenomenon.

Finally, since membranes are not perfectly permselective, they also allow the transport of water, mainly by two mechanisms: osmosis and electroosmosis. The first one results from osmotic pressure difference between the diluted and concentrated solutions. In the second mechanism, ions passing through the membrane are accompanied by a solvation shell of water molecules (23). These phenomena are more significant in systems with differences between the concentration of the compartments and under low applied current densities (291,292). Therefore, the water transport through the membranes may also have influenced the ion transfer in the two experiments assessed herein, which may have occurred with greater intensity in the underlimiting test. As can be seen in Figure 44, in the last cycle, which had the greatest concentration difference between the dilute and concentrate compartments, the highest differences between the PE% of the underlimiting and overlimiting tests were obtained. Some authors verified that these phenomena of water transport can limit the usefulness of electrodialysis as a method of concentrating electrolyte solutions (293).

5.3.2.3.   Mass balance

A mass balance for each species (copper, zinc and EDTA) was performed with their molar flow rates in each cycle, as well as for the system considering all the inputs and outputs of the 4 cycles (overall mass balance), as shown in Figure 45.
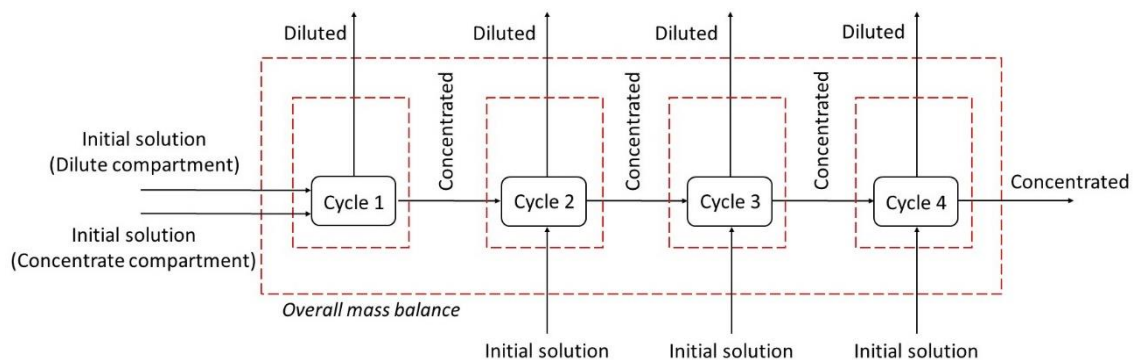
Figure 45 - Representation of the mass balance calculated for each cycle and for the overall system.

The results are presented in Table 17, which shows the percentage of the species leaving each control volume (diluted + concentrated solutions) in relation to the species entering it. The values slightly above 100 % in the mass balance of some species (~3 %) are due to the deviations of the chemical analysis.

Table 17 - Mass balance of metals and EDTA for each cycle and for the overall system of electrodialysis.

Mass balance for the underlimiting test (%)			
Cycle	Cu	Zn	EDTA
1st	91	100	102
2nd	95	96	102
3rd	98	97	99
4th	99	97	100
Overall system	91	93	102
Mass balance for the overlimiting test (%)			
Cycle	Cu	Zn	EDTA
1st	98	98	98
2nd	100	99	103
3rd	98	100	101
4th	103	102	100
Overall system	101	101	102

Note that in the underlimiting test, only 91 % and 93 % of Cu and Zn, respectively, of the initial solution were present in the final solutions (dilute+concentrate compartments), while in the overlimiting test, the overall mass balance of metals is complete (100 %).

As in the underlimiting experiment water splitting (and the reaction of protons with insoluble species) did not occur, part of the metals remained in the solid state and were not quantified in chemical analysis, which explains their values below 100 %. These results finally confirm that the overlimiting experiment led to the reaction of protons with insoluble species of copper and zinc present in the working solution, which allowed the metals passage to the concentrate compartment.

5.3.3. Chronopotentiometric measurements after the electrodialysis tests

The cation- and anion-exchange membranes were forwarded to chronopotentiometric measurements after both electrodialysis tests, for evaluating their transport properties, such as the limiting current density and

ohmic resistance. The virgin membranes, without being exposed to electrodialysis, were also evaluated.

Figure 46 presents the current-voltage curves obtained for the AEMs (Figure 46a) and CEMs (Figure 46b), by chronopotentiometry, whereas Table 18 presents the obtained values of limiting current density and ohmic resistance. The errors between the results from the duplicate curves, which are lower than 4 %, are also present in Table 18.
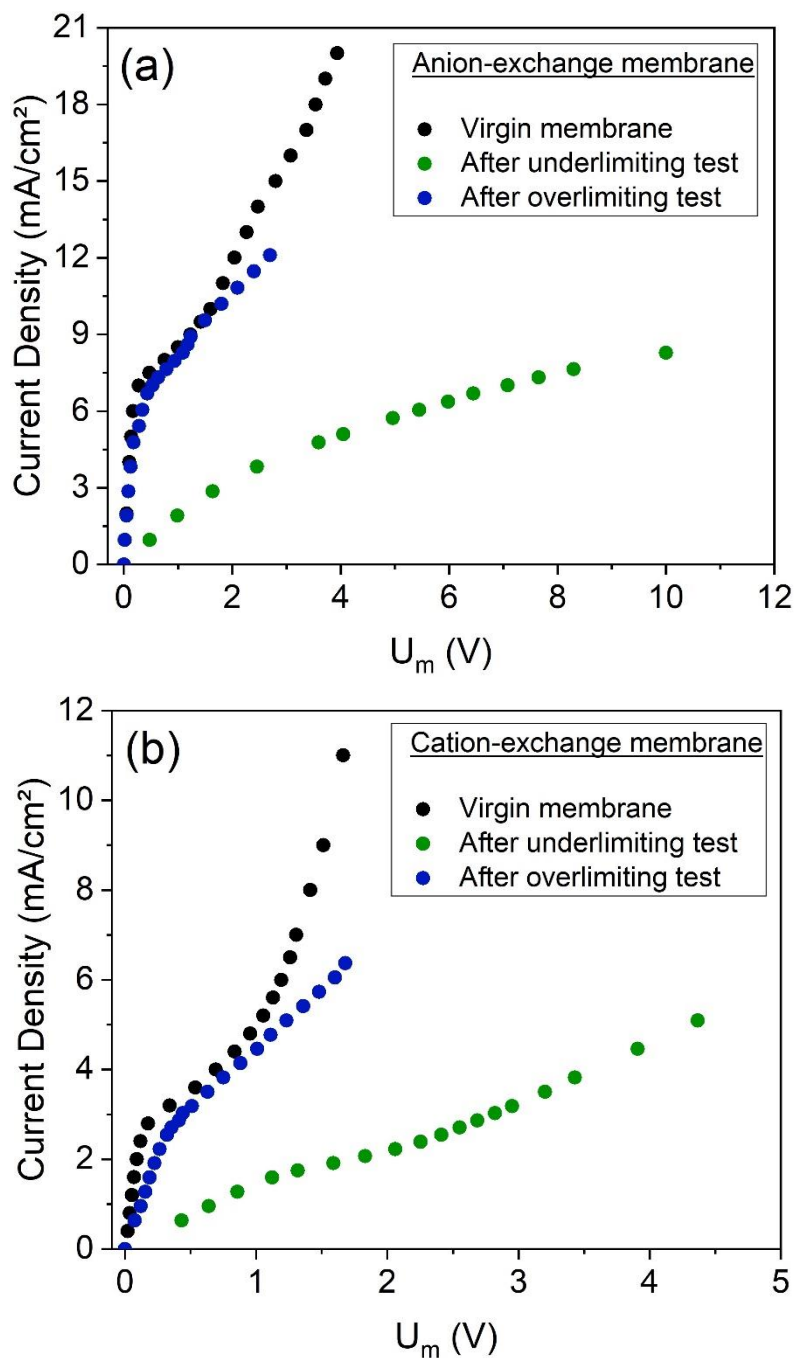
Figure 46 - Current-voltage curves obtained by chronopotentiometry of the a) AEM and b) CEM virgin and after the underlimiting and overlimiting experiments.

Table 18 - Limiting current density and ohmic resistance of both virgin membranes and after electrodialysis.

	Anion-exchange membrane				Cation-exchange membrane			
	i_{lim} (mA/cm²)	Error (%)	Ohmic Resistance ($\Omega.cm^2$)	Error (%)	i_{lim} (mA/cm²)	Error (%)	Ohmic Resistance ($\Omega.cm^2$)	Error (%)
Virgin	6.9	2.2	28	0.3	2.7	2.1	44	3.4
After ED (underlimiting)	3.7	0.9	572	2.0	1.6	0.2	672	1.9
After ED (overlimiting)	6.3	0.4	31	3.2	2.6	1.7	118	3.9

According to Figure 46, the behaviors of the CVCs and the properties obtained for the membranes from the underlimiting test are very distant from the virgin membranes. In turn, the CVCs of the membranes used in the overlimiting test are very close to the virgin membranes. Hence, the overlimiting operation did not cause remarkable modifications in the limiting current density or in the ohmic resistance.

The CVCs of the membranes used in the overlimiting test suggest the lower tendency of fouling occurrence when operating in this condition, which may be explained by the intense electroconvective vortices. Bukhovets et al. (224) proposed the "washing out" effect of electroconvection on organic fouling. According to the authors, the water splitting phenomenon at the AEM enhances the flux of hydroxyl ions and, together with electroosmotic convection and the effect of current exaltation, contributes to "washing out" the species fouled. Hence, considering the differences in the current-voltage curves of the CEMs and AEMs after each electrodialysis (Figure 46) and the intense occurrence of water splitting in the overlimiting test, it may be suggested that in this experiment, fouling/scaling occurrence was not verified in either membrane. Finally, although the "washing out" phenomenon is valid only for anion-exchange membranes, the results here show that the overlimiting operation also helps to mitigate scaling in cation-exchange membranes, but with lower intensity than for AEMs.

Figure 47 shows chronopotentiograms constructed for the anion- (Figure 47a) and cation-exchange membranes (Figure 47b) after both

electrodialysis: the overlimiting and underlimiting test, besides for the virgin membranes. In Figure 47, the current density applied to the AEMs was 7.6 mA/cm², whereas for the CEMs it was 3.2 mA/cm². The potential drop presented is the total one, for showing the influence of electrodialysis also on the ohmic resistance, although in some comparisons of different membranes, some authors represent the "reduced potential drop" by excluding the ohmic potential drop (146). All curves obtained were typical of monopolar membranes, without formation of additional inflexion points during the concentration polarization or the relaxation of the system.
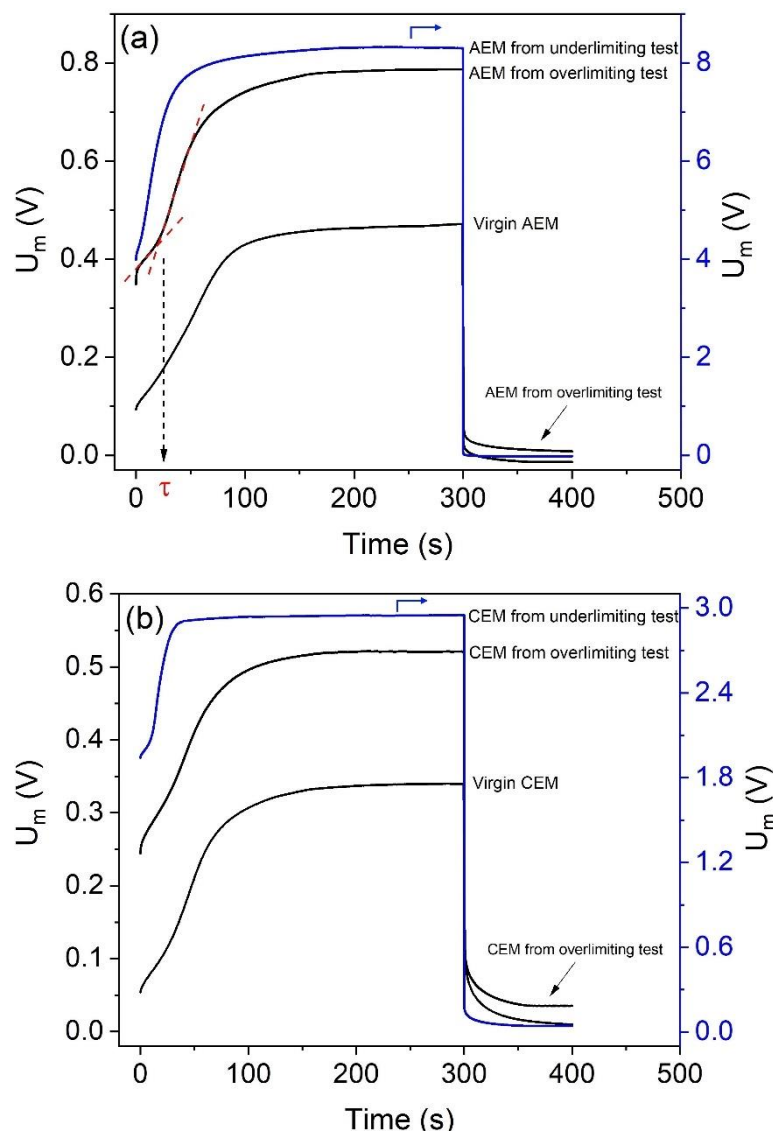
Figure 47 - Chronopotentiograms for the (a) AEMs under 7.6 mA/cm² and b) CEMs under 3.2 mA/cm². The membranes represented are the virgin ones and those used in electrodialysis in overlimiting and underlimiting condition.

For the anion-exchange membranes (Figure 47a), the initial voltage of the virgin one was close to 0.1 V, whereas for the membranes used in electrodialysis, higher voltage values were obtained, especially for the AEM from the underlimiting test. This occurred mainly due to the greater ohmic resistance after the electrodialysis (253). For the cation-exchange membranes (Figure 47b), similar behaviors of the AEMs were obtained: for the virgin CEM, the initial voltage was close to 0.05 V, whereas for the membranes used in electrodialysis, higher voltage values were obtained.

Differences between transition times (τ) were also verified. This can be experimentally determined by the intersection of tangential lines of the first and second stages of the chronopotentiograms, as represented in Figure 47a. For 7.6 mA/cm², the transition time obtained for the virgin AEM was approximately 28 seconds, whereas for the membranes used in the overlimiting and underlimiting tests it was 24 s and 6 s, respectively. Hence, the time elapsed until the depletion of counterions in the diffusion boundary layer in the underlimiting test is lower, which means the concentration polarization occurs earlier. This may be explained by the fouling occurrence and the reduction of the fraction of conductive area in the underlimiting test, as verified in the CVC evaluation. For the cation-exchange membranes, transition times also showed differences between the experiments. For 3.2 mA/cm², the transition time obtained for the virgin CEM was 29 seconds, whereas for the membrane after the overlimiting and underlimiting tests, it was 27 s and 11 s, respectively. As verified for the anion-exchange membrane, lower τ values for the CEM after the underlimiting test are due to the fouling/scaling occurrence. In Figure 47, the potential drop values during the relaxation of the system, i.e. when the current was switched-off, showed the following order: membranes from underlimiting test > membranes from overlimiting test > virgin membranes. The highest potential drop values for the membranes from the underlimiting test are also due to the presence of fouled species.

The relationship between transition time (τ) and fouling/scaling may also be evaluated by using the modified Sand's equation (153) (Equation 38). This equation shows that the $i\tau^{1/2}$ values are constant, independent of current density at a given concentration of electrolytes and it allows the determination of the fraction of conductive area (ε).

$$i\tau^{1/2} = \frac{\varepsilon C_0 z_j F(\pi D)^{1/2}}{2(\bar{t_j} - t_j)}$$ Equation 38

Figure 48 shows the dependence of transition time on current density represented in Sand's coordinates for each membrane used in the electrodialysis tests, in addition to the virgin membranes. Here, the plotted transition times were those associated to current densities at least 1.5 times higher than the limiting current density of the membranes, as suggested by Mareev et al. (147).
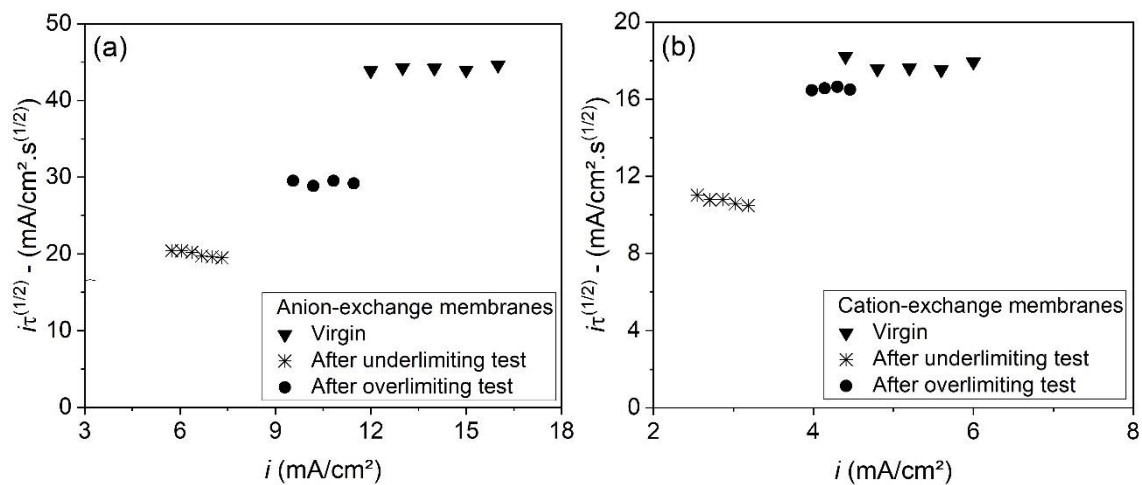
Figure 48 - Dependence of $i\tau^{1/2}$ on current density for the (a) anion-exchange membranes and (b) cation-exchange membranes after the underlimiting and overlimiting tests, besides for the virgin membranes.

As can be seen in Figure 48, the $i\tau^{1/2}$ values of the anion- (Figure 48a) and cation-exchange membranes (Figure 48b) were fairly constant, independent of the current density, and showed the following order: virgin membranes > membranes from the overlimiting test > membranes from the underlimiting test. This supports the previous discussion about the fraction of conductive area: membranes from the underlimiting test present the lowest ε values due to the occurrence of fouling/scaling. These results confirm the lower tendency of fouling occurrence at both membranes when operating in overlimiting condition. Finally, the greater heterogeneity (lower ε) of the membrane after the underlimiting test may also have favored the "funnel effect" (235), which occurs due to the accumulation of current lines within the well conducting areas of the membrane

surface. This also leads to the reduction of transition time, since the potential drop increases more rapidly (218).

5.3.4. Cleaning of the membranes

Considering the proximity between the current-voltage curves of the virgin membranes and those obtained after the electrodialysis in overlimiting condition, an alkaline cleaning procedure was performed with the anion- and cation-exchange membranes used in the underlimiting test, as detailed in Figure 16. After each cleaning step (with NaOH solutions in 0.1, 0.5 and 1.0 mol/L), current-voltage curves were constructed, by chronopotentiometry.

5.3.4.1.   Evaluation of current-voltage curves

The current-voltage curves obtained after each cleaning step are shown in Figure 49, whereas the limiting current densities, ohmic resistances (R_1) and overlimiting resistances (R_3) determined from the curves are shown in Table 19.
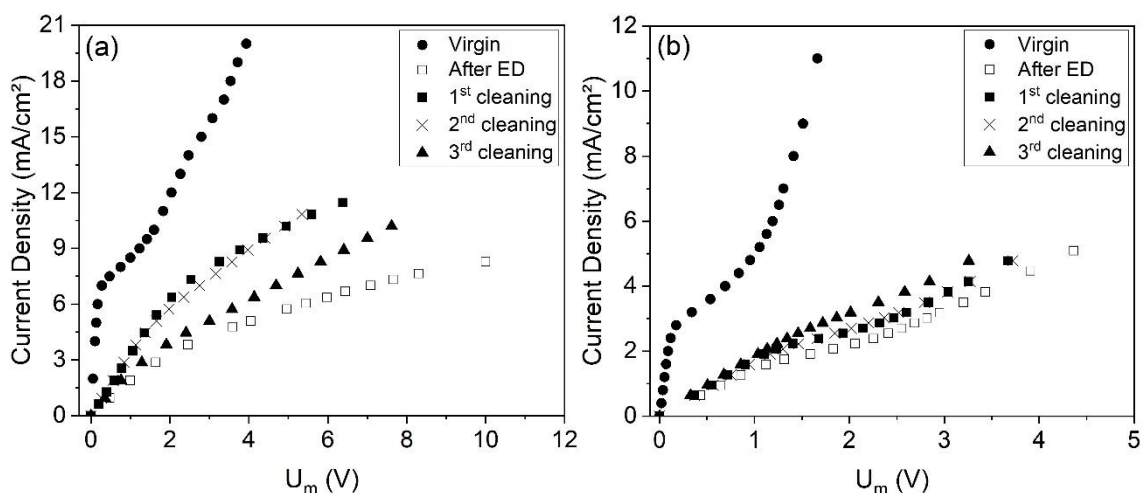
Figure 49 - Current-voltage curves of the a) AEM and b) CEM before the ED (virgin), after the ED (underlimiting test) and after the 1st, 2nd and 3rd cleaning step.

Table 19 - Limiting current density and electric resistances (R_1 and R_3) of both membranes after the cleaning steps.

	Anion-exchange membrane			Cation-exchange membrane		
	i_{lim}	R_1	R_3	i_{lim}	R_1	R_3
	(mA/cm²)	(Ω.cm²)	(Ω.cm²)	(mA/cm²)	(Ω.cm²)	(Ω.cm²)
Virgin	6.9	28	189	2.7	44	89
After electrodialysis	3.7	572	2333	1.6	672	734
1st cleaning	6.8	305	1060	2.1	582	659
2nd cleaning	5.4	298	720	1.9	591	730
3rd cleaning	3.2	398	941	2.4	549	746

According to Figure 49 and Table 19, the first cleaning (0.1 mol NaOH/L) seems to be the most suitable to recover the original features of the anion-exchange membrane after long-term electrodialysis. After the first cleaning, the i_{lim} was increased by 84 %, whereas the ohmic (R_1) and overlimiting resistances (R_3) were decreased by 47 % and 55 %, respectively. Despite the decrease in R_3 of the AEM (69 %) after the 2nd cleaning (0.5 mol NaOH/L), R_1 was not affected. Moreover, the 2nd cleaning caused a decrease in i_{lim}, which was not expected. This may have occurred due to the degradation of the AEM, since all the chronopotentiometric tests were conducted using the same electrolyte. This will be discussed further on.

The 3rd cleaning (1.0 mol NaOH/L) caused an inversion in the behavior of the properties of the AEM: a great increase in R_1 and R_3 if compared to the 2nd cleaning, and a decrease in the limiting current density. This also may have occurred due to the degradation of the AEM. Sata et al. (294) showed that AEMs deteriorate from three parts: the mechanical support (backing fabric), the polymer matrix, and the anion-exchange groups fixed on it. Besides, Merle et al. (295) verified that quaternary ammonium sites, present in the HDX200 membrane, are unstable under alkaline conditions and can be degraded following two main pathways: elimination and/or nucleophilic substitution (296). Hence, the degradation of the AEM by the NaOH solution reduced its fraction of conductive area. This caused the decrease in the limiting current density after the 2nd and, mainly, the 3rd cleaning step.

The increase in R_1 after the 3rd cleaning supports the suggestion regarding the decrease of ε, since the increase in the inhomogeneity enhances the membrane resistance due to the more tortuous counterion pathway (36). Besides, the degradation of the quaternary ammonium sites reduced the attraction between membrane and ions, which also increased the ohmic resistance (108).

Finally, the increase in R_3 after the 3rd cleaning is also in agreement with the reduction of ε, since Choi and Moon (215) verified that the conversion of quaternary amines into their tertiary and neutral forms leads to an increase in the plateau length. As this property represents the energy requirement for destroying the diffusion boundary layer and for changing the main mass transfer mechanism from diffusion and migration to electroconvection (143), the increase in plateau length disfavors the onset of overlimiting phenomena. Therefore, the overlimiting resistance, R_3, increased when the inhomogeneity degree of the membrane increased. Similar results were obtained by Ibanez et al. (216).

Concerning the cation-exchange membrane, the cleaning steps presented similar results on the ohmic and overlimiting resistances. Although the 3rd cleaning was the most efficient to approximate the i_{lim} and the ohmic resistance to the virgin membrane, its use is not recommended, since the 1st cleaning presented similar results and is less harmful to the membrane. The overlimiting resistances also did not show differences after each cleaning, except for the 1st one, which was responsible for the lowest R_3 value.

The differences between the properties values after each cleaning are less evident for the CEM than for the AEM; this occurred since anion-exchange membranes are more susceptible to degradation than cation-exchange ones (297). Hence, the NaOH solutions were not able to degrade the CEM so intensively as the AEM. These results are going to be further discussed in the FTIR-ATR and SEM-EDS evaluations

5.3.4.2.   Evaluation of chronopotentiometric curves

Chronopotentiometric curves were constructed for evaluating the influence of each cleaning step on the concentration polarization, transition times and the tendency of precipitates formation. The potential drop shown in the

chronopotentiograms is the total one (measured), for showing the influence of the cleaning procedure also on the ohmic resistance.

5.3.4.2.1.   Chronopotentiograms of the anion-exchange membrane

Chronopotentiometric curves of the anion-exchange membrane under three current densities after each cleaning step are presented in Figure 50.
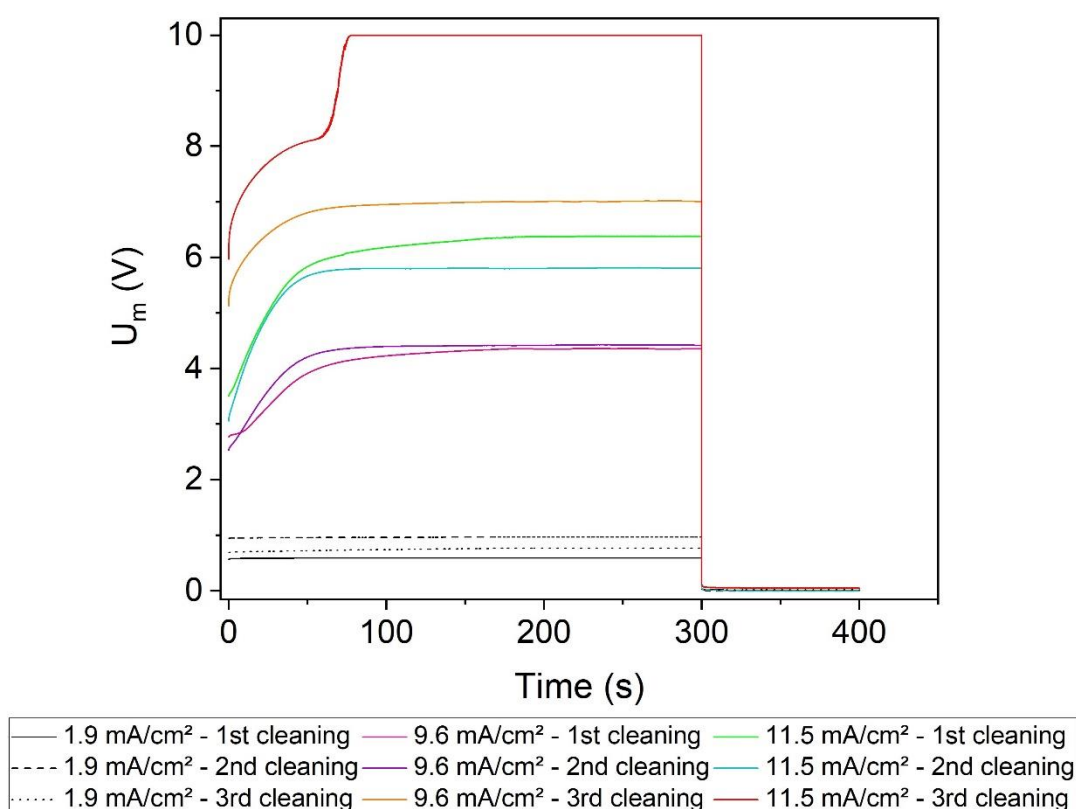
Figure 50 - Chronopotentiograms for the anion-exchange membrane after each cleaning step.

For the AEM, interesting behaviors may be verified in function of the increase in the current density. Under 1.9 mA/cm², the curves showed a constant behavior over time, without inflection points. Therefore, under this condition, migration and diffusion are the main mass transfer mechanisms.

Under application of current densities above the limiting one, an inflection point related to the occurrence of intense concentration polarization can be noted. For 9.6 mA/cm², the curves obtained after the 1st and 2nd cleaning steps are very close, especially at the steady-state condition. However, the curve of the

3rd cleaning under 9.6 mA/cm² is quite distant from the others and presents a higher voltage value. The same behavior can be seen for 11.5 mA/cm²; the final voltage of the curve obtained after the 1st cleaning is slightly higher than the 2nd one, whereas the final voltage of the curve of the 3rd cleaning is much higher than the others. This occurred because of the higher potential drop at the beginning of the ChP for the membrane of the 3rd cleaning. This is related to the ohmic potential drop, U_Ω, over the membrane and two adjacent solutions, where the concentrations are not yet affected by polarization concentration (52,146). As the main contribution of the U_Ω is given by the diluted diffusion boundary layer, the higher U_Ω value after the 3rd cleaning indicates an increase in the resistance of the polarized DBL and, consequently, in the overall cell voltage (142). In electrodialysis, this ohmic drop must be minimized, since energy inputs and electricity costs are directly affected by the cell voltage (57).

Another behavior can be seen in the chronopotentiograms: an unexpected increase in the voltage in the curve of the 3rd cleaning under application of 11.5 mA/cm² and the achievement of the maximum potential of the potentiostat/galvanostat (10 V). This is a typical behavior of precipitate formation on the surface of the membrane or inside it (172). Since all the chronopotentiograms were constructed using the same electrolyte (working solution of electrodialysis), this behavior supports the suggestion of the membrane degradation by the NaOH in 1.0 mol/L. As mentioned, quaternary amines are unstable at alkaline pH values and can be converted into tertiary ones, which have higher catalytic activity towards water splitting than the quaternary amines (118). Hence, the 3rd cleaning may have led to the decrease of quaternary ammonium groups in favor of tertiary amines (298,299) and, during chronopotentiometry, intense water splitting occurred at the AEM. This led to the intense migration of hydroxyl ions through the membrane, whereas protons accumulated on its cathodic side, causing a pH decrease. According to the speciation diagram constructed with the composition of the working solution of electrodialysis (Figure 38), ZnO and mainly CuO are present in the solution from pH values of approximately 8.3 and 7, respectively. Hence, these species may have been responsible for the non-expected increase in the potential drop after the 3rd cleaning. These results indicate that the cleaning with NaOH in 1.0 mol/L is not recommended for the anion-exchange membrane.

5.3.4.2.2.   Chronopotentiograms of the cation-exchange membrane

Figure 51 shows chronopotentiometric curves constructed for the cation-exchange membrane after each cleaning step.
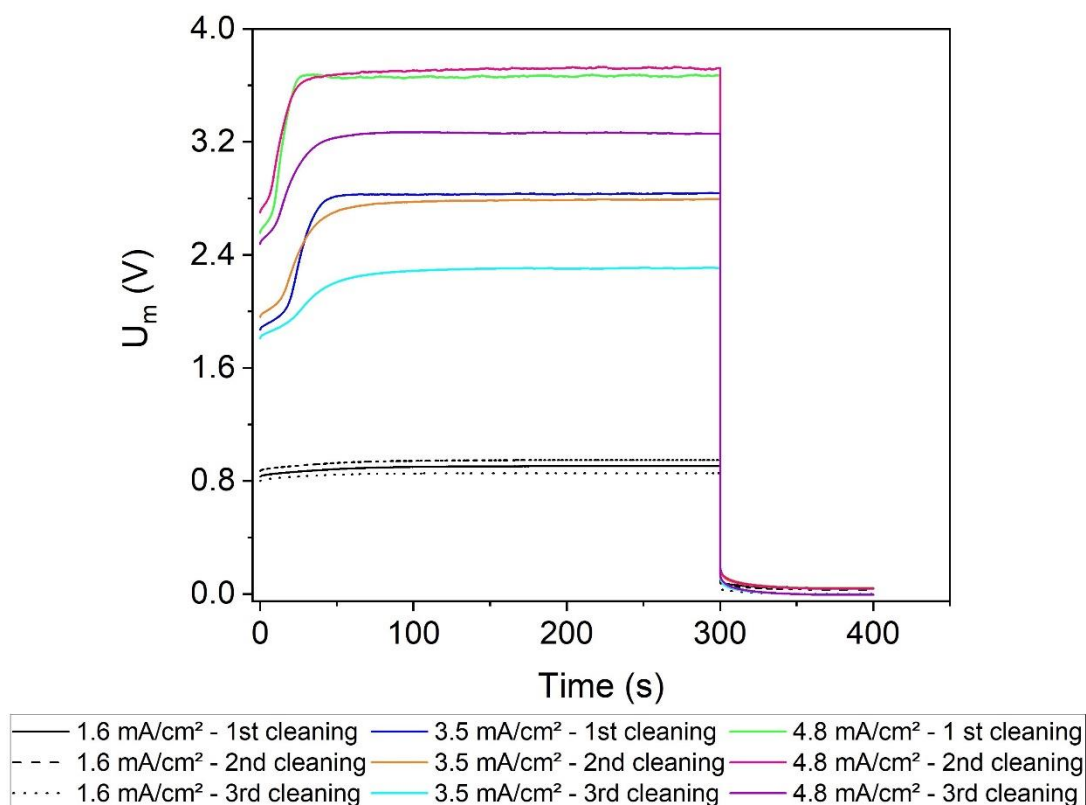
Figure 51 - Chronopotentiograms for the cation-exchange membrane after each cleaning step.

Under application of i = 1.6 mA/cm², migration and diffusion control the ion transfer, since the system is in underlimiting condition, i.e., intense concentration polarization did not occur. Under current densities above the limiting one (3.5 and 4.8 mA/cm²), the behavior of the curves of the 1st and 2nd cleaning steps are very similar, as well as their values of final potential drop. However, lower voltage values were obtained after the 3rd cleaning. The same trend was verified for the U_Ω values. These results are in accordance with the R_1 values presented in Table 19, which were calculated by the slope of the CVCs.

For the cation-exchange membranes, atypical behaviors, such as an unexpected increase in potential drop, were not verified in the

chronopotentiograms. As mentioned, anion-exchange membranes are more susceptible to degradation than cation-exchange membranes. Therefore, the functional groups of the CEM were not degraded as occurred for the AEM. Besides, anion-exchange membranes are more susceptible to the occurrence of water splitting than the cation-exchange ones (215), which also explains the absence of precipitates on its surface during chronopotentiometry.

5.3.4.3.   FTIR-ATR analysis

A FTIR-ATR analysis was performed for evaluating the modifications on the AEM and CEM structure after the cleaning procedure. Both membranes exhibit modifications on their spectral profile after electrodialysis and the cleaning procedure, especially in the frequency region between 1750 – 750 cm^{-1}.

5.3.4.3.1.   Anion-exchange membrane

Figure 52 presents the infrared spectra for the virgin and cleaned anion-exchange membrane after the electrodialysis test.

Figure 52 - IR spectra of the virgin anion-exchange membrane and after 344 hours of electrodialysis (underlimiting test) + three cleaning steps.

In Figure 52, the peaks at 2916 and 2848.5 cm^{-1} correspond to $v_{as,s}CH_2$, respectively (299), where indexes "*as*" and "*s*" refer to asymmetric and symmetric vibrations, respectively. Both peaks are present in the used AEM with lower

intensity, which means that it was degraded by electrodialysis or by the cleaning procedure.

A new peak at 1600.7 cm^{-1} appeared after the membrane use and, as showed by Kołodyńska et al. (300), this may be due to the presence of [Cu(EDTA)]$^{2-}$. Besides, Sawyer and Mckinnie (301) found a peak at 1605 cm^{-1} that corresponds to the -COO$^-$ present in the complex formed by EDTA and copper ions. Hence, this indicates that the cleaning procedure was not able to completely remove this species from the anion-exchange membrane or a species was deposited on the membrane surface after the last chronopotentiometric evaluation.

The peaks at 1463.8 and 1365.4 cm^{-1} are present in both spectra and are related to the -CH$_2$- (299,302,303). A decrease in the intensity of the peak at 1463.8 cm^{-1} can be noted after the membrane use, which occurred due to its degradation. Conversely, the intensity of the peak at 1365.4 cm^{-1} increased. This may be a consequence of the presence of a species composed of EDTA, since Esteban et al. (304) found a band assigned to N-H$^+$ deformation at 1364 cm^{-1} in the solid sample of EDTA disodium salt.

From 1365.4 to 750 cm^{-1}, all the bands showed higher intensity after the membrane use, which may be attributed to the fouling occurrence. At 1261.3 cm^{-1}, a new band was observed. In general, this peak is attributed to the C-O (305) or C-N stretching vibrations (306). However, this may also be related to the deposition of any species with EDTA, since Lanigan and Pidsosny (307) evaluated a sample of EDTA and found a peak at 1262 cm^{-1} related to -COO$^-$. At 1224.7 cm^{-1}, there is a peak for both anion-exchange membranes and this corresponds to the N-C stretching vibrations from the quaternary ammonium functional sites (277).

A peak is present at 1091.6 cm^{-1} only for the used membrane. Lanigan and Pidsosny (307) found a peak at 1109 cm^{-1} associated with the Cu-EDTA complex. Besides, the authors verified that the complexation of EDTA with Cu^{2+} or Zn^{2+} leads to a shift in the bands, and the shift degree depends on the ionic or covalent character of the complex formed. As the peak obtained at 1091.6 cm^{-1} is close to that found by Lanigan and Pidsosny (307) (1109 cm^{-1}), the appearance of this band may be a consequence of the formation of a complex of EDTA + copper or zinc ions. Besides, the results from Esteban et al. (304) supports this

suggestion, since they found a peak at 1090 cm^{-1}, which corresponds to the C-N asymmetric stretching of an EDTA disodium salt sample.

At 1033.7 cm^{-1} the band is present in the virgin membrane and in the used one, but its intensity is greater in the latter. For the virgin membrane, this peak is related to the v(N-C) stretching vibrations from the quaternary ammonium functional sites (308), whereas for the used one, this is related to the fouling occurrence. Lanigan and Pidsosny (307) found a peak at 1020 cm^{-1} related to the δOH(COOH) present in a sample of EDTA disodium salt. Sawyer and Mckinnie (301) found a peak at 1025 cm^{-1} that corresponds to the -COO- of the complex of EDTA with copper ions. Hence, the higher intensity of the band at 1033.7 cm^{-1} in the used membrane may be due to a complex with metals and EDTA, besides the v(N-C) stretching vibrations from the quaternary ammonium.

The bands at 975.9, 889.1 and 858.2 cm^{-1} are present in both AEMs and are associated with the C-H presence (273,300,309). The peak at 827.4 cm^{-1} also corresponds to the C-H and is present only in the virgin membrane, which suggests its degradation after its use. Finally, the peak at 802.3 cm^{-1}, in general, is also related to the C-H, but as it is present only in the used membrane, this may be related to the deposition of any specie.

5.3.4.3.2.   Cation-exchange membrane

The infrared spectra for the virgin and cleaned cation-exchange membrane after 344 hours of electrodialysis is shown in Figure 53.
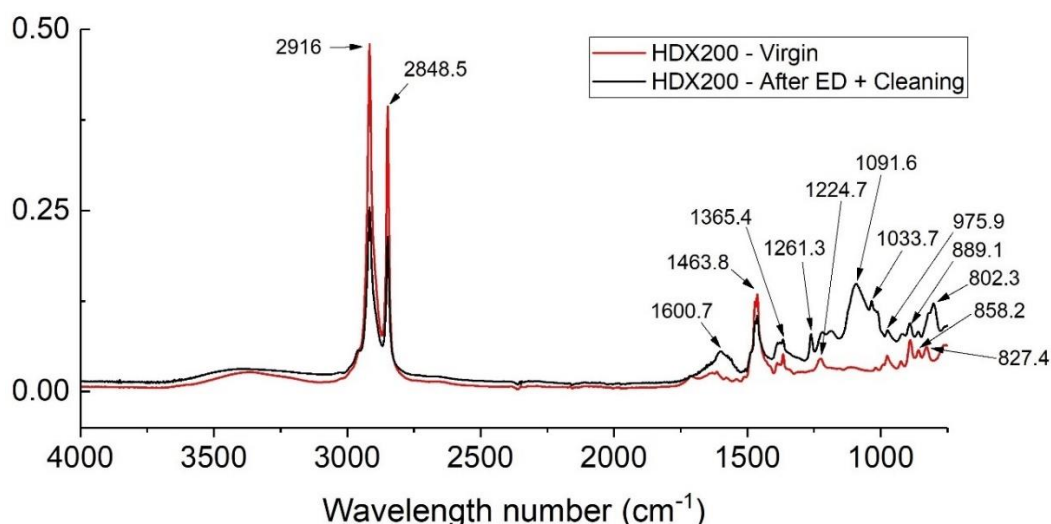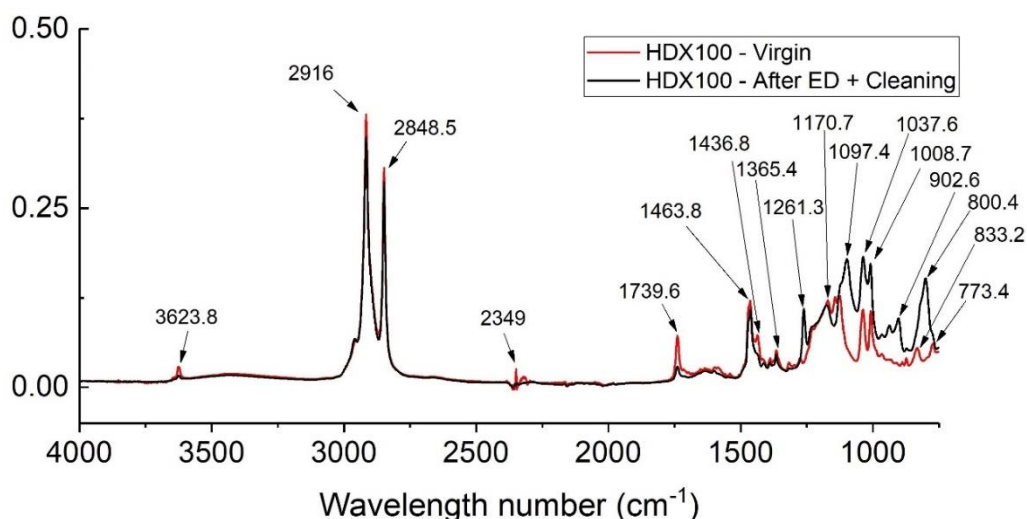
Figure 53 - IR spectra of the virgin cation-exchange membrane and after 344 hours of electrodialysis (underlimiting test) + three cleaning steps.

The peak at 3623.8 cm^{-1} corresponds to the OH stretching (310) and is present only in the virgin membrane, since it was degraded after being used. The bands at 2916 cm^{-1} and 2848.5 cm^{-1} correspond to the $\nu_{as,s}CH_2$, respectively (299). For the CEM, these peaks did not show lower intensities after the membrane usage, as verified for the AEM. This may be explained by the lower degradation of the CEM, since the transfer of most species in solution occurred through the AEM, including the complexes and the OH$^-$ ions. Besides, the higher degradation of the fixed groups of the AEM may be a consequence of the current induced membrane discharge (CIMD) effect. In this case, the hydroxyl ions caused the decomposition of the quaternary groups (113,215), and this does not occur at CEMs. These results are in accordance with the chronopotentiometric curves.

The peak at 2349 cm^{-1} is related to the CO_2 present in the air (306). The band at 1739.6 cm^{-1} corresponds to the C=O stretching (311,312) and for the used membrane, a decrease in its intensity was verified. Both CEMs showed a peak related to the bending of -CH$_2$- at 1463.8 cm^{-1}, whereas only the virgin membrane presented a peak related to the CH$_2$ group at 1436.8 cm^{-1} (277,302). A peak at 1365.4 cm^{-1} was observed for both membranes and this corresponds to δC-H (303).

The first peak that appeared only for the used CEM can be seen at 1261.3 cm^{-1}. Sawyer and Mckinnie (301) found a peak at 1260 cm^{-1}, which was

associated with the -COO- group or C-N bond present in a sample of EDTA disodium salt. Besides, the authors found a peak at 1255 cm^{-1} that was related to the -COO$^-$ group present in a Cu-EDTA complex. Hence, the peak at 1261.3 cm^{-1} found in the present work suggests the fouling/scaling occurrence.

At 1170.7 cm^{-1}, a peak that corresponds to the $-SO_3^-$ functional groups was verified for the virgin and used CEM with the same intensity. At 1097.4 cm^{-1}, another band was obtained only for the used membrane, which also suggests fouling/scaling. Sawyer and Mckinnie (301) found a peak at 1110 cm^{-1} associated with the C-N present in a complex of Zn-EDTA and a peak at 1120 cm^{-1} related to the C-N present in a sample of EDTA disodium salt. As discussed for the AEM in section 5.3.4.3.1 , the complexation of EDTA with Cu^{2+} or Zn^{2+} ions leads to a shift in the bands, and the shift degree depends on the ionic or covalent character of the complex formed (307). Hence, the peak at 1170.7 cm^{-1} may be related to any insoluble species, probably with EDTA.

The bands at 1037.6 cm^{-1} and 1008.7 cm^{-1} correspond to the $-SO_3$ functional groups (273,277) and are present in the spectra of both CEMs, but with higher intensity for the used membrane. These peaks may be related to the fouling/scaling occurrence, since Wang et al. (313) found a peak at 1043 cm^{-1} assigned to the v_{as}(C-N) present in a sample of EDTA, whereas Lanigan and Pidsosny (307) found a peak at 1008 cm^{-1} assigned to $vC-C(CH_2COOH)$. The peaks at 902.6 cm^{-1} and 800.4 cm^{-1} are present only at the used CEM, which may be also associated with the agglomeration of any species with EDTA. This is supported by the work of Lanigan and Pidsosny (307), since they found a peak at 915 cm^{-1} related to the $vC-C(CH_2COO^-)$ present in a sample of EDTA disodium salt.

Finally, the bands at 833.2 cm^{-1} and 773.4 cm^{-1} are present only in the spectra of the virgin CEM, indicating its degradation after its use. Both peaks correspond to the C-H bending (314–316). In general, the AEM showed more peaks related to degradation and fouling occurrence than the CEM.

5.3.4.4.   <u>SEM/EDS analysis</u>

Scanning electron microscopy (SEM) analysis was performed after the cleaning procedure for evaluating modifications in the structures of the anion- and

cation-exchange membranes. Dispersive energy spectroscopy (EDS) analysis through point scan was also performed for qualitatively characterizing the samples. The SEM images are present in Figure 54 for the anion-exchange membrane HDX200 and in Figure 55 for the cation-exchange membrane HDX100.
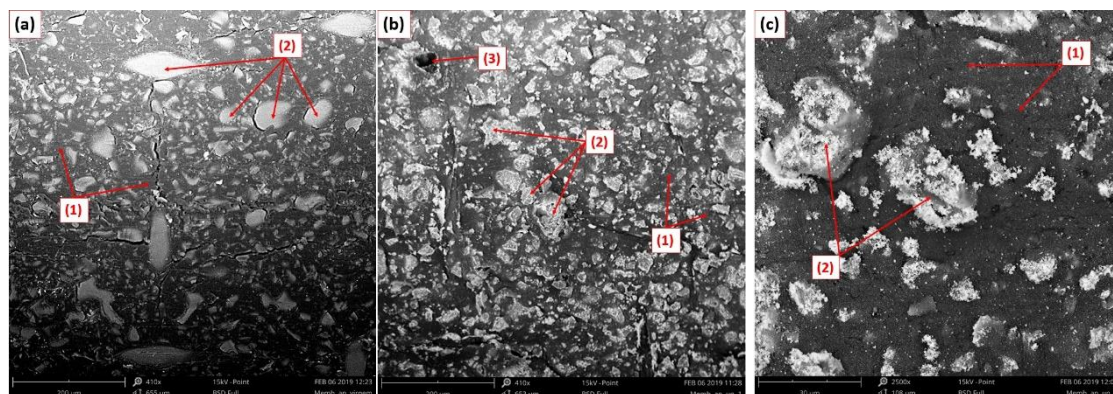
Figure 54 - SEM images of the a) virgin anion-exchange membrane HDX200 (655µm) and after the cleaning and chronopotentiometric procedures at b) 653µm and c) 108µm.
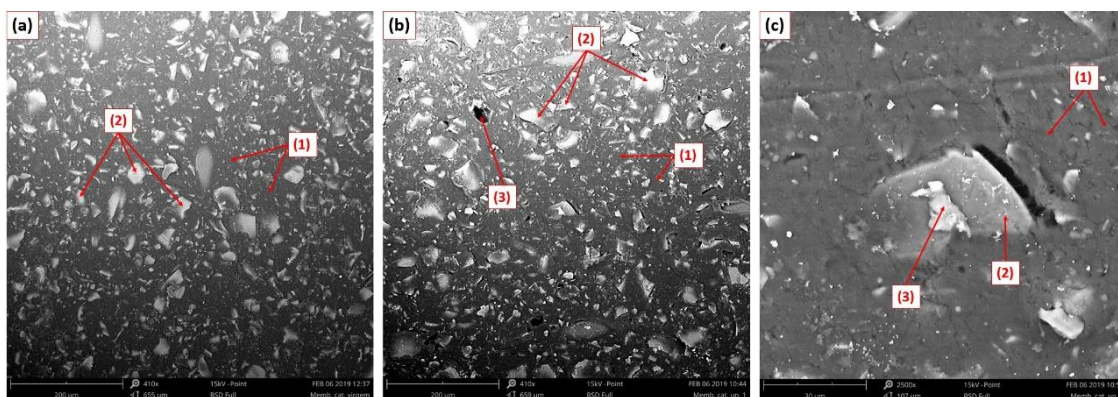
Figure 55 - SEM images of the a) virgin cation-exchange membrane HDX100 (655µm) and after the cleaning and chronopotentiometric procedures at b) 659µm and c) 107µm.

Both membranes have their structures characterized by clearly distinct conductive and nonconductive regions, since there are dispersed agglomerates of ion-exchange particles typical of heterogeneous membranes. Nonconductive regions are shown at points 1 of Figure 54 (a,b,c) and Figure 55 (a,b,c), whereas conductive regions with functional groups are presented at points 2 of Figure 54a and Figure 55a. Point 2 of Figure 54b and Figure 55b also show conductive

regions in the membranes after electrodialysis but, in this case, the EDS analysis showed the presence of some species agglomerated on the fixed charges.

For the AEM, the species agglomerated can be clearly seen in Figure 54c (point 2) and are composed mainly of zinc, which may be present as an oxide (ZnO) or complexed with EDTA [$Zn(EDTA)^{2-}$ or $Zn(EDTA)OH^{3-}$]. The presence of an agglomerate of zinc at the AEM is a consequence of the inefficiency of the cleaning procedure for removing the scaled/fouled species or due to the last chronopotentiometric test performed after the 3rd cleaning. These results confirm those presented in the FTIR-ATR analysis.

For the cation-exchange membrane, the agglomeration of species at the fixed charges is shown in Figure 55c; at point 2, the functional group can be seen, whereas at point 3 an agglomerate of sodium is shown. The sodium was attracted to the fixed charges since the membrane cleaning was conducted with NaOH solutions.

Finally, the degradation of the polymer structure was also observed; points 3 of Figure 54b and Figure 55b show some cavities, which appeared because of the exposure of the membranes to the extremely alkaline solutions (317). These cavities are present exactly on the fixed charges, which means that the concentration of active functional groups was reduced in both membranes. The presence of these cavities finally confirms the results obtained in the evaluation of current-voltage and chronopotentiometric curves (section 5.3.4.1 and section 5.3.4.2), since the decrease in the fraction of conductive area of the membranes was suggested. Some authors reported that membranes ageing affects the polymeric chains more than the ion-exchange groups, which leads to the loss of permselectivity (318,319). Hence, the use of 1.0 mol NaOH/L solution is not appropriate to clean ion-exchange membranes used in electrodialysis.

5.3.5. Conclusions

The treatment of wastewater from the brass electroplating industry was evaluated by two long-term electrodialysis tests: one in underlimiting condition (344 h) and another in overlimiting one for both membranes (186 h). The final conductivities of the concentrated solutions obtained in the overlimiting

test were higher than in the underlimiting one, due to the difference in the species that migrated through the membranes in each experiment. Percent concentrations and percent extractions higher than 340 % and 85 %, respectively, were obtained for copper, zinc and EDTA in the overlimiting test after four cycles of electrodialysis.

The results suggest the occurrence of intense water splitting on the cathodic side of the AEM. Although this phenomenon is undesirable in electrodialysis, herein its occurrence accounted for the highest percent concentrations obtained for copper, zinc and EDTA in the overlimiting test. The water splitting phenomenon, the reaction of protons with complexes and insoluble species, the intense electric field and electroconvection allowed the migration of the ions Cu^{2+} and Zn^{2+} from the AEM to the CEM, which favored their extraction. The improvements in the overlimiting test were obtained due to the electrodialysis current mode used herein, since the concentrate compartments of the cation- and anion-exchange membranes were connected to the same reservoir.

After the electrodialysis, chronopotentiometric tests performed for the CEMs and AEMs showed that the overlimiting operation did not cause remarkable modifications in the limiting current density or in the ohmic resistance, differently from the underlimiting test, since electroconvective vortices minimized fouling and scaling at both membranes. A three-stage alkaline procedure for cleaning the membranes was tested after the chronopotentiometric tests and the most suitable solution for recovering the features of the membranes is 0.1 mol NaOH/L. Current-voltage and chronopotentiometric curves, FTIR-ATR and SEM/EDS analyses showed that the most alkaline solution degraded the membranes.

Considering the species that remained in the diluted solutions, the passage of cations through the CEM, and the lower fouling/scaling at the membranes, the electrodialysis in overlimiting condition was more advantageous than in the underlimiting one. Small intermembrane distances are recommended for the system evaluated in this work, since we verified that it plays an important role in the ionic transfer mainly when water splitting is dominant. Finally, this electrodialysis system has a very promising applicability mainly to treating solutions with complexes and insoluble species, exploiting the phenomenon of water splitting.

5.4. Topic IV: Evaluation of brass electrodeposition at RDE from cyanide-free bath and the recovery of the metals and EDTA extracted, by electrodialysis, on the bath

In this topic, a rotating disc electrode was used to construct voltammetric curves and to evaluate the influence of the rotation speed, the galvanostatic/potentiostatic mode and the charge density on the quality of brass electrodeposition with EDTA. The recovery of EDTA, copper and zinc ions extracted in section 5.3, by electrodialysis, was also assessed in function of the quality of the electrodeposits.

5.4.1. Voltammetric study

5.4.1.1.   Influence of the rotation speed

The influence of the rotation speed on the voltammetric curves was assessed using solutions with the metals together and separated. Figure 56 presents the cathodic peaks of the voltammetric curves obtained for the solution with 0.15 M EDTA, 3 M NaOH and (a) 0.06 M Cu^{2+}, (b) 0.14 M Zn^{2+} and (c) the original bath (Cu, Zn, EDTA and NaOH) under rotation speeds (ω) between 0-2500 rpm. As observed, the increase in the electrode rotation caused a displacement of the curves toward more negative values of current densities. For the agitated solutions, typical plateaus of mass-controlled processes were obtained, mainly for copper-EDTA solutions (Figure 56a). From these plateaus, the limiting current density may be determined, which enhances with the rotation speed of the electrode. Figure 56(d) shows the cyclic voltammetric curves without agitation for the same solutions, where several anodic peaks can be observed.
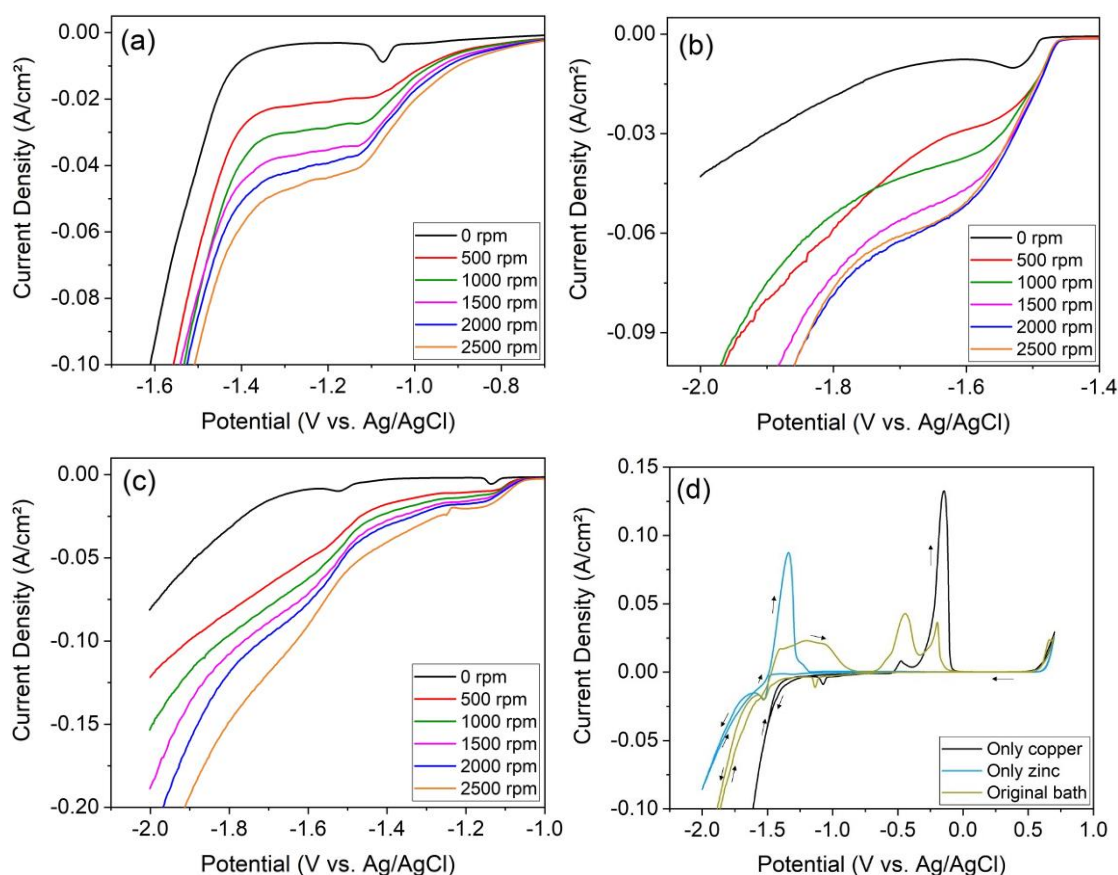
Figure 56 - Cathodic peaks of the cyclic voltammetric curves constructed for solutions with 0.15 M EDTA, 3 M NaOH and (a) 0.06 M Cu^{2+}, (b) 0.14 M Zn^{2+} and (c) the original bath. Figure (d) shows the cyclic curves without agitation for the same solutions of Figures (a, b,c).

From the curves of Figure 56(a) and (b), current values (*I*) were determined at some potentials for solutions with copper-EDTA and zinc-EDTA, respectively, under rotation speeds from 500 to 2500 rpm. Then, the Koutecky-Levich equation (320) (Equation 39) was used for determining the diffusion coefficient (D_0) of the metal ions.

$$\frac{1}{I} = \frac{1}{I_k} + \frac{1}{I_d} = \frac{1}{nFkC_0} + \frac{1}{0.62nFAC_0D_0^{2/3}v^{-1/6}\omega^{1/2}} \qquad \text{Equation 39}$$

In Equation 39, *I* is the measured current, I_k and I_d are the kinetic and diffusion currents, respectively, *n* the number of electrons, *F* the Faraday constant, *k* the kinetic rate constant, *A* the disc area, C_0 the bulk concentration, v the kinematic viscosity (considered as 0.01 cm²/s) and ω the rotation speed in

rad/s. The Koutecky-Levich plots (I^{-1} vs. $\omega^{-1/2}$) for the solution with copper, EDTA and NaOH are shown in Figure 57.
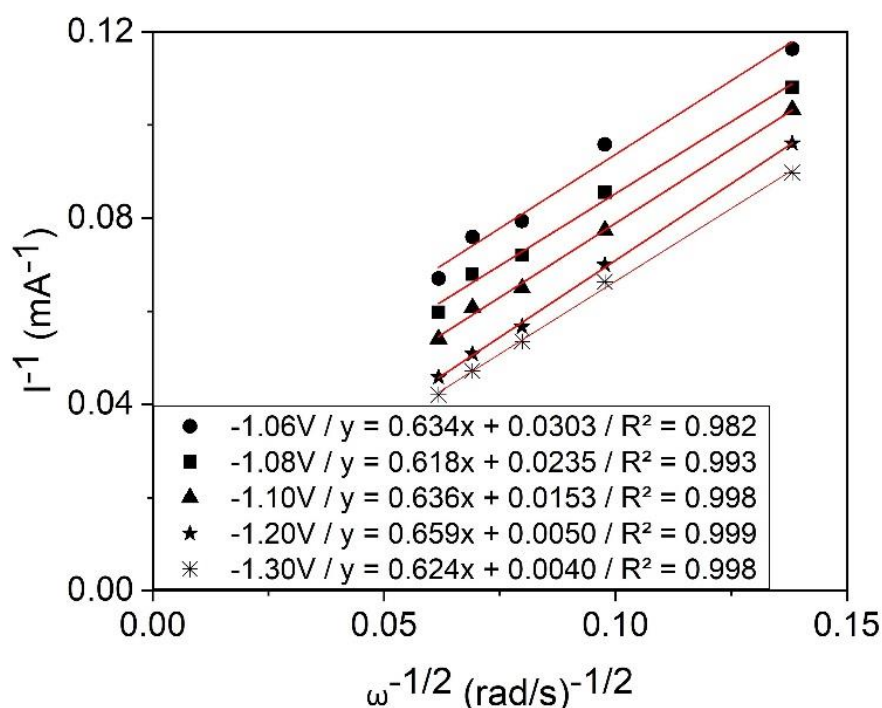
Figure 57 - Koutecky-Levich plots obtained for the solution with copper, EDTA and NaOH.

For the copper-EDTA solution, the curves obtained in Figure 57 for each potential are linear and present virtually the same slope. This means that the equation is valid for the system Cu-EDTA, which is under mass transport control at -1.30 V due to the proximity to the zero intercept. At the other potential values, the reaction is limited by a combination of mass transport and sluggish kinetics. The diffusion coefficient obtained for copper-EDTA was 2.9×10^{-6} cm²/s. This value of diffusion coefficient is comparable to that found in literature for copper-EDTA ($3\text{-}4\times10^{-6}$ cm²/s) (321) and for other complexes with copper, such as copper-sorbitol (2.4×10^{-6} cm²/s) (322), copper–citrate (2.1×10^{-6} cm²/s) (323) and copper-glycerol (3.5×10^{-6} cm²/s) (321). For zinc-EDTA, the diffusion coefficient could not be determined, since the curves obtained were not a straight line. As can be seen in the voltammograms of zinc solutions (Figure 56b), the rotation speed caused a vertical displacement of the curves. Therefore, for any potential between approximately -1.5 V and -1.7 V, the curves are in different

conditions depending on the rotation speed (see 500 rpm and 2500 rpm). This may be explained by the more negative reduction potential of zinc than copper since the effect of hydrogen evolution on the deposition of the former is higher. Besides, the non-linearity of the curves obtained for the solution with zinc-EDTA may suggest a kinetic limitation (324,325).

For the agitated solutions with only copper (Figure 56a) a reduction plateau at approximately -1.0 V begins to appear. We can infer that at this potential, a primary bulk nucleation and growth of copper on 1010 steel occurred. The well-defined reduction peak for the solution without agitation shows that the mass transfer controls the system, as confirmed by the Koutecky-Levich plots. In turn, at the beginning of the reduction in the systems under agitation, the electrodeposition is controlled by charge transfer. For the solution with only zinc without agitation (Figure 56b), a well-defined reduction peak can be seen at approximately -1.5 V, whereas for the solutions with zinc under agitation, the current density negatively increased without achieving a well-defined plateau. As already mentioned, this may have occurred due to the mixed (charge and mass transport) control of the Zn-EDTA system, besides the greater influence of hydrogen evolution on the deposition of zinc than of copper.

The voltammetric curve for the original bath (Figure 56c) showed a peak at approximately -1.1 V, which is related to the deposition of copper. Another peak was verified at approximately -1.5 V with and without agitation due to the reduction of zinc. For the agitated solutions, the curves also showed plateaus instead of well-defined peaks, as verified for the static solution.

Figure 56d shows that at potential values more positive than the crossover potential, which is that related to the null current density ($i = 0$), we can see anodic peaks related to the oxidation of the separated metals or together in the bath. For the solution with only copper, the potentials of the two oxidation peaks were the same of the original bath, but with different intensities. For the solution with only zinc, a change in the curve behavior can be seen by a shoulder at the end of the oxidation peak, which may be associated with the dissolution of some different species of zinc that was deposited during the reduction step. It can be also seen that the oxidation peak is well defined when zinc is the only metal in solution, but the peak becomes quite large in the presence of copper, exhibiting a very different behavior. By analyzing the curves of Figure 56d, the formation of several

Cu-Zn alloys may be suggested or, at least, intermediate phases. For both curves present in Figure 56d, the exponential growth of the anodic current at potentials over 0.5 V is due to oxygen evolution. The distance between the reduction potential and the oxidation potential is larger for the solutions with only copper than zinc, implying more intense irreversibility for the former.

Finally, the decrease in the current density at potentials more negative than -1.5 V can be attributed to the hydrogen evolution. This indicates that the use of EDTA is more interesting than pyrophosphate and glycerol-zincate due to their higher limiting potential with respect to the hydrogen evolution (-1.3 V and -1.2 V, respectively) (73). However, the peak of zinc deposition is very close to the beginning of the hydrogenation. As will be discussed, this influences the quality of the deposits.

5.4.1.2.   Influence of ions concentration

The influence of copper and zinc concentration was evaluated. Curves of cyclic voltammetry with solutions of 0.15 M EDTA, 3 M NaOH and Cu^{2+} in 0.03 M, 0.06 M and 0.1 M and Zn^{2+} in 0.06 M, 0.1 M and 0.14 M were constructed (Figure 58).
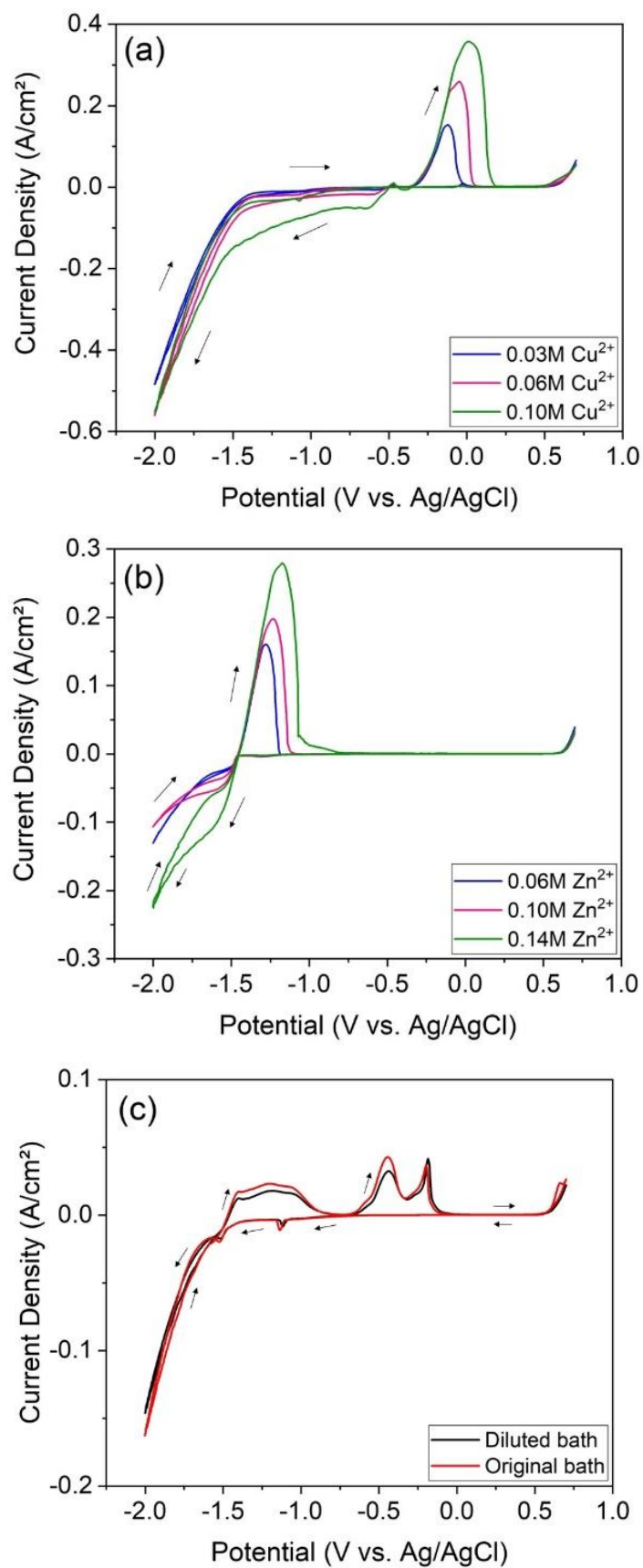
Figure 58 - Cyclic voltammetric (CV) curves of solutions with 0.15 M EDTA, 3 M NaOH and (a) Cu^{2+} and (b) Zn^{2+} under 500 rpm. Figure (c) presents the CV of the bath with 25 % (v/v) of the solution from electrodialysis without agitation.

Accroding to Figure 58, the increase in the concentration of the metals has a similar effect to the rotation speed, that is, a shift of the curve occurs towards more negative and positive current densities related to the reduction and oxidation of the metals, respectively. A cyclic voltammetry for the bath with 25 % (v/v) of the solution from electrodialysis is also shown in Figure 58. We can see that the dilution of the bath virtually did not alter the cyclic voltammetric curve. Hence, deposits with similar qualities may be expected.

5.4.2. Electrodeposition tests

5.4.2.1.   Potentiostatic mode

Deposits in potentiostatic mode were obtained at potential values between -1.3 V and -1.5 V and rotation speeds from 0 to 1500 rpm. The duration of the electrodepositions was 2.5 min. Table 20 shows the Cu/Zn proportions, determined by SEM/EDS, and the deposition images.

Table 20 - Proportion of Cu/Zn and deposits images for different potentials applied and rotation speeds.

Potential (V)	Rotation speed (rpm)			
	0	500	1000	1500
-1.30				
	8.8	4.7	4.8	4.1
-1.35				
	5.9	3.2	3.3	4.0
-1.40				
	3.2	2.5	2.7	2.4
-1.45				
	0.9	1.4	1.6	1.9
-1.50				
	0.7	1.0	0.9	0.9

As can be seen, the experiments performed without agitation generated homogeneous deposits, with brightness and different colors depending on the applied potential. At -1.3 V, the electrode presents a color typical of copper, since the amount of this metal deposited was much higher than zinc (Cu/Zn of 8.8). At -1.35 V, the color resembles copper, but lighter, due to the greater presence of zinc. At -1.40 V, a typical brass deposit was obtained, with Cu/Zn ratio of 3.2. At -1.45 V, the electrode showed a darker color, whereas at -1.5 V, the deposit was black. The darkening of the deposits at potentials of -1.45 V and -1.50 V can be justified by the proximity to the region of hydrogen evolution, since the hydrogenation changes the properties of the deposit especially in the presence of zinc. It is known that the presence of EDTA increases the hydrogen entry into the electrode during the H_2 evolution (326), which also facilitates its darkening at negative potentials.

Figure 59 shows the SEM images of the deposits obtained potentiostatically at -1.45 V (Figure 59a) and -1.50 V (Figure 59b) without

agitation. For potentials of -1.3 V, -1.35 V and -1.40 V, the SEM images are not shown, since they were very similar to that obtained at -1.45 V (Figure 59a), with a very homogeneous coating and some disperse globular crystallites. EDS analysis indicates that the whole surface, including the crystallites, presented very similar Cu/Zn proportions. At -1.5 V (Figure 59b) the SEM image greatly differed from the others. In this case, the deposit showed polyhedral crystallites. This type of deposit is caused by the hydrogen evolution. For all the tested conditions, the absence of cracks suggests that the deposit of brass is not under stress, which means that the use of EDTA is more promising than other alternative complexing agents, such as glycerol and pyrophosphate (73).
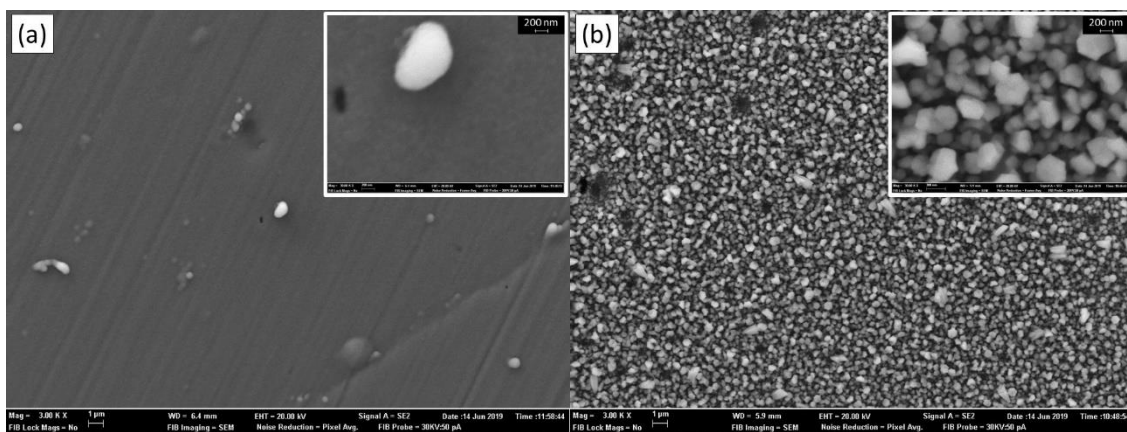
Figure 59 - SEM images of the Cu-Zn deposits obtained in the potentiostatic mode at a) -1.45 V and b) -1.5 V.

According to Table 20, the rotation of the electrode altered the color of the deposits compared to the static mode, since it decreased the Cu/Zn proportion. Although the potentials of copper reduction are less negative than zinc, the latter has a higher concentration than the former. Therefore, as verified by the voltammetric curve, we can suggest that the electrode rotation enhanced the influence of hydrogen evolution. Hence, the convection associated with the higher concentration of zinc favored its deposition. This behavior was mainly seen at potentials of -1.3 V, -1.35 V and -1.4 V. At the most negative potentials (-1.45 V and -1.5 V) the rotation did not cause remarkable changes in Cu/Zn proportions, especially at -1.5 V. At these two potentials, the evolution of the hydrogen was also responsible for the convection in the region near the electrode, therefore, the rotation no longer caused an increase in the zinc deposition.

The deposits became darker with the rotating speed increasing, since the agitation favors the hydrogen evolution (327). However, the darkening did not occur at -1.30 V, since the agitated electrodes presented a very homogeneous deposit, typical of brass and with brightness. These results suggest that instead of applying negatively high potentials in the absence of agitation, operating at -1.3 V with agitation may be more interesting, since quite uniform brass deposits are obtained, possibly with lower energy consumption.

Musa et al. (70) evaluated the effect of agitation on the electrodeposition of brass with cyanide as complexing agent and verified the inverse behavior; the forced convection favored the transport of copper to the electrode and disfavored the deposition of zinc. Besides the differences between the properties of cyanide and EDTA, the proportion of metals in the bath evaluated by the authors was 70%Cu and 30%Zn, exactly the inverse of that evaluated by us. In turn, Gómez and Vallés (328) evaluated the effect of rotation on Zn and Co deposits and noted that forced convection increased the zinc deposition in various times tested.

In general, the experiments under rotation of 500, 1000 and 1500 rpm presented a brass appearance with similar colors for each applied potential and similar Cu/Zn proportions. Monev et al. (329) studied the behavior of the evolution of hydrogen during electrodeposition of zinc on steel and verified that varying the rotation speed of the electrode between approximately 325 – 3845 rpm, the rate of hydrogenation did not change. In this case, the rate determining step of the hydrogen evolution process is electron transfer. We can suggest, therefore, that the Cu/Zn proportion virtually did not vary with the increase of rotation speed from 500 to 1500 rpm, since the hydrogenation remained constant and this determined the proportion of the metals deposited at each potential.

SEM images also showed changes between the deposits obtained with and without agitation, as shown in Figure 60 for -1.45 V. The morphologies obtained under all rotation speeds were very similar (Figure 60b and Figure 60c), showing a cluster of spherical particles that had their amount and size increased with the increasing rotation speed. However, both are very different from those obtained without agitation (Figure 60a). This is in accordance with the visual appearance of the electrodes shown in Table 20. Without agitation, disperse crystallites were obtained, whereas under agitation, they were agglomerated in bigger and circular formats.
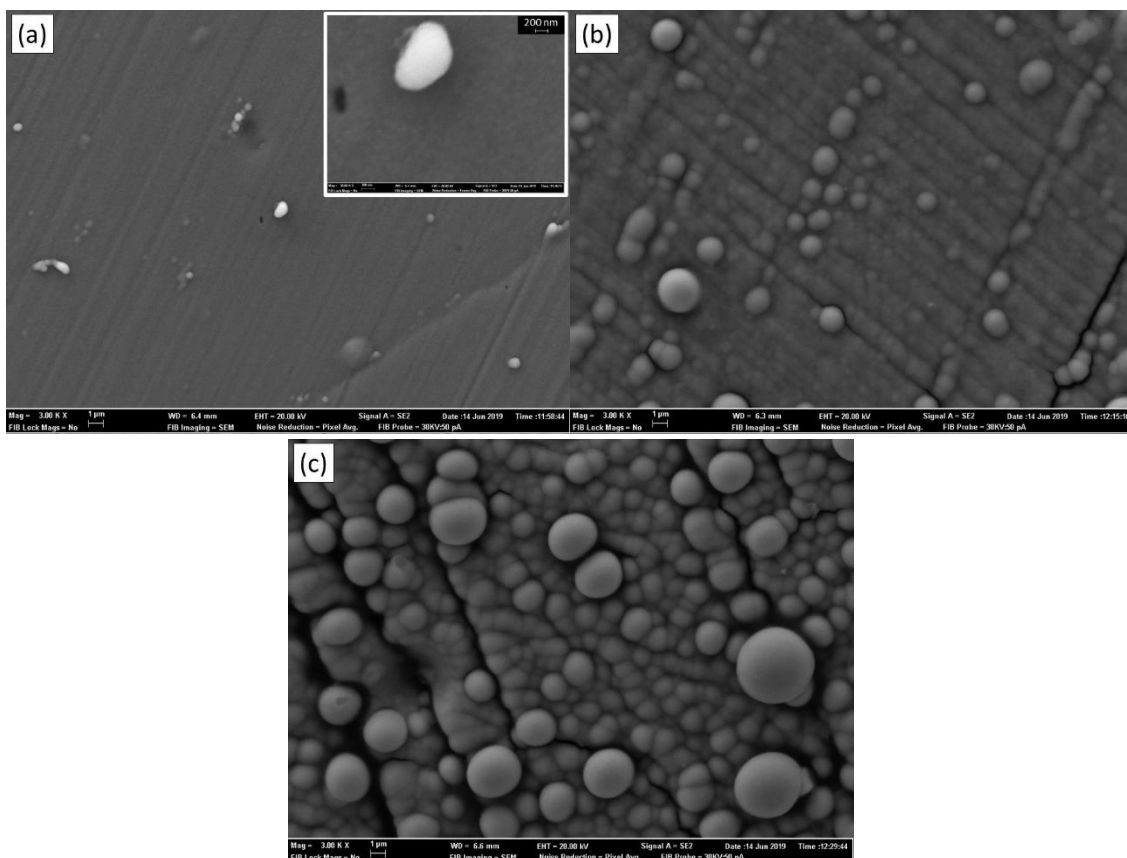
Figure 60 - SEM images of the Cu-Zn deposits obtained at -1.45 V under a) 0 rpm, b) 500 rpm and c) 1500 rpm.

5.4.2.2. Galvanostatic mode

For approximating the results to the industrial conditions, electrodepositions in galvanostatic mode were performed by applying the average of the final values of current density obtained in the potentiostatic curves. Here, the experiments were conducted without agitation with duration of 2.5 min, except in the charge density evaluation. Table 21 shows the applied current density values, the Cu/Zn proportions obtained and the visual aspect of the deposits. As verified, the Cu/Zn proportions were very close to those obtained in the potentiostatic mode (compared to Table 20). However, the visual appearance of the deposits was affected and, in general, potentiostatic electrodepositions provided deposits with better quality.

Table 21 - Cu-Zn deposits obtained in galvanostatic mode without agitation.

Current density (mA/cm²)	Cu/Zn proportion	Visual aspect
-3.2	9.0	
-3.6	4.9	
-4.0	2.6	
-6.0	1.1	
-15.1	0.6	

The images obtained by SEM are also quite different for the applied current densities, as shown in Figure 61. Changes in the deposits can also be seen by comparing those obtained in potentiostatic mode (Figure 59) with those obtained in galvanostatic mode. This may be explained by the different mechanisms of deposition in each experiment. For -3.2 mA/cm² (Figure 61a), the deposit was homogeneous and covered by small coalesced globular crystallites; for -3.6, -4.0 and -6.0 mA/cm², the deposits were very similar (not shown). In Figure 61b, the presence of particles and clusters can be seen for -6.0 mA/cm²; their amount and size enhanced with the current density. Finally, for -15.1 mA/cm² (Figure 61c), polyhedral crystallites were present, as verified for the potentiostatic mode.
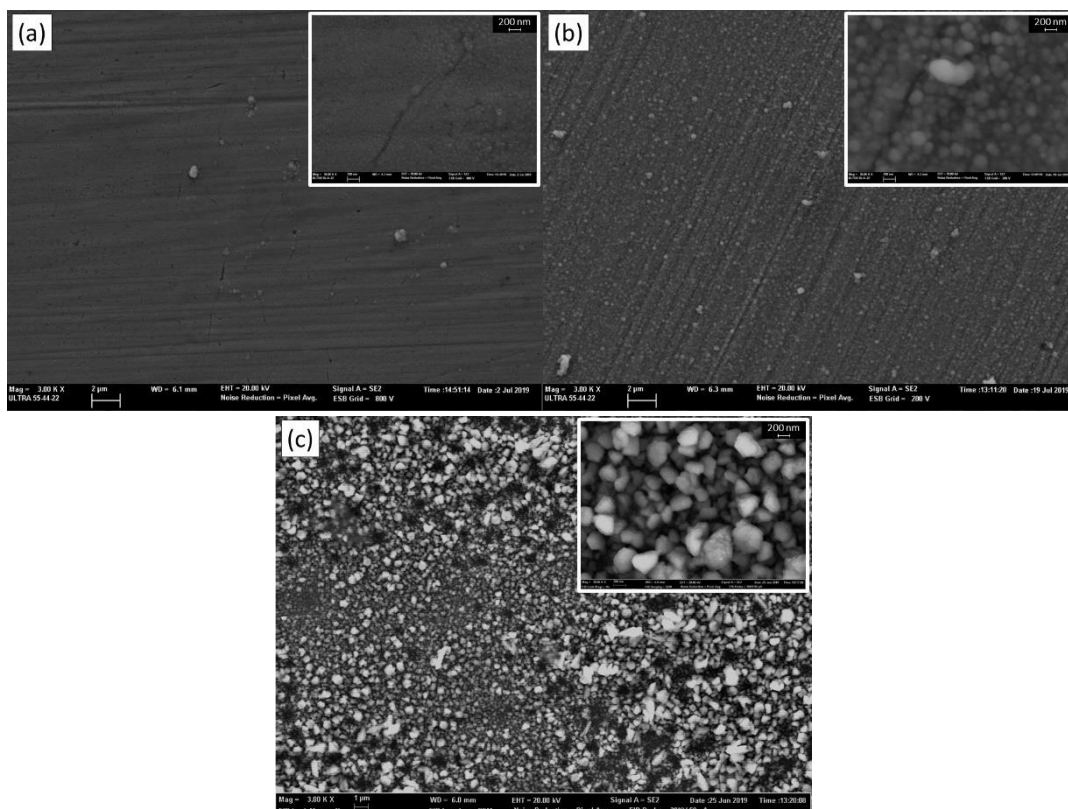
Figure 61 - SEM images of the Cu-Zn deposits obtained in galvanostatic mode at (a) -3.2 mA/cm², (b) -6.0 mA/cm², (c) -15.1 mA/cm².

The curves of potential *vs.* time obtained in the galvanostatic depositions are shown in Figure 62. We can note some changes of the curve behavior for each applied current density. A plateau at potential of approximately -1.1 V followed by a sudden drop of the potential can be seen, which is due to the reduction of copper. Then, the steady-state was achieved and, at this condition, both metals were electrodeposited. This steady-state condition occurred earlier with the increase in current density and the plateau related to the copper deposition was reduced. Hence, increasing the current density, both metals tend to be electrodeposited at the same time. This explains the differences of the SEM images presented in Figure 61. For all current densities, the final potentials achieved were very close to those values applied in the potentiostatic mode.
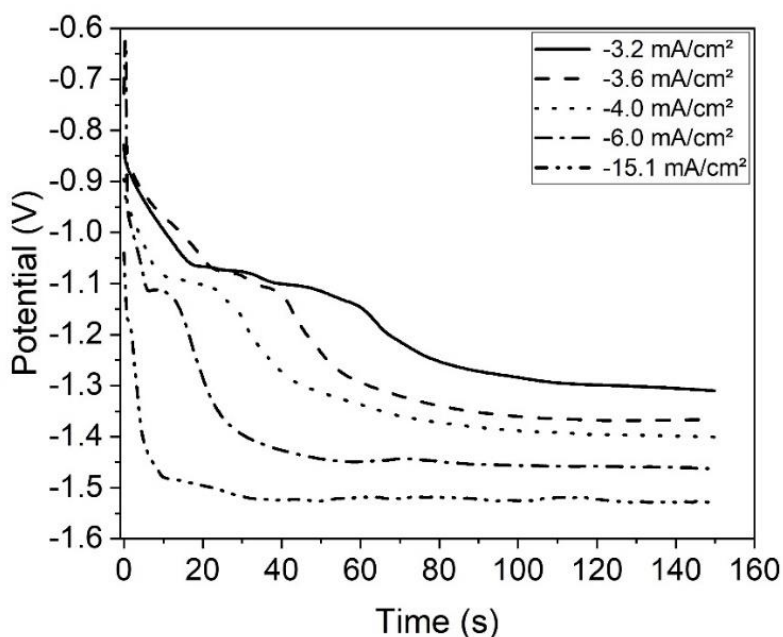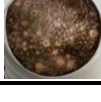
Figure 62 - Potential transients obtained for the galvanostatic electrodepositions.

5.4.2.2.1.   Influence of the charge density

The charge density was also evaluated in function of the Cu/Zn proportion and the visual aspect, as shown in Table 22. The experiments were performed by applying -4.0 mA/cm² (the current density related to the potential of -1.4 V) during different times and without agitation.

Table 22 - Influence of the charge density on the brass electrodeposition.

Time (s)	Charge density (C/cm²)	Cu/Zn proportion	Visual Aspect
75	0.3	27.8	
150	0.6	2.8	
248	1.0	5.2	
495	2.0	4.5	
2476	10.0	0.9	

According to Table 22, increasing the charge density, the quality of the deposits was affected. For 0.3 C/cm², the electrode showed a typical color of pure copper and a relatively homogeneous appearance. In this case, the time was not enough for the zinc deposition. For 0.6 C/cm² and 1.0 C/cm² the deposits were typical of brass, but, in the latter, the electrode began to darken, whereas at 10 C/cm² the electrode was almost completely black. This may have occurred due to the depletion of metal ions on the electrode surface, especially copper, since it was present in lower concentration, and the evolution of hydrogen. This is in accordance with the reduction of the Cu/Zn proportion at charge densities from 1 to 10 C/cm². These results show that, for the bath evaluated herein, operating under approximately 0.5 – 1.0 C/cm² is more interesting.

The SEM images (Figure 63) were also very different for each charge density. For 0.3 C/cm² and 0.6 C/cm², we can see that the coatings were made up of clusters grouped in nodules of different dimensions. For 1.0 C/cm², the clusters were also present with some large disperse crystallites. For 2.0 C/cm², the deposit exhibited coalesced globular crystallites of larger sizes. For all charge densities, no interstices were observed between the clusters, indicating that the coating covered the entire surface even for the lowest time evaluated.
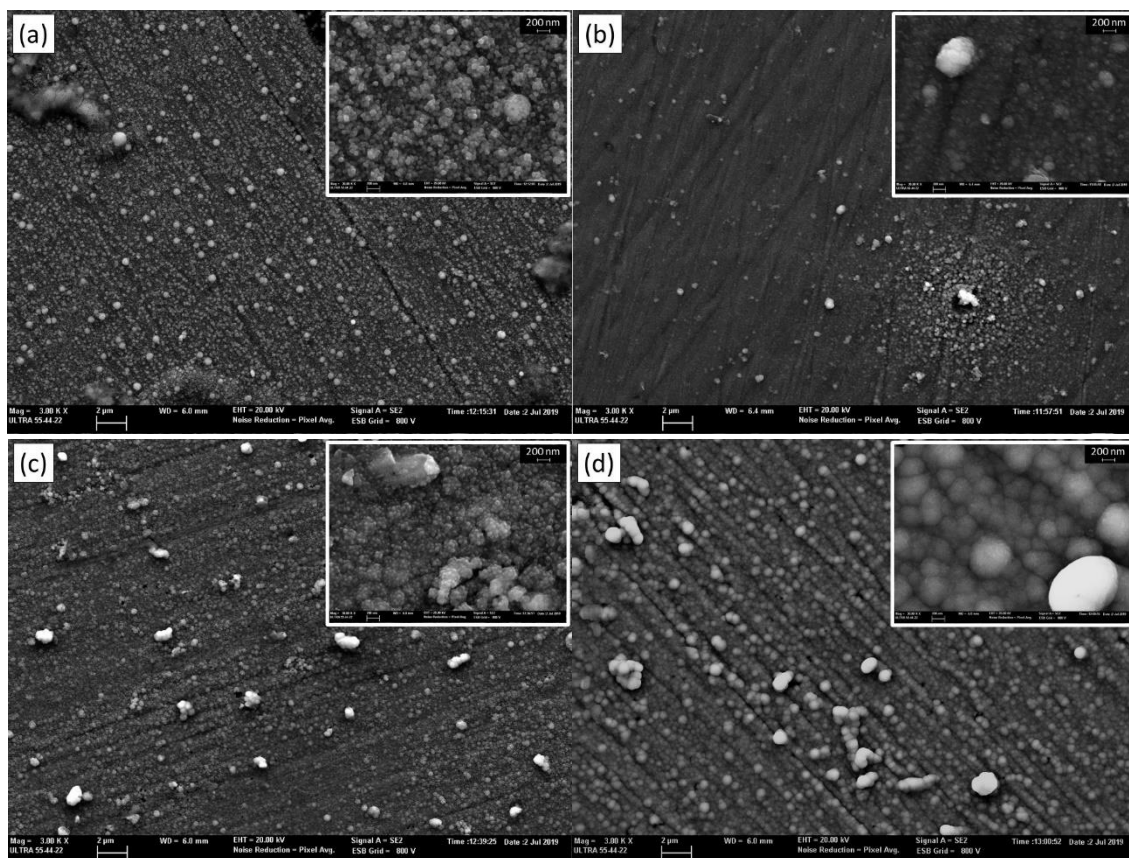
Figure 63 - SEM images of the Cu-Zn deposits obtained in galvanostatic mode at -4.0 mA/cm² and charge density of (a) 0.3 (b) 0.6 (c) 1.0 and (d) 2.0 C/cm².

5.4.2.3. Addition of the concentrated solution obtained from the wastewater treatment into the bath

To close the loop on the brass electrodeposition with EDTA and the treatment of the rinsing water generated in this process, we evaluated the dilution of the original bath (75 % v/v) with the concentrated solution obtained after the 4th cycle of the electrodialysis (25 % v/v) conducted in overlimiting condition in section 5.3. The electrodeposition tests were performed without agitation in potentiostatic (-1.3, -1.35, -1.4, -1.45, -1.5 V) and galvanostatic mode (-3.8, -4.2, -5.1 mA/cm²). Table 23 shows the composition of the solution tested here, whereas Table 24 shows the visual aspect of the electrodeposits obtained.

Table 23 - Conditions of the electrodeposition tests performed with solutions with 75 % (v/v) of the original bath and 25 % (v/v) of the solution from electrodialysis.

	Cu^{2+} (M)	Zn^{2+} (M)	EDTA (M)	Na^+ (M)	SO_4^{2-} (M)	Applied potential/current density
Original bath	0.06	0.14	0.15	3.0	0.2	
Electrodialysis	0.003	0.004	0.007	0.378	0.1	
Experiments performed in potentiostatic mode						
75 %Bath and 25 %ED	0.046	0.106	0.114	2.345	0.175	-1.30, -1.35, -1.40, -1.45, -1.50 (V)
Experiments performed in galvanostatic mode						
75 %Bath and 25 %ED	0.046	0.106	0.114	2.345	0.175	-3.8, -4.2, -5.1 (mA/cm²)

Table 24 - Cu-Zn deposits obtained in potentiostatic and galvanostatic mode, without agitation, with 75 % (v/v) of the original bath and 25 % (v/v) of the solution from electrodialysis.

Potentiostatic mode		
Potential (V)	Cu/Zn proportion	Visual aspect
-1.35	4.6	
-1.40	2.2	
-1.45	0.8	
-1.50	0.5	

Galvanostatic mode			
Current density (mA/cm²)	Charge density (C/cm²)	Cu/Zn proportion	Visual aspect
-3.8	0.56	4.7	
-4.2	0.63	2.8	
-5.1	0.76	1.1	

The deposits obtained potentiostatically at -1.35 V and -1.4 V were slightly opaque, whereas at -1.45 V the deposit was bright and uniform. At -1.5 V it was very dark, as also verified for the original bath without its dilution.

The deposits obtained galvanostatically also showed some visual differences compared to the potentiostatic mode especially at -5.1 mA/cm², although the final values of potential were very similar to those from the potentiostatic depositions. Considering the general deterioration of the quality of the deposits after the dilution of the original bath, this is not recommended.

5.4.2.4.   Concentration adjustment of the solution from electrodialysis

Considering the poor quality of the deposits obtained in section 5.4.2.3 after diluting the original bath, we evaluated the adjustment of the concentration of the solution obtained by electrodialysis under overlimiting condition until reaching the concentration of the original bath. Electrodepositions in potentiostatic   (-1.4 V   and   -1.45 V)   and   galvanostatic   mode (-4.0 and -6.0 mA/cm²) were performed and the results are shown in Table 25. The applied current densities in the galvanostatic experiments were the same of those applied using the original bath (Table 21).

Table 25 - Cu-Zn deposits obtained in potentiostatic and galvanostatic mode, without agitation, after the adjustment of the concentration of the ED solution.

Potentiostatic mode		
Applied potential (V)	Cu/Zn proportion	Visual aspect
-1.40	3.3	
-1.45	0.9	
Galvanostatic mode		
Current density (mA/cm²)	Cu/Zn proportion	Visual aspect
-4.0	3.8	
-6.0	1.7	

According to Table 25, the deposits were uniform, bright and presented different colors depending on the applied potential/current density. By comparing the coatings with the results showed for the original bath (Table 20 and Table 21), we can see that the values of Cu/Zn proportions and the colors of the deposits with the adjusted bath virtually did not change. It is known that the presence of neutral ions, such as Na^+ and SO_4^{2-}, in the bath may affect the quality of the electrodeposits due to the increase in the electrolyte conductivity. This occurs since neutral ions carry part of the current and hinder the transport of ions that are deposited on the electrode, generating more compact deposits (330,331). As

shown in Table 25, the different concentrations of OH^-, Na^+ and SO_4^{2-} in the adjusted bath did not damage the quality of the deposits. However, in industrial applications, the concentration of neutral ions may vary and this needs to be considered. Besides, additives are often introduced into industrial baths since they can control the deposition rate, alter the crystallization mechanisms, avoid excessive hydrogen formation, and improve the brightness of the deposits (64,84,322). As additives may improve the quality of the deposits, their presence in the electroplating bath may be considered in future works.

Figure 64 shows the SEM images for the deposits obtained potentiostatically and galvanostatically and as can be seen, their appearances are very similar to the deposits obtained with the original bath (Figure 59 and Figure 61). For the potentiostatic tests, a homogeneous surface was verified with some dispersed crystallites. For the galvanostatic tests, the presence of particles and clusters with similar characteristics can be seen, and their sizes enhanced with the current density.
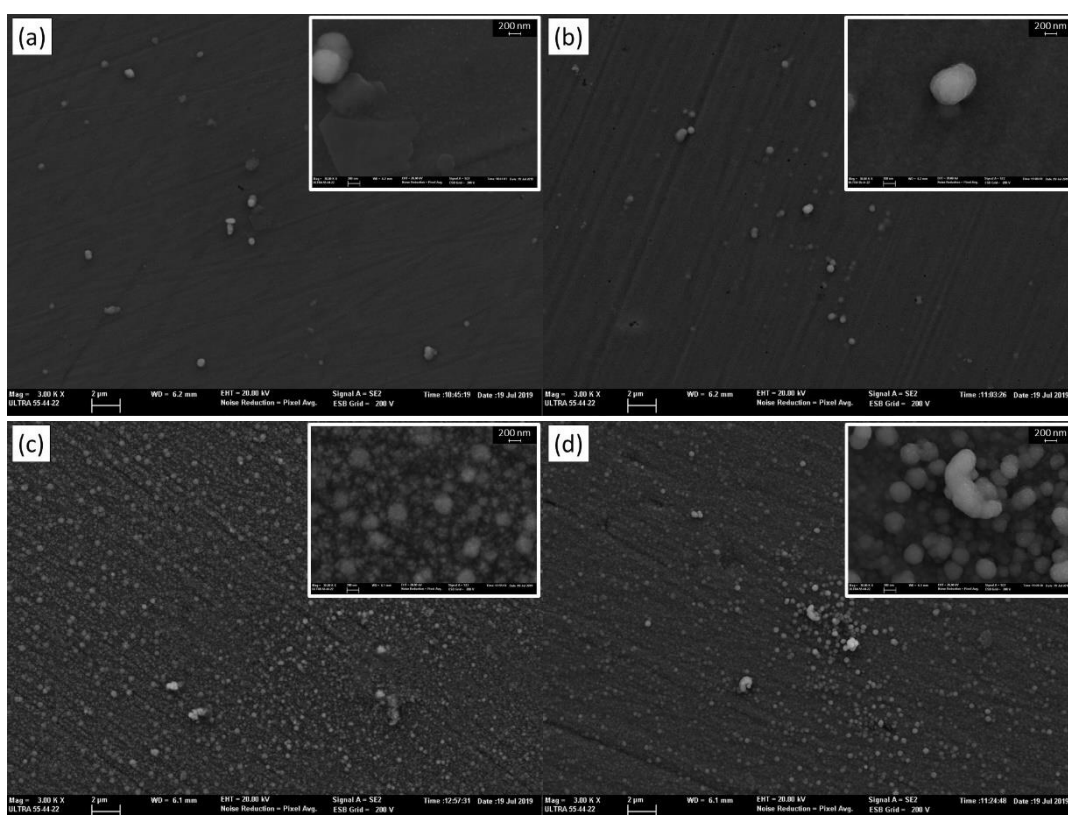
Figure 64 - SEM images of the Cu-Zn deposits obtained potentiostatically at (a) -1.4 V, (b) -1.45 V and galvanostatically at (c) -4.0 mA/cm² and (d) -6.0 mA/cm².

5.4.3. Conclusions

Studies of cyclic voltammetry and electrodeposition of brass on steel were performed at RDE using EDTA as complexing agent. The voltammetric curves and the quality of the deposits were assessed in function of the rotation speed, the potentiostatic/galvanostatic mode, the charge density and the bath concentration.

Voltammetric curves showed a typical displacement of the curves with the increase in rotation speed. This means that the solution agitation influences the peaks of reduction/oxidation and, mainly, the hydrogen evolution. According to the Koutecky-Levich equation, the deposition of copper is controlled by mass transport at -1.3 V and the diffusion coefficient of copper-EDTA complexes is 2.9×10^{-6} cm²/s. For zinc-EDTA solutions, the diffusion coefficient could not be determined by the equation and the deposition was suggested to be controlled by mass and charge transfer.

The electrodeposition study showed that the rotation speed influences the quality of the deposits. The agitation of the electrode led to the darkening of the deposits due to the hydrogen evolution and the lower proportion of Cu/Zn electrodeposited. However, for -1.3 V, very good deposits were obtained with typical color of brass and brightness. This suggests that operating at -1.3 V with agitation may be more interesting than at -1.4 V or -1.45 V, due to the lower energy consumption. The operation mode (potentiostiatic/galvanostatic) also influenced the quality of the deposits and, in general, potentiostatic electrodepositions provided deposits with better quality.

Finally, the recovery of the metals and EDTA from the rinsing water, treated by electrodialysis, on the bath was evaluated. The dilution of the original bath with 25 % v/v of the concentrated solution from electrodialysis is not recommended since it damaged the quality and generated opaque and non-uniform deposits. The concentration adjustment of the solution obtained by electrodialysis until reaching the concentration of the original bath was assessed. Very good deposits were obtained, showing that the different concentrations of OH^-, Na^+ and SO_4^{2-} did not damage it. For the bath evaluated herein, charge densities from 0.5 to 1.0 C/cm² must be used to guarantee the electrodeposition of zinc and avoid the darkening of the deposit.

6. FINAL CONCLUSIONS

The results showed that electrodialysis is a promising alternative for the treatment of wastewaters from the cyanide-free brass electroplating industry, especially if conducted at overlimiting current regimes. The results obtained by chronopotentiometry, concerning the transport properties of species across the membranes, agreed with those obtained in the electrodialysis tests. Finally, EDTA seems to be a good alternative to cyanide. Uniform electrodeposits, with typical color of brass, brightness and without cracks were obtained with the original bath and after the recovery of ions from electrodialysis, especially under agitation and at lower voltages than those already tested in literature.

6.1.   Final conclusions of topic I

- The limiting current density was not affected by the differences between the morphologies of HDX100 and PC-SK, since it showed an increase virtually linear with the increase in the Cu^{2+} concentration for both membranes.

- The increase in Cu^{2+} concentration led to an increase in the transport number in both membranes and, under all conditions tested, HDX100 presented greater values of $\overline{t_j}$ than PC-SK.

- Differences in the behavior of the ohmic resistance of the membranes suggested that the dominance of the pure membrane resistance occurred earlier for the PC-SK, with the increase in Cu^{2+} concentration. This occurred due to the higher local concentration of Cu^{2+} ions at the conductive regions of PC-SK than at HDX100, since the former is homogeneous and presents lower fraction of conductive area, water uptake and ion-exchange capacity.

- An increase in the plateau length of both membranes was verified with the increase in the concentration of Cu^{2+}, which occurred due to the greater concentration of K^+ ions from the KOH used to adjust the solution pH.

- Chronopotentiograms were also constructed using a more concentrated solution and both membranes. The PC-SK showed an additional inflexion point typical of bipolar membranes, which may be explained by the higher tendency of precipitates formation at its surface than at HDX100.

- At the end of the experiments, a blue solid material could be seen only at the surface of PC-SK, which is undesirable in electrodialysis.

- The use of the HDX membrane showed to be more appropriate than PC-SK for treating wastewaters with Cu^{2+} ions since the latter favors fouling/scaling.

6.2. Final conclusions of topic II

- For the solution with Cu^{2+}/Zn^{2+} molar ratio of 1.0 and pH 11, the formation of a precipitate at the AEM was suggested by the behavior of the current-voltage curve without a clear distinction between the 2nd and 3rd regions and by the chronopotentiograms, which showed oscillations in the potential drop.

- For the solution with Cu^{2+}/Zn^{2+} molar ratio of 1.0 and pH 12, two i_{lim} and two inflexion points were verified in the CVC and in the ChP, respectively. This was related to the competition between OH^-, SO_4^{2-} and $Zn(EDTA)^{2-}$ to cross the membrane.

- For the solution with Cu^{2+}/Zn^{2+} of 0.4 and pH 10, the formation of an insoluble species at the AEM was verified in the CVC and in ChPs. For solutions with Cu^{2+}/Zn^{2+} of 1.0 and 2.3, typical curves were obtained. Hence, in ED, the solution with Cu^{2+}/Zn^{2+} of 0.4 was used to assess the influence of the current regime and the presence of insoluble species on the extraction of ions.

- Typical CVCs and ChPs were obtained for solutions with Cu^{2+}/Zn^{2+} molar ratio of 1.0, pH 10 and $EDTA/Cu^{2+}$ molar ratios between 2 - 3.5. Hence, the addition of EDTA virtually did not affect the transport properties, which suggests that complexes with copper and zinc accounted for the alterations in transport properties more intensively than complexes without the metals.

6.3. Final conclusions of topic III

- The results of percent extraction, percent concentration and mass balance showed that the operation of electrodialysis in overlimiting condition enhanced the ion transfer through the membranes. Percent concentrations and percent extractions higher than 340 % and 85 %, respectively, were obtained for EDTA, Cu^{2+} and Zn^{2+} ions after the fourth cycle of ED.

- In the overlimiting test, water splitting occurred at the cathodic side of the AEM, which is generally undesirable in electrodialysis, leading to reactions of protons with complexes of EDTA-metals and insoluble species. This allowed the migration of free Cu^{2+} and Zn^{2+} from the AEM to the CEM as a result of the intense electric field and electroconvection. As the concentrate compartments of the CEM and AEM were connected to the same reservoir, overlimiting phenomena improved the extraction of ions.

- Chronopotentiometric tests performed with the membranes used in the electrodialysis tests showed that electroconvective vortices, in the overlimiting test, minimized fouling and scaling at both membranes.

- Among the NaOH solutions tested to clean the membranes after electrodialysis, the one with 0.1 mol NaOH/L was the most appropriate.

6.4.   Final conclusions of topic IV

- The solution agitation caused a displacement of the reduction and oxidation peaks of voltammetric curves and influenced mainly the hydrogen evolution.

- The deposition of copper is controlled by mass transport at -1.3 V, whereas the zinc deposition is controlled by mass and charge transfer. The diffusion coefficient of copper-EDTA complexes is 2.9×10^{-6} cm²/s.

- Electrodepositions at -1.3 V may be more interesting than at more negative voltages without agitation, since uniform brass electrodeposits, with brightness and without cracks were obtained.

- In general, electrodeposits obtained in potentiostatic mode showed better quality than those obtained in galvanostatic mode.

- The recovery of ions from the concentrated solution obtained by ED was also assessed. The dilution of the original bath with 25 % v/v of the solution from ED is not recommended since the quality of the deposits was deteriorated.

- Lastly, the concentration of EDTA, copper and zinc in the solution from ED was adjusted to reach the concentration of the original bath. The electrodeposits showed good quality, with similar colors and morphologies to those obtained with the original bath. Hence, different concentrations of OH^-, Na^+ and SO_4^{2-} ions in the bath do not damage the quality of deposits.

REFERENCES

1   Martín-Lara, M.A.; Blázquez, G.; Trujillo, M.C.; Pérez, A.; Calero, M. New treatment of real electroplating wastewater containing heavy metal ions by adsorption onto olive stone. **Journal of Cleaner Production**, v. 81, p. 120-129, 2014.

2   Winand, R. **Electrodeposition of Zinc and Zinc Alloys**. WILEY, 2011.

3   Rossi, A. A tartrate-based alloy bath for brass-plated steel wire production. **Journal of Applied Electrochemistry**, v. 22, p. 64–72, 1992.

4   Vreese, P. De; Skoczylas, A.; Matthijs, E.; Fransaer, J.; Binnemans, K. Electrodeposition of copper-zinc alloys from an ionic liquid-likecholine acetate electrolyte. **Electrochimica Acta**, v. 108, p. 788–794, 2013.

5   Rashwan, S.M. Electrodeposition of Zn–Cu coatings from alkaline sulphate bath containing glycine. **Transactions of the Institute of Metal Finishing**, v. 85, n. 4, p. 217–224, 2007.

6   Brenner, A. **Electrodeposition of Alloys**. New York: Academic Press, 1963.

7   Ramírez, C.; Calderón, J.A. Study of the effect of Triethanolamine as a chelating agent in the simultaneous electrodeposition of copper and zinc from non-cyanide electrolytes. **Journal of Electroanalytical Chemistry**, v. 765, p. 132–139, 2016.

8   Carlos, I.A.; Almeida, M.R.H. de. Study of the influence of the polyalcohol sorbitol on the electrodeposition of copper-zinc films from a non-cyanide bath. **Journal of Electroanalytical Chemistry**, v. 562, n. 2, p. 153–159, 2004.

9   Almeida, M.R.H. de; Barbano, E.P.; Zacarin, M.G.; Brito, M.M. de; Tulio, P.C.; Carlos, I.A. Electrodeposition of CuZn films from free-of-cyanide alkaline baths containing EDTA as complexing agent. **Surface and Coatings Technology**, v. 287, p. 103–112, 2016.

10   Almeida, M.R.H. de.; Barbano, E.P.; Carvalho, M.F. de; Carlos, I.A.; Siqueira, J.L.P.; Barbosa, L.L. Electrodeposition of copper-zinc from an alkaline bath based on EDTA. **Surface and Coatings Technology**, v. 206, n. 1, p. 95–102, 2011.

11   Babu, B.R.; Bhanu, S.U.; Meera, K.S. Waste Minimization in Electroplating Industries : A Review Waste Minimization in Electroplating Industries : A Review. **Journal of Environmental Science and Health Part C**, v. 27, p. 155–177, 2009.

12   Qin, J.J.; Wai, M.N.; Oo, M.H.; Wong, F.S. A feasibility study on the treatment and recycling of a wastewater from metal plating. **Journal of Membrane Science**, v. 208, n. 1–2, p. 213–221, 2002.

13   Fu, F.; Wang, Q. Removal of heavy metal ions from wastewaters: A review. **Journal of Environmental Management**, v. 92, n. 3, p. 407–418, 2011.

14   Weber, T.J. Wastewater Treatment. **Metal Finishing**, v. 105, n. 10, p. 699-714, 2007.

15   Korzenowski, C.; Rodrigues, M.A.S.; Bresciani, L.; Bernardes, A.M.; Ferreira, J.Z. Purification of spent chromium bath by membrane electrolysis. **Journal of Hazardous Materials**, v. 152, n. 3, p. 960–967, 2008.

16   Cavaco, S.A.; Fernandes, S.; Quina, M.M.; Ferreira, L.M. Removal of chromium from electroplating industry effluents by ion exchange resins. **Journal of Hazardous Materials**, v. 144, n. 3, p. 634–638, 2007.

17   Nagasawa, H.; Iizuka, A.; Yamasaki, A.; Yanagisawa, Y. Utilization of bipolar membrane electrodialysis for the removal of boron from aqueous solution. **Industrial and Engineering Chemistry Research**, v. 50, n. 10, p. 6325–6330, 2011.

18   Prochaska, K.; Antczak, J.; Regel-Rosocka, M.; Szczygiełda, M. Removal of succinic acid from fermentation broth by multistage process (membrane separation and reactive extraction). **Separation and Purification Technology**, v. 192, p. 360–368, 2018.

19   Maigrot, E. & Sabates, J. (1890). Apparat zur Lauterung von Zuckersaften mittels Elektrizitat.

20   Bittencourt, S.D.; Marder, L.; Benvenuti, T.; Ferreira, J.Z.; Bernardes, A.M. Analysis of different current density conditions in the electrodialysis of zinc electroplating process solution. **Separation Science and Technology**, v. 52, n. 13, p. 2079–2089, 2017.

21   Belova, E.I.; Lopatkova, G.Y.; Pismenskaya, N.D.; Nikonenko, V. V.; Larchet, C.; Pourcelly, G. Effect of anion-exchange membrane surface properties on mechanisms of overlimiting mass transfer. **Journal of Physical Chemistry B**, v. 110, n. 27, p. 13458–13469, 2006.

22   Pismenskaya, N.D.; Nikonenko, V. V.; Zabolotsky, V.I.; Sandoux, R.; Pourcelly, G.; Tskhay, A.A. Effects of the desalination chamber design on the mass-transfer characteristics of electrodialysis apparatuses at overlimiting current densities. **Russian Journal of Electrochemistry**, v. 44, n. 7, p. 818–827, 2008.

23   Strathmann, H. Ion-Exchange Membrane Processes in Water Treatment. In: **Sustainability Science and Engineering**. Elsevier, v.2.2010, p. 141-199.

24   Cohen, B.; Lazarovitch, N.; Gilron, J. Upgrading groundwater for irrigation using monovalent selective electrodialysis. **Desalination**, v. 431, p. 126-139, 2018.

25   Nath, K. (2008). Membrane separation processes. *Prentice-Hall*, 1–24.

26   Paidar, M.; Fateev, V.; Bouzek, K. Membrane electrolysis—History, current status and perspective. **Electrochimica Acta**, v. 209, p. 737–756, 2016.

27   Chang, J.H.; Ellis, A. V.; Tung, C.H.; Huang, W.C. Copper cation transport and scaling of ionic exchange membranes using electrodialysis under electroconvection conditions. **Journal of Membrane Science**, v. 361,

n. 1-2, p. 56–62, 2010.

28   Ilhan, F.; Kabuk, H.A.; Kurt, U.; Avsar, Y.; Sari, H.; Gonullu, M.T. Evaluation of treatment and recovery of leachate by bipolar membrane electrodialysis process. **Chemical Engineering and Processing: Process Intensification**, v. 75, p. 67–74, 2014.

29   Vera, E.; Ruales, J.; Dornier, M.; Sandeaux, J.; Sandeaux, R.; Pourcelly, G. Deacidification of clarified passion fruit juice using different configurations of electrodialysis. **Journal of Chemical Technology and Biotechnology**, v. 78, n. 8, p. 918–925, 2003.

30   Zayani, W.; Azizi, S.; El-Nasser, K.S.; Belgacem, Y. Ben; Ali, I.O.; Fenineche, N.; Mathlouthi, H. New nanoparticles of (Sm,Zn)-codoped spinel ferrite as negative electrode in Ni/MH batteries with long-term and enhanced electrochemical performance. **International Journal of Hydrogen Energy**, v. 44, n. 22, p. 11303–11310, 2019.

31   Chowdhury, N.R.; Kumar, R.; Kant, R. Theory for the chronopotentiometry on rough and finite fractal electrode: Generalized Sand equation. **Journal of Electroanalytical Chemistry**, v. 802, p. 64–77, 2017.

32   Xue, J.; Shao, M.; Shen, Q.; Liu, X.; Jia, H. Electrodeposition of Cu2O nanocrystalline on TiO2 nanosheet arrays by chronopotentiometry for improvement of photoelectrochemical properties. **Ceramics International**, v. 44, n. 10, p. 11039–11047, 2018.

33   Butylskii, D.Y.; Mareev, S.A.; Pismenskaya, N.D.; Apel, P.Y.; Polezhaeva, O.A.; Nikonenko, V.V. Phenomenon of two transition times in chronopotentiometry of electrically inhomogeneous ion exchange membranes. **Electrochimica Acta**, v. 273, p. 289–299, 2018.

34   Mareev, S.A.; Nebavskiy, A. V.; Nichka, V.S.; Urtenov, M.K.; Nikonenko, V. V. The nature of two transition times on chronopotentiograms of heterogeneous ion exchange membranes: 2D modelling. **Journal of Membrane Science**, v. 575, p. 179–190, 2019.

35   Martí-Calatayud, M.C.; García-Gabaldón, M.; Pérez-Herranz, V.; Sales, S.; Mestre, S. Synthesis and electrochemical behavior of ceramic cation-exchange membranes based on zirconium phosphate. **Ceramics International**, v. 39, n. 4, p. 4045–4054, 2013.

36   Martí-Calatayud, M.C.; Buzzi, D.C.; García-Gabaldón, M.; Bernardes, A.M.; Tenório, J.A.S.; Pérez-Herranz, V. Ion transport through homogeneous and heterogeneous ion-exchange membranes in single salt and multicomponent electrolyte solutions. **Journal of Membrane Science**, v. 466, p. 45–57, 2014.

37   Juškenas, R.; Karpavičiene, V.; Pakštas, V.; Selskis, A.; Kapočius, V. Electrochemical and XRD studies of Cu-Zn coatings electrodeposited in solution with d-mannitol. **Journal of Electroanalytical Chemistry**, v. 602, n. 2, p. 237–244, 2007.

38   Rousse, C.; Beaufils, S.; Fricoteaux, P. Electrodeposition of Cu-Zn thin films from room temperature ionic liquid. **Electrochimica Acta**, v. 107,

p. 624-631, 2013.

39   Gabe, D.R. Agitation: The most versatile degree of freedom for surface finishers. **Transactions of the Institute of Metal Finishing**, v. 81, n. 1, p. 7–12, 2003.

40   Clarke, C.J.; Browning, G.J.; Donne, S.W. An RDE and RRDE study into the electrodeposition of manganese dioxide. **Electrochimica Acta**, v. 51, n. 26, p. 5773–5784, 2006.

41   Finkelstein, D.A.; Kirtland, J.D.; Mota, N. Da; Stroock, A.D.; Abruña, H.D. Alternative oxidants for high-power fuel cells studied by rotating disk electrode (RDE) voltammetry at Pt, Au, and glassy carbon electrodes. **Journal of Physical Chemistry C**, v. 115, n. 13, p. 6073–6084, 2011.

42   Scarazzato, T.; Panossian, Z.; Tenório, J.A.S.; Pérez-Herranz, V.; Espinosa, D.C.R. Water reclamation and chemicals recovery from a novel cyanide-free copper plating bath using electrodialysis membrane process. **Desalination**, v. 436, p. 114–124, 2018.

43   Benvenuti, T.; Krapf, R.S.; Rodrigues, M.A.S.; Bernardes, A.M.; Zoppas-Ferreira, J. Recovery of nickel and water from nickel electroplating wastewater by electrodialysis. **Separation and Purification Technology**, v. 129, p. 106–112, 2014.

44   Benvenuti, T.; Siqueira Rodrigues, M.A.; Bernardes, A.M.; Zoppas-Ferreira, J. Closing the loop in the electroplating industry by electrodialysis. **Journal of Cleaner Production**, v. 155, p. 130–138, 2017.

45   Scarazzato, T.; Buzzi, D.C.; Bernardes, A.M.; Romano Espinosa, D.C. Treatment of wastewaters from cyanide-free plating process by electrodialysis. **Journal of Cleaner Production**, v. 91, p. 241–250, 2015.

46   Caprarescu, S.; Purcar, V.; Vaireanu, D.-I. Separation of Copper Ions from Synthetically Prepared Electroplating Wastewater at Different Operating Conditions using Electrodialysis. **Separation Science and Technology**, v. 47, p. 2273–2280, 2012.

47   Bleha, M.; Tishchenko, G.; Šumberová, V.; Kůdela, V. Characteristic of the critical state of membranes in ED-desalination of milk whey. **Desalination**, v. 86, n. 2, p. 173–186, 1992.

48   Ghalloussi, R.; Chaabane, L.; Larchet, C.; Dammak, L.; Grande, D. Structural and physicochemical investigation of ageing of ion-exchange membranes in electrodialysis for food industry. **Separation and Purification Technology**, v. 123, p. 229–234, 2014.

49   Rodrigues, M.A.S.; Korzenovski, C.; Gondran, E.; Bernardes, A.M.; Ferreira, J.Z. Evaluation of changes on ion-selective membranes in contact with zinc-cyanide complexes. **Journal of Membrane Science**, v. 279, n. 1-2, p. 140–147, 2006.

50   Zhang, Y.; Liu, R.; Lang, Q.; Tan, M.; Zhang, Y. Composite anion exchange membrane made by layer-by-layer method for selective ion separation and water migration control. **Separation and Purification Technology**, v. 192,

p. 278–286, 2018.

51   Le, X.T. Contribution to the study of properties of Selemion AMV anion exchange membranes in acidic media. **Electrochimica Acta**, v. 108, p. 232–240, 2013.

52   Andreeva, M.A.; Gil, V.V.; Pismenskaya, N.D.; Dammak, L.; Kononenko, N.A.; Larchet, C.; Grande, D.; Nikonenko, V.V. Mitigation of membrane scaling in electrodialysis by electroconvection enhancement, pH adjustment and pulsed electric field application. **Journal of Membrane Science**, v. 549, p. 129–140, 2018.

53   Martí-Calatayud, M.C.; García-Gabaldón, M.; Pérez-Herranz, V. Study of the effects of the applied current regime and the concentration of chromic acid on the transport of Ni^{2+} ions through Nafion 117 membranes. **Journal of Membrane Science**, v. 392–393, p. 137–149, 2012.

54   Mikhaylin, S.; Nikonenko, V.; Pismenskaya, N.; Pourcelly, G.; Choi, S.; Kwon, H.J.; Han, J.; Bazinet, L. How physico-chemical and surface properties of cation-exchange membrane affect membrane scaling and electroconvective vortices: Influence on performance of electrodialysis with pulsed electric field. **Desalination**, v. 393, p. 102–114, 2015.

55   Pismenskaia, N.; Sistat, P.; Huguet, P.; Nikonenko, V.; Pourcelly, G. Chronopotentiometry applied to the study of ion transfer through anion exchange membranes. **Journal of Membrane Science**, v. 228, n. 1, p. 65-76, 2004.

56   Wilhelm, F.G.; Vegt, N.F.A. Van der; Wessling, M.; Strathmann, H. Chronopotentiometry for the advanced current-voltage characterisation of bipolar membranes. **Journal of Electroanalytical Chemistry**, v. 502, n. 1-2, p. 152–166, 2001.

57   García-Gabaldón, M.; Pérez-Herranz, V.; Ortega, E. Evaluation of two ion-exchange membranes for the transport of tin in the presence of hydrochloric acid. **Journal of Membrane Science**, v. 371, n. 1–2, p. 65–74, 2011.

58   Chen, C.; Yoshiba, M.; Nagoshi, T.; Chang, T.M.; Yamane, D.; Machida, K.; Masu, K.; Sone, M. Pulse electroplating of ultra- fine grained Au films with high compressive strength. **Electrochemistry Communications**, v. 67, p. 51–54, 2016.

59   Fresner, J.; Schnitzer, H.; Gwehenberger, G.; Planasch, M.; Brunner, C.; Taferner, K.; Mair, J. Practical experiences with the implementation of the concept of zero emissions in the surface treatment industry in Austria. **Journal of Cleaner Production**, v. 15, n. 13–14, p. 1228–1239, 2007.

60   Viguri, J.R.; Andrés, A.; Irabien, A. Waste minimisation in a hard chromiun plating small medium enterprise (SME). **Waste Management**, v. 22, p. 931-936, 2002.

61   Dini, J.W., Snyder, D.D. Electrodeposition of Copper. In: **Modern Electroplating**. Hoboken, NJ, USA: John Wiley & Sons, Inc., 2011, p. 33-78.

62   Endres, F.M.; , Douglas; Abbott, A. **Electrodeposition from Ionic Liquids**. Wiley-VCH, 2008.

63   Peng, C.; Liu, Y.; Bi, J.; Xu, H.; Ahmed, A.S. Recovery of copper and water from copper-electroplating wastewater by the combination process of electrolysis and electrodialysis. **Journal of Hazardous Materials**, v. 189, n. 3, p. 814–820, 2011.

64   Carrillo-Abad, J.; García-Gabaldón, M.; Pérez-Herranz, V. Electrochemical recovery of zinc from the spent pickling solutions coming from hot dip galvanizing industries. Galvanostatic operation. **International Journal of Electrochemical Science**, v. 7, n. 6, p. 5442–5456, 2012.

65   Carrillo-Abad, J.; García-Gabaldón, M.; Pérez-Herranz, V. Study of the zinc recovery from spent pickling baths by means of an electrochemical membrane reactor using a cation-exchange membrane under galvanostatic control. **Separation and Purification Technology**, v. 132, p. 479–486, 2014.

66   Carrillo-Abad, J.; García-Gabaldón, M.; Ortega, E.; Pérez-Herranz, V. Recovery of zinc from spent pickling solutions using an electrochemical reactor in presence and absence of an anion-exchange membrane: Galvanostatic operation. **Separation and Purification Technology**, v. 98, p. 366–374, 2012.

67   Carrillo-Abad, J.; García-Gabaldón, M.; Pérez-Herranz, V. Treatment of spent pickling baths coming from hot dip galvanizing by means of an electrochemical membrane reactor. **Desalination**, v. 343, p. 38–47, 2014.

68   Carrera, J.A.; Bringas, E.; Román, M.F.S.; Ortiz, I. Selective membrane alternative to the recovery of zinc from hot-dip galvanizing effluents. **Journal of Membrane Science**, v. 326, n. 2, p. 672–680, 2009.

69   Bagotsky, V.S. **Fundamentals of Electrochemistry**. New Jersey: Wiley Interscience, 2006.

70   Musa, A.Y.; Slaiman, Q.J.M.; Kadhum, A.A.H.; Takriff, M.S. Effects of Agitation, Current Density and Cyanide Concentration on Cu-Zn Alloy Electroplating. **European Journal of Scientific Research**, v. 22, n. 4, p. 517–524, 2008.

71   Strow, H. Electroplating Solutions. **Environmental Technology**, v. 105, n. 10, p. 163–167, 2007.

72   Ballesteros, J.C.; Torres-Martínez, L.M.; Juárez-Ramírez, I.; Trejo, G.; Meas, Y. Study of the electrochemical co-reduction of Cu^{2+} and and Zn^{2+} ions from an alkaline non-cyanide solution containing glycine. **Journal of Electroanalytical Chemistry**, v. 727, p. 104–112, 2014.

73   Vagramyan, T.; Leach, J.S..; Moon, J.R. On the problems of electrodepositing brass from non-cyanide electrolytes. **Electrochimica Acta**, v. 24, p. 231–236, 1979.

74   Almeida, M.R.H. de; Barbano, E.P.; Carvalho, M.F. de; Tulio, P.C.; Carlos, I.A. Copper–zinc electrodeposition in alkaline-sorbitol medium:

Electrochemical studies and structural, morphological and chemical composition characterization. **Applied Surface Science**, v. 333, p. 13–22, 2015.

75   Assaf, F.H.; Rehim, S.S.A.E.; Mohamed, A.S.; Zaky, A.M. Electroplating of brass from citrate-based alloy baths. **Indian Journal of ChemicalTechnology**, v. 2, p. 147–152, 1995.

76   Senna, L.F.; Díaz, S.L.; Sathler, L. Electrodeposition of copper-zinc alloys in pyrophosphate-based electrolytes. **Journal of Applied Electrochemistry**, v. 33, n. 12, p. 1155–1161, 2003.

77   Despić, A.R.; Marinović, V.; Jović, V.D. Kinetics of deposition and dissolution of brass from the pyrophosphate-oxalate bath. **Journal of Electroanalytical Chemistry**, v. 339, n. 1–2, p. 473–488, 1992.

78   Fujiwara, Y.; Enomoto, H. Characterization of Cu-Zn alloy deposits from glucoheptonate baths. **Surface and Coatings Technology**, v. 35, n. 1–2, p. 113–124, 1988.

79   Krishnan, R.; Muralidharan, V.; Natarajan, S. A non- cyanide brass plating bath. **Bulletin of Electrochemistry**, v. 12, p. 274–277, 1996.

80   Barbano, E.P.; Oliveira, G.M. de; Carvalho, M.F. de; Carlos, I.A. Copper-tin electrodeposition from an acid solution containing EDTA added. **Surface and Coatings Technology**, v. 240, p. 14–22, 2014.

81   Oliveira, G.M. de; Carlos, I.A. Silver–zinc electrodeposition from a thiourea solution with added EDTA or HEDTA. **Electrochimica Acta**, v. 54, n. 8, p. 2155–2163, 2009.

82   Rekab, K.; Lepeytre, C.; Goettmann, F.; Dunand, M.; Guillard, C.; Herrmann, J.-M. Degradation of a cobalt(II)–EDTA complex by photocatalysis and H2O2/UV-C. Application to nuclear wastes containing 60Co. **Journal of Radioanalytical and Nuclear Chemistry**, v. 303, n. 1, p. 131–137, 2015.

83   Oztekin, Y.; Yazicigil, Z. Recovery of metals from complexed solutions by electrodeposition. **Desalination**, v. 190, n. 1–3, p. 79–88, 2006.

84   Fashu, S.; Gu, C.D.; Zhang, J.L.; Huang, M.L.; Wang, X.L.; Tu, J.P. Effect of EDTA and NH4Cl additives on electrodeposition of Zn−Ni films from choline chloride-based ionic liquid. **Transactions of Nonferrous Metals Society of China**, v. 25, n. 6, p. 2054–2064, 2015.

85   Nasef, M.M.; Guven, O. Radiation-grafted copolymers for separation and purification purposes: Status, challenges and future directions. **Progress in Polymer Science**, v. 37, n. 12, p. 1597–1656, 2012.

86   Shan, C.; Xu, Z.; Zhang, X.; Xu, Y.; Gao, G.; Pan, B. Efficient removal of EDTA-complexed Cu(II) by a combined Fe(III)/UV/alkaline precipitation process: Performance and role of Fe(II). **Chemosphere**, v. 193, p. 1235-1242, 2017.

87   Mohsen-Nia, M.; Montazeri, P.; Modarress, H. Removal of Cu^{2+} and Ni^{2+} from wastewater with a chelating agent and reverse osmosis processes.

Desalination, v. 217, n. 1–3, p. 276–281, 2007.

88   Ujang, Z.; Anderson, G.K. Application of low-pressure reverse osmosis membrane for Zn^{2+} and Cu^{2+} removal from wastewater. **Water Science and Technology**, v. 34, n. 9, p. 247–253, 1996.

89   Huang, Y.; Koseoglu, S. Separation of heavy metals from industrial waste streams by membrane separation technology. **Waste Management**, v. 13, p. 481–501, 1993.

90   Huang, T.C.; Wang, J.K. Selective transport of metal ions through cation exchange membrane in the presence of a complexing agent. **Industrial & Engineering Chemistry Research**, v. 32, n. 1, p. 133–139, 1993.

91   Ju, F.; Hu, Y. Removal of EDTA-chelated copper from aqueous solution by interior microelectrolysis. **Separation and Purification Technology**, v. 78, n. 1, p. 33–41, 2011.

92   Chaudhary, A.J.; Donaldson, J.D.; Grimes, S.M.; Yasri, N.G. Separation of nickel from cobalt using electrodialysis in the presence of EDTA. **Journal of Applied Electrochemistry**, v. 30, n. 4, p. 439–445, 2000.

93   Labbe, M.; Fenyo, J.-C.; Selegny, E. Separation of Nickel and Cobalt by Electrodialysis Using Ion-Exchange Membranes in the Presence of EDTA. **Separation Science**, v. 10, n. 3, p. 307–322, 1975.

94   Kubal, M.; Machula, T.; Strnadová, N. Separation of Calcium and Cadmium by Electrodialysis in the Presence of Ethylenediaminetetraacetic Acid. **Separation Science and Technology**, v. 33, n. 13, p. 1969–1980, 1998.

95   Cherif, A.T.; Elmidaoui, A.; Gavach, C. Separation of Ag^+, Zn^{2+} and Cu^{2+} ions by electrodialysis with monovalent cation specific membrane and EDTA. **Journal of Membrane Science**, v. 76, n. 1, p. 39–49, 1993.

96   Rozhkova, M.V.; Shaposhnik, V.A.; Strygina, I.P.; Artemova, L.V. Separation of cations with different charges in electrodialysis with the use of complex-formation. **Russian journal of electrochemistry**, v. 32, n. 2, p. 237–240, 1996.

97   Iizuka, A.; Yamashita, Y.; Nagasawa, H.; Yamasaki, A.; Yanagisawa, Y. Separation of lithium and cobalt from waste lithium-ion batteries via bipolar membrane electrodialysis coupled with chelation. **Separation and Purification Technology**, v. 113, p. 33–41, 2013.

98   Almeida, M.R.H. de.; Barbano, E.P.; Carvalho, M.F. de; Carlos, I.A.; Siqueira, J.L.P.; Barbosa, L.L. Electrodeposition of copper-zinc from an alkaline bath based on EDTA. **Surface and Coatings Technology**, v. 206, n. 1, p. 95–102, 2011.

99   Daylan, B.; Ciliz, N.; Mammodov, A. Hazardous process chemical and water consumption reduction through cleaner production application for a zinc electroplating industry in Istanbul. **Resources, Conservation and Recycling**, v. 81, p. 1–7, 2013.

100   Associação Brasileira de Normas Técnicas (2004). NBR 10.004/2004: Resíduos sólidos – Classificação. Rio de Janeiro. 77.

101 European Parliament and Council. Directive (2008). Directive 2008/98/EC of the European Parliament and of the Council of 19 November 2008 on waste and repealing certain directives. Official Journal of the European Union. 312.

102 Paulino, A.T.; Minasse, F.A.S.; Guilherme, M.R.; Reis, A. V.; Muniz, E.C.; Nozaki, J. Novel adsorbent based on silkworm chrysalides for removal of heavy metals from wastewaters. **Journal of Colloid and Interface Science**, v. 301, n. 2, p. 479–487, 2006.

103 Huisman, J.L.; Schouten, G.; Schultz, C. Biologically produced sulphide for purification of process streams, effluent treatment and recovery of metals in the metal and mining industry. **Hydrometallurgy**, v. 83, n. 1–4, p. 106–113, 2006.

104 Fornari, P.; Abbruzzese, C. Copper and nickel selective recovery by electrowinning from electronic and galvanic industrial solutions. **Hydrometallurgy**, v. 52, n. 3, p. 209–222, 1999.

105 Keeley, J.; Smith, A.D.; Judd, S.J.; Jarvis, P. Reuse of recovered coagulants in water treatment: An investigation on the effect coagulant purity has on treatment performance. **Separation and Purification Technology**, v. 131, p. 69–78, 2014.

106 Kongsricharoern, N.; Polprasert, C. Electrochemical precipitation of chromium (Cr^{6+}) from an electroplating wastewater. **Water Science and Technology**, v. 31, n. 9, p. 109–117, 1995.

107 Bernardes, A.M.; Costa, R.F.D.; Fallavena, V.L.V.; Rodrigues, M.A.S.; Trevisan, M.D.; Ferreira, J.Z. Electrochemistry as a clean technology for the treatment of effluents: The application of electrodialysis. **Metal Finishing**, v. 98, n. 11, p. 52–114, 2000.

108 Nagarale, R.K.; Gohil, G.S.; Shahi, V.K. Recent developments on ion-exchange membranes and electro-membrane processes. **Advances in Colloid and Interface Science**, v. 119, n. 2–3, p. 97–130, 2006.

109 Baker, R. **Membrane Technology and Applications**. California: WILEY, 2004.

110 Yamauchi, A.; Sayed, A.M. EL; Mizuguchi, K.; Kodama, M.; Sugito, Y. Ion transport behavior in diffusion layer of new designed ion exchange-mosaic composite polymer membrane. **Journal of Membrane Science**, v. 283, n. 1–2, p. 301–309, 2006.

111 Strathmann, H. **Ion-exchange Membrane Separation Processes**. Elsevier, 2004.

112 Campione, A.; Gurreri, L.; Ciofalo, M.; Micale, G.; Tamburini, A.; Cipollina, A. Electrodialysis for water desalination: A critical assessment of recent developments on process fundamentals, models and applications. **Desalination**, v. 434, p. 121–160, 2018.

113 Nikonenko, V. V.; Kovalenko, A. V.; Urtenov, M.K.; Pismenskaya, N.D.; Han, J.; Sistat, P.; Pourcelly, G. Desalination at overlimiting currents: State-

of-the-art and perspectives. **Desalination**, v. 342, p. 85–106, 2014.

114 Kontturi, K.; Murtomäki, L.; et al. **Ionic Transport Processes in Electrochemistry and Membrane Science**. Oxford University Press, 2008.

115 Mohammadi, T.; Moheb, A.; Sadrzadeh, M.; Razmi, A. Modeling of metal ion removal from wastewater by electrodialysis. **Separation and Purification Technology**, v. 41, n. 1, p. 73–82, 2005.

116 Martí-Calatayud, M.C.; Buzzi, D.C.; García-Gabaldón, M.; Ortega, E.; Bernardes, A.M.; Tenório, J.A.S.; Pérez-Herranz, V. Sulfuric acid recovery from acid mine drainage by means of electrodialysis. **Desalination**, v. 343, p. 120–127, 2014.

117 Strathmann, H. Electrodialysis, a mature technology with a multitude of new applications. **Desalination**, v. 264, n. 3, p. 268–288, 2010.

118 Garcia-Vasquez, W.; Dammak, L.; Larchet, C.; Nikonenko, V.; Grande, D. Effects of acid-base cleaning procedure on structure and properties of anion-exchange membranes used in electrodialysis. **Journal of Membrane Science**, v. 507, p. 12–23, 2016.

119 Labbé, D.; Araya-Farias, M.; Tremblay, A.; Bazinet, L. Electromigration feasibility of green tea catechins. **Journal of Membrane Science**, v. 254, n. 1–2, p. 101–109, 2005.

120 Bazinet, L.; Ippersiel, D.; Mahdavi, B. Fractionation of whey proteins by bipolar membrane electroacidification. **Innovative Food Science and Emerging Technologies 5**, v. 5, p. 17–25, 2004.

121 Kaláb, J.; Palatý, Z. Electrodialysis of oxalic acid: batch process modeling Jiří. **Chemical Papers**, v. 66, n. 12, p. 1118–1123, 2012.

122 Ferrer, J.S.J.; Laborie, S.; Durand, G.; Rakib, M. Formic acid regeneration by electromembrane processes. **Journal of Membrane Science**, v. 280, n. 1–2, p. 509–516, 2006.

123 Gonçalves, F.; Fernandes, C.; Santos, P.C. dos.; Pinho, M.N. de. Wine tartaric stabilization by electrodialysis and its assessment by the saturation temperature. **Journal of Food Engineering**, v. 59, n. 2–3, p. 229–235, 2003.

124 Marder, L.; Bittencourt, S.D.; Zoppas Ferreira, J.; Bernardes, A.M. Treatment of molybdate solutions by electrodialysis: The effect of pH and current density on ions transport behavior. **Separation and Purification Technology**, v. 167, p. 32–36, 2016.

125 Peraki, M.; Ghazanfari, E.; Pinder, G.F.; Harrington, T.L. Electrodialysis: An application for the environmental protection in shale-gas extraction. **Separation and Purification Technology**, v. 161, p. 96–103, 2016.

126 Velizarova, E.; Ribeiro, A.B.; Ottosen, L.M. A comparative study on Cu, Cr and As removal from CCA-treated wood waste by dialytic and electrodialytic processes. **Journal of Hazardous Materials**, v. 94, n. 2, p. 147–160, 2002.

127 Koene, L.; Janssen, L.J.J. Removal of nickel from industrial process liquids. **Electrochimica Acta**, v. 47, n. 5, p. 695–703, 2001.

128 Smara, A.; Delimi, R.; Chainet, E.; Sandeaux, J. Removal of heavy metals from diluted mixtures by a hybrid ion-exchange/electrodialysis process. **Separation and Purification Technology**, v. 57, n. 1, p. 103–110, 2007.

129 Amado, F.D.R.; Rodrigues, L.F.; Rodrigues, M.A.S.; Bernardes, A.M.; Ferreira, J.Z.; Ferreira, C.A. Development of polyurethane/polyaniline membranes for zinc recovery through electrodialysis. **Desalination**, v. 186, n. 1–3, p. 199–206, 2005.

130 Cifuentes, L.; García, I.; Arriagada, P.; Casas, J.M. The use of electrodialysis for metal separation and water recovery from CuSO4-H2SO4-Fe solutions. **Separation and Purification Technology**, v. 68, n. 1, p. 105–108, 2009.

131 Cifuentes, L.; Crisóstomo, G.; Ibáñez, J.P.; Casas, J.M.; Alvarez, F.; Cifuentes, G. On the electrodialysis of aqueous H2SO4-CuSO4 electrolytes with metallic impurities. **Journal of Membrane Science**, v. 207, n. 1, p. 1-16, 2002.

132 Scarazzato, T.; Panossian, Z.; Tenório, J.A.S.; Pérez-Herranz, V.; Espinosa, D.C.R. A review of cleaner production in electroplating industries using electrodialysis. **Journal of Cleaner Production**, v. 168, p. 1590-1602, 2017.

133 Wu, G.M.; Lin, S.J.; Yang, C.C. Preparation and characterization of high ionic conducting alkaline non-woven membranes by sulfonation. **Journal of Membrane Science**, v. 284, n. 1–2, p. 120–127, 2006.

134 Berezina, N.P.; Kononenko, N.A.; Dyomina, O.A.; Gnusin, N.P. Characterization of ion-exchange membrane materials: Properties vs structure. **Advances in Colloid and Interface Science**, v. 139, n. 1–2, p. 3–28, 2008.

135 Aouad, F.; Lindheimer, A.; Chaouki, M.; Gavach, C. Loss of permselectivity of anion exchange membranes in contact with zinc chloride complexes. **Desalination**, v. 121, n. 1, p. 13–22, 1999.

136 Aouad, F.; Lindheimer, A.; Gavach, C. Transport properties of electrodialysis membranes in the presence of Zn^{2+} complexes with Cl^{-}. **Journal of Membrane Science**, v. 123, n. 2, p. 207–223, 1997.

137 Ma, H.; Yue, S.; Li, H.; Wang, Q.; Tu, M. Recovery of lactic acid and other organic acids from food waste ethanol fermentation stillage: Feasibility and effects of substrates. **Separation and Purification Technology**, v. 209, p. 223–228, 2019.

138 Szczygiełda, M.; Antczak, J.; Prochaska, K. Separation and concentration of succinic acid from post-fermentation broth by bipolar membrane electrodialysis (EDBM). **Separation and Purification Technology**, v. 181, p. 53–59, 2017.

139 Melnikov, S.; Kolot, D.; Nosova, E.; Zabolotskiy, V. Peculiarities of

transport-structural parameters of ion-exchange membranes in solutions containing anions of carboxylic acids. **Journal of Membrane Science**, v. 557, p. 1–12, 2018.

140   Marder, L.; Ortega Navarro, E.M.; Perez-Herranz, V.; Bernardes, A.M.; Ferreira, J.Z. Evaluation of transition metals transport properties through a cation exchange membrane by chronopotentiometry. **Journal of Membrane Science**, v. 284, n. 1–2, p. 267–275, 2006.

141   Herraiz-Cardona, I.; Ortega, E.; Pérez-Herranz, V. Evaluation of the Zn^{2+} transport properties through a cation-exchange membrane by chronopotentiometry. **Journal of Colloid and Interface Science**, v. 341, n. 2, p. 380–385, 2010.

142   Marder, L.; Ortega Navarro, E.M.; Pérez-Herranz, V.; Bernardes, A.M.; Ferreira, J.Z. Chronopotentiometric study on the effect of boric acid in the nickel transport properties through a cation-exchange membrane. **Desalination**, v. 249, n. 1, p. 348–352, 2009.

143   Martí-Calatayud, M.C.; García-Gabaldón, M.; Pérez-Herranz, V.; Ortega, E. Determination of transport properties of Ni(II) through a Nafion cation-exchange membrane in chromic acid solutions. **Journal of Membrane Science**, v. 379, n. 1–2, p. 449–458, 2011.

144   Krol, J.J.; Wessling, M.; Strathmann, H. Chronopotentiometry and overlimiting ion transport through monopolar ion exchange membranes. **Journal of Membrane Science**, v. 162, n. 1–2, p. 155–164, 1999.

145   Larchet, C.; Nouri, S.; Auclair, B.; Dammak, L.; Nikonenko, V. Application of chronopotentiometry to determine the thickness of diffusion layer adjacent to an ion-exchange membrane under natural convection. **Advances in Colloid and Interface Science**, v. 139, n. 1–2, p. 45–61, 2008.

146   Gil, V.V.; Andreeva, M.A.; Jansezian, L.; Han, J.; Pismenskaya, N.D.; Nikonenko, V.V.; Larchet, C.; Dammak, L. Impact of heterogeneous cation-exchange membrane surface modification on chronopotentiometric and current–voltage characteristics in NaCl, CaCl2 and MgCl2 solutions. **Electrochimica Acta**, v. 281, p. 472–485, 2018.

147   Mareev, S.A.; Butylskii, D.Y.; Pismenskaya, N.D.; Nikonenko, V. V. Chronopotentiometry of ion-exchange membranes in the overlimiting current range. Transition time for a finite-length diffusion layer: Modeling and experiment. **Journal of Membrane Science**, v. 500, p. 171–179, 2016.

148   Sistat, P.; Pourcelly, G. Chronopotentiometric response of an ion-exchange membrane in the underlimiting current-range. Transport phenomena within the diffusion layers. **Journal of Membrane Science**, v. 123, p. 121–131, 1997.

149   Sand, H.J.S. On the Concentration at the Electrodes in a Solution , with special reference to the Liberation of Hydrogen by Electrolysis of a Mixture of Copper Sulphate and Sulphuric Acid. **Journal The London, Edinburgh, and Dublin Philosophical Magazine and Journal of Science**, v. 17, n. 496–534, 1899.

150 Lerche, D.; Wolf, H. Quantitative Characterisation of current-induced diffusion layers at cation-exchange membranes. I. investigations of temporal and local behaviour of concentration profile at constant current density. **Bioelectrochemistry and Bioenergetics**, v. 2, n. 4, p. 293–302, 1975.

151 Audinos, R.; Pichelin, G. Characterization of electrodialysis membranes by chronopotentiometry. **Desalination**, v. 68, n. 2–3, p. 251–263, 1988.

152 Nebavskaya, K.A.; Sarapulova, V. V.; Sabbatovskiy, K.G.; Sobolev, V.D.; Pismenskaya, N.D.; Sistat, P.; Cretin, M.; Nikonenko, V. V. Impact of ion exchange membrane surface charge and hydrophobicity on electroconvection at underlimiting and overlimiting currents. **Journal of Membrane Science**, v. 523, p. 36–44, 2017.

153 Choi, J.-H.; Moon, S.-H. Pore size characterization of cation-exchange membranes by chronopotentiometry using homologous amine ions. **Journal of Membrane Science**, v. 191, n. 1–2, p. 225–236, 2001.

154 Lide, D.R. **Handbook of Chemistry and Physics**. New York: CRC Press, 1997.

155 Mareev, S.A.; Butyl'skii, D.Y.; Kovalenko, A. V.; Pis'menskaya, N.D.; Dammak, L.; Larchet, C.; Nikonenko, V. V. Inclusion of the concentration dependence of the diffusion coefficient in the sand equation. **Russian Journal of Electrochemistry**, v. 52, n. 10, p. 996–1000, 2016.

156 Vobeckà, L.; Svoboda, M.; Beneš, J.; Belloň, T.; Slouka, Z. Heterogeneity of heterogeneous ion-exchange membranes investigated by chronopotentiometry and X-ray computed microtomography. **Journal of Membrane Science**, v. 559, p. 127–137, 2018.

157 Boucher, M.; Turcotte, N.; Guillemette, V.; Lantagne, G.; Chapotot, A.; Pourcelly, G.; Sandeaux, R.; Gavach, C. Recovery of spent acid by electrodialysis in the zinc hydrometallurgy industry: Performance study of different cation-exchange membranes. **Hydrometallurgy**, v. 45, n. 1–2, p. 137–160, 1997.

158 Tugas, I.; Pourcelly, G.; Gavach, C. Electrotransport of protons and chloride ions in anion exchange membranes for the recovery of acids. Part I. Equilibrium properties. **Journal of Membrane Science**, v. 85, n. 2, p. 183-194, 1993.

159 Tugas, I.; Lambert, J.M.; Maillols, J.; Bribes, J.L.; Pourcelly, G.; Gavach, C. Identification of the ionic species in anion exchange membranes equilibrated with sulphuric acid solutions by means of Raman spectroscopy and radiotracers. **Journal of Membrane Science**, v. 78, n. 1–2, p. 25–33, 1993.

160 Chapotot, A.; Pourcelly, G.; Gavach, C. Transport competition between monovalent and divalent cations through cation-exchange membranes. Exchange isotherms and kinetic concepts. **Journal of Membrane Science**, v. 96, n. 3, p. 167–181, 1994.

161 Schneider, E.W.; Verbrugge, M.W. Radiotracer method for simultaneous

measurement of cation, anion and water transport through ion-exchange membranes. **Applied Radiation and Isotopes**, v. 44, n. 10–11, p. 1399-1408, 1993.

162 Larchet, C.; Auclair, B.; Nikonenko, V. Approximate evaluation of water transport number in ion-exchange membranes. **Electrochimica Acta**, v. 49, n. 11, p. 1711–1717, 2004.

163 Auclair, B.; Nikonenko, V.; Larchet, C.; Métayer, M.; Dammak, L. Correlation between transport parameters of ion-exchange membranes. **Journal of Membrane Science**, v. 195, n. 1, p. 89–102, 2001.

164 Stránská, E. Relationships between transport and physical–mechanical properties of ion exchange membranes. **Desalination and Water Treatment**, v. 56, n. 12, p. 3220–3227, 2015.

165 Kang, M.S.; Choi, Y.J.; Lee, H.J.; Moon, S.H. Effects of inorganic substances on water splitting in ion-exchange membranes: I. Electrochemical characteristics of ion-exchange membranes coated with iron hydroxide/oxide and silica sol. **Journal of Colloid and Interface Science**, v. 273, n. 2, p. 523–532, 2004.

166 Kang, M.S.; Choi, Y.J.; Choi, I.J.; Yoon, T.H.; Moon, S.H. Electrochemical characterization of sulfonated poly(arylene ether sulfone) (S-PES) cation-exchange membranes. **Journal of Membrane Science**, v. 216, n. 1–2, p. 39–53, 2003.

167 Choi, Y.J.; Song, J.H.; Kang, M.S.; Seo, B.K. Preparation and electrochemical characterizations of anion-permselective membranes with structurally stable ion-exchange sites. **Electrochimica Acta**, v. 180, p. 71-77, 2015.

168 Kim, D.H.; Park, J.H.; Seo, S.J.; Park, J.S.; Jung, S.; Kang, Y.S.; Choi, J.H.; Kang, M.S. Development of thin anion-exchange pore-filled membranes for high diffusion dialysis performance. **Journal of Membrane Science**, v. 447, p. 80–86, 2013.

169 Kang, Y.S.; Moon, S.-H.; Park, J.-S.; Seo, S.-J.; Lee, M.-J.; Choi, Y.-W.; Kang, M.-S.; Kim, D.-H. Pore-filled anion-exchange membranes for non-aqueous redox flow batteries with dual-metal-complex redox shuttles. **Journal of Membrane Science**, v. 454, p. 44–50, 2013.

170 Mikhaylin, S.; Bazinet, L. Fouling on ion-exchange membranes: Classification , characterization and strategies of prevention and control. **Advances in Colloid and Interface Science**, v. 229, p. 34–56, 2016.

171 Martí-Calatayud, M.C.; García-Gabaldón, M.; Pérez-Herranz, V. Mass Transfer Phenomena during Electrodialysis of Multivalent Ions: Chemical Equilibria and Overlimiting Currents. **Applied Sciences**, v. 8, n. 9, p. 1566, 2018.

172 Martí-Calatayud, M.C.; García-Gabaldón, M.; Pérez-Herranz, V. Effect of the equilibria of multivalent metal sulfates on the transport through cation-exchange membranes at different current regimes. **Journal of Membrane Science**, v. 443, p. 181–192, 2013.

173 Wilhelm, F.G.; Vegt, N.F.A. Van Der; Strathmann, H.; Wessling, M. Comparison of bipolar membranes by means of chronopotentiometry. **Journal of Membrane Science**, v. 199, n. 1, p. 177–190, 2002.

174 Taky, M.; Pourcelly, G.; Gavach, C.; Elmidaoui, A. Chronopotentiometric response of a cation exchange membrane in contact with chromiumIII solutions. **Desalination**, v. 105, n. 3, p. 219–228, 1996.

175 Freijanes, Y.; Barragán, V.M.; Muñoz, S. Chronopotentiometric study of a Nafion membrane in presence of glucose. **Journal of Membrane Science**, v. 510, p. 79–90, 2016.

176 Shahi, V.K.; Thampy, S.K.; Rangarajan, R. Chronopotentiometric studies on dialytic properties of glycine across ion-exchange membranes. **Journal of Membrane Science**, v. 203, n. 1–2, p. 43–51, 2002.

177 Park, J.S.; Choi, J.H.; Yeon, K.H.; Moon, S.H. An approach to fouling characterization of an ion-exchange membrane using current-voltage relation and electrical impedance spectroscopy. **Journal of Colloid and Interface Science**, v. 294, n. 1, p. 129–138, 2006.

178 Kang, M.-S.; Cho, S.-H.; Kim, S.-H.; Choi, Y.-J.; Moon, S.-H. Electrodialytic separation characteristics of large molecular organic acid in highly water-swollen cation-exchange membranes. **Journal of Membrane Science**, v. 222, n. 1–2, p. 149–161, 2003.

179 Nunes, S.P.; Peinemann, K.-V. **Membrane Technology in the Chemical Industry**. Weinheim, Germany: WILEY-VCH Verlag GmbH & Co. KGaA, 2006.

180 Cooke, B.A. Concentration polarization in electrodialysis-I. The electrometric measurement of interfacial concentration. **Electrochimica Acta**, v. 3, n. 4, p. 307–317, 1961.

181 Cooke, B.A.; Walt, S.J. Van der Concentration polarization in electrodialysis-III. Practical electrodialysis systems. **Electrochimica Acta**, v. 5, n. 3, p. 216–228, 1961.

182 Forgacs, C. **Theoretical and practical aspects of scale control in electrodialysics desalination apparatus**. Dechema Monograph, 1962.

183 Sata, T. **Ion Exchange Membranes: Preparation, Characterization, Modification and Application**. Cambridge: Royal Society of Chemistry, 2004.

184 Długołecki, P.; Ogonowski, P.; Metz, S.J.; Saakes, M.; Nijmeijer, K.; Wessling, M. On the resistances of membrane, diffusion boundary layer and double layer in ion exchange membrane transport. **Journal of Membrane Science**, v. 349, n. 1–2, p. 369–379, 2010.

185 Nikonenko, V. V; Pismenskaya, N.D.; Belova, E.I.; Sistat, P.; Huguet, P.; Pourcelly, G.; Larchet, C. Intensive current transfer in membrane systems : Modelling , mechanisms and application in electrodialysis. **Advances in Colloid and Interface Science**, v. 160, n. 1–2, p. 101–123, 2010.

186 Sang, S.; Wu, Q.; Huang, K. A discussion on ion conductivity at cation

exchange membrane/solution interface. **Colloids and Surfaces A: Physicochemical and Engineering Aspects**, v. 320, n. 1–3, p. 43–48, 2008.

187 Levich, V.G. **Physicochemical Hydrodynamics**. New Jersey: Englewood Cliffs, 1962.

188 Helfferich, F.G. **Ion Exchange**. New York: McGraw-Hill, 1962.

189 Peers, A.M. . **Discussions of the Faraday Society**, p. 21–24, 1956.

190 Levich, V. **Physicochemical Hydrodynamics**. NJ: Prentice Hall, 1962.

191 Ashrafi, A.M.; Gupta, N.; Neděla, D. An investigation through the validation of the electrochemical methods used for bipolar membranes characterization. **Journal of Membrane Science**, v. 544, p. 195–207, 2017.

192 Güler, E.; Baak, W. van; Saakes, M.; Nijmeijer, K. Monovalent-ion-selective membranes for reverse electrodialysis. **Journal of Membrane Science**, v. 455, p. 254–270, 2014.

193 Volodina, E.; Pismenskaya, N.; Nikonenko, V.; Larchet, C.; Pourcelly, G. Ion transfer across ion-exchange membranes with homogeneous and heterogeneous surfaces. **Journal of Colloid and Interface Science**, v. 285, n. 1, p. 247–258, 2005.

194 Lee, H.J.; Hong, M.K.; Han, S.D.; Shim, J.; Moon, S.H. Analysis of fouling potential in the electrodialysis process in the presence of an anionic surfactant foulant. **Journal of Membrane Science**, v. 325, n. 2, p. 719-726, 2008.

195 Długołęcki, P.; Anet, B.; Metz, S.J.; Nijmeijer, K.; Wessling, M. Transport limitations in ion exchange membranes at low salt concentrations. **Journal of Membrane Science**, v. 346, n. 1, p. 163–171, 2010.

196 Pismenskaya, N.; Nikonenko, V.; Auclair, B.; Pourcelly, G. Transport of weak-electrolyte anions through anion exchange membranes - Current-voltage characteristics. **Journal of Membrane Science**, v. 189, n. 1, p. 129–140, 2001.

197 Melnikova, E.D.; Pismenskaya, N.D.; Bazinet, L.; Mikhaylin, S.; Nikonenko, V. V. Effect of ampholyte nature on current-voltage characteristic of anion-exchange membrane. **Electrochimica Acta**, v. 285, p. 185–191, 2018.

198 Scarazzato, T.; Panossian, Z.; García-Gabaldón, M.; Ortega, E.M.; Tenório, J.A.S.; Pérez-Herranz, V.; Espinosa, D.C.R. Evaluation of the transport properties of copper ions through a heterogeneous ion-exchange membrane in etidronic acid solutions by chronopotentiometry. **Journal of Membrane Science**, v. 535, p. 268–278, 2017.

199 Zook, J.M.; Bodor, S.; Gyurcsányi, R.E.; Lindner, E. Interpretation of chronopotentiometric transients of ion-selective membranes with two transition times. **Journal of Electroanalytical Chemistry**, v. 638, n. 2, p. 254–261, 2010.

200 Dalla Costa, R.F.; Klein, C.W.; Bernardes, A.M.; Ferreira, J.Z. Evaluation of

the electrodialysis process for the treatment of metal finishing wastewater. **Journal of the Brazilian Chemical Society**, v. 13, n. 4, p. 540–547, 2002.

201 Długołecki, P.; Ogonowski, P.; Metz, S.J.; Saakes, M.; Nijmeijer, K.; Wessling, M. On the resistances of membrane, diffusion boundary layer and double layer in ion exchange membrane transport. **Journal of Membrane Science**, v. 349, n. 1–2, p. 369–379, 2010.

202 Długołecki, P.; Anet, B.; Metz, S.J.; Nijmeijer, K.; Wessling, M. Transport limitations in ion exchange membranes at low salt concentrations. **Journal of Membrane Science**, v. 346, n. 1, p. 163–171, 2010.

203 Nouri, S.; Dammak, L.; Bulvestre, G.; Auclair, B. Comparison of three methods for the determination of the electrical conductivity of ion-exchange polymers. **European Polymer Journal**, v. 38, n. 9, p. 1907–1913, 2002.

204 Post, J.W.; Saakes, M.; Rijnaarts, H.H.M.; Galama, A.H.; Veerman, J.; Vermaas, D.A.; Nijmeijer, K. Membrane resistance: The effect of salinity gradients over a cation exchange membrane. **Journal of Membrane Science**, v. 467, p. 279–291, 2014.

205 Galama, A.H.; Hoog, N.A.; Yntema, D.R. Method for determining ion exchange membrane resistance for electrodialysis systems. **Desalination**, v. 380, p. 1–11, 2016.

206 Silva, R.F.; Francesco, M. De; Pozio, A. Tangential and normal conductivities of Nafion® membranes used in polymer electrolyte fuel cells. **Journal of Power Sources**, v. 134, n. 1, p. 18–26, 2004.

207 Stodollick, J.; Femmer, R.; Gloede, M.; Melin, T.; Wessling, M. Electrodialysis of itaconic acid: A short-cut model quantifying the electrical resistance in the overlimiting current density region. **Journal of Membrane Science**, v. 453, p. 275–281, 2014.

208 Choi, Y.J.; Park, J.M.; Yeon, K.H.; Moon, S.H. Electrochemical characterization of poly(vinyl alcohol)/formyl methyl pyridinium (PVA-FP) anion-exchange membranes. **Journal of Membrane Science**, v. 250, n. 1-2, p. 295–304, 2005.

209 Choi, J.-H.; Lee, H.-J.; Moon, S.-H. Effects of Electrolytes on the Transport Phenomena in a Cation-Exchange Membrane. **Journal of colloid and interface science**, v. 238, n. 1, p. 188–195, 2001.

210 Choi, E.Y.; Strathmann, H.; Park, J.M.; Moon, S.H. Characterization of non-uniformly charged ion-exchange membranes prepared by plasma-induced graft polymerization. **Journal of Membrane Science**, v. 268, n. 2, p. 165-174, 2006.

211 Kniaginicheva, E.; Pismenskaya, N.; Melnikov, S.; Belashova, E.; Sistat, P.; Cretin, M.; Nikonenko, V. Water splitting at an anion-exchange membrane as studied by impedance spectroscopy. **Journal of Membrane Science**, v. 496, p. 78–83, 2015.

212 Ruíz-Bauzá, V.M.B.C. Current–Voltage Curves for Ion-Exchange Membranes: A Method for Determining the Limiting Current Density.

Journal of Colloid and Interface Science, v. 205, p. 365–373, 1998.

213 Gil, V. V.; Andreeva, M.A.; Pismenskaya, N.D.; Nikonenko, V. V.; Larchet, C.; Dammak, L. Effect of counterion hydration numbers on the development of Electroconvection at the surface of heterogeneous cation-exchange membrane modified with an MF-4SK film. **Petroleum Chemistry**, v. 56, n. 5, p. 440–449, 2016.

214 Nikonenko, V. V.; Uzdenova, A.M.; Kovalenko, A. V.; Urtenov, M.K.; Mareev, S.A.; Pis'menskaya, N.D.; Pourcelly, G. Effect of electroconvection and its use in intensifying the mass transfer in electrodialysis (Review). **Russian Journal of Electrochemistry**, v. 53, n. 10, p. 1122–1144, 2017.

215 Choi, J.H.; Moon, S.H. Structural change of ion-exchange membrane surfaces under high electric fields and its effects on membrane properties. **Journal of Colloid and Interface Science**, v. 265, n. 1, p. 93–100, 2003.

216 Ibanez, R.; Stamatialis, D.F.; Wessling, M. Role of membrane surface in concentration polarization at cation exchange membranes. **Journal of Membrane Science**, v. 239, n. 1, p. 119–128, 2004.

217 Sarapulova, V.; Nevakshenova, E.; Nebavskaya, X.; Kozmai, A.; Aleshkina, D.; Pourcelly, G.; Nikonenko, V.; Pismenskaya, N. Characterization of bulk and surface properties of anion-exchange membranes in initial stages of fouling by red wine. **Journal of Membrane Science**, v. 559, p. 170–182, 2018.

218 Dammak, L.; Larchet, C.; Andreeva, M.A.; Pismenskaya, N.D.; Nikonenko, V.V.; Gil, V.V.; Grande, D.; Kononenko, N.A. Effect of homogenization and hydrophobization of a cation-exchange membrane surface on its scaling in the presence of calcium and magnesium chlorides during electrodialysis. **Journal of Membrane Science**, v. 540, p. 183–191, 2017.

219 Rubinstein, I.; Zaltzman, B. Electro-osmotically induced convection at a permselective membrane. **Physical Review E**, v. 62, n. 2, p. 2238–2251, 2000.

220 Balster, J.; Yildirim, M.H.; Stamatialis, D.F.; Ibanez, R.; Lammertink, R.G.H.; Jordan, V.; Wessling, M. Morphology and Microtopology of Cation-Exchange Polymers and the Origin of the Overlimiting Current. **Journal of Physical Chemistry B**, v. 111, p. 2152–2165, 2007.

221 Akberova, E.M.; Vasil'eva, V.I.; Zabolotsky, V.I.; Novak, L. Effect of the sulfocation-exchanger dispersity on the surface morphology, microrelief of heterogeneous membranes and development of electroconvection in intense current modes. **Journal of Membrane Science**, v. 566, p. 317-328, 2018.

222 Cardoso, D.; Stéphano, L.; Antônio, M.; Rodrigues, S.; Moura, A.; Alberto, J.; Tenório, S. Water recovery from acid mine drainage by electrodialysis. **Minerals Engineering**, v. 40, p. 82–89, 2013.

223 Meng, H.; Deng, D.; Chen, S.; Zhang, G. A new method to determine the optimal operating current (Ilim′) in the electrodialysis process. **Desalination**, v. 181, n. 1–3, p. 101–108, 2005.

224 Bukhovets, A.; Eliseeva, T.; Dalthrope, N.; Oren, Y. The influence of current density on the electrochemical properties of anion-exchange membranes in electrodialysis of phenylalanine solution. **Electrochimica Acta**, v. 56, n. 27, p. 10283–10287, 2011.

225 Simons, R. Strong electric field effects on proton transfer between membrane-bound amines and water. **Nature**, v. 30, n. 5725, p. 824–826, 1979.

226 Frilette, V.J. Electrogravitational transport at synthetic ion exchange membrane surfaces. **Journal of Physical Chemistry**, v. 61, n. 2, p. 168-174, 1957.

227 Rubinshtein, I.; Zaltzman, B.; Pretz, J.; Linder, C. Experimental verification of the electroosmotic mechanism of overlimiting conductance through a cation exchange electrodialysis membrane. **Russian Journal of Electrochemistry**, v. 38, n. 8, p. 853–863, 2002.

228 Rubinstein, I.; Zaltzman, B. Electro-Osmotic Slip of the Second Kind and Instability in Concentration Polarization At Electrodialysis Membranes. **Mathematical Models and Methods in Applied Sciences**, v. 11, n. 02, p. 263–300, 2001.

229 Pundik, T.; Rubinstein, I.; Zaltzman, B. Bulk electroconvection in electrolyte. **Physical Review E - Statistical, Nonlinear, and Soft Matter Physics**, v. 72, n. 6, p. 1–8, 2005.

230 Rubinstein, I.; Kedem, B.; Zaltzman O. Electric fields in and around ion-exchange membranes. **Journal of Membrane Science**, v. 125, p. 17–21, 1997.

231 Rubinstein, I. Electroconvection at an electrically inhomogeneous permselective interface. **Physics of Fluids A**, v. 3, n. 10, p. 2301–2309, 1991.

232 Rubinstein, S.M.; Manukyan, G.; Staicu, A.; Rubinstein, I.; Zaltzman, B.; Lammertink, R.G.H.; Mugele, F.; Wessling, M. Direct observation of a nonequilibrium electro-osmotic instability. **Physical Review Letters**, v. 101, n. 23, p. 1–4, 2008.

233 Dukhin, S.S. Electrokinetic phenomena of the second kind and their applications. **Advances in Colloid and Interface Science**, v. 35, n. C, p. 173–196, 1991.

234 Mishchuk, N.A. Electro-osmosis of the second kind near the heterogeneous ion-exchange membrane. **Colloids and Surfaces A: Physicochemical and Engineering Aspects**, v. 140, p. 75–89, 1998.

235 Rubinstein, I.; Zaltzman, B.; Pundik, T. Ion-exchange funneling in thin-film coating modification of heterogeneous electrodialysis membranes. **Physical Review E - Statistical Physics, Plasmas, Fluids, and Related Interdisciplinary Topics**, v. 65, n. 4, p. 10, 2002.

236 Urtenov, M.K.; Uzdenova, A.M.; Kovalenko, A. V.; Nikonenko, V. V.; Pismenskaya, N.D.; Vasil'eva, V.I.; Sistat, P.; Pourcelly, G. Basic

mathematical model of overlimiting transfer enhanced by electroconvection in flow-through electrodialysis membrane cells. **Journal of Membrane Science**, v. 447, p. 190–202, 2013.

237 Druzgalski, C.L.; Andersen, M.B.; Mani, A. Direct numerical simulation of electroconvective instability and hydrodynamic chaos near an ion-selective surface. **Physics of Fluids**, v. 25, n. 11, p. 110804, 2013.

238 Maletzki, F.; Rösler, H.W.; Staude, E. Ion transfer across electrodialysis membranes in the overlimiting current range: stationary voltage current characteristics and current noise power spectra under different conditions of free convection. **Journal of Membrane Science**, v. 71, n. 1–2, p. 105-116, 1992.

239 Rubinstein, I.; Shtilman, L. Voltage against current curves of cation exchange membranes. **Journal of the Chemical Society, Faraday Transactions 2: Molecular and Chemical Physics**, v. 75, n. 6, p. 231-246, 1979.

240 Zabolotsky, V.I.; Nikonenko, V. V; Pismenskaya, N.D.; Laktionov, E. V; Urtenov, M.K.; Strathmann, H.; Wessling, M.; Koops, G.H. Coupled transport phenomena in overlimiting current electrodialysis. **Separation and Purification Technology**, v. 14, p. 255–267, 1998.

241 Urtenov, M.A.K.; Kirillova, E. V.; Seidova, N.M.; Nikonenko, V. V. Decoupling of the Nernst-Planck and Poisson equations. Application to a membrane system at overlimiting currents. **Journal of Physical Chemistry B**, v. 111, n. 51, p. 14208–14222, 2007.

242 Mishchuk, S.S.; Dukhin, N.A. Unlimited increase in the current through an ionite granule. **Kolloid. Zh.**, v. 49, n. 8, p. 1197, 1987.

243 Rubinstein, I.; Staude, E.; Kedem, O. Role of the membrane surface in concentration polarization at ion-exchange membrane. **Desalination**, v. 69, n. 2, p. 101–114, 1988.

244 Nikonenko, V.; Zabolotsky, V.; Larchet, C.; Auclair, B.; Pourcelly, G. Mathematical description of ion transport in membrane systems. **Desalination**, v. 147, n. 1–3, p. 369–374, 2002.

245 Zabolotsky, V.I.; Novak, L.; Kovalenko, A. V.; Nikonenko, V. V.; Urtenov, M.H.; Lebedev, K.A.; But, A.Y. Electroconvection in systems with heterogeneous ion-exchange membranes. **Petroleum Chemistry**, v. 57, n. 9, p. 779–789, 2017.

246 Davidson, S.M.; Wessling, M.; Mani, A. On the Dynamical Regimes of Pattern-Accelerated Electroconvection. **Scientific Reports**, v. 6, p. 1–10, 2016.

247 Mishchuk, N., Dukhin, S. Interfacial Electrokinetics and Electrophoresis. In: A V. Delgado (Ed.); **Interfacial Electrokinetics and Electrophoresis**. CRC Press, 2001, p. 241.

248 Pismenskiy, A.; Nikonenko, V.; Urtenov, M.; Pourcelly, G. Mathematical modelling of gravitational convection in electrodialysis processes.

Desalination, v. 192, n. 1–3, p. 374–379, 2006.

249 Mareev, S.; Kozmai, A.; Nikonenko, V.; Belashova, E.; Pourcelly, G.; Sistat, P. Chronopotentiometry and impedancemetry of homogeneous and heterogeneous ion-exchange membranes. **Desalination and Water Treatment**, v. 56, p. 3207–3210, 2015.

250 Mareev, S.A.; Nichka, V.S.; Butylskii, D.Y.; Urtenov, M.K.; Pismenskaya, N.D.; Apel, P.Y.; Nikonenko, V. V Chronopotentiometric Response of an Electrically Heterogeneous Permselective Surface: 3D Modeling of Transition Time and Experiment. **The Journal of Physical Chemistry C**, v. 120, n. 24, p. 13113–13119, 2016.

251 Belashova, E.D.; Melnik, N.A.; Pismenskaya, N.D.; Shevtsova, K.A.; Nebavsky, A. V.; Lebedev, K.A.; Nikonenko, V. V. Overlimiting mass transfer through cation-exchange membranes modified by Nafion film and carbon nanotubes. **Electrochimica Acta**, v. 59, p. 412–423, 2012.

252 Pismenskaya, N.D.; Nikonenko, V. V.; Melnik, N.A.; Shevtsova, K.A.; Belova, E.I.; Pourcelly, G.; Cot, D.; Dammak, L.; Larchet, C. Evolution with time of hydrophobicity and microrelief of a cation-exchange membrane surface and its impact on overlimiting mass transfer. **Journal of Physical Chemistry B**, v. 116, n. 7, p. 2145–2161, 2012.

253 Korzhova, E.; Pismenskaya, N.; Lopatin, D.; Baranov, O.; Dammak, L.; Nikonenko, V. Effect of surface hydrophobization on chronopotentiometric behavior of an AMX anion-exchange membrane at overlimiting currents. **Journal of Membrane Science**, v. 500, p. 161–170, 2015.

254 Belova, E.; Lopatkova, G.; Pismenskaya, N.; Nikonenko, V.; Larchet, C. Role of water splitting in development of electroconvection in ion-exchange membrane systems. **Desalination**, v. 199, n. 1–3, p. 59–61, 2006.

255 Volgin, V.M.; Davydov, A.D. Natural-Convective Instability of Electrochemical Systems: A Review*. **Elektrokhimiya**, v. 42, n. 6, p. 567-608, 2006.

256 Volgin, V.M.; Volgina, O. V.; Bograchev, D.A.; Davydov, A.D. Simulation of ion transfer under conditions of natural convection by the finite difference method. **Journal of Electroanalytical Chemistry**, v. 546, p. 15–22, 2003.

257 Nikonenko, V. V.; Pismenskaya, N.D.; Belova, E.I.; Sistat, P.; Huguet, P.; Pourcelly, G.; Larchet, C. Intensive current transfer in membrane systems: Modelling, mechanisms and application in electrodialysis. **Advances in Colloid and Interface Science**, v. 160, n. 1–2, p. 101–123, 2010.

258 Pismenskaya, N.D.; Nikonenko, V. V; Belova, E.I.; Lopatkova, G.Y.; Sistat, P.; Pourcelly, G.; Larshe, K. Coupled convection of solution near the surface of ion-exchange membranes in intensive current regimes. **Russian Journal of Electrochemistry**, v. 43, n. 3, p. 307–327, 2007.

259 Zabolotsky, V.I.; Nikonenko, V. V.; Pismenskaya, N.D. On the role of gravitational convection in the transfer enhancement of salt ions in the course of dilute solution electrodialysis. **Journal of Membrane Science**, v. 119, n. 2, p. 171–181, 1996.

260 Simons, R. Water splitting in ion exchange membranes. **Electrochimica Acta**, v. 30, n. 3, p. 275–282, 1985.

261 Simons, R. Electric field effects on proton transfer between ionizable groups and water in ion exchange membranes. **Electrochimica Acta**, v. 29, n. 2, p. 151–158, 1984.

262 Zabolotskii, V.I.; Shel'deshov, N. V; Gnusin, N.P. Dissociation of Water Molecules in Systems with Ion-exchange Membranes. **Russian Chemical Reviews**, v. 57, n. 8, p. 801–808, 1988.

263 Krol, J.J.; Wessling, M.; Strathmann, H. Concentration polarization with monopolar ion exchange membranes: Current-voltage curves and water dissociation. **Journal of Membrane Science**, v. 162, n. 1–2, p. 145–154, 1999.

264 Kang, M.-S.; Choi, Y.-J.; Moon, S.-H. Effects of charge density on water splitting at cation-exchange membrane surface in the over-limiting current region. **Korean Journal of Chemical Engineering**, v. 21, n. 1, p. 221–229, 2004.

265 Elattar, A.; Elmidaoui, A.; Pismenskaia, N.; Gavach, C.; Pourcelly, G. Comparison of transport properties of monovalent anions through anion-exchange membranes. **Journal of Membrane Science**, v. 143, n. 1–2, p. 249–261, 1998.

266 Malek, P.; Ortiz, J.M.; Richards, B.S.; Schäfer, A.I. Electrodialytic removal of NaCl from water: Impacts of using pulsed electric potential on ion transport and water dissociation phenomena. **Journal of Membrane Science**, v. 435, p. 99–109, 2013.

267 Mikhaylin, S.; Nikonenko, V.; Pourcelly, G.; Bazinet, L. Intensification of demineralization process and decrease in scaling by application of pulsed electric field with short pulse/pause conditions. **Journal of Membrane Science**, v. 468, p. 389–399, 2014.

268 Mishchuk, N.A.; Verbich, S. V.; Gonzales-Caballero, F. Concentration Polarization and Specific Selectivity of Membranes in Pulse Mode. **Colloid Journal**, v. 63, n. 5, p. 586–594, 2001.

269 Kharkats, Y.I. The mapping of faradic efficiencies in large electrodialysis units. **Sov Electrochem**, v. 21, p. 917, 1985.

270 Andersen, M.B.; Soestbergen, M. Van; Mani, A.; Bruus, H.; Biesheuvel, P.M.; Bazant, M.Z. Current-induced membrane discharge. **Physical Review Letters**, v. 109, n. 10, p. 1–5, 2012.

271 Slouka, Z.; Senapati, S.; Yan, Y.; Chang, H.C. Charge inversion, water splitting, and vortex suppression due to DNA sorption on ion-selective membranes and their ion-current signatures. **Langmuir**, v. 29, n. 26, p. 8275–8283, 2013.

272 Ogutveren, U.B.; Koparal, S.; E. Ozel. Electrodialysis for the removal of copper ions from wastewater. **Journal of Environmental Science and Health . Part A: Environmental Science and Engineering and**

Toxicology, v. 32, p. 749–761, 2008.

273 Caprarescu, S.; Corobea, M.C.; Purcar, V.; Spataru, C.I.; Ianchis, R.; Vasilievici, G.; Vuluga, Z. San copolymer membranes with ion exchangers for Cu(II) removal from synthetic wastewater by electrodialysis. **Journal of Environmental Sciences (China)**, v. 35, p. 27–37, 2015.

274 Alebrahim, M.F.; Khattab, I.A.; Sharif, A.O. Electrodeposition of copper from a copper sulfate solution using a packed-bed continuous-recirculation flow reactor at high applied electric current. **Egyptian Journal of Petroleum**, v. 24, n. 3, p. 325–331, 2015.

275 Puigdomench, I. (2001). Hydra Medusa — Make Equilibrium Diagrams using Sophisticated Algorithms.

276 Vogel, C.; Meier-Haack, J. Preparation of ion-exchange materials and membranes. **Desalination**, v. 342, p. 156–174, 2014.

277 Garcia-Vasquez, W.; Ghalloussi, R.; Dammak, L.; Larchet, C.; Nikonenko, V.; Grande, D. Structure and properties of heterogeneous and homogeneous ion-exchange membranes subjected to ageing in sodium hypochlorite. **Journal of Membrane Science**, v. 452, p. 104–116, 2014.

278 Sistat, P.; Pourcelly, G. Chronopotentiometric response of an ion-exchange membrane in the underlimiting current-range. Transport phenomena within the diffusion layers. **Journal of Membrane Science**, v. 123, n. 1, p. 121-131, 1997.

279 Nightingale, E.R. Phenomenological Theory of Ion Solvation. Effective Radii of Hydrated Ions. **The Journal of Physical Chemistry**, v. 63, n. 9, p. 1381-1387, 1959.

280 Logette, S.; Eysseric, C.; Pourcelly, G.; Lindheimer, A.; Gavach, C. Selective permeability of a perfluorosulphonic membrane to different valency cations. Ion-exchange isotherms and kinetic aspects. **Journal of Membrane Science**, v. 144, n. 1–2, p. 259–274, 1998.

281 Shahi, V.K.; Thampy, S.K.; Rangarajan, R. Studies on transport properties of surfactant immobilized anion-exchange membrane. **Journal of Membrane Science**, v. 158, n. 1–2, p. 77–83, 1999.

282 Izquierdo-Gil, M.A.; Barragán, V.M.; Villaluenga, J.P.G.; Godino, M.P. Water uptake and salt transport through Nafion cation-exchange membranes with different thicknesses. **Chemical Engineering Science**, v. 72, p. 1–9, 2012.

283 Nikonenko, V.; Lebedev, K.; Manzanares, J.A.; Pourcelly, G. Modelling the transport of carbonic acid anions through anion-exchange membranes. **Electrochimica Acta**, v. 48, n. 24, p. 3639–3650, 2003.

284 Prochaska, K.; Woźniak-Budych, M.J. Recovery of fumaric acid from fermentation broth using bipolar electrodialysis. **Journal of Membrane Science**, v. 469, p. 428–435, 2014.

285 Kumar, M.; Tripathi, B.P.; Shahi, V.K. Ionic transport phenomenon across sol-gel derived organic-inorganic composite mono-valent cation selective

membranes. **Journal of Membrane Science**, v. 340, n. 1–2, p. 52–61, 2009.

286 Belloň, T.; Polezhaev, P.; Vobecká, L.; Svoboda, M.; Slouka, Z. Experimental observation of phenomena developing on ion-exchange systems during current-voltage curve measurement. **Journal of Membrane Science**, v. 572, p. 607–618, 2019.

287 Baes, C.F.; Mesmer, R.E. **The Hydrolysis of Cations**. New York, London, Sydney, Toronto.: John Wiley & Sons, 1976.

288 Lindsay, W.L. **Chemical Equilibria in Soils**. New York: John Wiley and Sons, 1979.

289 Ganych, V.V.; Zabolotskii, V.I.; Shel'deshov, N.V. Electrolytic dissociation of water molecules in systems comprising solutions and MA-40 anion-exchange membranes modified with transition metal ions. **Sov. Electrochemistry**, v. 28, n. 9, p. 1138–1143, 1992.

290 Zabolotskii, V.I.; Ganych, V.V.; Sheldeshov, N.V. Effect of Copper Complexes with the Ionogenic Groups of the MA-40 Anion-Exchange Membrane on the Dissociation Rate of Water Molecules in the Electric Field. **Sov. Electrochemistry**, v. 27, n. 10, p. 1098, 1991.

291 Indusekhar, V.K.; Krishnaswamy, N. Water transport studies on interpolymer ion-exchange membranes. **Desalination**, v. 52, n. 3, p. 309-316, 1985.

292 Lakshminarayaniah, N. Electro-osmotic permeability of ion-exchange resin membranes. **Proceedings of the Indian Academy of Sciences - Section A**, v. 55, n. 4, p. 200–212, 1962.

293 Saakes, M.; Galama, A.H.; Post, J.W.; Bruning, H.; Rijnaarts, H.H.M. Seawater predesalination with electrodialysis. **Desalination**, v. 342, p. 61-69, 2013.

294 Sata, T.; Tsujimoto, M.; Yamaguchi, T.; Matsusaki, K. Change of anion exchange membranes in an aqueous sodium hydroxide solution at high temperature. **Journal of Membrane Science**, v. 112, n. 2, p. 161–170, 1996.

295 Merle, G.; Wessling, M.; Nijmeijer, K. Anion exchange membranes for alkaline fuel cells: A review. **Journal of Membrane Science**, v. 377, n. 1-2, p. 1–35, 2011.

296 Couture, G.; Alaaeddine, A.; Boschet, F.; Ameduri, B. Progress in Polymer Science Polymeric materials as anion-exchange membranes for alkaline fuel cells. **Progress in Polymer Science**, v. 36, n. 11, p. 1521–1557, 2011.

297 Ghalloussi, R.; Garcia-vasquez, W.; Chaabane, L.; Dammak, L.; Larchet, C.; Deabate, S. V Ageing of ion-exchange membranes in electrodialysis : A structural and physicochemical investigation. **Journal of Membrane Science**, v. 436, p. 68–78, 2013.

298 Cope, A.C., Trumbull, E.R. Olefins from amines: the hofmann elimination reaction and amine oxide pyrolysis. In: **Organic Reactions**. John Wiley &

Sons, Inc., 2004,

299 Kuć, M.; Cieślik-Boczula, K.; ̃wiątek, P.; Jaszczyszyn, A.; Gąsiorowski, K.; Malinka, W. FTIR-ATR study of the influence of the pyrimidine analog of fluphenazine on the chain-melting phase transition of sphingomyelin membranes. **Chemical Physics**, v. 458, p. 9–17, 2015.

300 Kołodyńska, D.; Hubicki, Z.; Pasieczna-Patkowska, S. FT-IR/PAS Studies of Cu(II)-EDTA Complexes Sorption on the Chelating Ion Exchangers. **Acta Physica Polonica A**, v. 116, n. 3, p. 340–343, 2009.

301 Sawyer, D.T.; McKinnie, J.M. Properties and Infrared Spectra of Ethylenediaminetetraacetic Acid Complexes. II. Chelates of Divalent Ions. **Journal of the American Chemical Society**, v. 82, n. 16, p. 4191–4196, 1960.

302 Cheng, J.; Yang, X.; Dong, L.; Yuan, Z.; Wang, W.; Wu, S.; Chen, S.; Zheng, G.; Zhang, W.; Zhang, D.; Wang, H. Effective nondestructive evaluations on UHMWPE/Recycled-PA6 blends using FTIR imaging and dynamic mechanical analysis. **Polymer Testing**, v. 59, p. 371–376, 2017.

303 Grochowicz, M.; Kierys, A. TG/DSC/FTIR studies on the oxidative decomposition of polymer-silica composites loaded with sodium ibuprofen. **Polymer Degradation and Stability**, v. 138, p. 151–160, 2017.

304 Esteban, M.F.G.; Serrano, R.V.; Vilchez, F.G. Synthesis and vibrational study of some polydentate ligands. **Spectrochimica Acta Part A: Molecular Spectroscopy**, v. 43, n. 8, p. 1039–1043, 1987.

305 Srinivasan, S.; Gunasekaran, S.; Ponnambalam, U.; Savarianandam, A.; Gnanaprakasam, S.; Natarajan, S. Spectroscopic and thermodynamic analysis of enolic form of 3-oxo-L-gulofuranolactone. **Indian Journal of Pure and Applied Physics**, v. 43, n. 6, p. 459–462, 2005.

306 Hosakun, Y.; Halász, K.; Horváth, M.; Csóka, L.; Djoković, V. ATR-FTIR study of the interaction of CO_2 with bacterial cellulose-based membranes. **Chemical Engineering Journal**, v. 324, p. 83–92, 2017.

307 Lanigan, K.C.; Pidsosny, K. Reflectance FTIR spectroscopic analysis of metal complexation to EDTA and EDDS. **Vibrational Spectroscopy**, v. 45, n. 1, p. 2–9, 2007.

308 Caprarescu, S.; Radu, A.-L.; Purcar, V.; Ianchis, R.; Sarbu, A.; Ghiurea, M.; Nicolae, C.; Modrogan, C.; Vaireanu, D.-I.; Périchaud, A.; Ebrasu, D.-I. Adsorbents/ion exchangers-PVA blend membranes: Preparation, characterization and performance for the removal of Zn^{2+} by electrodialysis. **Applied Surface Science**, v. 329, p. 65–75, 2015.

309 Hébert, P.; Rille, A. Le; Zheng, W.Q.; Tadjeddine, A. Vibrational spectroscopic study of the adsorption of pyridine at the Au(111)-electrolyte interface by in situ difference frequency generation. **Journal of Electroanalytical Chemistry**, v. 447, n. 1–2, p. 5–9, 1998.

310 Nakanishi, K.; Solomon, P.H. **Infrared Absorption Spectroscopy**. San Francisco : Holden-Day: 1977.

311 Amado, F.D.R.; Rodrigues, M.A.S.; Morisso, F.D.P.; Bernardes, A.M.; Ferreira, J.Z.; Ferreira, C.A. High-impact polystyrene/polyaniline membranes for acid solution treatment by electrodialysis: Preparation, evaluation, and chemical calculation. **Journal of Colloid and Interface Science**, v. 320, n. 1, p. 52–61, 2008.

312 Benavente, L.; Coetsier, C.; Venault, A.; Chang, Y.; Causserand, C.; Bacchin, P.; Aimar, P. FTIR mapping as a simple and powerful approach to study membrane coating and fouling. **Journal of Membrane Science**, v. 520, p. 477–489, 2016.

313 Wang, C.; Bai, X.; Liu, S.; Liu, L. Synthesis of cobalt-aluminum spinels via EDTA chelating precursors. **Journal of Materials Science**, v. 39, n. 20, p. 6191–6201, 2004.

314 Wu, K.H.; Wang, Y.R.; Hwu, W.H. FTIR and TGA studies of poly (4-vinylpyridine- co-divinylbenzene)–Cu (II) complex. **Polymer Degradation and Stability**, v. 79, p. 195–200, 2003.

315 Mitić, Ž.; Cakić, M.; Nikolić, G. Fourier-Transform IR spectroscopic investigations of Cobalt(II)-dextran complexes by using D2O isotopic exchange. **Spectroscopy**, v. 24, n. 3–4, p. 269–275, 2010.

316 Xia, Q.; Zhao, X.J.; Chen, S.J.; Ma, W.Z.; Zhang, J.; Wang, X.L. Effect of solution-blended poly(styrene-co-acrylonitrile) copolymer on crystallization of poly(vinylidene fluoride). **Express Polymer Letters**, v. 4, n. 5, p. 284-291, 2010.

317 Komkova, E.N.; Stamatialis, D.F.; Strathmann, H.; Wessling, M. Anion-exchange membranes containing diamines : preparation and stability in alkaline solution. **Journal of Membrane Science**, v. 244, p. 25–34, 2004.

318 Dammak, L.; Larchet, C.; Grande, D. Ageing of ion-exchange membranes in oxidant solutions. **Separation and Purification Technology**, v. 69, p. 43–47, 2009.

319 Bulejko, P.; Weinertová, K. Properties and structure of heterogeneous ion-exchange membranes after exposure to chemical agents. **Journal of Solid State Electrochemistry**, v. 21, p. 111–124, 2017.

320 Tabakovic, I.; Riemer, S.; Jayaraju, N.; Venkatasamy, V.; Gong, J. Relationship of Fe^{2+} concentration in solution and current efficiency in electrodeposition of CoFe films. **Electrochimica Acta**, v. 58, n. 1, p. 25–32, 2011.

321 Almeida, M.R.H. de.; Carlos, I.A.; Barbosa, L.L.; Carlos, R.M.; Lima-Neto, B.S.; Pallone, E.M.J.A. Voltammetric and morphological characterization of copper electrodeposition from non-cyanide electrolyte. **Journal of Applied Electrochemistry**, v. 32, n. 7, p. 763–773, 2002.

322 Barbosa, L.L.; Almeida, M.R.H. de; Carlos, R.M.; Yonashiro, M.; Oliveira, G.M.; Carlos, I.A. Study and development of an alkaline bath for copper deposition containing sorbitol as complexing agent and morphological characterization of the copper film. **Surface and Coatings Technology**, v. 192, n. 2–3, p. 145–153, 2005.

323   Ying, R.Y. Electrodeposition of copper-nickel alloys from citrate solutions on a rotating disk electrode I. Experimental results. **Journal of the Electrochemical Society**, v. 135, n. 12, p. 2957–2964, 1988.

324   Losada, J.; Peso, I. Del; Beyer, L. Redox and electrocatalytic properties of electrodes modified by films of polypyrrole nickel(II) Schiff-base complexes. **Journal of Electroanalytical Chemistry**, v. 447, n. 1–2, p. 147–154, 1998.

325   Razmi, H.; Azadbakht, A. Electrochemical characteristics of dopamine oxidation at palladium hexacyanoferrate film, electroless plated on aluminum electrode. **Electrochimica Acta**, v. 50, n. 11, p. 2193–2201, 2005.

326   Flis-Kabulska, I. Effect of anodic prepolarization on hydrogen entry into iron at cathodic potentials in 0.1 M NaOH without and with EDTA or sodium molybdate. **Electrochimica Acta**, v. 55, n. 17, p. 4895–4901, 2010.

327   Dorsch, R.K. Simultaneous electrodeposition of nickel and hydrogen on a rotating disk electrode. **Journal of Electroanalytical Chemistry and Interfacial Electrochemistry**, v. 21, n. 3, p. 495–508, 2006.

328   Gómez, E.; Vallés, E. Electrodeposition of zinc + cobalt alloys: inhibitory effect of zinc with convection and pH of solution. **Journal of Electroanalytical Chemistry**, v. 397, n. 1–2, p. 177–184, 1995.

329   Monev, M.; Mirkova, L.; Krastev, I.; Tsvetkova, H.; Rashkov, S.; Richtering, W. Effect of brighteners on hydrogen evolution during zinc electroplating from zincate electrolytes. **Journal of Applied Electrochemistry**, v. 28, n. 10, p. 1107–1112, 1998.

330   Wranglen, G. Electrodeposition of Metal Powders. **Journal of The Electrochemical Society**, v. 97, n. 11, p. 353, 2007.

331   Zeiri, L.; Younes, O.; Efrima, S.; Deutsch, M. Interfacial Electrodeposition of Silver. **The Journal of Physical Chemistry B**, v. 101, n. 45, p. 9299–9308, 1997.

APPENDIX

The EDTA dissociation follows reactions (A1) - (A6):

$H^+ + EDTA^{4-} \leftrightarrow HEDTA^{3-}$	log K = 11.24	(A1)
$2H^+ + EDTA^{4-} \leftrightarrow H_2EDTA^{2-}$	log K = 18.04	(A2)
$3H^+ + EDTA^{4-} \leftrightarrow H_3EDTA^-$	log K = 21.19	(A3)
$4H^+ + EDTA^{4-} \leftrightarrow H_4EDTA$	log K = 23.42	(A4)
$5H^+ + EDTA^{4-} \leftrightarrow H_5EDTA^+$	log K = 22.12	(A5)
$6H^+ + EDTA^{4-} \leftrightarrow H_6EDTA^{2+}$	log K = 21.62	(A6)
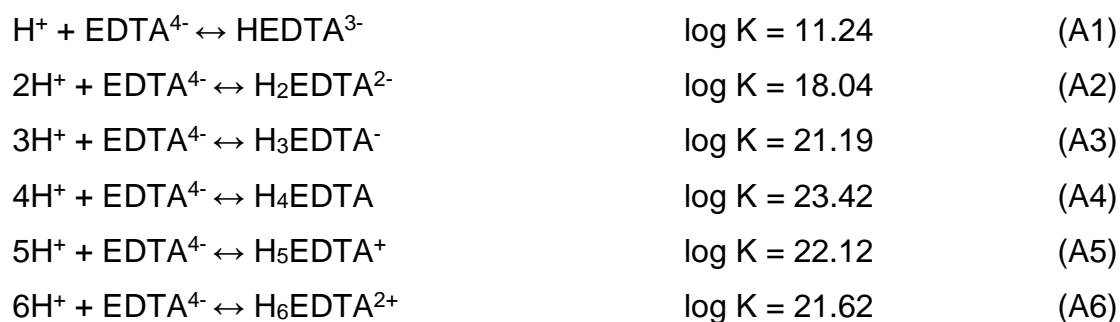
The reactions of chelation mechanism between EDTA and copper ions are (A7) - (A10):

$Cu^{2+} + EDTA^{4-} \leftrightarrow Cu(EDTA)^{2-}$	log K = 20.57	(A7)
$Cu^{2+} + EDTA^{4-} \leftrightarrow H^+ + Cu(EDTA)OH^{3-}$	log K = 8.5	(A8)
$2H^+ + Cu^{2+} + EDTA^{4-} \leftrightarrow Cu(H_2EDTA)$	log K = 26.35	(A9)
$H^+ + Cu^{2+} + EDTA^{4-} \leftrightarrow Cu(HEDTA)^-$	log K = 24.12	(A10)
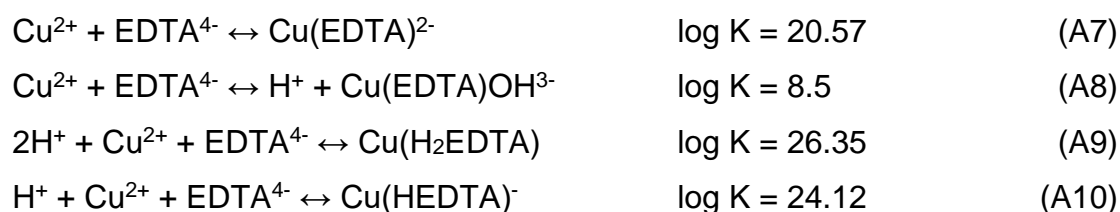
In aqueous solution, soluble copper hydroxides can also be formed as shown by reactions (A11) - (A17)

$Cu^{2+} \leftrightarrow H^+ + CuOH^+$	log K = -7.96	(A11)
$Cu^{2+} \leftrightarrow 2H^+ + Cu(OH)_2$	log K = -16.24	(A12)
$Cu^{2+} \leftrightarrow 3H^+ + Cu(OH)^{3-}$	log K = -26.7	(A13)
$Cu^{2+} \leftrightarrow 4H^+ + Cu(OH)_4^{2-}$	log K = -39.6	(A14)
$2Cu^{2+} \leftrightarrow H^+ + Cu_2OH^{3+}$	log K = -6.7	(A15)
$2Cu^{2+} \leftrightarrow 2H^+ + Cu_2(OH)_2^{2+}$	log K = -10.35	(A16)
$3Cu^{2+} \leftrightarrow 4H^+ + Cu_3(OH)_4^{2+}$	log K = -21.1	(A17)
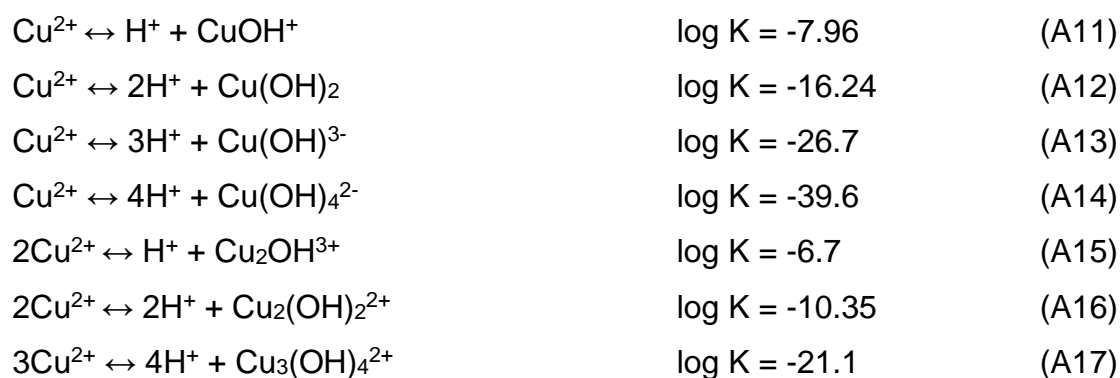
The reactions of chelation mechanism between EDTA and zinc ions are (A18) - (A21):

$Zn^{2+} + EDTA^{4-} \leftrightarrow Zn(EDTA)^{2-}$	log K = 18.0	(A18)
$Zn^{2+} + EDTA^{4-} \leftrightarrow H^+ + Zn(EDTA)OH^{3-}$	log K = 5.48	(A19)
$2H^+ + Zn^{2+} + EDTA^{4-} \leftrightarrow Zn(H_2EDTA)$	log K = 22.96	(A20)

$H^+ + Zn^{2+} + EDTA^{4-} \leftrightarrow Zn(HEDTA)^-$ log K = 21.45   (A21)
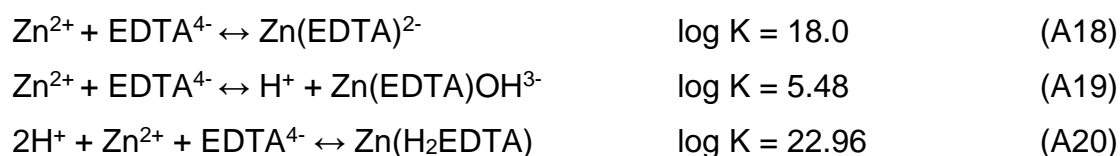
Reactions (A22) - (A28) present the formation of soluble hydroxides with zinc.

$Zn^{2+} \leftrightarrow 2H^+ + Zn(OH)_2$ log K = -16.4   (A22)

$Zn^{2+} \leftrightarrow 3H^+ + Zn(OH)_3^-$ log K = -28.2   (A23)

$Zn^{2+} \leftrightarrow 4H^+ + Zn(OH)_4^{2-}$ log K = -41.3   (A24)

$2Zn^{2+} \leftrightarrow 6H^+ + Zn_2(OH)_6^{2-}$ log K = -54.3   (A25)

$2Zn^{2+} \leftrightarrow H^+ + Zn_2OH^{3+}$ log K = -9.0   (A26)

$4Zn^{2+} \leftrightarrow 4H^+ + Zn_4(OH)_4^{4+}$ log K = -27.0   (A27)

$Zn^{2+} \leftrightarrow H^+ + ZnOH^+$ log K = -7.5   (A28)
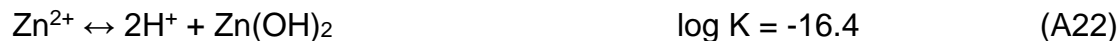
Reactions (A29) - (A33) show the mechanism of the formation of insoluble complexes involving copper, zinc and EDTA:

$Cu^{2+} \leftrightarrow 2H^+ + Cu(OH)_2$ (solid)   log K = -8.64   (A29)

$Cu^{2+} \leftrightarrow 2H^+ + CuO$ (crystal)   log K = -7.675   (A30)

$4H^+ + EDTA^{4-} \leftrightarrow H_4EDTA$ (solid)   log K = 27.22   (A31)

$Zn^{2+} \leftrightarrow 2H^+ + Zn(OH)_2$ (solid)   log K = -12.45   (A32)

$Zn^{2+} \leftrightarrow 2H^+ + ZnO$ (crystal)   log K = -11.2   (A33)
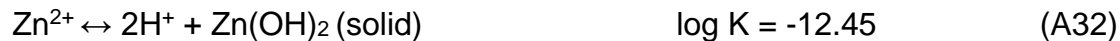
The formation of other soluble and insoluble sulfate and sodium compounds from the copper and zinc sulfate and NaOH used for the pH adjustment, respectively, are shown by reactions (A34) - (A52):

$H^+ + SO_4^{2-} \leftrightarrow HSO_4^-$ log K = 1.98   (A34)

$Cu^{2+} + SO_4^{2-} \leftrightarrow CuSO_4$ log K = 2.31   (A35)

$Cu^{2+} + SO_4^{2-} \leftrightarrow CuSO_4$(solid)   log K = -3.01   (A36)

$2Cu^{2+} + SO_4^{2-} \leftrightarrow 2H^+ + CuO.CuSO_4$ (solid)   log K = -11.53   (A37)

$3Cu^{2+} + SO_4^{2-} \leftrightarrow 4H^+ + Cu_3SO_4(OH)_4$ (solid)   log K = -8.29   (A38)

$4Cu^{2+} + SO_4^{2-} \leftrightarrow 6H^+ + Cu_4SO_4(OH)_6$ (solid)   log K = -15.34   (A39)

$Zn^{2+} + SO_4^{2-} \leftrightarrow ZnSO_4$ log K = 2.37   (A40)

$Zn^{2+} + SO_4^{2-} \leftrightarrow ZnSO_4$ (solid)   log K = -3.01   (A41)

$Zn^{2+} + 2SO_4^{2-} \leftrightarrow Zn(SO_4)_2^{2-}$ log K = 3.28   (A42)

$Zn^{2+} + 3SO_4^{2-} \leftrightarrow Zn(SO_4)_3^{4-}$ log K = 1.7   (A43)

$Zn^{2+} + 4SO_4^{2-} \leftrightarrow Zn(SO_4)_4^{6-}$	log K = 1.7	(A44)
$2Zn^{2+} + SO_4^{2-} \leftrightarrow 2H^+ + Zn_2(OH)_2SO_4$ (solid)	log K = -7.5	(A45)
$3Zn^{2+} + 2SO_4^{2-} \leftrightarrow 2H^+ + Zn_3O(SO_4)_2$ (solid)	log K = -19.02	(A46)
$4Zn^{2+} + SO_4^{2-} \leftrightarrow 6H^+ + Zn_4(OH)_6SO_4$ (solid)	log K = -28.4	(A47)
$Na^+ \leftrightarrow H^+ + NaOH$	log K = -14.18	(A48)
$Na^+ + SO_4^{2-} \leftrightarrow NaSO_4^-$	log K = 0.7	(A49)
$2Na^+ + SO_4^{2-} \leftrightarrow Na_2SO_4$ (solid)	log K = 0.179	(A50)
$Na^+ + EDTA^{4-} \leftrightarrow Na(EDTA)^{3-}$	log K = 2.8	(A51)
$2H^+ + EDTA^{4-} + 2Na^+ \leftrightarrow Na_2(H_2EDTA)$ (solid)	log K = 20.4	(A52)